LOW ORDER HARMONICS MITIGATION IN GRID CONNECTED, PARALLEL PV INVERTERS

Suriana Binti Salimin

A Thesis Submitted for the Degree of

Doctor of Philosophy

School of Electrical, Electronics, and Computer Engineering

Newcastle University

October 2014

Abstract

This research is concerned with the problem of network power quality when grid connected systems are used to feed the network distribution grid. A parallel connection of photovoltaic (PV) system is the main interest of study for this research. This type of PV system uses power electronic components such as inverter and current controller that produce harmonics which adversely affect the power quality of the distribution network. Development and simulation of current controller using the proportional resonance (PR) scheme is considered to overcome the harmonic problems in single and parallel PV inverters. This scheme eliminates specific harmonic in the low order part. The control parameter randomisation technique is added to the scheme to produce a more efficient current controller system. Thus, the inverter harmonic performance (inverter output current) is improved. This concept is extended to parallel inverter based systems, where opportunities for harmonic cancellation improve the inverter harmonic performance further. Experimental hardware setup using TMS320F2812 is also developed to verify the promising simulation results.

Keywords: Harmonics, current controller, parallel, PV inverter, grid connected system.

Acknowledgements

First and foremost, I would love to express my sincere gratitude to my supervisors, Dr. Matthew Armstrong and Dr. Bashar Zahawi. My main supervisor, Dr. Matthew Armstrong is the most important person that helped, guided, supported, advised, and determined to keep giving me valuable ideas and information throughout this project.

My utmost appreciation also goes to the staffs especially from the mechanical workshop, electrical workshop, and electronic workshop for their guidance and support. Thank you very much to Stephen Mitchell, Stephen Robson, Jeff, Darren, and the others! Many thanks to all my colleagues in the Power Electronics, Drives and Machines Research Group for their friendship and help.

Special thanks to my husband, Khairul, as well as my precious forever babies, Danish, Daania dan Dalila for always be with me upon the completion of this study. Not to forget, my family and friends who prayed for my success.

Thank you very much.

Without those whom I mentioned above, this PhD project will not be accomplished.

Table of Contents

List of Figures

List of Tables

List of Abbreviations and Symbols

Abbreviations

DG	Distributed Generation
PV	Photovoltaic
DC	Direct Current
AC	Alternating Current
PWM	Pulse Width Modulation
L	Inductor
LC	Inductor and Capacitor
LCL	Inductor, Capacitor and Inductor
MPPT	Maximum Power Point Tracking
RMS	Root Mean Square
IEEE	Institute of Electrical and Electronic Engineers (USA)
PI	Proportional and Integral
PR	Proportional and Resonant
HC	Harmonic Compensator
DSP	Digital Signal Processing
PR+HC	Proportional Resonant with Harmonic Compensator
THD	Total Harmonic Distortion
LV	Low Voltage
UPS	Uninterruptible Power Supply
WAC	Weighted Average Current
PLL	Phase Locked Loop
CPWM	Centered Pulse Width Modulation
SHMPWM	Selective Harmonic Mitigation Pulse Width Modulation
SHEPWM	Selective Harmonic Elimination Pulse Width Modulation

OSPWM	Optimal Sinusoidal Pulse Width Modulation
SMC	Sliding Mode Control
FFT	Fast Fourier Transform
THIPWM	Third Harmonic Injection Pulse Width Modulation
ACSC	Average Current Sharing Center
NSPWM	Non-sinusoidal Pulse Width Modulation
NSHVC	Non-sinusoidal Hysterisis Voltage Control
APF	Active Power Filter
DIRS	Direct Injection Random Signal
IGBT	Insulated Gate Bipolar Transistor
ADC	Analogue to Digital Converter
DAC	Digital to Analogue Converter
ZOH	Zero Order Hold
PID	Proportional Integral Derivative
P	Proportional
I	Integral
ESR	Equivalent Series Resistance

Symbols

f	Frequency
kWp	KiloWatt power
G_{PR}	Proportional-Resonant Current Controller
G_{HC}	Harmonic Compensator Current Controller
K_P	Proportional gain
K_I	Integral gain
V_{PV}	Output voltage of Photovoltaic
R_P	Random gain component
V_{dc}	DC output voltage
$V_{control}/V_{sin}$	Voltage of control signal
V_{tri}	Voltage of triangular waveform
G_{PI}	Proportional-Integral Current Controller
ω_o	Fundamental frequency (rad/s)
T	Sampling time (s)
Hz	Hertz (frequency)
$G_{PRmodified}$	Modified Proportional-Resonant Current Controller
R_{KP}	Randomized proportional gain
C_f	Filter capacitance value
L_f	Filter inductance value
L_g	Grid inductance value
R_{Lf}	Resistance value of the inductor of the filter
R_{Cf}	Resistance value of the capacitor of the filter
R_g	Resistance value of the grid
V_{PCC}	Voltage at the point of common coupling
V_x	Voltage at inverter output

H_{Lf}	Transfer function of the filter
I_x	Output inverter current
I_g	Grid current
I_{Cf}	Filter capacitance current
I_o	Output current from the filter
H_{Lg}	Transfer function of the grid impedance
c_{pk}	Peak of the carrier signal
$m_s(t)$	Modulating signal
$c(t)$	Carrier signal
d	Duty cycle
ω_c	Cut-off frequency
K_{c3}	Resonant gain at three times of fundamental frequency
K_{c5}	Resonant gain at five times of fundamental frequency
K_{c7}	Resonant gain at seven times of fundamental frequency
V_G	Background grid voltage
I_{ref}	Reference current

Chapter 1: Introduction

1.1 Chapter Introduction

The first chapter of this thesis provides an overview on distributed generation (DG). This is the technical area in which this work aims to make a valid contribution to knowledge. The main advantages of DG technology are described and the recent annual growth statistics for application of renewable energy systems is presented.

This thesis will specifically concentrate on small scale grid connected photovoltaic (PV) systems. Therefore, the second half of the chapter provides a brief discussion on Photovoltaic (PV) systems, highlighting the technological challenges which exist within these systems and the opportunities for further research. The final section of this chapter summarises the aims and objectives of this research project.

1.2 Overview on Distributed Generation (DG)

Throughout the whole of the modern era, each century has seen an increase in energy consumption, which is intrinsically linked to the continual increase in worldwide human population. This can be seen in Table 1-1 as proposed by R. DeGunther [1]. With the well recognised depletion of traditional fossil fuels such as coal, oil and gas, distributed generation technologies or embedded generation is rapidly becoming a significant and important matter worldwide. Typically, these generation systems are connected at strategic places within the power distribution network and much closer to the end users than conventional power stations. Based on P. Chiradeja and Y. Ma, et al [2, 3], the key advantages of this type of electricity generation are as follows:

i- It can reduce transmission losses as the plant is installed near its application.

ii- It has satisfying power supply demand where the energy can always be utilized whenever needed by users. For instance in the event of line outage or scheduled interruption.

Table 1-1 Population and Energy Consumption Over Time.

Date	**Population (billions)**	**Consumption (kWh/day)**
5000 bc	0.1	9.4
0 ad	0.3	10.1
1850	1.3	12.0
1980	4.4	51.0
2000	6.0	230
2050	9.0	1000?

Distributed generation uses renewable energy sources that include solar, wind, wave, hydro power and biomass. They convert these natural sources to usable electricity. Often, they are of small scale, scattered and close to the loads and their control devices [4, 5]. Renewable sources play an important role in order to reduce the environmental pollution and thus decrease the worries of global warming and climate changes [6]. As known by many, traditional energy sources such as petroleum, natural gas and coal are major contributors' to the pollution of the environment. It has been stated in literature that:

"All fossil fuels produce carbon dioxide, a greenhouse gas when burned. When there is insufficient air, all fossil fuels produce highly toxic carbon monoxide" [7].

1.2.1 *Electricity from Solar*

Generally, there is an upward trend in the utilisation of renewable energy sources for electricity generation. However, as shown in Figure 1-1, grid connected photovoltaic (PV) systems have experienced a particularly rapid growth (60%) in demand between the end of year 2004 and 2009 with a 53% increase in capacity for 2009 alone. Being so popular, photovoltaic generation systems are now readily integrated into distribution systems worldwide [8].

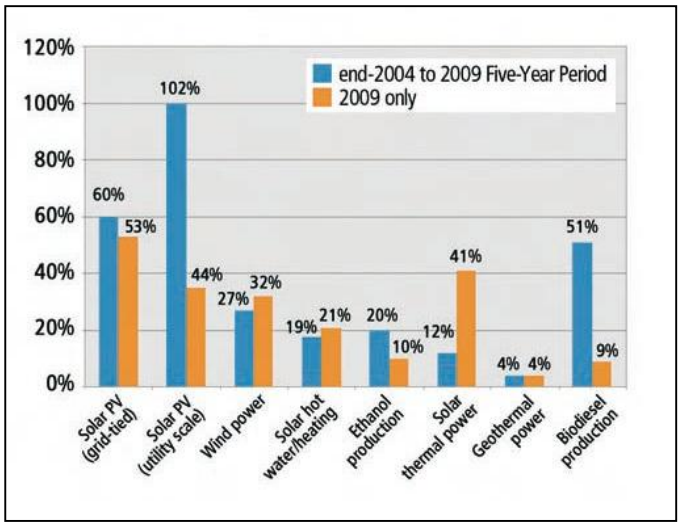

Figure 1-1: Average annual growth rates of renewable energy capacity, end 2004 to 2009[9].

It is estimated that the future lifespan of the Sun is approximately 4 to 5 billion years. For this reason, it is generally assumed that the Sun represents an energy that is to all intents and purposes, inexhaustible [10]. Furthermore, it is one of the cleanest energy sources. With regards to grid connected systems, PV technology is generally acknowledged to be one of the more reliable and low maintenance solutions, compared to alternative systems such as wind turbine generators. When operating, there are typically no moving parts which need to be replaced when broken. Instead, the PV panels generally only require scheduled inspection and cleaning. Furthermore, PV systems are very flexible and can be installed anywhere significant levels of sun can reach such as rooftops of industrial, commercial and residential buildings. The electricity can also be sold to the utility grid if extra power is generated.

Below are the lists of the advantages according to Foster R. et al [10]:

a) High reliability.

b) Low operating costs.

c) Local fuel (not imported fossil fuel).

d) Long, useful life.

e) Clean energy.

f) No on-site operator required.

g) Low operation and maintenance costs.

More explanation on PV systems is provided in the next section.

1.3 Background of grid connected PV Inverter

Renewable energy generating systems can be readily used to supply standalone load systems. However, there is an increasing trend to also connect PV systems to the utility grid. In such systems, the grid receives the electrical energy generated by the PV inverter system [11]. The basic concept of a PV grid connected inverter system is illustrated in Figure 1-2.

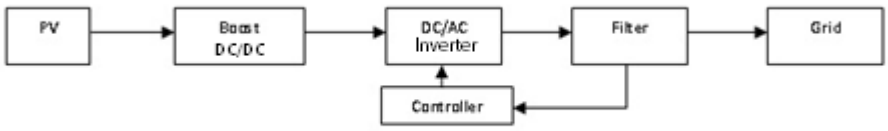

Figure 1-2: Basic concept of grid connected inverter.

Based on Figure 1-2, the basic concept of grid connected inverter consists of:

a) PV array – A PV array is assembled from several PV modules made of multiple solar cells to capture the sunlight and converts it to a DC voltage [12, 13].
b) DC/DC boost converter – The input of the converter varies due to the DC voltage variation from the PV array whilst the output from the converter is controlled to follow a constant desired voltage value [14]. The purpose is to increase the low input voltage to a standard DC bus voltage value; i.e. 400 V(DC) [15]. The performance depends on its design as well as its operating conditions. Regardless of the weather and temperature, maximum output power can be achieved through the implementation of a good maximum power point tracking (MPPT) algorithm [16].
c) DC/AC inverter – An inverter converts the DC voltage to an AC voltage, typically using Pulse Width Modulation (PWM) switching techniques. In addition, the inverter must be controlled to ensure that the voltage is synchronised to the grid supply voltage. This ensures unity power factor operation and optimum real power transfer to the grid.
d) Filter – A low pass filter is used to block and prevent high frequency components from entering the grid. These high frequency components come from the PWM switching frequency of the DC/AC inverter, which is typically in the kilohertz range. The types of filter used can be of inductive (L) type, inductive and capacitive (LC) type and inductive, capacitive, and inductive (LCL) type. Hanju Cha and Trung-Kien Vu [17] detail the advantages and disadvantages of each type of filter.
e) Controller – This inverter current controller minimises the error between the inverter output current and controller reference current. The intention is to keep the signal sinusoidal, with very low distortion, and to maintain a power factor close to unity [18-20].

Typically, PV arrays can be configured into four different types of topology; centralized technology, single-string technology, a multi-string technology, and an AC-cell or AC module technology [21]. In the paper by Xiaojin Wu et al [22], the first three arrangements are described. A centralized technology is a conventional arrangement where several PV modules are connected in series to make a string of PV modules.

Then, strings of PV modules are connected in parallel to form the PV array and feed the inverter. This is illustrated in the Figure 1-3.

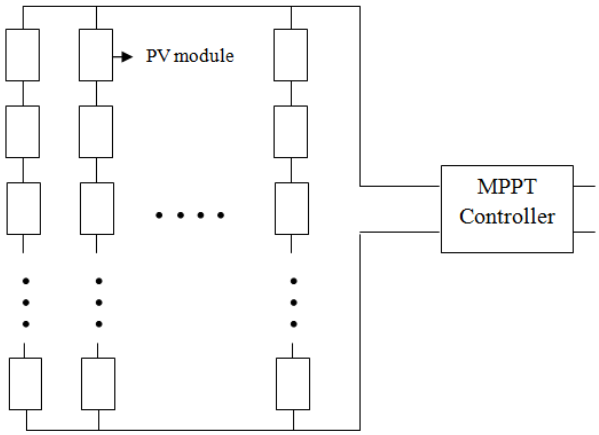

Figure 1-3: Centralised technology PV arrangement.

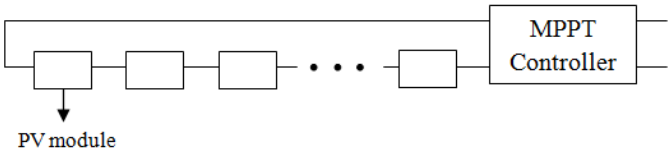

Figure 1-4: Single-string technology PV arrangement.

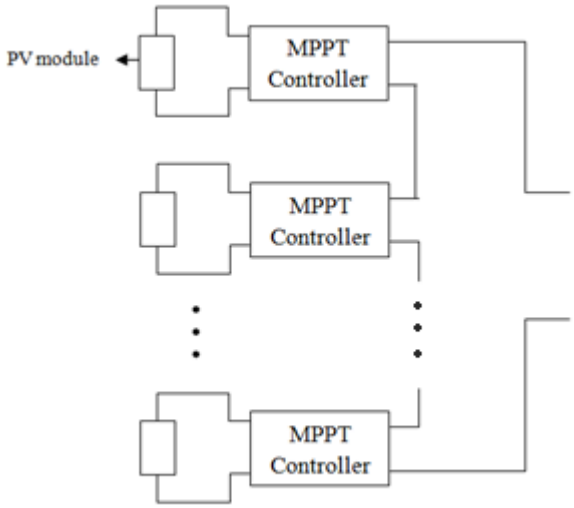

Figure 1-5: Multi-string technology PV arrangement.

The second configuration is the single-string technology shown in Figure 1-4. It consists of several PV modules connected together in series to form the PV array. The third configuration is the multi-string technology shown in Figure 1-5, which consists of a PV module with its own DC/DC converter, connected in parallel, and fed to a single DC/AC inverter. All three configurations have a maximum power point tracking (MPPT) controller which is used to draw the maximum power from the array [23].

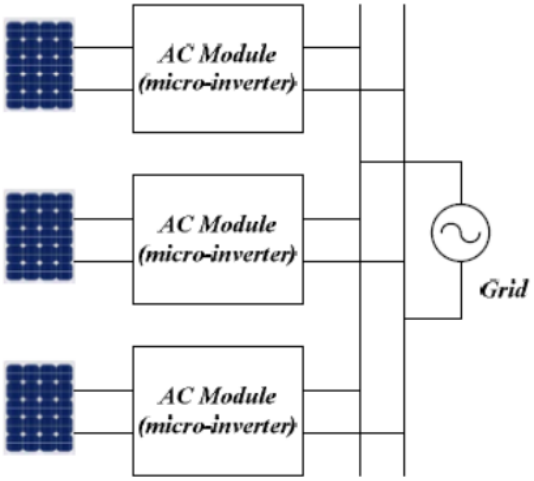

Figure 1-6: AC cell PV arrangement [24].

The last configuration is also called micro-inverter technology [25] (Figure 1-6). It is a system which combines a PV module and an AC module inverter to feed the grid. All of these arrangements and configurations have their own advantages and disadvantages comprising of complexity, efficiency, reliability, and more. The key points are summarised in Table 1-2.

Table 1-2: Advantages and disadvantages of PV array configuration [22, 26, 27].

	Advantages	Disadvantages
Centralized Technology	1. PV array arrangement generates higher voltage and current suitable for large scale systems (>1 MW). 2. Simple and low cost as only one MPPT controller is used.	1. The MPPT controller considers the PV modules arrangement as one whole thus makes the output power smaller.
Single-string Technology	1. PV array arrangement generates higher voltage and low current which is easy to assemble based on power demands.	1. One shaded PV module can cause large power dissipation on that module as the photocurrent in that particular module may drop.
Multi-string Technology	1. Each PV module has its own MPPT controller thus maximum power is drawn.	1. Complicated and costly 2. Shading problem is reduced as only one module in series.
Micro inverter technology	1. The output from this technology can be directly connected to AC system.	1. Has an additional up-front cost.

Regardless of the PV array arrangement, these inverter systems do have their drawbacks that generally arise from the switching process and non-linearity in the components of the power electronic converter system. Briefly, the purpose of these electronic components is to integrate the PV system into the supply grid and ensure that it complies with a host of power quality recommendations and standards [28]. The inverter for instance has to fulfil several important functions before the current may be fed into the supply grid [29]. Firstly, it must shape the current into a sinusoidal waveform where a controller is used and secondly, it must invert the DC current into an AC current with a correct switching. In doing so, it is very difficult to avoid levels of distortion in the conversion and control process. The result is undesirable current and voltage harmonics appearing in the inverter output which can potentially contribute to a lower power quality grid network with increased risk of disruption.

Power quality is defined as the voltage and current provided by the grid that can be successfully utilized by the user without interference or interruption [30]. For good power quality operation, it is important that the current harmonics produced at the output of the inverter do not exceed the national Point of Common Coupling standards [31]. The impact of these harmonics include variation in root mean square (RMS) voltage, disturbance of electronic components and stress on insulation materials [32]. Other impacts are discussed in Chapter 2. Therefore, it is vital to reduce the harmonic level to be under the limit as recommended in IEEE 929-2000 [31].

1.3.1 *Parallel Inverter System*

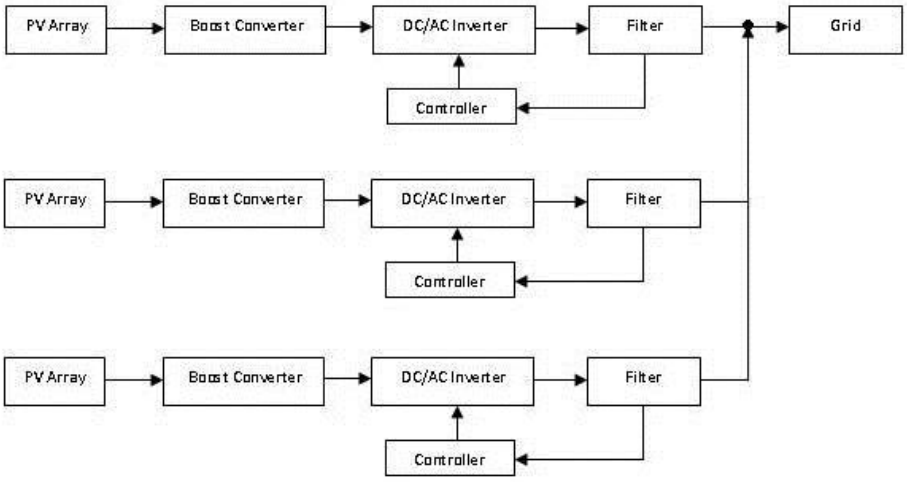

Figure 1-7: Parallel arrangement of grid connected system.

Parallel inverter systems are commonly used to increase the power rating of the PV system and maximise the return of power to the network. In this system, several individually controlled inverter units are connected to the grid via a common point of coupling. Each inverter output voltage should be synchronised to the grid voltage and inject unity power factor current into the network. The synchronization method of individual inverter units, together with the interaction between closely coupled systems can potentially increase the production of low order harmonics [33]. This is also agreed by Cespedes M. And J. Sun [34] where it is stated that unintended interactions may occur because each of the inverters has its own dynamic system. He also grouped the unintended interaction into the low frequency region; not more than the fundamental frequency, medium frequency region; between the fundamental frequency and the

crossover frequency, and the high frequency region; more than the crossover frequency. Each of them comes from different sources with its own ways of mitigation. The main point is that the unintended interaction between the inverters may affect the power quality of the network. Figure 1-7 shows an example arrangement of several PV inverter systems connected in parallel with the supply grid. It can be seen that each PV system has its own inverter and controller system.

1.4 Aims and Objectives

This chapter has highlighted the types of PV inverter system which are commonly used in practice. The need for good power quality operation has been described and the causes and impacts of harmonic generation are stated. Even today, with modern devices and control methods, the issue of power quality remains a problem which all manufacturers must address. For this reason, this research aims to propose a method to eliminate the low order harmonics production in a parallel PV inverter system connected to the supply grid. As a result, the work primarily concentrates on the output side (AC) of the system which consists of the DC/AC inverter, the current controller, the low pass (LC) filter and the supply grid.

With this in mind, the thesis has the following objectives:

a) To demonstrate the low-order harmonic performance of a single-phase grid connected inverter using the classical proportional integral (PI) control methods.

b) To show that the low order harmonic performance of a grid-connected inverter can be improved by replacing the PI controller with a proportional resonance (PR) current controller scheme.

c) To explore that the addition of harmonic compensators (HC) and controller parameter randomisation techniques can further improve the harmonic performance of a parallel connected inverter systems.

   Studies on proportional resonant controllers with harmonic compensators (PR+HC) have been carried out previously. A full literature review on this topic

is presented in Chapter 2. However, to the best of the authors' knowledge, no studies have attempted to model the PR+HC controller and make better analysis specifically to grid connected system.

d) To validate the above points in simulation and experimentally.

1.5 Thesis Outline

This thesis consists of 8 chapters. This Chapter has discussed the background of PV inverter system and has set out the aims and objectives of the research project. Chapter 2 presents a literature review of relevant previous work in the field of PV inverter systems. Chapter 3 focuses on the different control methods to be applied in this project; the conventional PI controller scheme, the PR+HC controller scheme and the modified PR+HC controller scheme. Chapter 4 is written to model the grid connected inverters. Chapter 5 demonstrates the simulation results when using the three controller schemes. Chapters 6 and Chapter 7 demonstrate the experimental results when using the three controller schemes with a stand-alone system and a grin connected system. Finally, Chapter 8 presents the conclusion of this research project.

1.6 Chapter Summary

This chapter has described the background to distributed generation and the reasons for its continuing popularity compared to traditional forms of fossil fuel based generation. The concept of single and parallel PV inverter systems has been discussed. Furthermore, relevant to this thesis, the basic causes of harmonic generation have been set out, and the need to meet the appropriate grid connection standards has been set out. At the end of this chapter, the aims and objectives of the research project are identified.

In this research project, the main contributions to knowledge include:

a) Modelling the inverter system with a PR+HC current controller. This controller includes additional harmonic compensation terms, e.g. for the 3rd, 5th, and 7th harmonic orders, which can reduce low order harmonics injection into the grid. In Chapter 4, frequency domain results demonstrate the increased impedance to these components, and the resulting power quality benefits.

b) For a stand-alone inverter, improved harmonic performance can be achieved by randomizing, within limits, the integral gain of a PI controller. Hence, the technique can also be considered for grid connected applications. Previous research has typically concentrated on modifying the proportional controller only.

c) In this thesis, a PR controller employing parameter randomisation techniques is employed. The author believes that this is the first time that such a technique has been applied. In this thesis, simulation and practical results demonstrate that a modified PR controller technique improves the harmonic performance of individual and parallel connected inverter systems. In Chapter 7, the harmonic profiles of the parallel inverters system show no correlation between the inverters. This leads to a better total harmonic value (THD) value. Overall a 19% improvement, compared to a conventional PI current controller, is achieved.

This research has resulted in the following publication:

- S. Salimin, M. Armstrong and B. Zahawi, "Randomized Integral Gain of Pi Current Controller for A Single Pv Inverter System," *Engineering*, Vol. 5 No. 1B, 2013, pp. 221-225.

Chapter 2: Literature Review

2.1 Chapter Introduction

The chapter begins with an overview of harmonic injection. A brief explanation on what harmonics are; as well as their potential impacts, is discussed. Following this, four types of harmonics are identified. The work from a significant number of papers is discussed in the area of harmonic injection and harmonic mitigation techniques for both single and multiple/parallel grid-connected inverter systems. On a broader level, additional papers concentrating on harmonic generation from engineering fields other than grid-connected inverters are then reviewed. Finally, from the literature review, the direction and objectives of this research project are compiled and explained.

2.2 Reviews on Harmonic Injection

The most significant discussion in any grid-connected system is the current or voltage harmonic injection into the grid. In general, harmonics are considered to be undesirable voltage or current frequency components that can arise in an electrical system or power network. They normally appear at frequencies which are an integer multiples of the fundamental frequency of the system [35]. In grid connected inverter systems, the fundamental frequency is normally 50 Hz or 60 Hz, depending on the country of concern. The mathematical definition of a single harmonics is:

$$f_n = nf_1 \qquad (\text{where } f_1 \text{ is the fundamental frequency and n = 1,2,3,…})$$

When this harmonic is added to the magnitude of fundamental frequency, a distorted current or voltage waveform is produced. In grid-connected systems, harmonic emissions not only depends on the characteristics of the grid network, but also on the location of PV installation within the network and the behaviour of the inverter system itself [36, 37]. For instance, installing the PV inverter system closer to the secondary side of the pole transformer, the effects of the harmonics are less than installing the PV closer to loads [38].

In PV grid connected system, concerns have been raised by several relevant bodies about the injection of harmonics into the network. Impacts of harmonic currents according to [33, 39-41] include:

a) Communication interference.
b) Heating problems that lead to over-current, insulation breakdown, cable corrosion –due to 'skin effects' of copper.
c) Solid state device malfunctions.
d) Voltage distortion that will reduce reliability electrical and electronic systems.

Papaioannou et al [42] describe the impact of the connection of PV inverter systems to the low voltage (LV) distribution network. The investigation took place in Greece involving a 20 kWp PV system connection under different weather conditions. Results from the harmonic behaviour examination show the significant presence of 3^{rd}, 5^{th}, and 7^{th} order harmonics current. Furthermore, Kotsopoulos et al., 2005 [43] reported that when many inverters are operating in parallel, resonance caused by the interaction between the inverter output filter capacitance with the grid is also a big issue. A case in point is failure to the power factor correction capacitors. A report by Caamano et al [32] mentioned a wide range of harmonic impacts to the network components and AC side of the inverter system. These include variation in RMS voltage and flicker, disturbances of electronic component, overloading of passive filters, stress on insulation materials, and many more.

H. Soo et al [44] stated a different view about low-order harmonics; one of four types of harmonics injection. The paper demonstrated that the low order harmonic profile of the inverter output current can be affected by the operating conditions of the grid voltage, variations in the grid impedance, and the connection of other non-linear loads to the network. IEEE 929-2000 [31] sets limitation on the level of harmonic injection into the grid which is permissible. Table 2-1 shows the recommended individual current harmonic limitations for general distribution systems. The current THD must also be less than 5% of the fundamental frequency at the rated output power of the inverter. In addition, an individual voltage distortion limit of 3% and overall voltage THD of less than 5% is defined by IEEE 519-1992 [45].

Table 2-1: IEEE standard on harmonic limitation [45].

Harmonic Order (Odd)	Limit
$3^{rd} – 9^{th}$	< 4%
$11^{th} – 15^{th}$	< 2%
$17^{th} – 21^{st}$	< 1.5%
$23^{rd} – 33^{rd}$	< 0.6%
Above 33^{rd}	< 0.3%

These recommendations apply to single inverter installations only. The author is unaware of any recommendations relating to parallel connected systems. Indeed, this may be difficult to enforce, as it is often the case that individual inverter units are connected to the grid separately, and co-incidentally form a parallel operating system with existing installations. For example, consider the case where a domestic customer has a PV installation at home. The engineer installing the system will typically only concern themselves with the immediate installation, not the neighbouring devices.

The various types of harmonics are often being categorised as PWM or switching harmonics [33], low-order harmonics [33], and DC current injection [46]. A. Testa et al [47] has also demonstrated that inter-harmonics and sub-harmonics can be included as an additional source of harmonic pollution which may need to be considered. A brief explanation of these types of harmonic is described in the following section.

2.2.1 *Types of Harmonic*

a) Low-order Harmonics

Low-order harmonics are components at frequencies close to the fundamental frequency. Their origin is often from the deficiencies in the inverter output current controller. Besides, extrinsic sources such as connection to a distorted grid can also produce low-order harmonics. As stated by Abeyasekera et al [48], in order to remove low-order harmonics, it requires a bulky and costly output filter. Therefore, it is common to ensure that a robust current control loop is applied. Several PWM inverter

switching techniques and control methods have been proposed to specifically reduce and eliminate low-order harmonics. They are broadly discussed in sub-section 2.3.

b) PWM/Switching Harmonics

Switching harmonics are the high order harmonics generally in kHz range. They are generated because of the side effect of high frequency inverter switching and can be filtered relatively easily by using a low pass filter at the inverter output. In a study by H.Zhang et al [49], equations to calculate switching harmonic components are derived for the purpose of minimizing the dc link capacitor. S. Ma et al [50] has proposed two techniques as a solution for switching harmonics problem. They are the zero voltage switching half cycle and voltage phase compensation and their effectiveness is confirmed.

c) Inter-harmonics and Sub-harmonics

Inter-harmonics and sub-harmonics on the other hand are components at variable frequencies that are not in integer multiples of fundamental frequency. The detection and measurement of the frequencies are difficult to trace and there is still unanswered questions on how to accurately measure and eliminate them from systems. Voltage or current distortion from inter-harmonics may arise from effects such as sub-synchronous oscillations, voltage fluctuation and disturbance in fluorescent lamps, arcing loads, variable speed electric drives, static converters and ripple controllers [47, 51]. Chun Li et al [52] have carried out experiment work and field tests on inter-harmonics where the result illustrated the difficulties in the analysis. Z. Leonowizc [53] has also shown a method called a root-music method that can be used to estimate the signal parameters of sub-harmonics and inter-harmonics; however, the computation is complex.

d) DC Current Injection

The last type of harmonic is DC current injection. Power electronic converters are one of the major sources of DC current being injected into the grid. DC components can shift the operating point of distribution transformers [54] and this is highly undesirable. For this reason, network operators often set a limit of close to zero for the DC component. Often, a mains frequency transformer is used to couple the inverter to the network, and prevent any DC current components from entering the grid. [55].

Avoiding the use of an isolation transformer in PV systems is now being the trend where the cost and weight can be reduced [56].

2.3 Reviews of Previous Works

To date, a considerable amount of literature has been published to improve the harmonic performance of grid connected inverters, all with their associated merits and disadvantages. It is always possible to make the improvements by improving the power electronic converter hardware; inverter topology, PWM switching schemes, filter arrangements, and so on. Alternatively, it is also possible to enhance the performance and robustness of the inverter current controller.

The following discussion is divided into three sections. In the first section, several papers on harmonic performance improvements of a single grid-connected PV inverter system are described. This is then followed by a review of the harmonic performance of parallel grid-connected inverter systems. The final section is a discussion of harmonic performance in other application areas, such as uninterruptible power supply (UPS) and AC motor drives.

2.3.1 *Single Connected PV System*

In 1973, a generalized technique of harmonic elimination in the half-bridge and full-bridge output waveforms was proposed by Patel and Hoft [57]. In this work, output waveforms for both the half-bridge and full-bridge are 'chopped' *M* times per half cycle. An *M* equation is then obtained through several steps of derivation which can best be solved by computational techniques. Whilst complex, solutions for eliminating the 5^{th}, 7^{th}, 11^{th}, 13^{th}, and 17^{th} can be obtained.

Then, in the study by Teodorescu et al [58], a new control structure was proposed to mitigate high harmonic distortion problems which arise from the imperfect compensation action of a grid voltage feed forward PI controller. This new structure uses a P+Resonant (PR) controller to control the fundamental current and several generalized integrators in a harmonic compensator (HC) for THD level reduction. The harmonics of interest were the 3^{rd}, 5^{th}, and 7^{th} components.

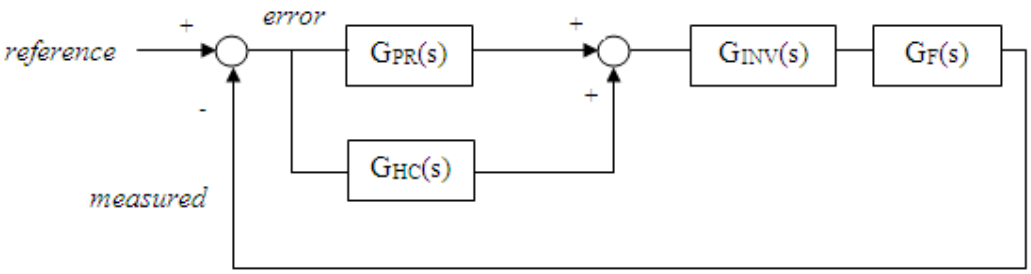

Figure 2-1: The current loop of PV inverter with PR and HC.

Figure 2-1 illustrates the block diagram of the proposed control strategy where G_{PR} is the PR current controller and G_{HC} is the harmonic compensator. PR controller was designed first without the compensator until the correct tuning of the proportional gain, K_P and resonant gain, K_R is determined. This was then followed with the addition of HC. From the paper [59], Observation from the Bode graph for PR + HC shows a peak gain exists at the harmonics frequencies of interest where this gain cannot be found in the PR graph. Interestingly, controller dynamic remains unchanged and this is being the key point to compensate the selective harmonic components. Tests to compare the spectrum for PI, PR and the proposed structure, PR + HC, were done. Results show much improvement in the interested harmonics order and the THD level is also decreased [59].

In another study by Su et al [59], a proportional resonant (PR) controller scheme is also used to achieve a high quality sinusoidal output current waveform in a single phase PV inverter. By simulation, it is shown that the THD obtained for the output current is 2.72%, which is clearly acceptable [60].

A different research study on the proportional resonant (PR) control system has also been carried out by Guoqiao et al [60, 61]. In his papers, a new current feedback method for the PR controller is proposed. In the first paper, instead of taking the inverter output current or the grid current as the feedback, he suggests to use the weighted average value (WAC) of the inverter output current and the grid current as the current feedback method. In the second paper, he recommends splitting the capacitor of the LCL filter into two parts (C_1 and C_2) and to take the current flowing between the two capacitors as the feedback current for the PR controller. From the experimental results for both

proposed methods [61, 62], two conclusions are drawn. Firstly, the control system is reduced from a third order system to a first order system; this can be proved by deriving the transfer function solution for the system. Secondly, less phase error and lower current THD are achieved when compared to using the inverter output current feedback.

Castilla M. et al [62] proposed a different way of using the resonant harmonic compensator. Instead of connecting the resonant harmonic compensator in parallel with the tracking regulator, the paper presented the compensator to be in series with the tracking regulator. Experimental results show that this location prevents the need of PLL algorithm. This is because this technique alone can provide accurate synchronization with grid voltage. In addition, the grid current distortion is also slightly lower when compared to the conventional harmonic compensator connection.

A novel harmonic elimination PWM technique is introduced by Villarreal-Ortiz et al [63] where the location of the commutation angles is derived from a closed-form equation based on a centroid algorithm. This technique is named Centroid PWM (CPWM) and is suitable to use for online control applications. In the study, Villarreal-Ortiz et al achieve lower THD levels when using the proposed technique compared to PWM techniques carried out in previous studies.

Leopoldo et al [64] proposed a new method to generate the switching pattern of three-level PWM inverters. This is called selective harmonic mitigation PWM (SHMPWM). Initially, the paper revised the selective harmonic elimination PWM (SHEPWM) technique from previous works where the need for tuned filters is essential to minimise uncontrolled non-eliminated harmonics (thus increasing the volume, weight and cost of the system). Using the proposed strategy, an advance on previous methods is achieved by considering the harmonics, THD, and local grid standards as a global problem. The switching pattern is reformulated as a nonlinear optimization problem and solved using a general purpose optimization heuristic algorithm. The method is claimed to be very versatile and can be tuned to meet any grid code in the calculation process. The study considered grid codes EN 50160 and CIGRE WG 36-05 and 15 switching angles. Results highlighted low harmonic levels when using the SHMPWM technique, hence avoiding the use of the costly tuned filters in the system. Experiment

in order to compare the technique with previous ones that are optimal sinusoidal PWM (OSPWM) and SHEPWM methods was carried out [65]. At first, result for SHEPWM was studied and showed zero harmonic content up to the 43^{rd} order but the 45^{th} and 49^{th} order had important content, 8.1% and 16.9% respectively. Result was slightly different with OSPWM method where the switching harmonic was inside the restrictive band. Both previous methods did not comply with the harmonic grid codes limitation. Conversely, grid codes stated earlier was fulfilled with the proposed SHMPWM technique.

Following that, in another study by Qunhai Huo et al [65], innovation of the conventional PI current control mode was made due to poor control effects in PI current loop control where the exponential sliding mode control (SMC) is proposed to be used in the control loop. In the paper, the chosen sliding model and existence of SMC as well as SMC stability analysis using Lyapunov theorem was derived. Simulation was done and output current waveforms were compared between the proposed method and conventional PI controller. Results showed a high degree of ripple and sawtooth-like waveform in the output current of conventional PI controller. In contrast, a smooth sin waveform can be seen in the result showing greatly reduced ripple phenomenon. In addition, the FFT analysis showed an improvement in THD to 0.91% rather than 24.75%. To conclude, the system stability is theoretically confirmed their report of the poor control effects when using the conventional one. However, this study only provides strong theoretical support in designing hardware but has not been able to demonstrate and implement it.

The most recent research was presented by Jevraj and Nasrudin [18]. They claimed that there is a limitation in harmonic reduction when using a typical single-phase three level inverter. This is because the harmonic components of output voltage are determined by the carrier frequency and the switching functions. Therefore, in order to tackle this limitation, a five level inverter topology is introduced for PV systems where instead of one reference signal, the new inverter topology uses two where they took turn to be compared with the carrier signal at one time. The idea behind this topology is to generate five level of output voltage; $+V_{PV}$, $+1/2V_{PV}$, 0, $-1/2V_{PV}$, $-V_{PV}$; where V_{PV} is the voltage across the DC-DC boost converter. Furthermore, the proposed topology uses an auxiliary circuit between the DC-DC boost converter and the inverter. Results are

compared with the results of three-level inverter system. The lower THD measurement for the proposed inverter proved that harmonic content can be reduced as the number of output levels increases. However, the measured PV system efficiency is low because of the auxiliary circuit.

2.3.2 *Parallel Connected PV System*

PV systems which are connected in parallel are commonly found in many networks. Such an arrangement is often used to increase the power delivered to the network. In this topology, each PV array has its own inverter and controller system, but is connected in parallel at a common point of coupling to the supply network. However, research studies into low order harmonics injection in parallel inverter systems, and methods to eliminate them, are not so popular compared to single connected inverter systems.

In a study by Younis et al [66, 67], a new configuration of parallel inverter system is presented. The design is based on a parallel three inverter system, where a resistor is used in series at the inverter output to minimise circulating current flow in the inverters. The paper also explains how the use of a third harmonic injection PWM (THIPWM) can be employed for further THD reduction. Results compare single inverter operation to parallel inverter operation, and show an improvement in current and voltage THD performance when the inverters are connected in parallel.

Another study by Armstrong et al [33] presents an inverter current controller with simple parameter randomization as an alternative to inter-inverter communications, for the purpose of introducing harmonic cancellation between individual inverter units. In the study, three independent inverters with conventional current control technique are tested and shown to exhibit very similar harmonic performance due to a strong correlation with the grid synchronisation process and the dynamics of the grid itself; harmonics between the 3^{rd} and 15^{th} are particularly predominant. When the three inverters are connected together in parallel with a common point of coupling to the network, a similar trend in harmonic performance is observed in each inverter unit.

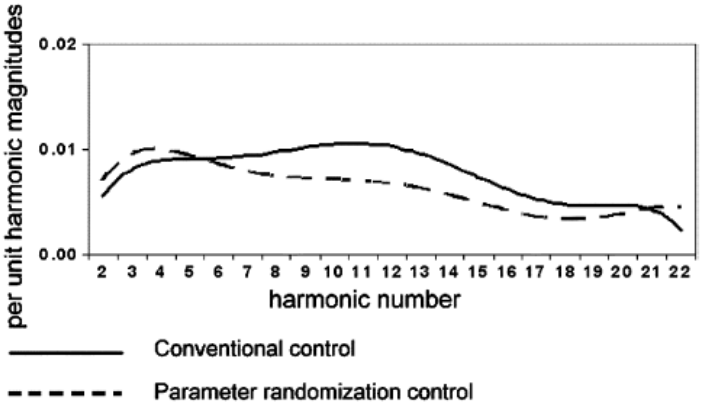

Figure 2-2 Harmonic trend line of parallel inverter system using conventional control and parameter randomization control technique [33].

In order to prevent these harmonics from becoming stronger when more and more inverters were connected in parallel, a modification of the current controller was made. The new technique is called the current controller parameter randomization technique where a random gain component, *Rp*, was added to the original proportional gain, *Kp*. With this technique, results showed an uncorrelated trend lines for both individual inverter and parallel inverter system. From Figure 2-2, although the harmonics between the 3rd and 11th remain the dominant one, magnitude of these harmonics was reduced on average and additional reduction was also achieved in the higher harmonics order. This confirmed a lower THD level. However, a limitation of the method proposed can be observed from the result shown in Figure 2-2 where a greater value can be seen in the 3rd and 5th harmonic orders.

Recently, A.M. Roslan et al [68] introduced an adaptive gain scheduling in the controller of parallel inverters. Instead of using the conventional PI current controller, it uses a PR current controller in the study because of its many advantages compared to conventional PI. The study focused on the instantaneous average current sharing between two inverters when the condition of line impedance varied. Two gain schedulers are used in two different location of each inverter. The model of the parallel system using the proposed technique is explained clearly in the paper. The impact of this technique can be seen in the inverter output current of each inverter. Final results show a better performance regarding the current and power sharing of parallel inverter

systems under variable line impedance but a study of low order harmonics performance has not been carried out.

M. Jafari et al [69] has also presented a method regarding the average current sharing. The proposed method uses a reference current which is taken from the average current sharing centre (ACSC) and is claimed to be the most robust scheme in average current sharing literature group. This is because it provides robust stability and performance under filter and load parameter variations. The study begins with analysis of a single inverter system both with linear and non-linear load and followed with the multi-inverter systems analysis. However, evidence from hardware experimental results is not stated for verification of simulation findings.

2.3.3 *General Review on Harmonic Performance Improvements*

In addition to reviewing the performance of inverters focusing in grid connected PV system, several papers proposing ideas on improving the inverter performance in different areas have also been noticed. This includes improvement in the controller for islanding inverters, UPS as well as AC motor drives and vector-controlled drive. During the islanding mode, instead of using the non- sinusoidal PWM (NSPWM), Khodsuz M. and A. Sheikholeslami [70] has presented a different technique known as non-sinusoidal hysteresis voltage control (NSHVC). The paper briefly explained how the nonlinear load can cause problems especially when the supply grid is off. Several advantages and features of the proposed technique have also been listed. Simulation of NSHVC and NSPWM are performed and compared. When the new controller technique is used, a significant reduction in THD and the harmonic components are noticed from the results shown.

In a recent study, B. Geethalakshmi et al [71] has proposed a shunt active power filter (APF) in order to compensate for the current harmonic components produced by nonlinear loads such as current and voltage source inverter. The APF is realized by using a 5 level H-bridge inverter. From the simulation results, based on several APF performance verification including unbalanced supply voltage and dynamic load variation, the proposed technique has proved to reduce the magnitude of significant harmonics as well as the line current THD.

In her study on harmonics reduction, Najwa Mahamad et al [72] divided the harmonics generated into three types; the positive-sequence harmonics which are of the 7^{th}, 13^{th},

and 19th components, the negative-sequence harmonics which are of the 5th, 11th, and 17th components that can totalled up the THD current of the system, and lastly the zero-sequence harmonics which are of the triplen harmonics such as the 3rd, 9th, and 15th harmonic components and can cause overheating on the neutral wire of the three phase power distribution system. In order to reduce the harmonics, the paper proposed an employment of a transformer and LC filter. From the experimental result, using the transformer alone can only reduce a small amount of harmonics current magnitude. However, after implementing the combination of the transformer and the LC filter, the harmonic in line current and neutral current is reduced to the standard of IEEE.

In 2008, A. Zabihinejad and J.S. Moghani [73] has proposed a new method called Direct Injection of Random Signal (DIRS) in order to reduce the inverter output current and voltage THD of an induction motor drive. In their study, a random signal is applied in the control scheme and has caused a variance in the output current and voltage THD. Results show that varying the random signal by 30% has best improved the output voltage harmonic spectrum characteristics. In addition, the harmonic components are also well distributed.

2.4 Research Idea

In this research, a "hybrid controller" is proposed where the features from promising techniques or schemes above will be combined to produce a new control scheme capable of minimising the low order harmonics in the parallel grid connected inverter system. The positive features of selective harmonic compensation scheme; which can compensate the low-order harmonics of particularly the 3rd, 5th, and 7th, and the random signal injection; which can reduced the harmonic magnitude of the 9th to 17th orders are used together in the current controller system for this research project in order to produce a computationally efficient controller. So far, no research studies have been found to apply these two methods together and use it in any inverter applications. Therefore, the combining methods are proposed here to reduce the harmonic magnitude of the low order harmonics spectrum between the 3rd and 19th of the grid connected system.

2.5 Chapter Summary

From this chapter, an overview of the harmonics injection has been explained. The definition of harmonics as well as its impacts is discussed. Besides, the four types of harmonics that are the low order harmonics, switching harmonics, dc current injection and inter harmonics are also mentioned in this chapter. This chapter has also discussed a large amount of papers on previous works about the harmonics injection and the solving methods with first; on a single grid connected inverter system and second; on a parallel grid connected inverter system. Furthermore, a few papers about harmonics injection from other area that grid connected inverter are also reviewed. At the end of this chapter, the idea of the research project is clarified.

Chapter 3: Methodology

3.1 Chapter Introduction

At the beginning of this chapter, two forms of PWM technique are discussed. Following that, the advantages of a digital system is explained. Three types of controller systems; the conventional PI current controller, the PR current controller, and the modified PR current controller, are also discussed in detail towards the end of this chapter.

3.2 Identification of the system to be studied

In order to start simulating the project models, these two main parts or systems must be identify and understood first; the PWM technique and the inverter current control method. PWM is used as a switching technique to drive the gates of the inverter. Whereas, the current control technique is used to respond and compensate for any error in the inverter current. Synchronization to the grid voltage is usually desirable and will also be implemented by the current controller; this is vital to have a unity power factor injection. Details are discussed next.

3.2.1 *PWM Technique*

There are two forms of switching techniques that can be used to drive the gate signals for inverters; the bipolar PWM switching technique and the unipolar PWM switching technique. Here, both of them is briefly discussed.

1. Bipolar PWM Switching Technique

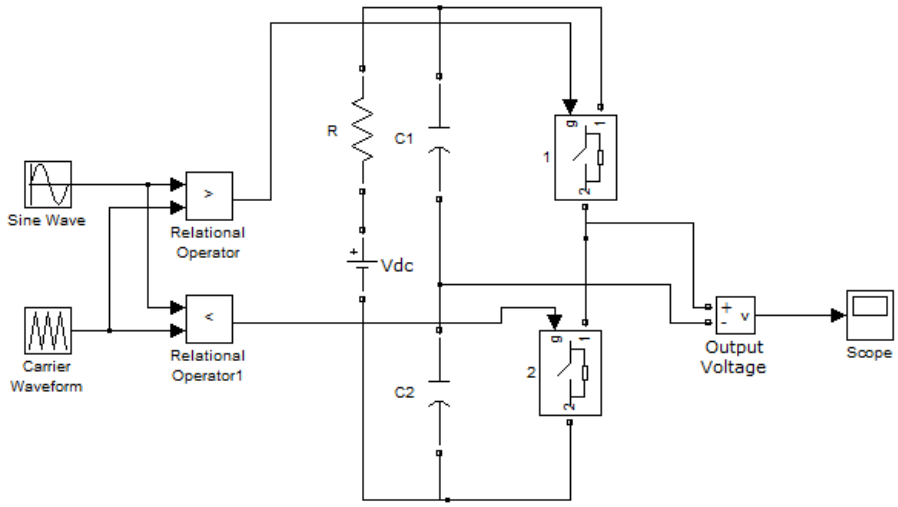

Figure 3-1: Bipolar PWM switching.

This technique is normally used with a half-bridge inverter where it compares a sine wave that acts as the control wave with a carrier wave which is normally in a triangular form. It is shown in Figure 3-1 above. The process is quite simple. Whenever the voltage of the sine wave is bigger than the carrier wave, switch 1 will turn on and the output will then be $+{}^{V_{dc}}/_{2}$. But when the voltage of the sine wave is smaller than the carrier wave, switch 2 will turn on and the output will become $-{}^{V_{dc}}/_{2}$. This process is illustrates in Figure 3-2.

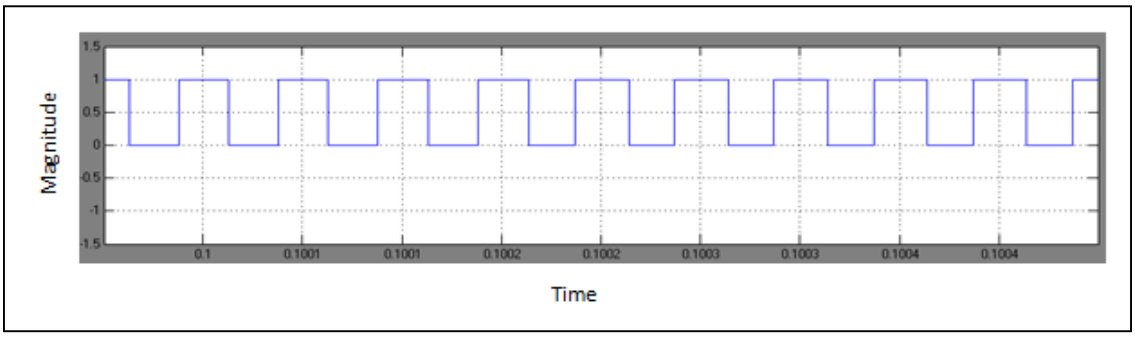

(a)

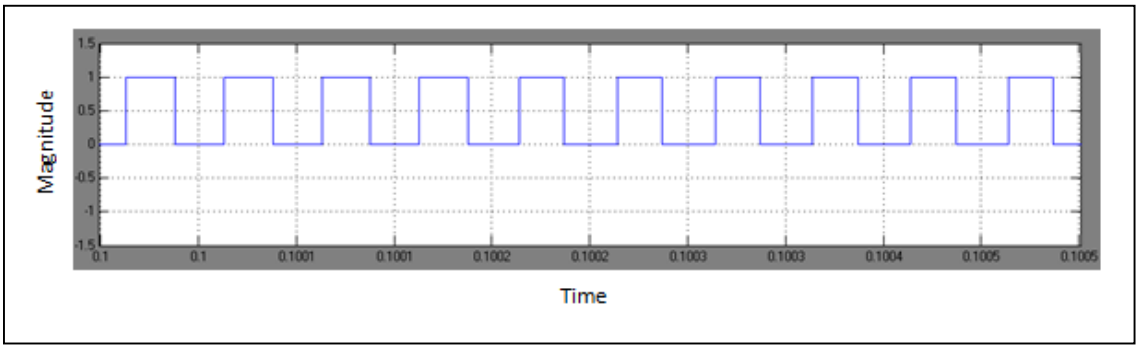

(b)

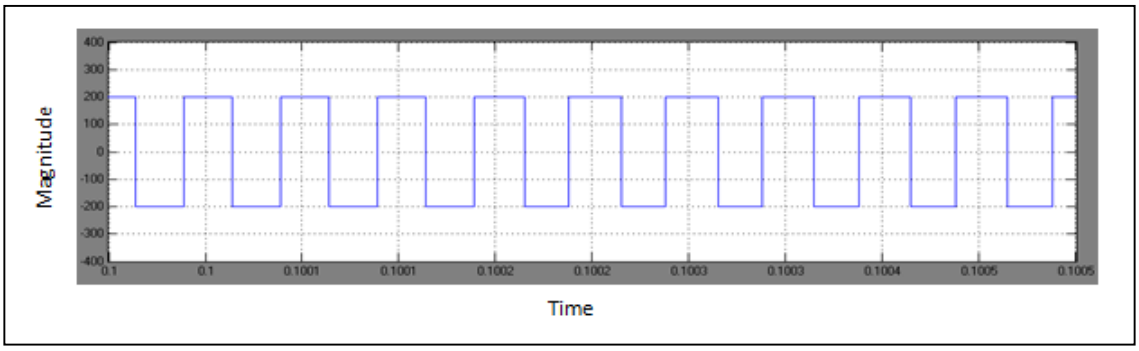

(c)

Figure 3-2: Waveforms of (a) $\boldsymbol{V_{control} > V_{tri}}$ which turns on Gate 1;

(b) $\boldsymbol{V_{control} < V_{tri}}$ which turns on Gate 2 ; and (c) Output voltage.

2. Unipolar PWM Switching Technique

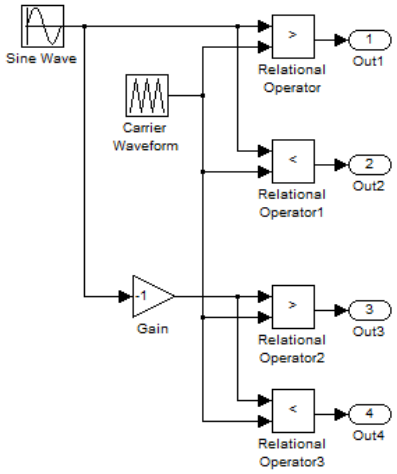

Figure 3-3: Unipolar PWM unit.

In this project, a unipolar PWM technique is used as the switching technique for the H-bridge inverter. This is because this switching technique offers a higher efficiency and higher power output than bipolar switching technique [74]. Moreover, less electro-magnetic interference (EMI) can be achieved when using unipolar switching [75]. T.Abeyasekera [76] also mentioned two advantages of a unipolar PWM technique. First, it has less dv/dt stress on the load as the voltage goes from 0 to $+V_{dc}$ or from 0 to $-V_{dc}$. Second, it has significant reduction in DC link voltage ripple thus reducing the size of the capacitors. The model of an inverter with a unipolar switching technique is as Figure 3-3. This PWM unit is then connected to an H-bridge inverter (see Figure 3-4). In the early stage where basic simulation is run, IGBTs with internal diodes were used as the switching devices. For later simulations (Chapter 5) and experimental hardware (Chapter 6 and Chapter 7) purpose, MOSFETs are used because they are suitable for the conditions of the research; use less than 200 V DC supply, less than 1 kW system, and using 20 kHz switching frequency. 20 kHz is a typical switching frequency for a grid connected inverter system. It is chosen because it represents a good balance between conduction and switching losses in typical MOSFET switched applications. Furthermore, it is beyond the audible range of humans, which is highly desirable. Therefore, throughout this thesis, unless otherwise stated the chosen PWM

switching frequency for all simulation and experimental work is 20 kHz. This system works as described in the next page.

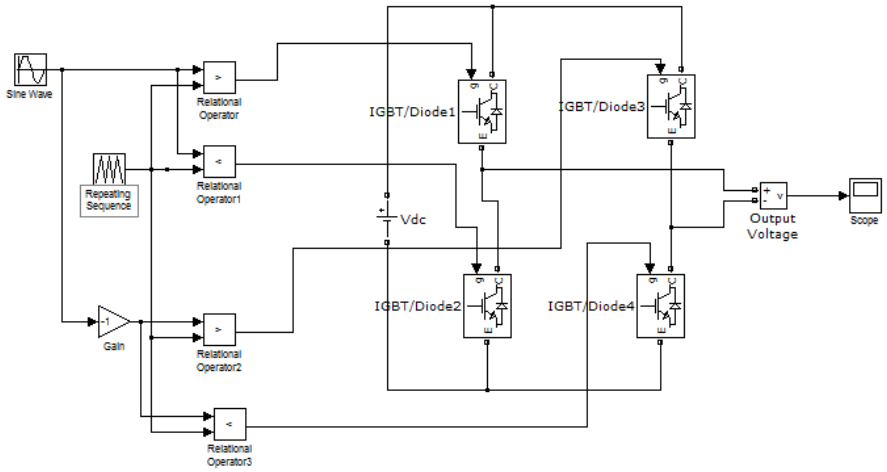

Figure 3-4: Unipolar PWM switching.

Based on Figure 3-3 and Figure 3-4, if

$V_{sin} > V_{tri}$; Out 1 will turn on Switch 1.

$V_{sin} < V_{tri}$; Out 2 will turn on Switch 2.

$-V_{sin} > V_{tri}$; Out 3 will turn on Switch 3.

$-V_{sin} > V_{tri}$; Out 4 will turn on Switch 4.

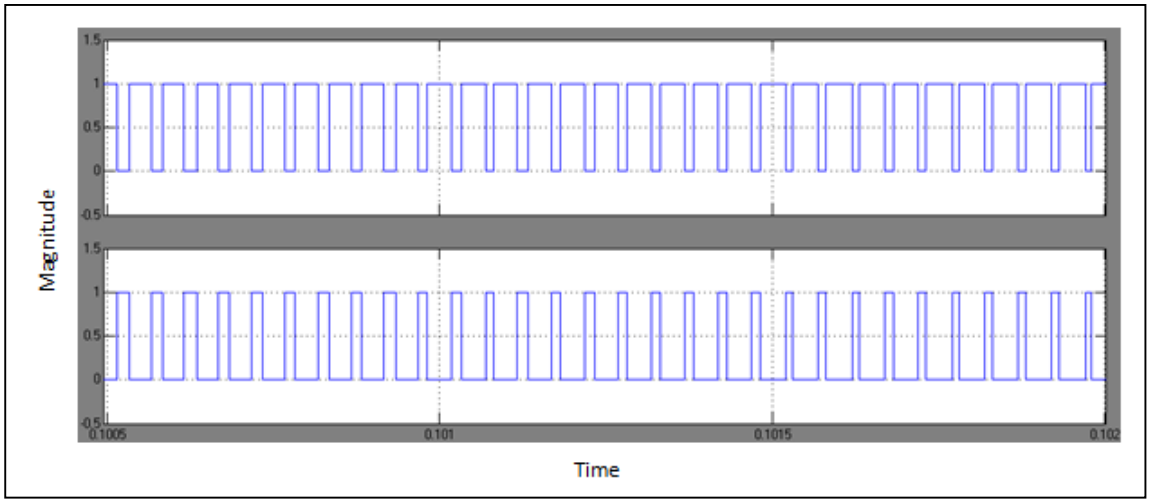

(a)

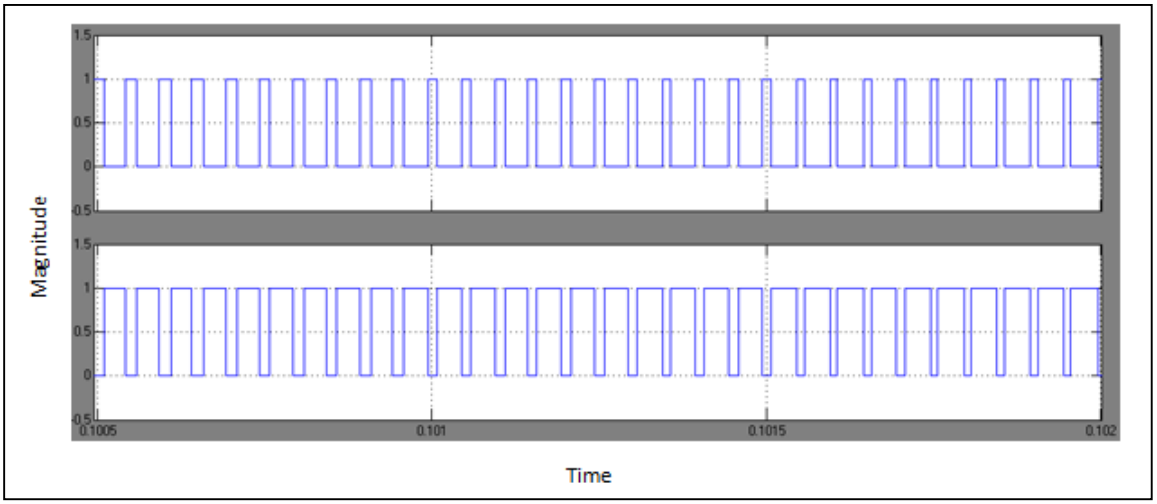

(b)

Figure 3-5: Waveforms at (a) Out1 and Out2 (b) Out3 and Out4.

(b)

Figure 3-5 are the examples of the waveforms that are being the gate signal for IGBT1, IGBT2, IGBT3, and IGBT4. When the combination of turning on and off above is compared, output results should be in a form of a modified sine wave with V_{peak} must equal to V_{dc}. Therefore, to ensure the PWM technique is working in the correct way, all the parameters involved are set as in Table 3-1 and the model is run for 0.2 s with maximum step size in the configuration parameters being changed to 1.0×10^{-6}. This is to confirm the sampling rate is enough without missing any important information. Output result agrees with the theory and is shown in Figure 3-6.

Table 3-1 System parameters.

Sine Wave	Frequency = 50 Hz Ma = 0.8
Carrier Wave	Frequency = 20 kHz Output values = [-1 1 -1]
Inverter Source	400 V_{dc}

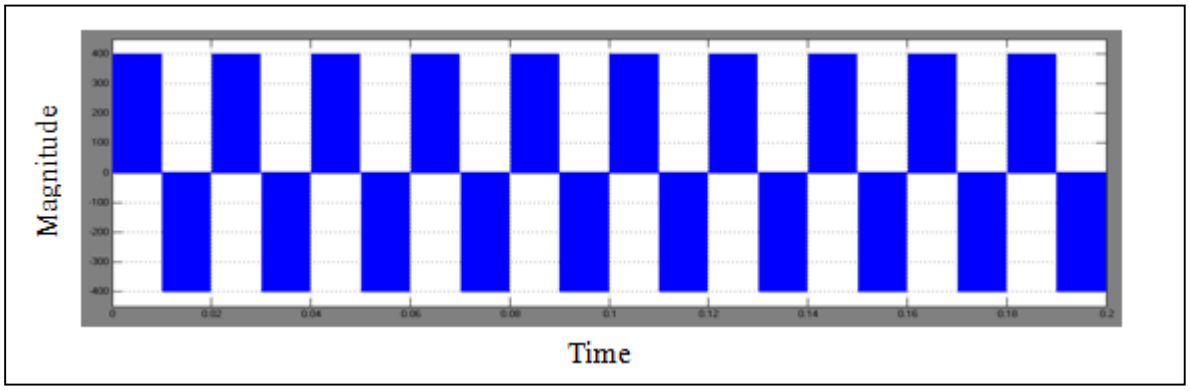

Figure 3-6: Inverter output voltage.

3.2.2 *Digital Control System*

The crucial part in the project is concerned with the control process. Better regulation of the current control system is important so that a unity power factor current is injected into the system. The idea of this project is to use a digital system rather than the analogue system. This is because digital system has the advantage of flexibility, accuracy, and easiness to monitor the parameters. Compared to the simple analogue controller system, the digital system uses a microprocessor as a main element with other small systems before and after it. These small systems are; sample and hold which

holds analogue signal at a constant value, analogue to digital converter (ADC) which converts analogue signals to digital number and digital to analogue converter (DAC) which converts the digital number back to an analogue signal [77]. The block diagram of digital control system in Figure 3-7 illustrates the process.

Figure 3-7: Digital control system.

The process starts as soon after a signal is identified. This signal is then sampled at a certain constant intervals periodically and held throughout the same intervals by a *zero-order hold* (ZOH) device to form a staircase-like sample. An analogue to digital converter is then used to convert the sample to discrete values in a finite time as demanded by the microprocessor. The major job of microprocessor is to control the incoming values so that it appears as nearly as demanded by the user. When the job is done, it has to be converted back to analogue signal via a digital to analogue converter. Again, a *zero-order hold* (ZOH) is a necessity.

3.3 Current Controllers

As mentioned in the previous chapters, this research project will demonstrate the efficiency of three different current controllers; the conventional PI control technique, the proportional resonance (PR) control technique and the modified proportional resonance control technique. All three of them will be discussed as in the following sub-sections.

3.3.1 *Conventional PI Control Technique*

In this project, rather than the proportional, integral and derivative (PID) system, only the proportional (P) and integral (I) terms are used in the current controller system. This type of controller is the most common controller applied as the inverter current feedback process. The term P will give an output that is proportional to the system error, which is the difference between the system output value and the desired value. It has a gain, K_P, which will multiply the error and response to it. The purpose is to reduce the rise time of the system. However, using this proportional term alone will result in having a system stationary error. In order to eliminate this error and complete the P

based control, the integral part is used. The output of the integral part is the multiplication of a gain, K_I and the summing of the previous errors to the current system error. This is a continuous process which will stop if the system signal or the system output value matches the desired value demanded by the user. The analogue PI transfer function is

$$G_{PI}(s) = K_P + \frac{K_I}{s}$$

(Eq. 3-1)

In the z-domain, the transfer function becomes

$$G_{PI}(z) = K_P + \frac{K_I}{1 - z^{-1}}$$

(Eq. 3-2)

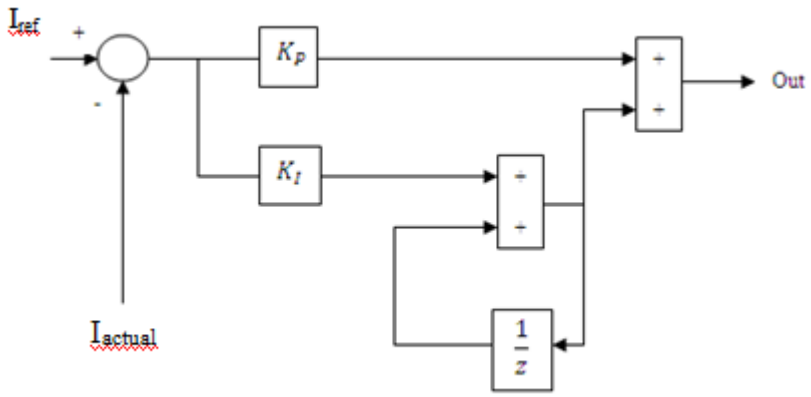

Figure 3-8: A PI current controller block diagram.

Figure 3-8 illustrates the PI current controller block diagram. The system actual current is compared to the reference current and will be used in the controlling process. The output signal after the process has been taken that is the Out1 is then used for the PWM inverter switching.

3.3.2 *Proportional Resonance Controller Scheme (PR)*

This second technique is called the proportional resonance control technique. In this technique, several harmonic current regulators work in parallel. By using this technique, the weakness of the PI current control technique regarding the steady state error can be dealt with [78]. This means that the measured output current will be equally same to the reference current or the demand current. Based on previous paper [58], the analogue transfer function of the PR current controller is defined as:

$$G_{PR}(s) = K_P + K_R \frac{s}{s^2 + \omega_o^2}$$

(Eq. 3-3)

By using the Tustin transformation, the analogue equation above is changed to the z domain known as the discrete function. This is done by substituting $\boldsymbol{s}$ with $\frac{\mathbf{2}}{\boldsymbol{T}}\frac{\mathbf{1-z^{-1}}}{\mathbf{1+z^{-1}}}$. Based on that, Eq. 3.3 is then transformed to:

$$G_{PR}(z) = K_P + K_R \frac{\frac{2}{T}\frac{1-z^{-1}}{1+z^{-1}}}{(\frac{2}{T}\frac{1-z^{-1}}{1+z^{-1}})^2 + \omega_o^2}$$

$$G_{PR}(z) = \frac{K_P\left[\left(\frac{2}{T}\frac{1-z^{-1}}{1+z^{-1}}\right)^2 + \omega_o^2\right] + K_R\left(\frac{2}{T}\frac{1-z^{-1}}{1+z^{-1}}\right)}{\left(\frac{2}{T}\frac{1-z^{-1}}{1+z^{-1}}\right)^2 + \omega_o^2}$$

$$G_{PR}(z) = \frac{K_P\left[\left(\frac{4}{T^2}\right)\left(\frac{1-2z^{-1}+z^{-2}}{1+2z^{-1}+z^{-2}}\right) + \omega_0^2\right] + \frac{2K_R}{T}\left(\frac{1-z^{-1}}{1+z^{-1}}\right)}{\left(\frac{4}{T^2}\right)\left(\frac{1-2z^{-1}+z^{-2}}{1+2z^{-1}+z^{-2}}\right) + \omega_0^2}$$

$$G_{PR}(z) = \frac{\left(\frac{4K_P}{T^2}\right)\left(\frac{1-2z^{-1}+z^{-2}}{1+2z^{-1}+z^{-2}}\right) + K_P\omega_0^2 + \frac{2K_R}{T}\left(\frac{1-z^{-1}}{1+z^{-1}}\right)}{\frac{4(1-2z^{-1}+z^{-2}) + T^2\omega_0^2(1+2z^{-1}+z^{-2})}{T^2(1+2z^{-1}+z^{-2})}}$$

(Eq. 3-4)

In order to get a simpler transfer function, some adjustments are made to the (Eq. 3-4) above. This is shown as in the next page.

$$G_{PR}(z) = \frac{\left(\frac{4K_P}{T^2}\right)\left(\frac{1-2z^{-1}+z^{-2}}{1+2z^{-1}+z^{-2}}\right) + K_P\omega_0^2\left(\frac{T^2(1+2z^{-1}+z^{-2})}{T^2(1+2z^{-1}+z^{-2})}\right) + \frac{2K_RT}{T^2}\left(\frac{1-z^{-2}}{1+2z^{-1}+z^{-2}}\right)}{\frac{4(1-2z^{-1}+z^{-2})+T^2\omega_0^2(1+2z^{-1}+z^{-2})}{T^2(1+2z^{-1}+z^{-2})}}$$

$$= \frac{4K_P(1-2z^{-1}+z^{-2}) + K_P\omega_0^2T^2(1+2z^{-1}+z^{-2}) + 2K_RT(1-z^{-2})}{4(1-2z^{-1}+z^{-2})+T^2\omega_0^2(1+2z^{-1}+z^{-2})}$$

$$= \frac{4K_P - 8K_Pz^{-1} + 4K_Pz^{-2} + K_P\omega_0^2T^2 + 2K_P\omega_0^2T^2z^{-1} + K_P\omega_0^2T^2z^{-2} + 2K_RT - 2K_RTz^{-2}}{4 - 8z^{-1} + 4z^{-2} + T^2\omega_0^2 + 2T^2\omega_0^2z^{-1} + T^2\omega_0^2z^{-2}}$$

$$= \frac{(4K_P + K_P\omega_0^2T^2 + 2K_RT) + (2K_P\omega_0^2T^2 - 8K_P)z^{-1} + (4K_P + K_P\omega_0^2T^2 - 2K_RT)z^{-2}}{(4 + T^2\omega_0^2) + (2T^2\omega_0^2 - 8)z^{-1} + (4 + T^2\omega_0^2)z^{-2}}$$

(Eq. 3-5)

By dividing the nominator and the denominator of the transfer function in (Eq. 3-5) above by $(4 + T^2\omega_0^2)$, the discrete form becomes:

$$G_{PR}(z) = \frac{\frac{(4K_P + K_P\omega_0^2T^2 + 2K_RT)}{(4 + T^2\omega_0^2)} + \frac{(2K_P\omega_0^2T^2 - 8K_P)}{(4 + T^2\omega_0^2)}z^{-1} + \frac{(4K_P + K_P\omega_0^2T^2 - 2K_RT)}{(4 + T^2\omega_0^2)}z^{-2}}{1 + \frac{(2T^2\omega_0^2 - 8)}{(4 + T^2\omega_0^2)}z^{-1} + z^{-2}}$$

(Eq. 3-6)

For simplification, the transfer function is re-written as:

$$G_{PR}(z) = \frac{b_o + b_1z^{-1} + b_2z^{-2}}{1 + a_1z^{-1} + a_2z^{-2}}$$

(Eq. 3-7)

where

$$b_o = \frac{\left(4K_P + K_P\omega_0^2T^2 + 2K_RT\right)}{(4 + T^2\omega_0^2)}$$

$$b_1 = \frac{\left(2K_P\omega_0^2T^2 - 8K_P\right)}{(4 + T^2\omega_0^2)}$$

$$b_2 = \frac{(4K_P + K_P\omega_0^2T^2 - 2K_RT)}{(4 + T^2\omega_0^2)}$$

$$a_1 = \frac{\left(2T^2\omega_0^2 - 8\right)}{\left(4 + T^2\omega_0^2\right)}$$

$$a_2 = 1$$

K_P and K_R are the proportional gain and the resonance gain, T is the sampling time and $\omega_o$is the fundamental frequency of the system in rad/sec. With the resonance part added to the proportional controller, the steady state error of the system is nearly eliminated. Substituting T with 50 µs and $\omega_o$with 2π x 50 Hz, the optimum proportional and resonance gains of the PR current controller technique can be achieved by trial and error tuning.

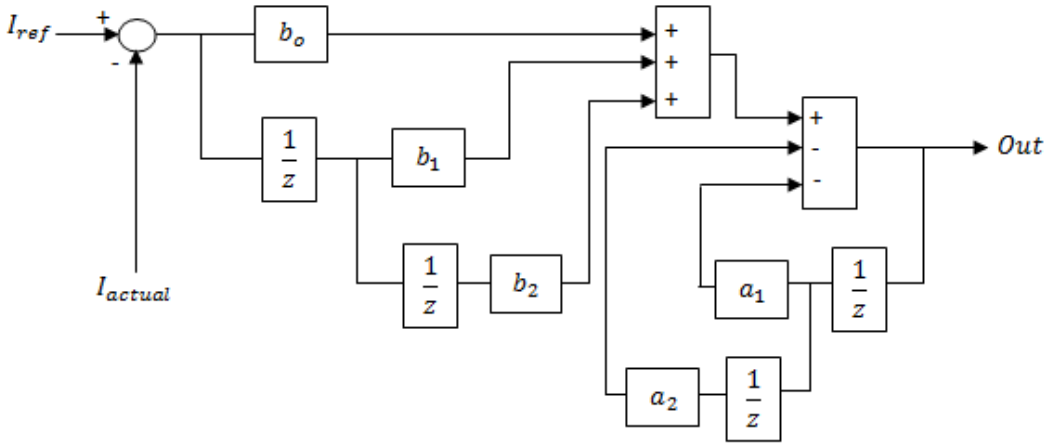

Figure 3-9 below shows the controller block diagram. The resulting output signal will be used in the inverter switching process.

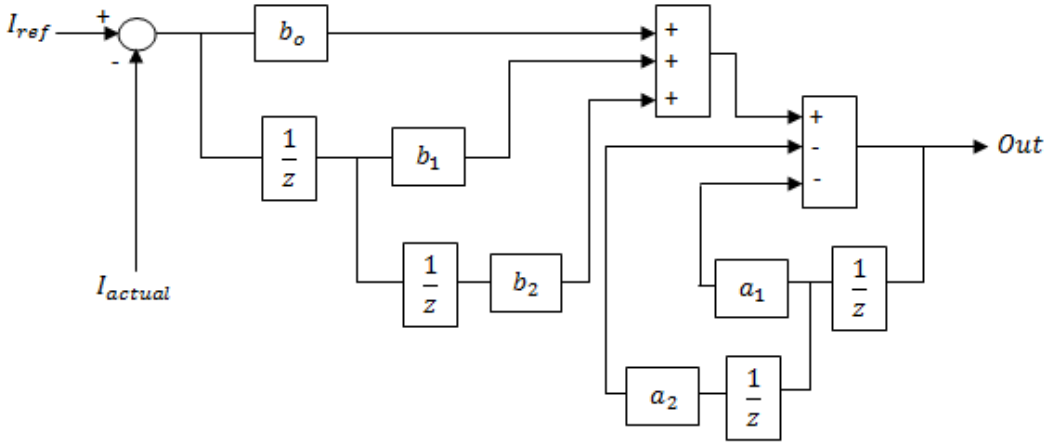

Figure 3-9: A proportional resonance (PR) current controller block diagram.

3.3.3 *Modified Proportional Resonance (PR) Technique*

The last and improved technique proposed in this research project is the modification of the proportional resonance technique above. Instead of using a fixed proportional gain, $K_{P,}$ a random signal is added to generate a new randomly varying proportional signal for the controller. This technique is expected to have an effect on the overall harmonic orders that will result in further decrement of the grid current THD both on single inverter system and parallel inverter system. Based on (Eq. 3-7), the discrete transfer function of the modified PR current controller is;

$$G_{PRmodified}(z) = \frac{b_o + b_1 z^{-1} + b_2 z^{-2}}{1 + a_1 z^{-1} + a_2 z^{-2}}$$

(Eq. 3-8)

Although the transfer function above looks no different with the proportional resonance control technique, modification is made to the b_o, b_1, and b_2 where;

$$b_o = \frac{(4R_{KP} + R_{KP}\omega_0^2 T^2 + 2K_R T)}{(4 + T^2\omega_0^2)}$$

$$b_1 = \frac{(2R_{KP}\omega_0^2 T^2 - 8R_{KP})}{(4 + T^2\omega_0^2)}$$

$$b_2 = \frac{(4R_{KP} + R_{KP}\omega_0^2 T^2 - 2K_R T)}{(4 + T^2\omega_0^2)}$$

a_1 and a_2 remain unchanged thus the values are identical to those obtained for the proportional resonance control method. In order to get the correct value for the randomized proportional gain, R_{KP}, a limit need to be set for both upper and lower value so as to maintain the stability of the output current result. This limitation is obtained by trial and error tuning where the edge where the output current starts to become unstable is taken as the upper and lower limit for the randomized proportional gain, R_{KP}. With the gain keeps changing within the limitation set each time, the output current is expected to maintain its shape and stability whilst at the same time its harmonic spectrum will results in the reduction of the THD.

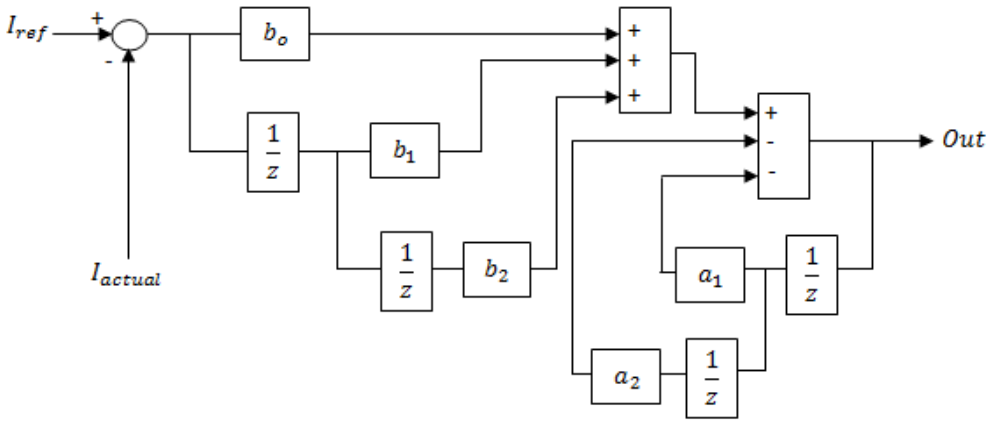

Figure 3-10: A modified PR current controller block diagram.

3.4 Chapter Summary

This chapter describes the fundamental operating principles of a single phase H-Bridge inverter. For this inverter topology, two PWM techniques are briefly discussed; bipolar and unipolar switching. The literature review shows that the Unipolar PWM switching scheme offers a number of advantages, including improved harmonic performance, less dv/dt stress on the semiconductor switches, and a reduction in the DC link voltage ripple which allows for a smaller DC link capacitor to be used [74] [76]. For these reasons, in this project, unipolar switching is selected as the preferred PWM control technique.

This chapter also introduces three control techniques that can be applied in grid connected inverter systems. The PI controller is described, as it is one of the most commonly understood control methods and is often used as a benchmark for assessing research results. A review of the PR controller is also presented, as this is becoming another popular control technique in inverter based systems. Compared to the PI controller, the literature suggests that the PR controller can be tuned to achieve better harmonic performance. Furthermore, it does not exhibit the steady state error associated with PI controller when tracking an AC reference signal.

Following this, the concept of PI parameter randomisation is introduced. Literature suggests that this is a good technique to apply in order to reduce the harmonic content of the inverter output; this is one of the main research objectives of this work. Based on these findings, a new control strategy is described which extracts the benefits of the

aforementioned techniques. Here, a PR controller with randomisation of the proportional gain is proposed. The remainder of this thesis will focus on testing the hypothesis that this proposed controller will yield better harmonic performance than conventional PI and PR control techniques.

Chapter 4: Modelling of Grid Connected, PV Inverter System

4.1 Introduction

This chapter is written to model the closed loop system of grid-connected PV inverter system. It begins with modelling the system impedances of the low pass filter, followed by modelling the current controllers and the PWM. Three types of current controllers are modelled here; the conventional PI current controller, the PR current controller, and the PR current controller with added harmonic compensators (PR+HC). At the end, the closed loop response is plotted, the system stability is analysed using the s-plane and the critical part is the range of controller gains that can be varied without making the system unstable can be determined.

4.2 Modelling of Grid Connected, Single PV Inverter System

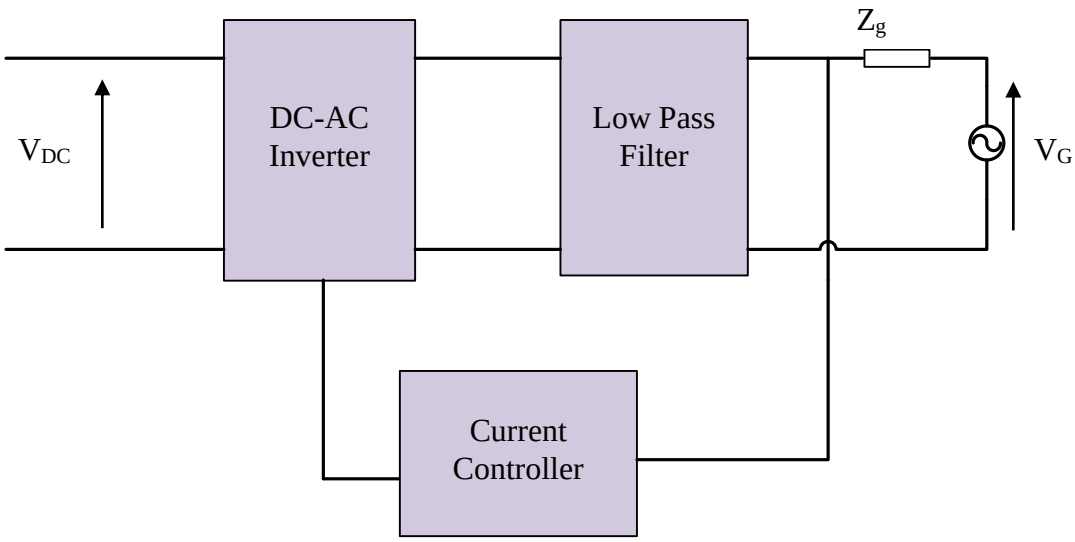

Figure 4-1: Basic arrangement of grid connected inverter system.

Figure 4-1 above shows the basic arrangement of a grid connected inverter system. In order to model the whole system, it is divided into three parts. First, the low pass filter is modelled using the system impedance. Second, the current controllers are modelled and last, the PWM switching is modelled. They are discussed and explained in the next sub-sections.

4.2.1 *Modelling of Low Pass Filter with System Impedance*

Ignoring the current control loop, the low pass filter consists of an inductance and capacitance with an equivalent resistance value in series (ESR). To model the system impedance, this will include the grid impedance at the output side of the filter thus forming a LCL circuit arrangement as in

Figure **4-2**. Next, the relation of the impedance is explained and discussed based on the diagram.

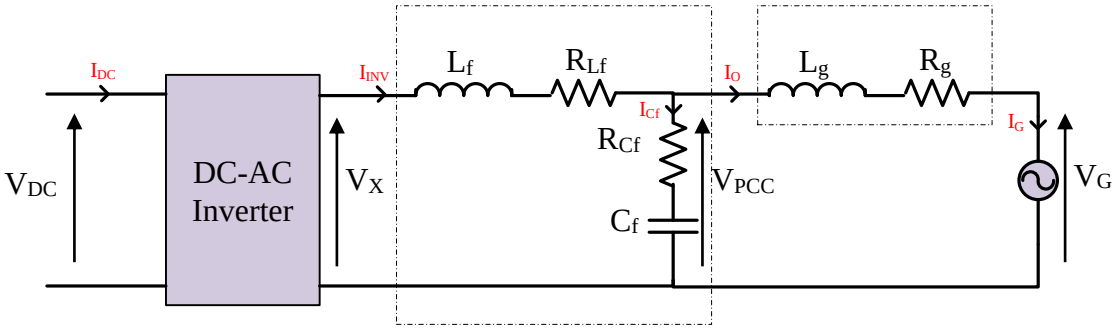

Figure 4-2: Equivalent circuit for low pass filter and the grid.

From the figure, L_f is the filter inductance, L_c is the filter capacitance, L_g is the grid inductance, and the three resistance; R_{Lf}, R_{Cf}, and R_g, are the respective ESR for the system. The relationship in time domain between the voltage at point of common coupling, V_{PCC}, and the voltage at inverter output, V_X can be expressed as:

$$V_X(t) - V_{PCC}(t) = L_f \frac{dI_X(t)}{dt} + R_{Lf} I_x(t)$$

(Eq. 4-1)

Whereas, in frequency domain, Laplace transform is made and given as:

$$V_X(s) - V_{PCC}(s) = L_f s I_X(s) + R_{Lf} I_X(s)$$

(Eq. 4-2)

In order to gain the Laplace transfer function of the low pass filter induction, it has to be represented by its output/input characteristics. Considering the equation above, the relationship becomes:

$$V_X(s) - V_{PCC}(s) = I_X(s)(L_f s + R_{Lf})$$

$$H_{Lf}(s) = \frac{I_X(s)}{V_X(s) - V_{PCC}(s)} = \frac{1}{L_f s + R_{Lf}}$$

(Eq. 4-3)

Next, the same steps are taken in order to get the Laplace transfer function for the filter capacitance branch. Equations below derived the steps.

$$V_{PCC}(t) = R_{Cf} I_{Cf}(t) + \frac{1}{C_f} \int I_{Cf} dt$$

(Eq. 4-4)

$$V_{PCC}(s) = R_{Cf} I_{Cf}(s) + \frac{1}{C_f s} I_{Cf}(s)$$

(Eq. 4-5)

$$V_{PCC}(s) = I_{Cf}(s)(R_{Cf} + \frac{1}{C_f s})$$

(Eq. 4-6)

Note that the current flowing through the filter capacitance branch is the current difference between the inverter output current, I_X and the grid current, I_g. Therefore, since $I_{Cf}(s) = I_X(s) - I_O(s)$, the equation above becomes

$$V_{PCC}(s) = \big(I_X(s) - I_O(s)\big)(\frac{R_{Cf} C_f s + 1}{C_f s})$$

(Eq. 4-7)

Finally, the Laplace transfer function is:

$$H_{Cf}(s) = \frac{V_{PCC}(s)}{I_X(s) - I_O(s)} = \frac{R_{Cf} C_f s + 1}{C_f s}$$

(Eq. 4-8)

For the grid impedance branch, the same steps are again used to express its Laplace transfer function. These are described in detail as in the following equations.

In time domain, the relationship is:

$$V_{PCC}(t) - V_G(t) = L_g \frac{dI_O(t)}{dt} + R_g I_O(t)$$

(Eq. 4-9)

In frequency domain, the equation above becomes:

$$V_{PCC}(s) - V_G(s) = L_g s I_O(s) + R_g I_O(s)$$

$$V_{PCC}(s) - V_G(s) = I_O(s)(L_g s + R_g)$$

(Eq. 4-10)

To obtain the Laplace transfer function for the grid impedance branch, the output/input characteristic is:

$$H_{Lg}(s) = \frac{I_O(s)}{V_{PCC}(s) - V_G(s)} = \frac{1}{L_g s + R_g}$$

(Eq. 4-11)

By combining the three transfer functions from (Eq. 4-3), (Eq. 4-8) and (Eq. 4-11), the relationship between the input and the output of the low pass filter and the grid can be made with the output current, I_O become the output and the inverter output voltage, V_X become the input. Figure 4-3 is the block diagram when the three transfer functions from the filter inductance branch, the filter capacitance branch and the grid impedance branch are linked together.

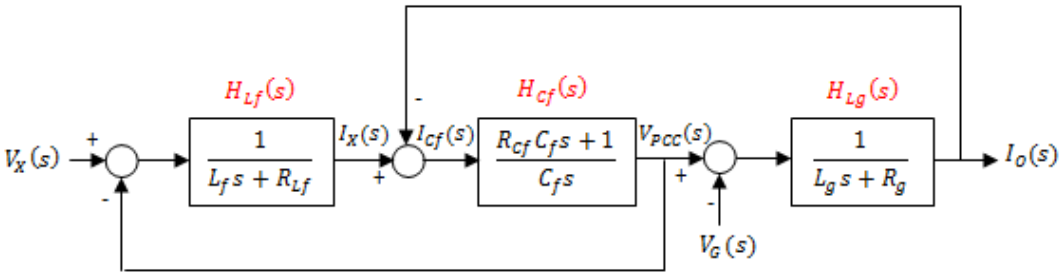

Figure 4-3: Block diagram of the low pass filter and grid impedance branch.

Based on Figure 4-3, a single Laplace transfer function of $I_O(s)/V_X(s)$ can be made. It is derived as followed [45].

$$I_O(s) = \{\left\{\left[\left(V_X(s) - V_{PCC}(s)\right)\frac{1}{L_f s + R_{Lf}}\right] - I_O(s)\right\}\frac{R_{Cf}C_f s + 1}{C_f s} - V_G(s)\}\frac{1}{L_g s + R_g}$$

$$I_O(s) = \{\left\{\frac{V_X(s) - V_{PCC}(s) - I_O(s)\left(L_f s + R_{Lf}\right)}{L_f s + R_{Lf}}\right\}\frac{R_{Cf}C_f s + 1}{C_f s} - V_G(s)\}\frac{1}{L_g s + R_g}$$

$$I_O(s) = \{\frac{\left[V_X(s) - V_{PCC}(s) - I_O(s)\left(L_f s + R_{Lf}\right)\right]\left(R_{Cf}C_f s + 1\right)}{C_f s\left(L_f s + R_{Lf}\right)} - V_G(s)\}\frac{1}{L_g s + R_g}$$

$$I_O(s) = \{\frac{\left[V_X(s) - V_{PCC}(s) - I_O(s)\left(L_f s + R_{Lf}\right)\right]\left(R_{Cf}C_f s + 1\right) - V_G(s)C_f s\left(L_f s + R_{Lf}\right)}{C_f s\left(L_f s + R_{Lf}\right)}\}\frac{1}{L_g s + R_g}$$

$$I_O(s) = \frac{\left[V_X(s) - V_{PCC}(s) - I_O(s)\left(L_f s + R_{Lf}\right)\right]\left(R_{Cf}C_f s + 1\right) - V_G(s)C_f s\left(L_f s + R_{Lf}\right)}{C_f s\left(L_f s + R_{Lf}\right)\left(L_g s + R_g\right)}$$

(Eq. 4-12)

(Eq. 4-11) can be rearranged to $V_{PCC}(s) - V_G(s) = I_O(s)(L_g s + R_g)$. This then gives:

$$V_{PCC}(s) = I_O(s)\left(L_g s + R_g\right) + V_G(s)$$

(Eq. 4-13)

Substituting both (Eq. 4-12) and (Eq. 4-13) gives:

$$I_O(s) = \frac{\left[V_X(s) - I_O(s)\left(L_g s + R_g\right) - V_G(s) - I_O(s)\left(L_f s + R_{Lf}\right)\right]\left(R_{Cf}C_f s + 1\right) - V_G(s)C_f s\left(L_f s + R_{Lf}\right)}{C_f s\left(L_f s + R_{Lf}\right)\left(L_g s + R_g\right)}$$

$$1 = \frac{\left[V_X(s) - I_O(s)\left(L_g s + R_g\right) - V_G(s) - I_O(s)\left(L_f s + R_{Lf}\right)\right]\left(R_{Cf}C_f s + 1\right) - V_G(s)C_f s\left(L_f s + R_{Lf}\right)}{I_O(s)C_f s\left(L_f s + R_{Lf}\right)\left(L_g s + R_g\right)}$$

$$0 = \frac{\left[V_X(s) - I_O(s)\left(L_g s + R_g\right) - V_G(s) - I_O(s)\left(L_f s + R_{Lf}\right)\right]\left(R_{Cf}C_f s + 1\right) - V_G(s)C_f s\left(L_f s + R_{Lf}\right)}{I_O(s)C_f s\left(L_f s + R_{Lf}\right)\left(L_g s + R_g\right)} - 1$$

$$0 = \frac{\left[V_X(s) - I_O(s)\left(L_g s + R_g\right) - V_G(s) - I_O(s)\left(L_f s + R_{Lf}\right)\right]\left(R_{Cf}C_f s + 1\right) - V_G(s)C_f s\left(L_f s + R_{Lf}\right) - I_O(s)C_f s\left(L_f s + R_{Lf}\right)\left(L_g s + R_g\right)}{I_O(s)C_f s\left(L_f s + R_{Lf}\right)\left(L_g s + R_g\right)}$$

(Eq. 4-14)

$$0 = \left[V_X(s) - I_O(s)\left(L_g s + R_g\right) - V_G(s) - I_O(s)\left(L_f s + R_{Lf}\right)\right]\left(R_{Cf}C_f s + 1\right) - V_G(s)C_f s\left(L_f s + R_{Lf}\right) - I_O(s)C_f s\left(L_f s + R_{Lf}\right)\left(L_g s + R_g\right)$$

$$0 = V_X(s)\left(R_{Cf}C_f s + 1\right) - I_O(s)\left(L_g s + R_g\right)\left(R_{Cf}C_f s + 1\right) - V_G(s)\left(R_{Cf}C_f s + 1\right) - I_O(s)\left(L_f s + R_{Lf}\right)\left(R_{Cf}C_f s + 1\right) - V_G(s)C_f s\left(L_f s + R_{Lf}\right) - I_O(s)C_f s\left(L_f s + R_{Lf}\right)\left(L_g s + R_g\right)$$

$$\begin{aligned} 0 = {} & V_X(s)\left(R_{Cf}C_f s + 1\right) - I_O(s)[\left(L_g s + R_g\right)\left(R_{Cf}C_f s + 1\right) + \left(L_f s + R_{Lf}\right)\left(R_{Cf}C_f s + 1\right) \\ & + C_f s\left(L_f s + R_{Lf}\right)\left(L_g s + R_g\right)] - V_G(s)[\left(R_{Cf}C_f s + 1\right) + C_f s\left(L_f s + R_{Lf}\right)] \end{aligned}$$

(Eq. 4-15)

$$\begin{aligned} & I_O(s)[\left(L_g s + R_g\right)\left(R_{Cf}C_f s + 1\right) + \left(L_f s + R_{Lf}\right)\left(R_{Cf}C_f s + 1\right) + C_f s\left(L_f s + R_{Lf}\right)\left(L_g s + R_g\right)] \\ & \qquad = V_X(s)\left(R_{Cf}C_f s + 1\right) - V_G(s)[\left(R_{Cf}C_f s + 1\right) + C_f s\left(L_f s + R_{Lf}\right)] \end{aligned}$$

$$\begin{aligned} & I_O(s)\left[\left(L_g R_{Cf}C_f s^2 + \left(L_g + R_g R_{Cf}C_f\right)s + R_g\right) + \left(L_f R_{Cf}C_f s^2 + \left(L_f + R_{Lf}R_{Cf}C_f\right)s + R_{Lf}\right)\right. \\ & \qquad \left. + C_f s\left(L_f L_g s^2 + \left(L_f R_g + R_{Lf}L_g\right)s + R_{Lf}R_g\right)\right] \\ & \qquad = V_X(s)(R_{Cf}C_f s + 1) - V_G(s)[C_f L_f s^2 + \left(R_{Cf}C_f + C_f R_L f\right)s + 1] \end{aligned}$$

(Eq. 4-16)

$$\begin{aligned} & I_O(s)[C_f L_f L_g s^3 + \left(L_g R_{Cf}C_f + L_f R_{Cf}C_f + C_f L_f R_g + C_f R_{Lf}L_g\right)s^2 \\ & \qquad + \left(L_g + R_g R_{Cf}C_f + L_f + R_{Lf}R_{Cf}C_f + C_f R_{Lf}R_g\right)s + R_g + R_{Lf}] \\ & \qquad = V_X(s)(R_{Cf}C_f s + 1) - V_G(s)[C_f L_f s^2 + \left(R_{Cf}C_f + C_f R_L f\right)s + 1] \end{aligned}$$

(Eq. 4-17)

From (Eq. 4-17**)**, it is clearly seen that $I_O(s)$ is the input and both $V_X(s)$ and $V_G(s)$ are the output of the low pass filter and grid impedance branch. In order to obtain the transfer function for the branch, the equation above is arranged to be as equation below:

$$G_{LCL}(s) = \frac{I_O(s)}{V_X(s)(R_{Cf}C_f s + 1) - V_G(s)[C_f L_f s^2 + \left(R_{Cf}C_f + C_f R_L f\right)s + 1]}$$

$$= \frac{1}{C_f L_f L_g s^3 + \left(L_g R_{Cf}C_f + L_f R_{Cf}C_f + C_f L_f R_g + C_f R_{Lf}L_g\right)s^2 + \left(L_g + R_g R_{Cf}C_f + L_f + R_{Lf}R_{Cf}C_f + C_f R_{Lf}R_g\right)s + R_g + R_{Lf}}$$

(Eq. 4-18)

4.2.2 *Modelling of PWM*

Whilst there are benefits associated with Unipolar PWM switching, both bipolar and unipolar PWM techniques results in the same average fundamental output voltage regardless of the switching behaviour. For control loop analysis, it has been shown that modelling the bipolar PWM strategy is significantly easier than that of the unipolar technique [44]. Therefore, for the control loop analysis only, the bipolar PWM technique is applied here. This is considered a valid "approximation" to the actual situation, provided we are only concerned with low frequency analysis below the PWM switching frequency (typically 20kHz); fortunately, this is the case here.

Figure 4.4 shows the single update PWM mode [79]. Here, the switching process is updated for each duty cycle. Based on the Figure 4-4, $m_c(t)$ is the output signal generated from the current controllers, $m_s(t)$ is the modulating signal and $c(t)$ is the carrier signal. The duty cycle d, is the fraction of time, which happens each time the modulating signal is higher than the carrier signal. This can be expressed by the value of a single update modulating signal in a cycle, $m_s nT_s$, divided by the peak of the carrier signal, c_{pk}. The sample and hold effects need also be considered in the modelling.

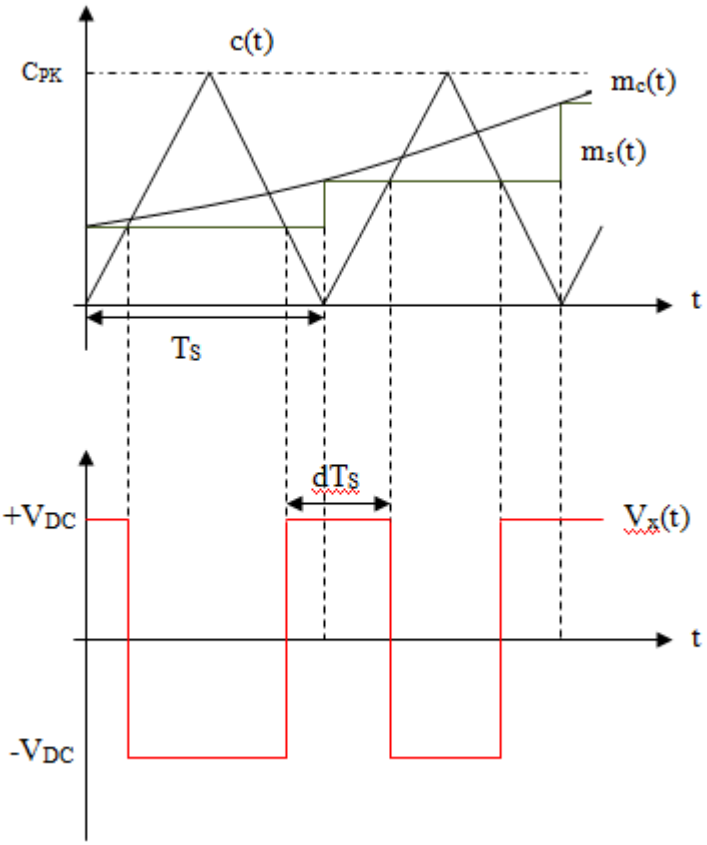

Figure 4-4: Single update PWM with triangular carrier waveform.

Equations below show the expression without and with the delay effects of sample and hold [79].

$$d = \frac{m_s n T_s}{c_{pk}} \, , n = 1,2,3,4, \ldots.$$

(Eq. 4-19)

$$d = \frac{m_c(s)}{c_{pk}} \frac{1 - s\frac{T_s}{4}}{1 + s\frac{T_s}{4}}$$

(Eq. 4-20)

In order to produce the output voltage of the H-bridge inverter, which goes from $-V_{DC}$ to $+V_{DC}$, it must depend on the PWM duty cycle. This is shown in equation below. In

order to simplify the analysis, it should be noted here that the voltage drop of the switches is ignored.

$$V_X(s) = 2dV_{DC}$$

$$V_X(s) = \frac{m_c(s)}{c_{pk}} \frac{1 - s\frac{T_s}{4}}{1 + s\frac{T_s}{4}} 2V_{DC}$$

(Eq. 4-21)

Re-arranging (Eq. 4-21), the output/input relationship of the PWM model is expressed as:

$$G_{PWM}(s) = \frac{V_X(s)}{m_c(s)} = 2\frac{1}{c_{pk}} \frac{1 - s\frac{T_s}{4}}{1 + s\frac{T_s}{4}} V_{DC}$$

(Eq. 4-22)

4.2.3 *Modelling of Current Controllers*

Chapter 3 has mentioned the transfer function for the current controllers used in this research project. They are again expressed as below:

a) Proportional Integral (PI) Current Controller

The Laplace transfer function for the output/input relationship of PI current controller is;

$$G_{PI}(s) = \frac{m_c(s)}{\varepsilon(s)} = \frac{K_P s + K_I}{s}$$

$$= \frac{K_P s + K_I}{s}$$

(Eq. 4-23)

K_P is the proportional gain and K_I is the integral gain of the controller system. Figure 4-5 shows the open loop Bode plot for the respective controller system. The chosen value used to develop the graph is 0.017 for K_P and 0.035 for K_I . These values are determined by a manual tuning approach in which the PI controller is initially

configured as a proportional only controller. The value of proportional gain is increased until the impact of continuing to increase the controller gain diminishes. The integral gain is then increased to reduce the steady state error. A small amount of fine tuning is applied until the best response is observed. At this point, the controller gains are recorded.

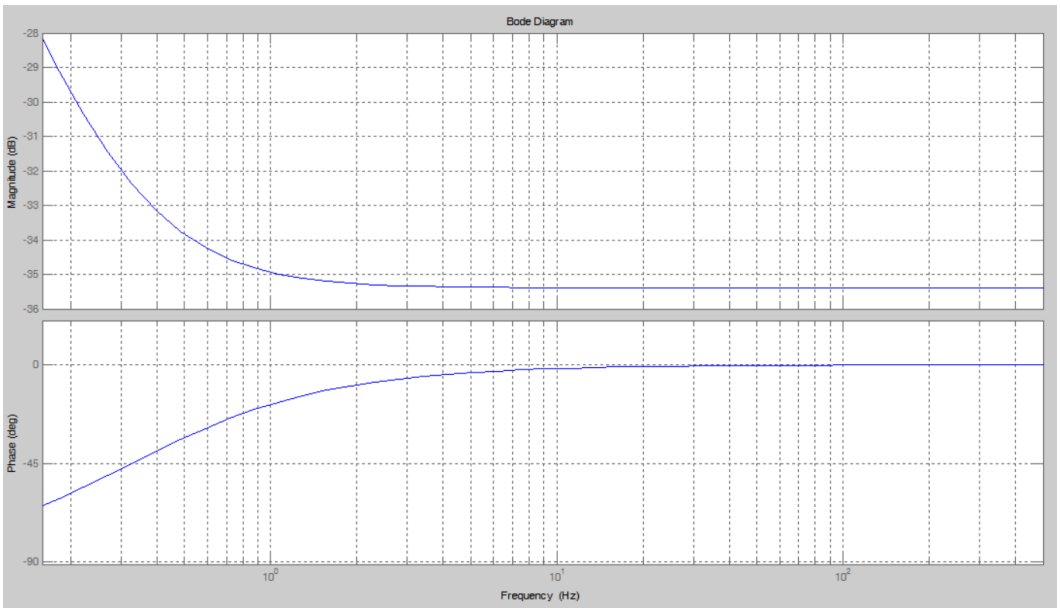

Figure 4-5: Open loop Bode plot for PI current controller scheme shows flat response at 50 Hz indicating no harmonic rejection at fundamental frequency.

b) Proportional Resonant (PR) Current Controller

The Laplace transfer function for PR current controller is;

$$G_{PR}(s) = \frac{m_c(s)}{\varepsilon(s)} = K_P + \frac{2K_R s}{s^2 + \omega_o^2}$$

$$= \frac{K_P(s^2 + \omega_o^2) + 2K_R s}{s^2 + \omega_o^2}$$

$$= \frac{K_P s^2 + 2K_R s + K_P \omega_o^2}{s^2 + \omega_o^2}$$

(Eq. 4-24)

However, as the ideal equation above is hard to implement in reality because of the round off and quantization error in digital transformation, a non ideal controller is used where a controller cut off frequency, ω_c is added to the system [58]. Furthermore, an increased ω_c will ensure the system stability and yield to a less sensitive controller [80]. This then makes the equation as:

$$G_{PR}(s) = \frac{m_c(s)}{\varepsilon(s)} = K_P + \frac{2K_R\omega_c s}{s^2 + 2\omega_c s + \omega_o^2}$$

$$= \frac{K_P(s^2 + 2\omega_c s + \omega_o^2) + 2K_R\omega_c s}{s^2 + 2\omega_c s + \omega_o^2}$$

$$= \frac{K_P s^2 + (2K_P\omega_c + 2K_R\omega_c)s + K_P\omega_o^2}{s^2 + 2\omega_c s + \omega_o^2}$$

(Eq. 4-25)

K_P is the controller proportional gain, K_R is the controller resonance gain of the system and ω_o on the other hand is equal to 2 times π times the fundamental frequency which is 315.159 rad/s.

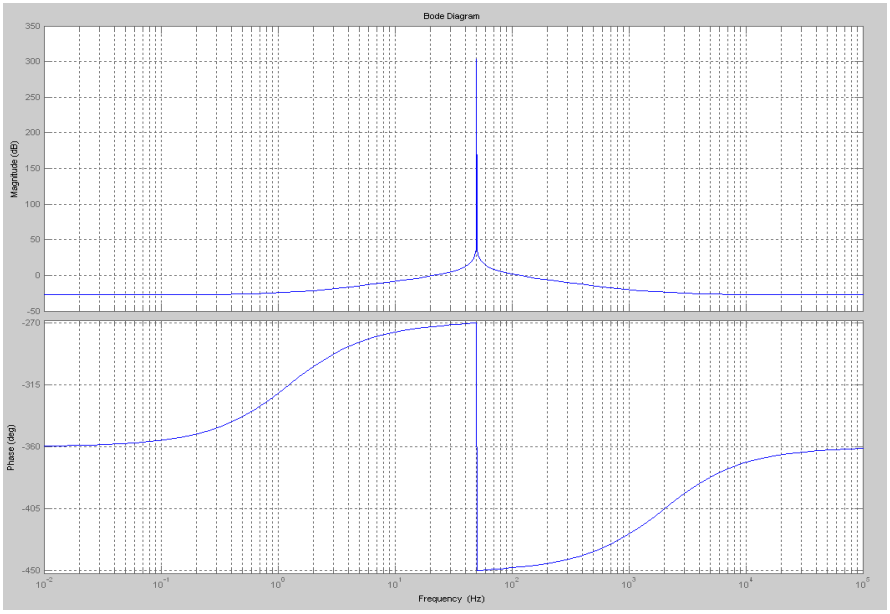

Figure 4-6: Open loop Bode plot of PR current controller scheme shows high magnitude at 50 Hz indicating good harmonic rejection at fundamental frequency.

The open loop Bode plot of the PR current controller without the cut off frequency ω_c is shown in Figure 4-6 with 0.046 and 580 for the K_P and K_R value respectively. Again,

the gain values are obtained in the simulation. Whereas the next following figure shows the open loop Bode plot of the PR current controller with the ω_c added and its effect if the value varies.

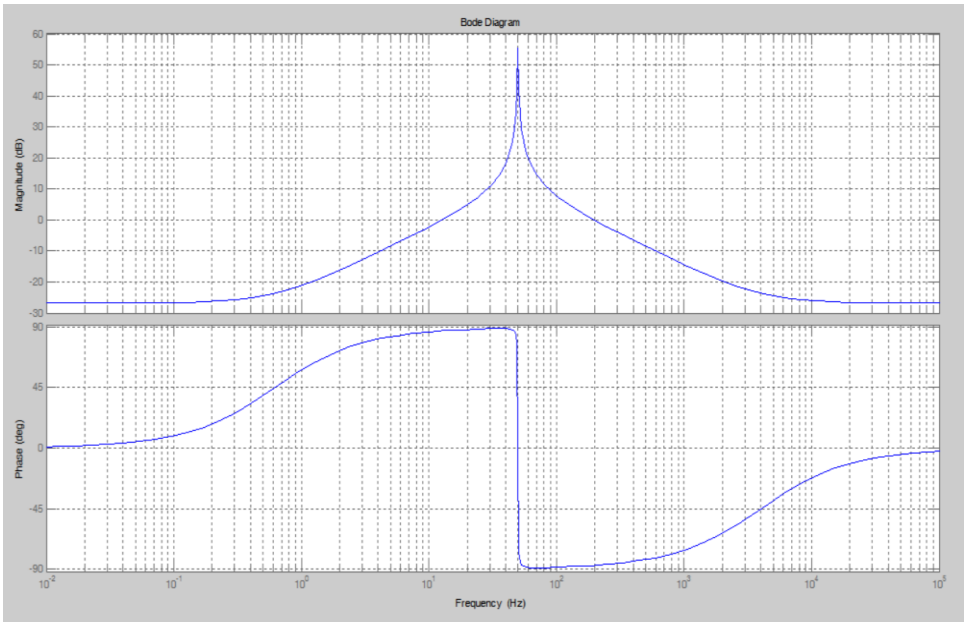

(a)

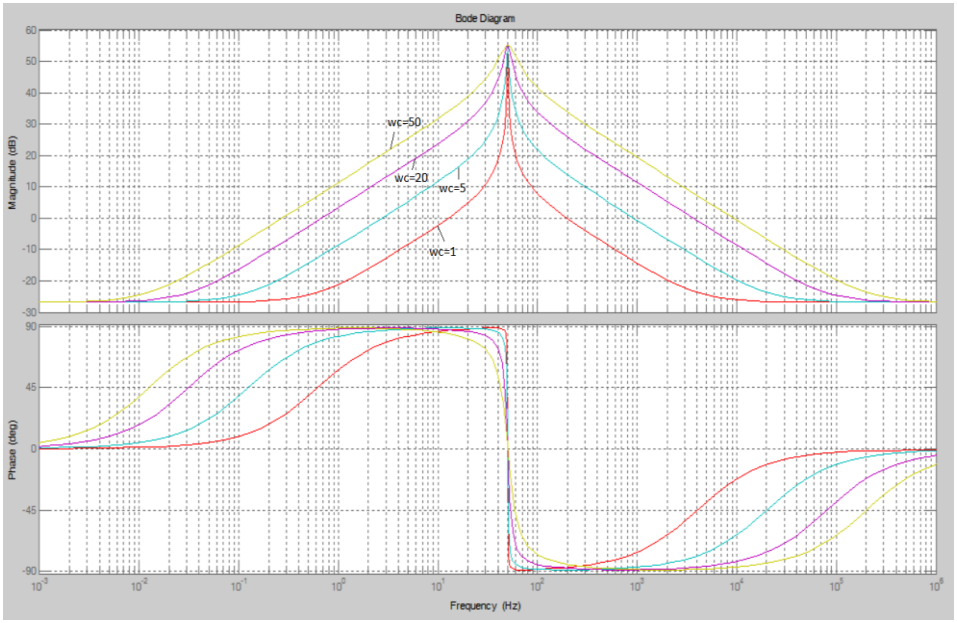

(b)

Figure 4-7: Open loop Bode plot of PR current controller scheme when (a) ω_c=1: wider magnitude response at 50 Hz shows less sensitive controller, and (b) ω_c=1, 5, 20, 50: sensitivity of the controller is reduced with increasing value of ω_c.

c) PR+HC Current Controller

The PR+HC scheme is the combination of the PR controller scheme but with harmonic compensators added. This depends on the number of harmonics that one needs to use in order to reduce the harmonics of interest. In this project, three harmonic compensators are modelled in the simulation; the 3rd harmonic order, the 5th harmonic order, and the 7th harmonic order. This is because these lower order harmonics are the most dominant harmonics and difficult to reduced. Therefore, the Laplace transfer function for the PR+HC current controller scheme with added ω_c is:

$$G_{PR+HC}(s) = \frac{m_c(s)}{\varepsilon(s)}$$

$$= K_P + \frac{2K_R\omega_c s}{s^2 + 2\omega_c s + \omega_o^2} + \frac{2K_{c3}\omega_{c3} s}{s^2 + 2\omega_{c3} s + 9\omega_o^2} + \frac{2K_{c5}\omega_{c5} s}{s^2 + 2\omega_{c5} s + 25\omega_o^2} + \frac{2K_{c7}\omega_{c7} s}{s^2 + 2\omega_{c7} s + 49\omega_o^2}$$

(Eq. 4-26)

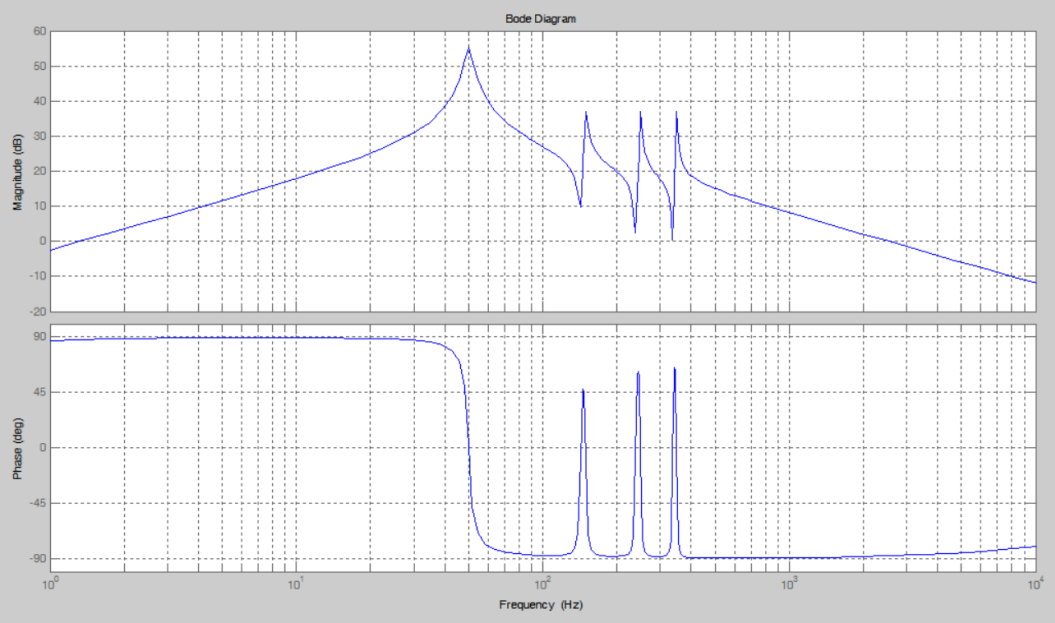

Figure 4-8: Open loop Bode plot of PR+HC current controller scheme with $\boldsymbol{\omega_c}$=10.

Based on (Eq. 4-26), K_P is the proportional gain, K_R is the resonant gain at fundamental frequency, K_{c3} is the resonant gain at three times the fundamental frequency, K_{c5} is the resonant gain at five times the fundamental frequency, and K_{c7} is the resonant gain at

seven times the fundamental frequency. The chosen values for all the gains mentioned are 0.046, 580, 70, 70, and 70 respectively which are obtained in the simulation earlier. The overall open loop Bode plot for PR+HC current controller is as in Figure 4-8.

4.2.4 *Model of Grid Connected, Single PV Inverter System*

By cascading (Eq. 4-18) and (Eq. 4-22) above with the chosen current controller ((Eq. 4-23**)**, (Eq. 4-25) or (Eq. 4-26)), the complete model of a grid connected, PV inverter system can be developed. This is illustrated in Figure 4-9.

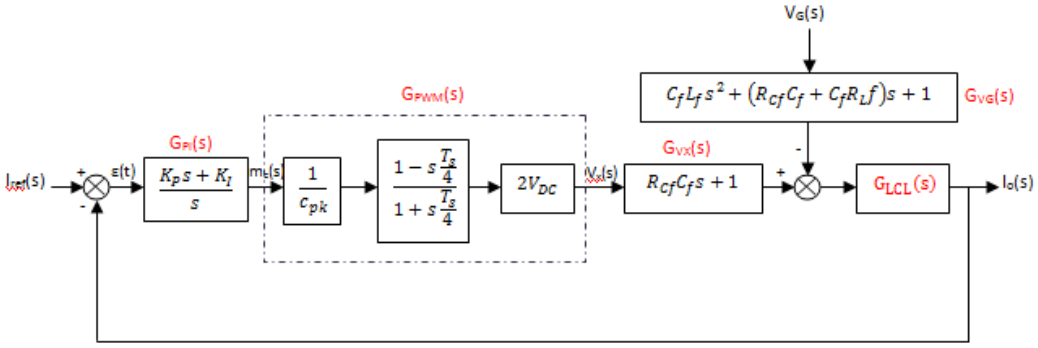

Figure 4-9: Model of grid connected inverter system with PI current controller.

From the figure, two input variables are observed which produce two different transfer function responses. One is the response when $V_G(s)$ is set to zero and the other one is the response when $I_{ref}(s)$ is set to zero. The overall closed loop response of the grid connected, single PV inverter system model is discussed further in the next sub-section.

4.3 Closed Loop Frequency Response

Earlier, two input variables are observed from the model in Figure 4-9. In order to get the overall closed loop response of the system model, each input is set to zero value for each time to develop two transfer functions. The mathematical expressions for the grid connected, inverter model with PI current controller are explained next.

When $V_G(s) = 0$;

$$\frac{I_o(s)}{I_{ref}(s)} = \frac{G_{PI}(s)G_{PWM}(s)G_{VX}(s)G_{LCL}(s)}{1 + G_{PI}(s)G_{PWM}(s)G_{VX}(s)G_{LCL}(s)}$$

$$I_o(s) = I_{ref}(s)\frac{G_{PI}(s)G_{PWM}(s)G_{VX}(s)G_{LCL}(s)}{1 + G_{PI}(s)G_{PWM}(s)G_{VX}(s)G_{LCL}(s)}$$

(Eq. 4-27)

When $I_{ref}(s) = 0$;

$$\frac{I_o(s)}{V_G(s)} = -\frac{G_{VG}(s)G_{LCL}(s)}{1 + G_{PI}(s)G_{PWM}(s)G_{VX}(s)G_{LCL}(s)}$$

$$I_o(s) = -V_G(s)\frac{G_{VG}(s)G_{LCL}(s)}{1 + G_{PI}(s)G_{PWM}(s)G_{VX}(s)G_{LCL}(s)}$$

(Eq. 4-28)

By adding (Eq. 4-27) and (Eq. 4-28), the closed loop response can be obtained.

$$I_o(s) = I_o(s)|_{V_G(s)=0} + I_o(s)|_{I_{ref}(s)=0}$$

$$I_o(s) = I_{ref}(s)\frac{G_{PI}(s)G_{PWM}(s)G_{VX}(s)G_{LCL}(s)}{1 + G_{PI}(s)G_{PWM}(s)G_{VX}(s)G_{LCL}(s)} - V_G(s)\frac{G_{VG}(s)G_{LCL}(s)}{1 + G_{PI}(s)G_{PWM}(s)G_{VX}(s)G_{LCL}(s)}$$

(Eq. 4-29)

Re-arranging (Eq. 4-29),

$$G_{CLPI}(s) = \frac{I_o(s)}{I_{ref}(s)} = \frac{G_{PI}(s)G_{PWM}(s)G_{VX}(s)G_{LCL}(s) - \frac{V_G(s)}{I_{ref}(s)}[G_{VG}(s)G_{LCL}(s)]}{1 + G_{PI}(s)G_{PWM}(s)G_{VX}(s)G_{LCL}(s)}$$

(Eq. 4-30)

Using the same steps, the closed loop response for the grid connected, inverter model with PR and PR+HC current controller can be obtained as in (Eq. 4-31) and (Eq. 4-32**)**.

$$G_{CLPR}(s) = \frac{I_o(s)}{I_{ref}(s)} = \frac{G_{PR}(s)G_{PWM}(s)G_{VX}(s)G_{LCL}(s) - \frac{V_G(s)}{I_{ref}(s)}[G_{VG}(s)G_{LCL}(s)]}{1 + G_{PR}(s)G_{PWM}(s)G_{VX}(s)G_{LCL}(s)}$$

(Eq. 4-31)

$$G_{CLPR+HC}(s) = \frac{I_o(s)}{I_{ref}(s)} = \frac{G_{PR+HC}(s)G_{PWM}(s)G_{VX}(s)G_{LCL}(s) - \frac{V_G(s)}{I_{ref}(s)}[G_{VG}(s)G_{LCL}(s)]}{1 + G_{PR+HC3}(s)G_{PWM}(s)G_{VX}(s)G_{LCL}(s)}$$

(Eq. 4-32)

Table 4.1 shows the list of parameters used in the system. These values are typical of a commercial scale single phase inverter system, and have been successfully applied in previous work [ref Hong]. For consistency, they are applied here also for the purposes of the Simulink simulation.

Table 4-1: List of parameters of grid connected model.

Parameter	**Value**
V_{DC}	400 V
C_{pk}	2
T_s	50 µs
L_f	1.6 mH
R_{Lf}	0.15 Ω
C_f	12 µF
R_{Cf}	0.0566 Ω
L_g	0.05 mH
R_g	0.1 Ω
V_g	$240\sqrt{2}$ V_{peak}
I_{ref}	20 A
K_P (PI)	0.017
K_I	0.035
K_P (PR and PR+HC)	0.046
K_R	580
HC_3, HC_5, HC_7	70

The following three figures below the Bode plot of the closed loop system response with PI, PR and PR+HC current controller together with its root locus.

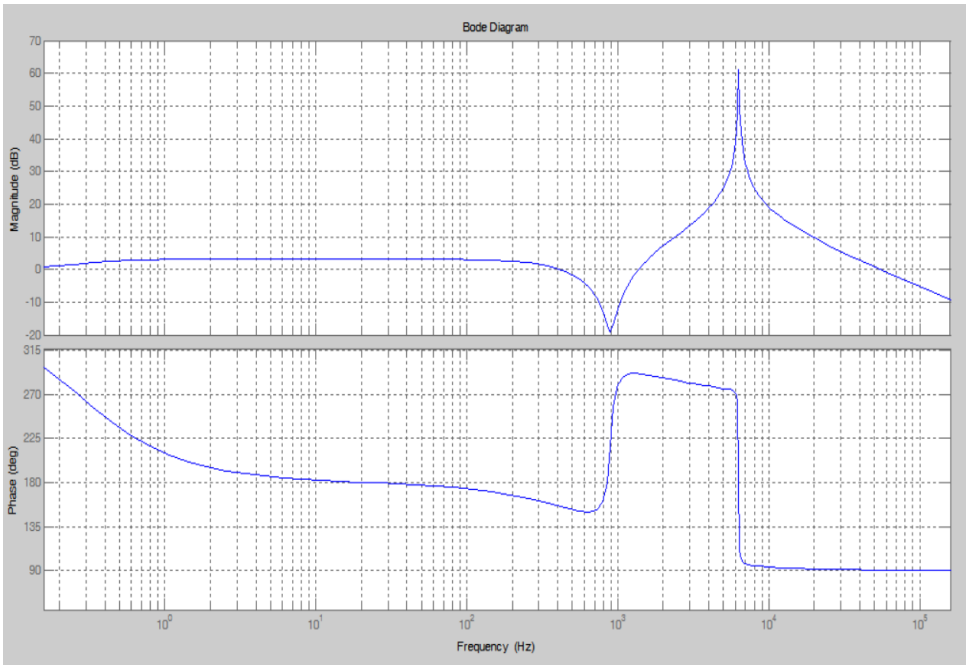

(a)

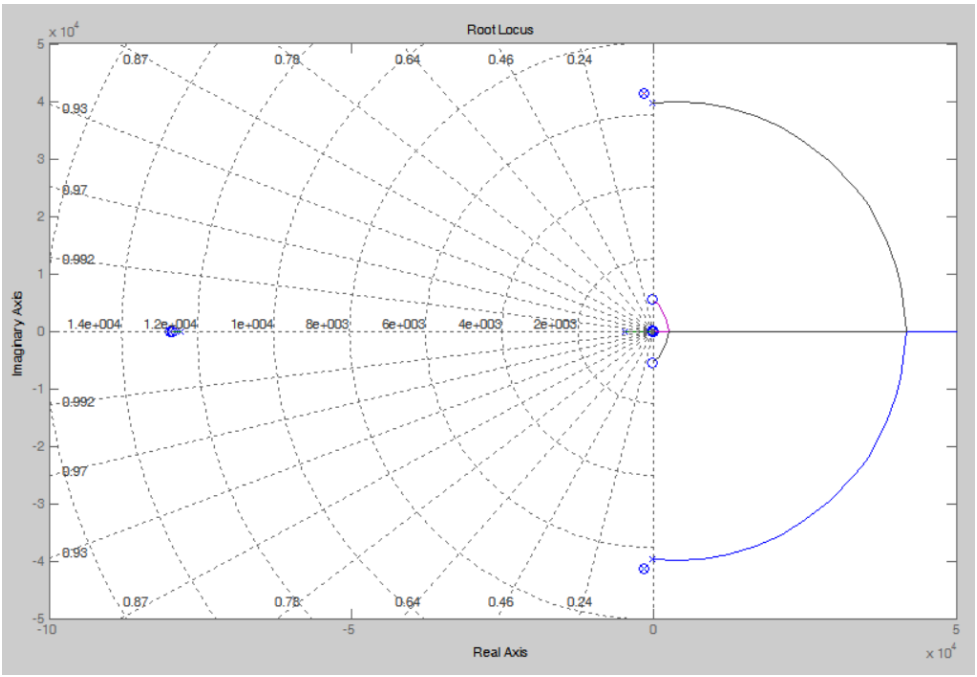

(b)

Figure 4-10: Closed loop response of the system with PI current controller. (a) Bode plot shows the attenuation of the low order harmonics, and controller resonant point at approximately 7 kHz, and (b) Root locus confirms the stability of the closed loop controller for the applied gains.

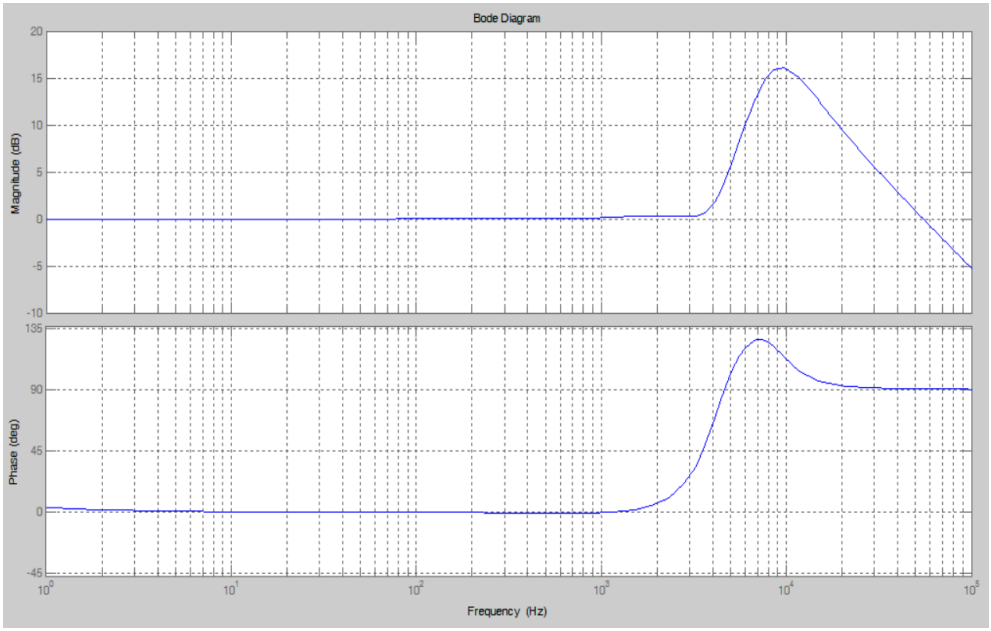

(a)

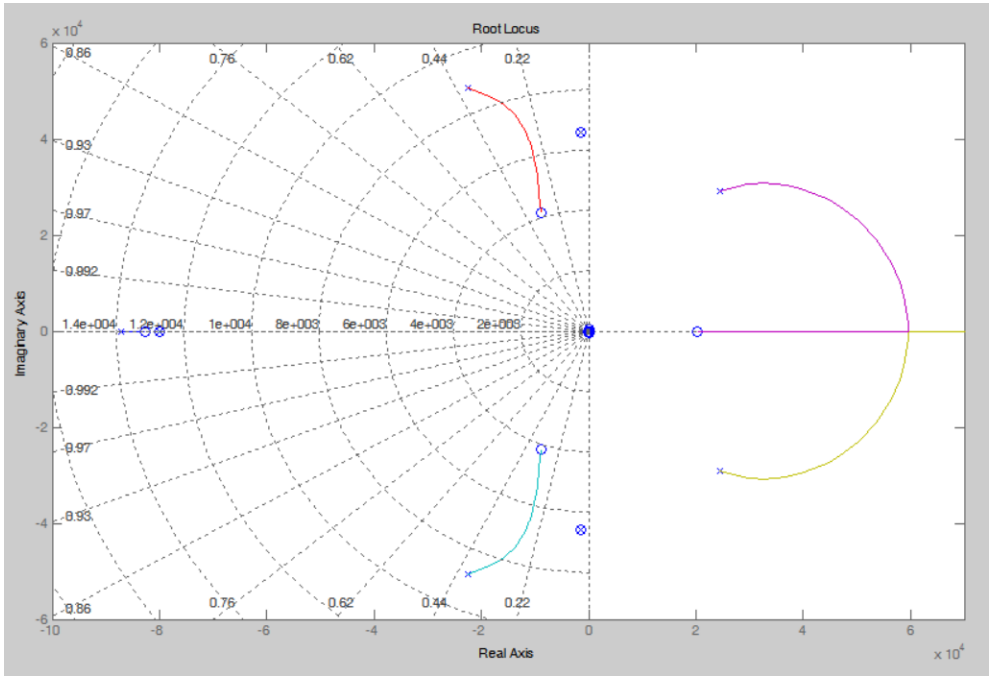

(b)

Figure 4-11: Closed loop response of the system with PR current controller. (a) Bode plot shows improved attenuation of low order harmonics, and lower impact of resonance (now at 10 kHz), and (b) Root locus confirms the stability of the closed loop controller for the applied gains.

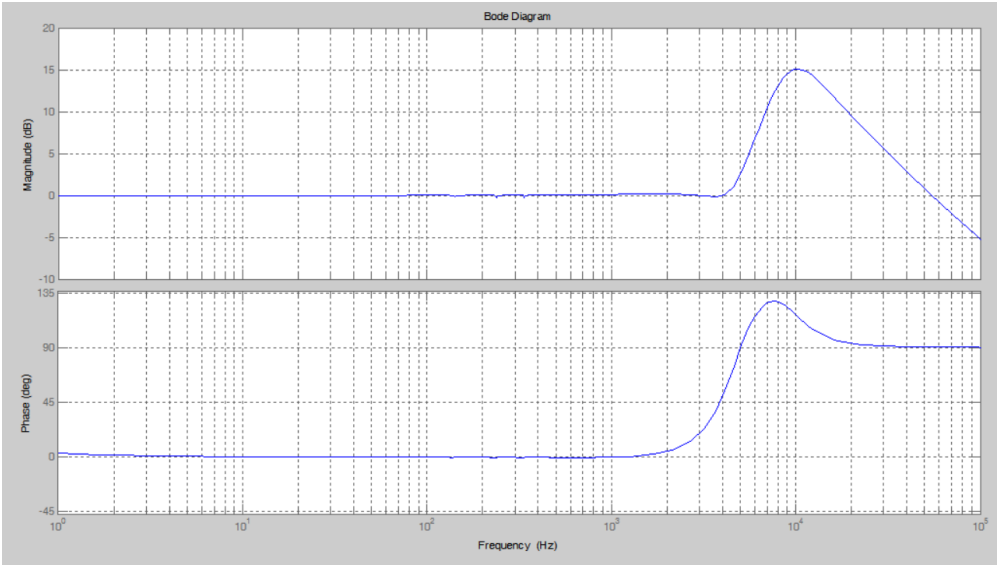

(a)

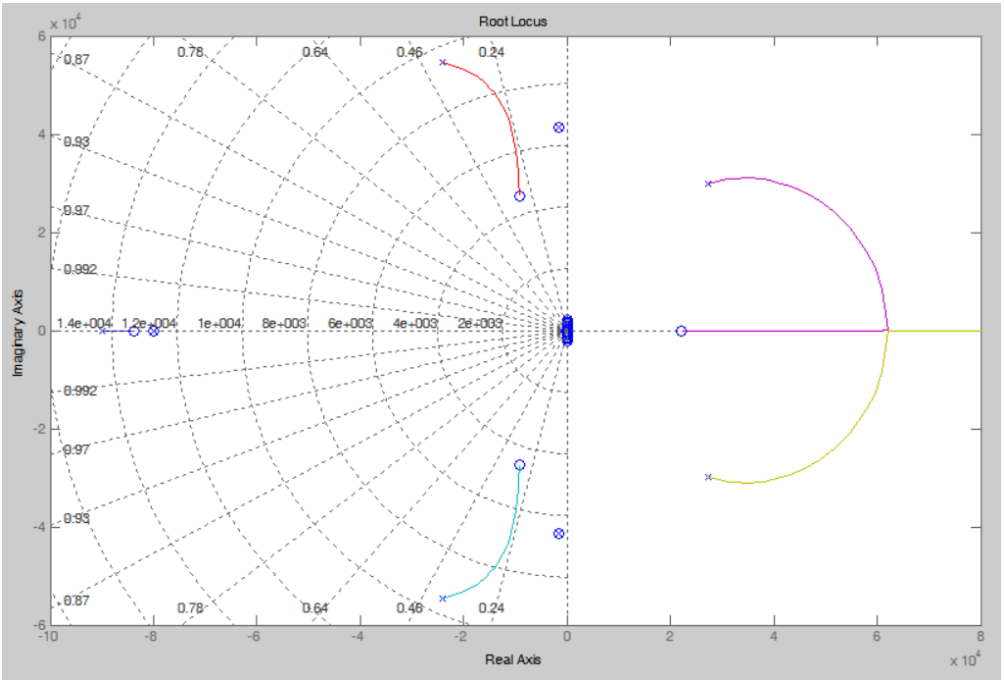

(b)

Figure 4-12: Close loop response of the system with PR+HC current controller. (a) Bode plot shows attenuation of low order harmonics, and further improvement of the resonant effect at 10 kHz, and (b) Root locus confirms the stability of the closed loop controller for the applied gains.

4.4 Discussion

Analysis of the PI controller bode plot shows that output gain of the controller is fairly uniform across the frequency range. For the PR controller, it is apparent that the controller can be tuned so that the control system has low impedance to the fundamental frequency of interest; in the case of a grid connected inverter system this is the network frequency – typically 50/60 Hz. This is one of the reasons that PR controller are becoming increasingly popular in distributed generation systems; it is well suited for readily injecting mains frequency signals into the grid, whilst presenting a higher impedance to other frequencies such as harmonics where it is preferential to minimise these components. The PR+HC takes this one step further, This controller includes additional harmonic compensation terms, which are tuned to specific harmonics which are desirable to mitigate. The example in this chapter has shown a typical application, which might be seen in a grid connected inverter system, where the HC terms are targeted towards the low order harmonics of the system. These are particularly troublesome in grid connected applications, since they are close to the fundamental frequency of the system, and thus immensely difficult to remove via traditional passive low pass filters. A typical passive low pass filter in a grid connected inverter might be designed around a cut of frequency in the range of 500 Hz – 1500 Hz, therefore 3^{rd}, 5^{th}, 7^{th} harmonic components are particularly troublesome. In the Bode of plot of the PR-HC, it is clear that the impedance to these components has been significantly increased (shown by the three "spikes" in the bode plot).

4.5 Chapter Summary

This chapter has explained the modelling process of a grid connected single inverter system employing three different types of controller. The approach to the modelling has been fully described, with full details on the development of the closed loop Laplace transfer function of each system. Based on an example set of gains used in each controller, it is clear to see that a robust control solution can be developed with each method. The key attributes of each controller have been shown via the frequency domain responses, and discussed. Whilst the PI controller produces a robust solution, the PR controller produces a solution which is better optimised to the injection of the fundamental frequency into the grid. Troublesome low order harmonic components can be mitigated further by the introduction of harmonic compensation (HC) terms. Care

must be taken when introducing these terms, since each adds complexity to the control structure and will require DSP resources when applied in practice.

Chapter 5: Simulations of Grid-Connected Inverter System with PI, PR and Modified PR Control

5.1 Chapter Introduction

Simulations are the assumptions of representations of the real model. Before any experimental hardware is developed, simulations are normally done in order to test the effectiveness of the proposed idea. Hence, the parameters used in the simulation process will be referred to in the future when developing the experimental hardware. In this chapter, simulations of a grid connected system are done using three control techniques that are the PI control, PR control and the modified PR control. At first, a single inverter system is simulated and followed by two inverter systems in parallel and connected to the same point in the supply grid.

5.2 Simulation of a single grid connected inverter

Before parallel inverter systems are simulated, a single connected inverter system is modelled initially using Matlab as the simulation tool. It comprises of PWM circuit, an H bridge inverter that consists of 4 mosfets with internal diodes, a low pass filter, current controller and the supply grid with grid impedance. The low pass filter consists of an inductance and a capacitor with values as listed in Table 5-1. It is designed so that the magnitude of frequencies lower than approximately of 1 kHz can pass through and magnitude of the frequencies higher than an approximate of 1 kHz is filtered. This is to prevent the unwanted switching frequency harmonics being injected to the grid.

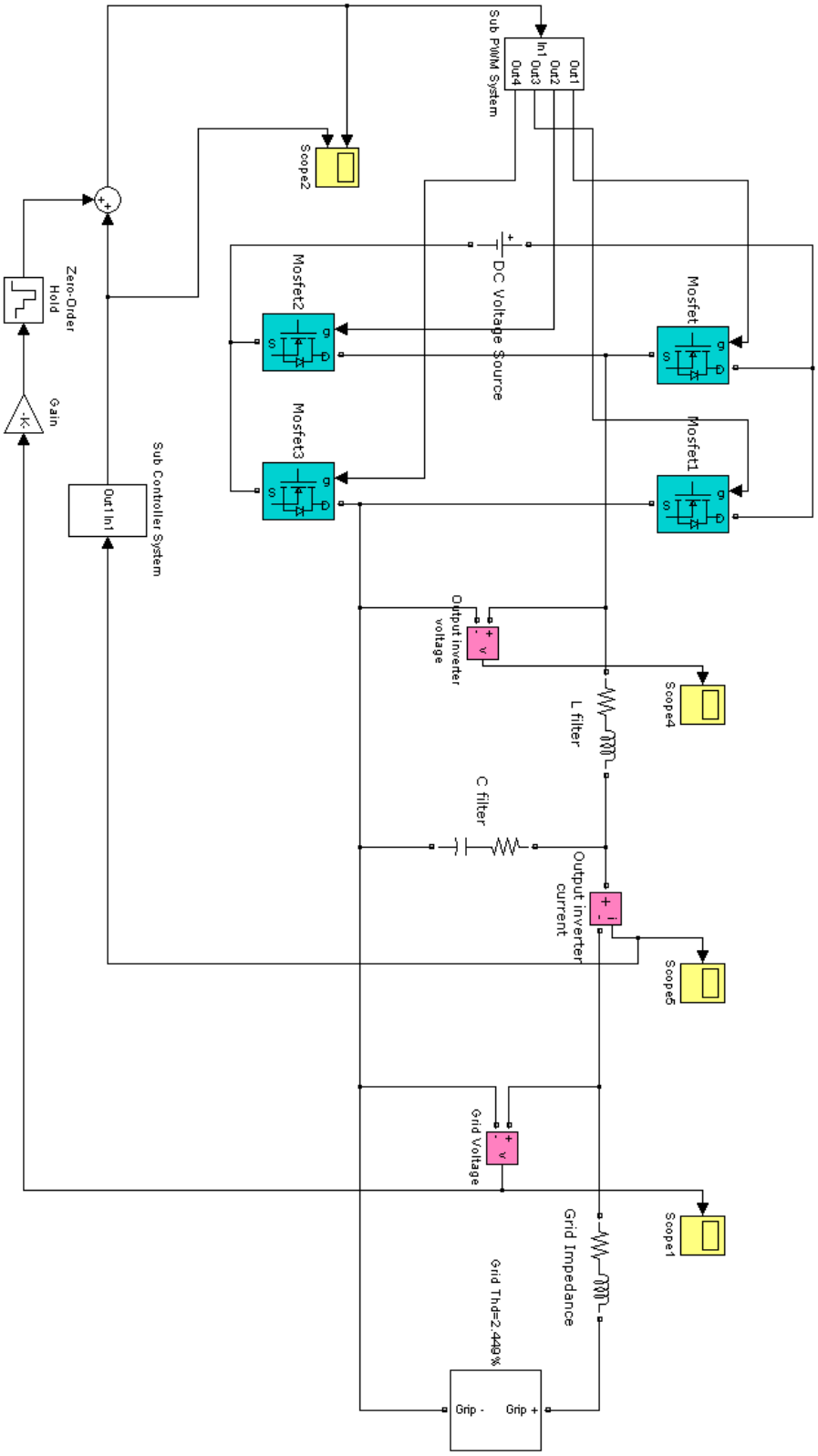

Figure 5-1: Simulink model of grid-connected inverter system.

Figure 5-1 shows a single inverter system model. The parameters are listed in Table 5-1.

Table 5-1: System parameters.

DC Voltage Source	400 V
Frequency	50 Hz
Filter Inductance and Resistance	L=1.6 mH, R=0.15 Ω
Filter Capacitance and Resistance	C=12 µF, R=0.0566 Ω
Filter Cut-Off Frequency	1148 Hz
Grid Voltage	240 V_{RMS}
Grid Impedance	R=0.1 Ω L=0.15 mH

Figure 5-2 is the grid model of 240 V_{RMS} which contains different magnitude and phase angle for each particular frequency of up to the 50th. In total, this will create an approximate background THD of 2.45% in the grid supply voltage. The harmonic data is based on experimental data acquired by a previous student in the Power Electronics, Drives and Machines laboratory at Newcastle University [44]. This data is readily available for simulation use by the research group.

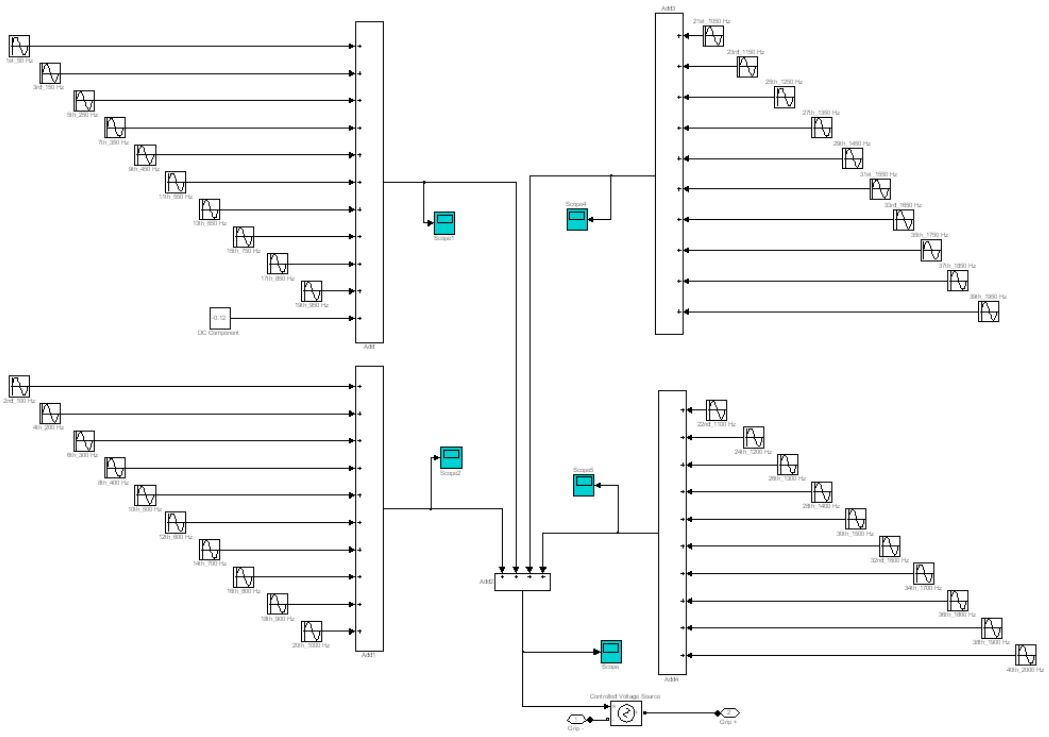

Figure 5-2: Grid model which contains a background THD of 2.45% [44].

Table 5-2: Grid model harmonic data [44].

Freq (Hz)	Amplitude (RMS)	Phase (deg)		Freq (Hz)	Amplitude (RMS)	Phase (deg)
50	241.72	320.29		1050	0.05	265.06
100	0.07	340.9		1100	0.01	277.76
150	3.56	90.01		1150	0.12	281.76
200	0.02	296.59		1200	0.01	49.23
250	3.45	98.5		1250	0.13	285.01
300	0.01	326.46		1300	0.01	151.49
350	2.45	253.58		1350	0.15	105.57
400	0.01	33.74		1400	0.01	103.03
450	1.09	303.98		1450	0.03	295.9
500	0.01	14.62		1500	0.01	98.5
550	0.5	91.26		1550	0.08	157.67
600	0	168.4		1600	0.01	175.79
650	1.37	13.7		1650	0.02	147.72
700	0.01	43.99		1700	0	335.9
750	0.73	313.33		1750	0.07	310.1
800	0.01	112.09		1800	0	204.46
850	0.7	350.93		1850	0.01	283.66
900	0.01	208.84		1900	0.01	20.7
950	0.2	167.34		1950	0.02	144.62
1000	0.01	316.74		2000	0	272.65

As there are three different digital current control methods used in this project, each is tested independently. The first simulation uses the conventional PI current controller, followed by the PR+HC and the modified PR+HC. The reference current is chosen to be 20 A peak as the system is assumed to work in a perfect sunny day with 3 kW output power. The simulation model samples the currents and voltages every 50 us. In addition, the PWM output is updated at the same rate. This simulates the basic operation of a real digital control system.

Such a set of conditions assumes close to full power operating conditions. Under these circumstances, the modulation index within the PWM is set to be very high. It is well known that the harmonic performance of grid connected inverters is typically best at full power, and that low modulation index operation can result in in greater harmonic distortion. This is because at low modulation indices, dead-time is a greater proportion of the pulse width. Therefore, the impact on low order harmonic distortion is greater.

Good quality dead-time compensation can mitigate the impact of this to some extent, but will not complete eliminate the phenomena. In a grid connected inverter PV system, such a scenario can potentially occur when there is a prolonged period of low irradiation. It is important to recognise, however, that such characteristics will apply regardless of the control strategy chosen. In most of the results presented in this thesis, a high modulation index is observed in the PWM unit, implying that the inverter is typically operating at high/full power conditions which is typically desirable where possible.

5.2.1 *Conventional PI control technique*

Figure 5-3 shows the PI controller model used in the simulation. The measured inverter output current will be *In1*. It is then compared with the I_{ref}, resulting an error which is used in the control process. The output of the current controller is then compared with a 20 kHz triangular wave signal to generate the PWM switching pattern to control the state of the H-Bridge power converter. Both gains; proportional gain and integral gain are tuned using a simple a manual tuning method until the output current matches the reference signal. Further fine tuning is then carried out to achieve an optimised current output, with good power quality (low harmonics). In this simulation, the gains used are 0.03 for K_P and 0.03 for K_I. The model is run for 1.0 s. Following this, FFT analysis is performed and the harmonic content of the output current waveform is recorded, up to the 20^{th} harmonic (1 kHz). Above this, the harmonics are significantly attenuated by the low pass filter. However, the overall THD of the current waveform is also recorded as an additional measure of power quality.

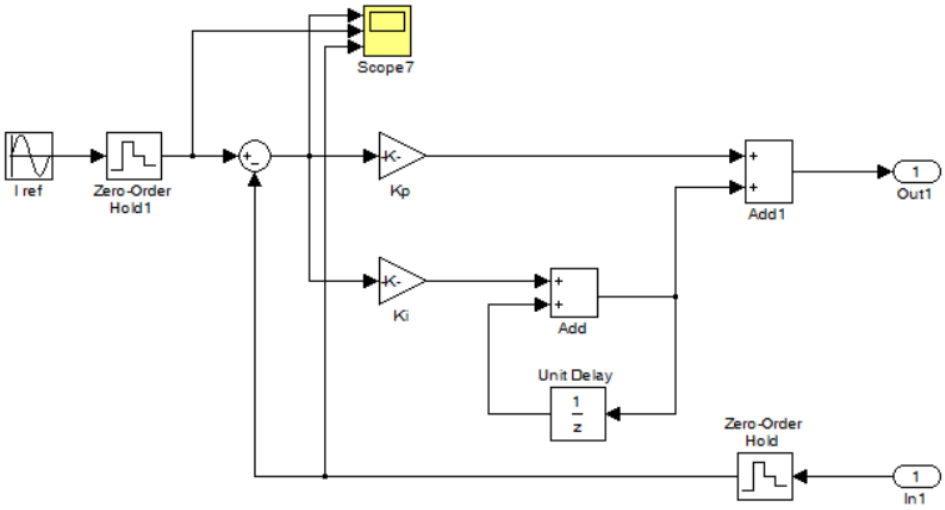

Figure 5-3: Conventional PI current controller digital Simulink model.

Figure 5-4 in the next page shows the screen shot of the reference current signal, the inverter output current signal, and the observed current error signal applied to the PI controller.

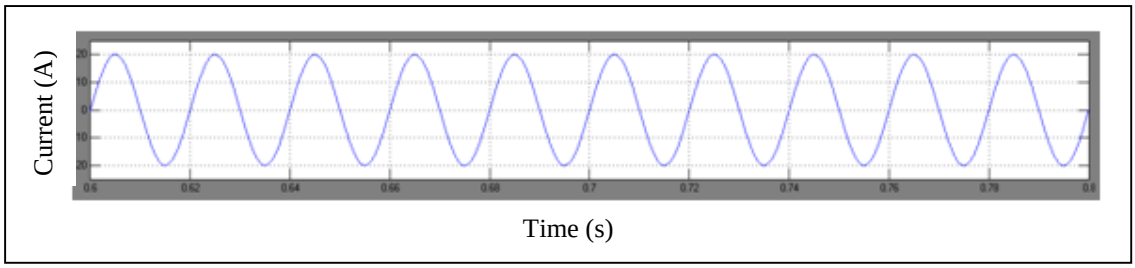

a)

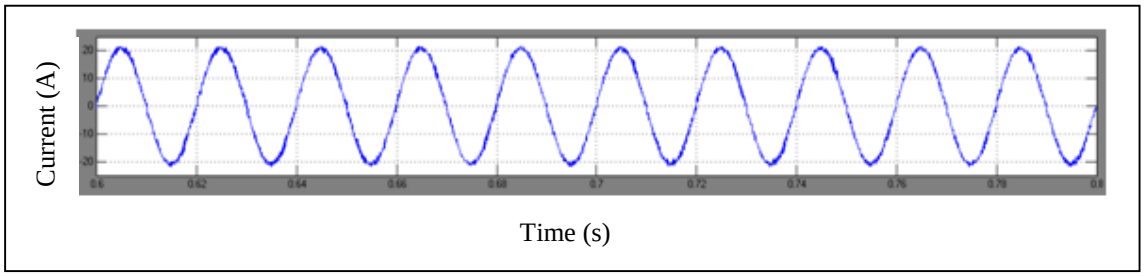

b)

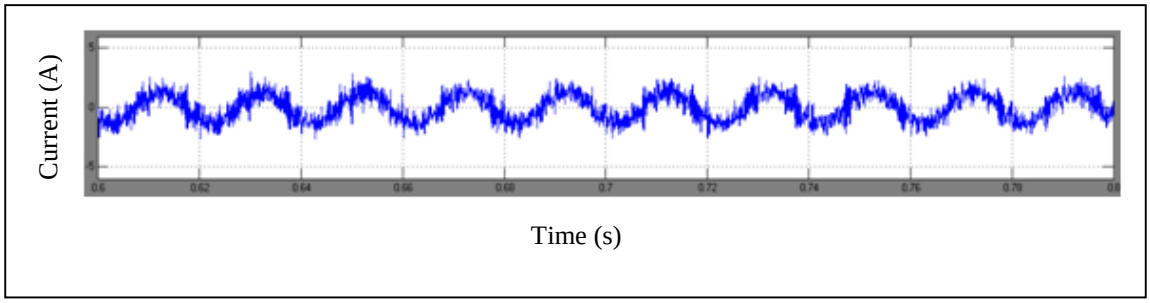

c)

Figure 5-4: Screen shot of (a) Reference current of PI controller with 20 A peak value, (b) Inverter output current of PI controller which shows a distorted waveform, and (c) Large magnitude error between reference current and inverter output current of PI controller.

With the chosen K_P and K_I value, when the model is run, the error between both the inverter output current and reference current is the smallest which is approximately 1.5 A peak. The harmonic spectrum for the inverter output current is measured using FFT Analysis. The sample taken for the analysis is 10 cycles starting from 0.6 s to 0.8 s. The low order harmonic data is then exported to Excel and post processed to produce the result illustrated in Figure 5-5 .

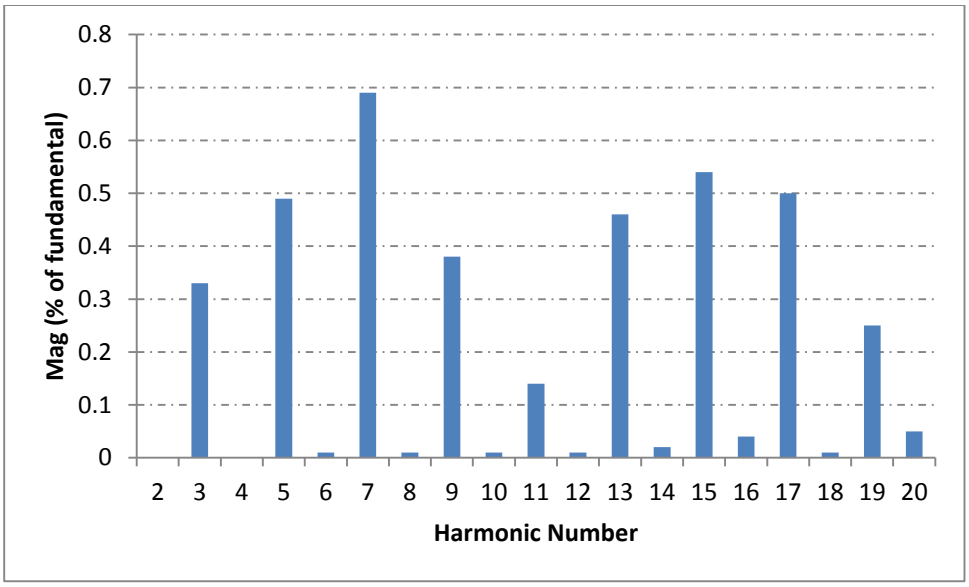

Figure 5-5: Low order harmonic spectrum of inverter output current with PI control ($K_P = 0.03\,, K_I = 0.03$)

The inverter output current shows a THD of 2.06 %, with high harmonics appear between the 3rd and 17th order. These low order harmonics are the prominent harmonics which are the focus to be eliminated or reduced in this research work. As mentioned previously, higher order harmonics beyond the 20th are less severe due to the 1 kHz cut off frequency of the low pass filter.

5.2.2 *Proportional resonance (PR) control technique*

Next, the same simulation model of a single inverter grid connected system is once again simulated. This time, instead of using the PI current control technique, the proportional resonance (PR) current control technique is implemented. Figure 5-6 shows the controller model of the PR technique. *In2* is the measured inverter output current whilst *Out2* is the output signal after the controlling process that will be used for PWM switching purposes. Based on Figure 5-6, several coefficients need to be determined carefully in targeting a reduction or elimination of the low order harmonics thus achieving a low THD value of the inverter output current. Chapter 3 has shown the equation for b_0, b_1, b_2, a_1 and a_2. For ease of simulation, the denominator from the equation is strategically replaced with a constant value for the controller, *const*. This leaves the b_0, b_1, b_2, a_1 and a_2 as one single value with only the proportional gain, K_P and the resonance gain, K_R to be tuned. Therefore

$$const = \frac{1}{4 + T^2{\omega_o}^2}$$

$$b_o = (4 + T^2{\omega_o}^2)K_P + 2TK_R$$

$$b_1 = (2T^2{\omega_o}^2 + 8)K_P$$

$$b_2 = (4 + T^2{\omega_o}^2)K_P - 2TK_R$$

$$a_1 = \frac{2T^2{\omega_o}^2 - 8}{4 + T^2{\omega_o}^2}$$

$$a_2 = 1$$

By inserting 50 µs for T (sampling time) and 2π times the fundamental frequency (50 Hz) for ω_o, all values, with the exception of K_P and K_R are obtained. Then, K_P and K_R need to be tuned so that the lowest inverter output current THD is achieved. Following a manual tuning method, the optimum output result is achieved when K_P is 0.04 and K_R is 700.

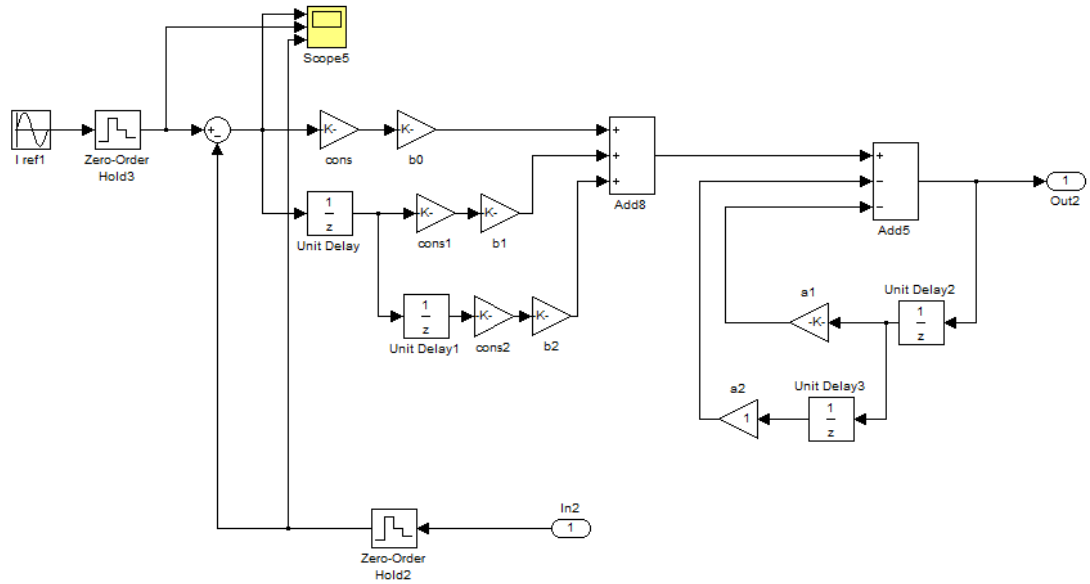

Figure 5-6: Simulink model of current controller using PR technique.

The reference current, measured inverter output current and the error can be seen in Figure 5-7. Based on the figure, the error current for the system using the PR control

technique is minimised when compared with the error current for the system using the PI control technique (Figure 5-4). This shows an advantage of the PR control system.

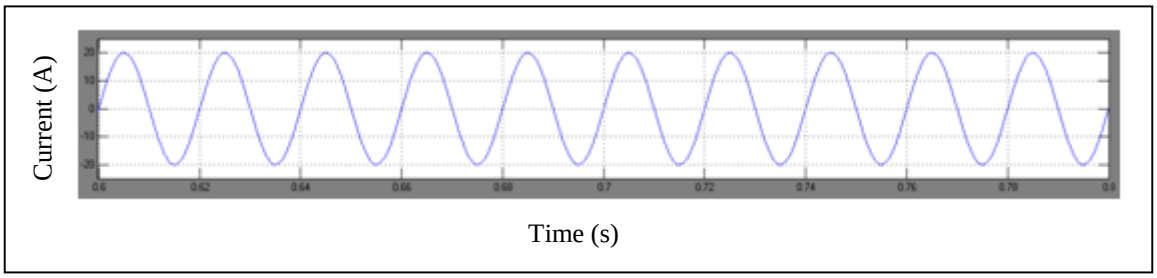

a)

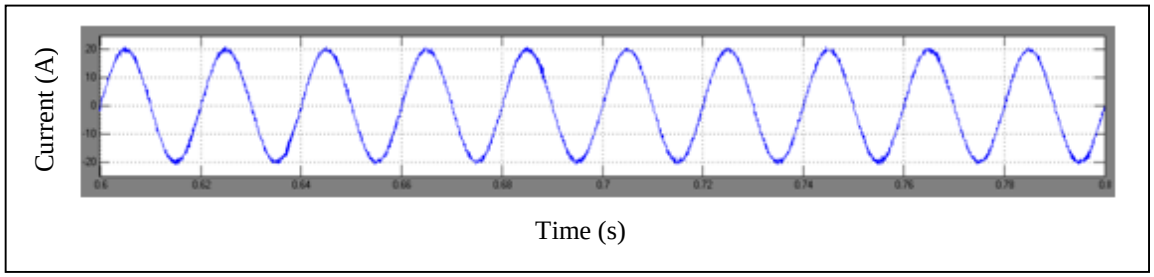

b)

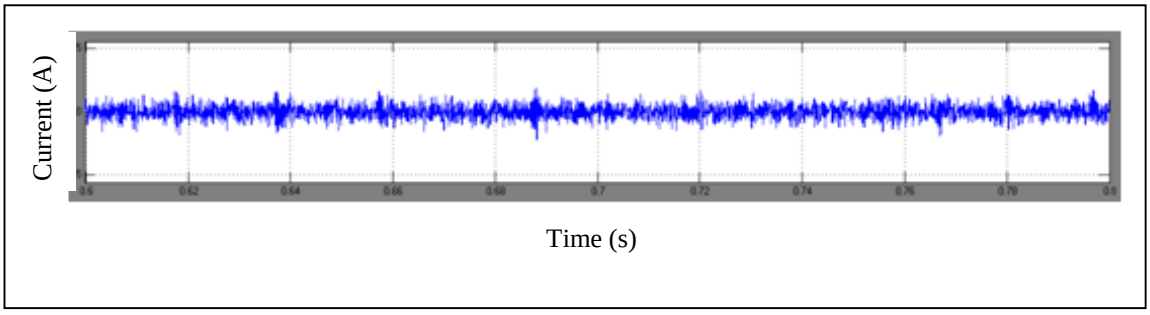

c)

Figure 5-7: Screen shot of (a) Reference current of PR controller with 20 A peak value, (b) Inverter output current of PR controller which shows smoother waveform compared to PI controller, and (c) Reduced error between reference current and inverter output current of PR controller.

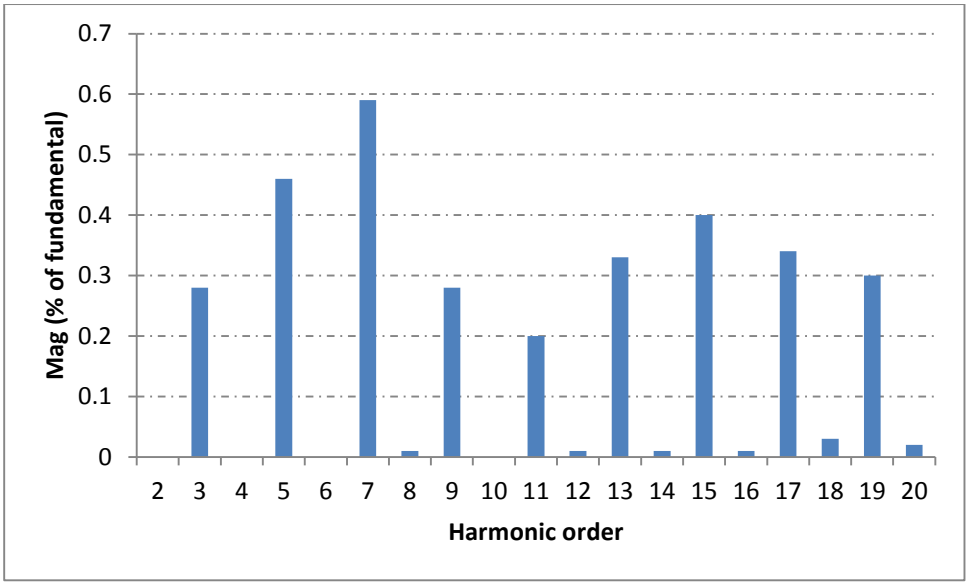

Figure 5-8: Low order harmonic spectrum of inverter output current with PR current controller.

Figure 5-8 shows the low order harmonic spectrum of the inverter output current after the data from FFT analysis in Simulink has been transferred to Excel. When run in the same length time as the system using PI current controller and sample time taken for the analysis made is also the same as the system using PI current controller, the THD achieved is 1.80% which is a reduction of approximately 13% from using the conventional PI control technique.

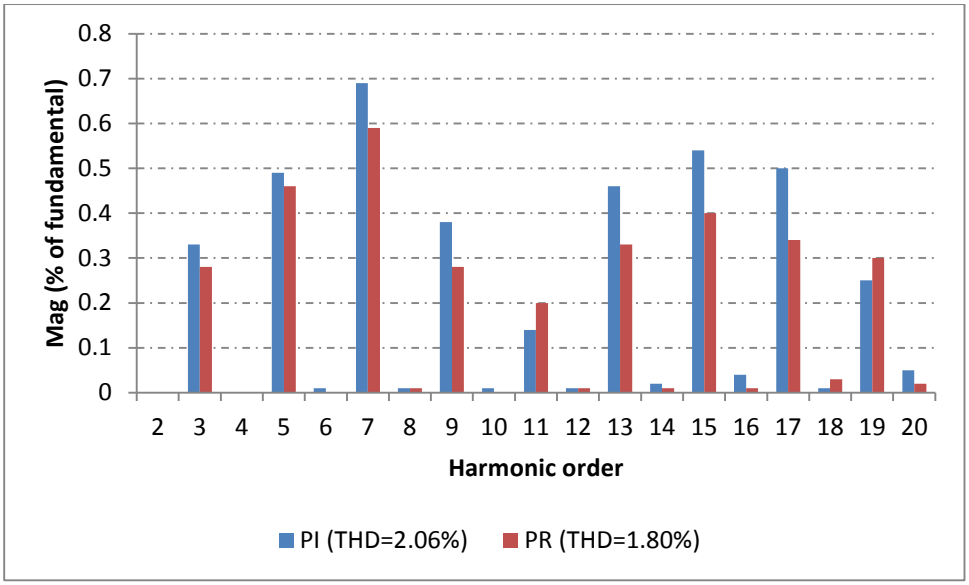

Figure 5-9: Comparison in the harmonic profile of PI and PR current controllers shows better reduction of harmonics magnitude with PR current controller.

Figure 5-9 illustrates the spectrums of Figure 5-5 and Figure 5-8 when they are set in a single bar graph. Besides the improvement in the THD, Figure 5-9 clearly shows that the harmonics magnitude between the 3rd and the 17th harmonic orders have also been reduced except for the 11th and 19th harmonic order. However, when observing the magnitude of the 11th harmonic, it is not a big concern here as it is the similar range of magnitude value that is between 0.1 and 0.2.

5.2.3 *Modified PR control technique*

As a novel approach, a slight modification is made to the proportional resonance (PR) current controller parameter. Instead of using the controller model as in Figure 5-6, the model as in Figure 5-10 is used in the simulation.

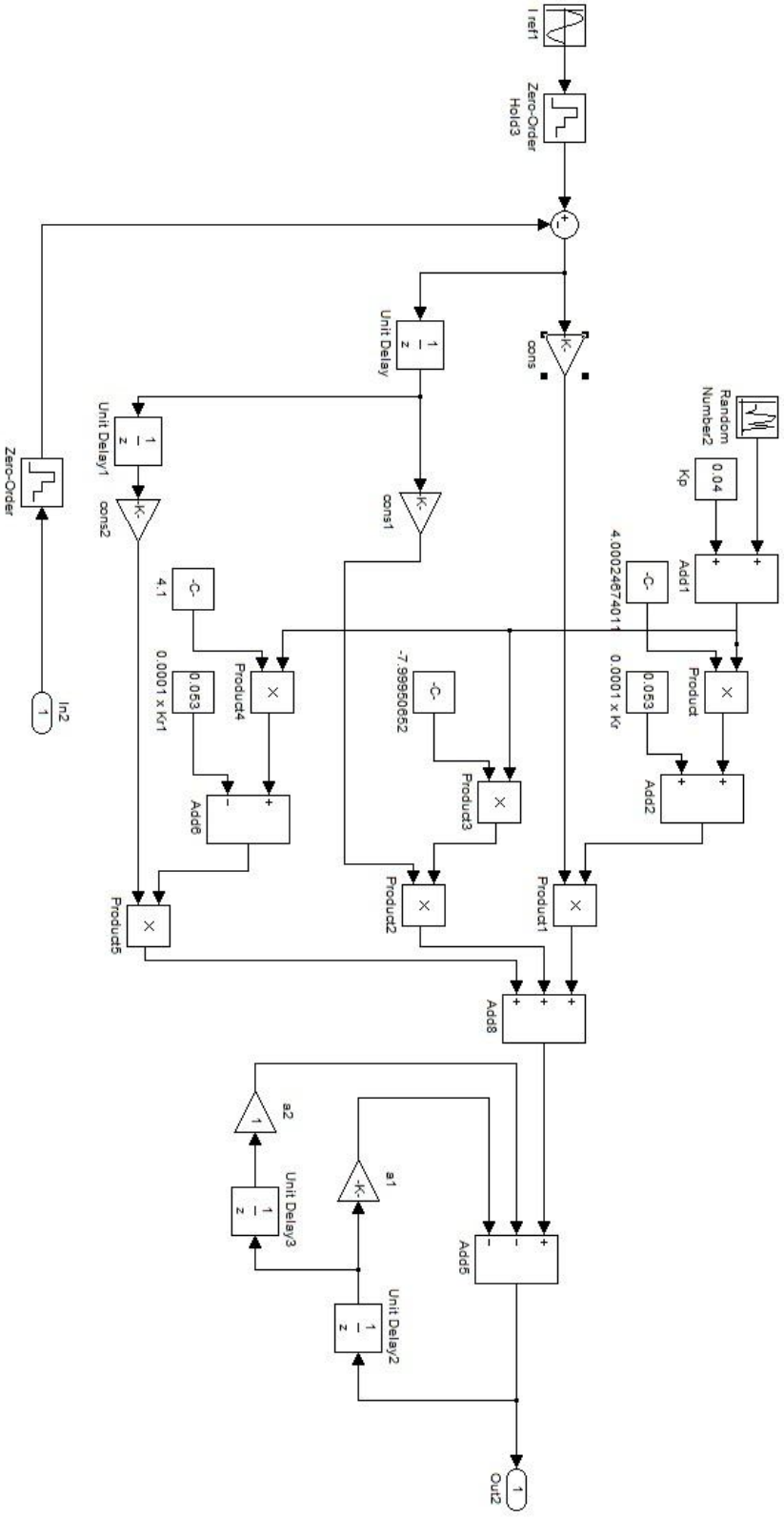

Figure 5-10: Simulink model of current controller using the modified PR control technique.

Based on Figure 5-10, it can be seen that the terms b_o, b_1, and b_2 that are used in the previous PR controller technique has been divided into several other fraction. The main thing to know is that all values in the b_o, b_1, and b_2 terms remain unchanged except for the proportional gain, K_P. This is because, the proportional part for this novel approach, R_{KP} is tuned randomly within a set limit. As illustrated in Figure 5-10, a random number block is used and added to the proportional gain, K_P, to become a new randomized proportional gain, R_{KP} for the controller process; a gain that varies within $K_P \pm 0.001$. The limit is chosen so that the THD as well as the harmonic spectrum of the inverter output current is in acceptable value and shape. Similar to the system with PR control technique, the value for K_P is 0.04 and K_R is 700. Below are the screen shots of the random signal generation.

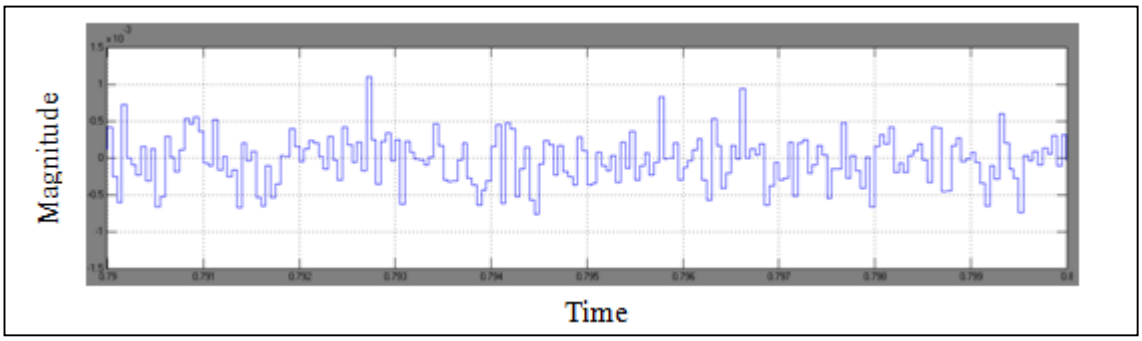

a)

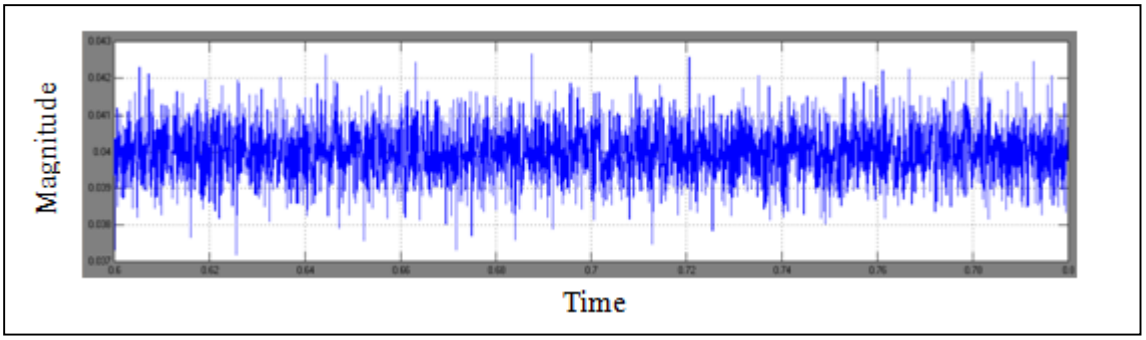

b)

Figure 5-11: Screen shot of (a) Random signal generation of the modified PR controller, and (b) The randomized proportional gain, R_{KP} signal which varies within a set limit.

If a fixed gain is used as for the system with PR current controller, the signal for K_P as in Figure 5-11(b) is maintained at 0.04 at all times. However, with this technique, the

proportional signal is randomly varies between 0.0395 to 0.0405. Beyond this limit, the signal of the inverter output current becomes unstable.

After the simulation of the modified control technique is run, FFT analysis of the inverter output current is once again captured and transferred using Excel. Result can be observed in Figure 5-12. From the figure, some addition and cancellation have occurred to the current harmonic profile as the effect of the randomly varying proportional gain. Most importantly, this addition and cancellation have further reduced the grid current THD from 1.80% to 1.78%. Though it is small, it is a good result where it clearly proves and shows that the modified PR control technique by adjusting the proportional gain randomly within a range that has been set is one important contribution to the knowledge and as a novel current controller for grid connected inverters. There are no extra circuits that need to be added thus no extra burden to the system when using this new technique.

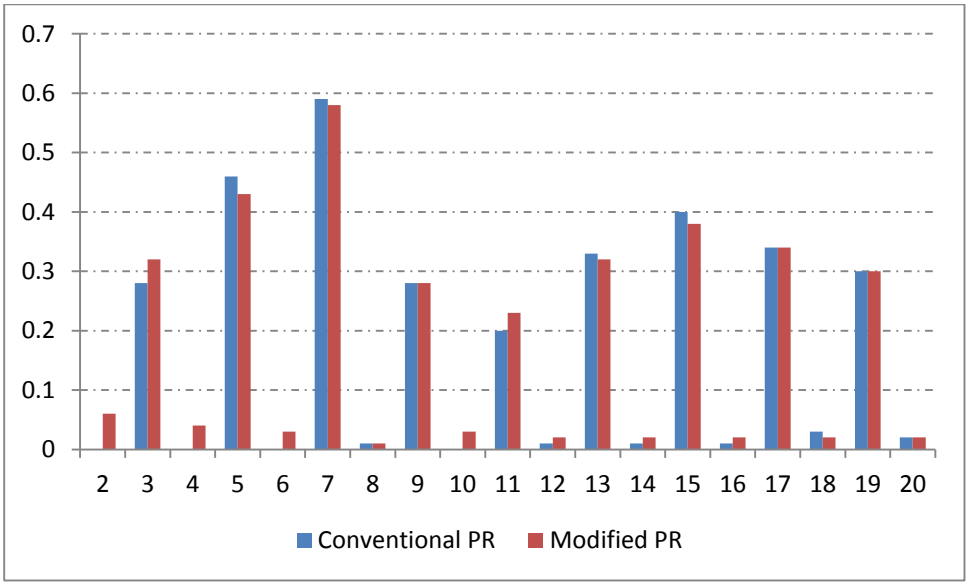

Figure 5-12: Harmonic profile of inverter output current with modified PR current controller shows better outcome compared to the conventional PR current controller.

5.3 Simulation of two grid connected inverters in parallel

The next step is to simulate two inverters in parallel with the grid. This is to prove that with the addition and cancellation of the harmonic trend, the proposed technique can further improved the THD of grid current. The simulation model of the parallel inverter system can be seen in Figure 5-13. The model is first run using the conventional PI

current controller and then followed by the proportional resonance (PR) current controller and the modified proportional resonance current controller. Details of the results are explained next.

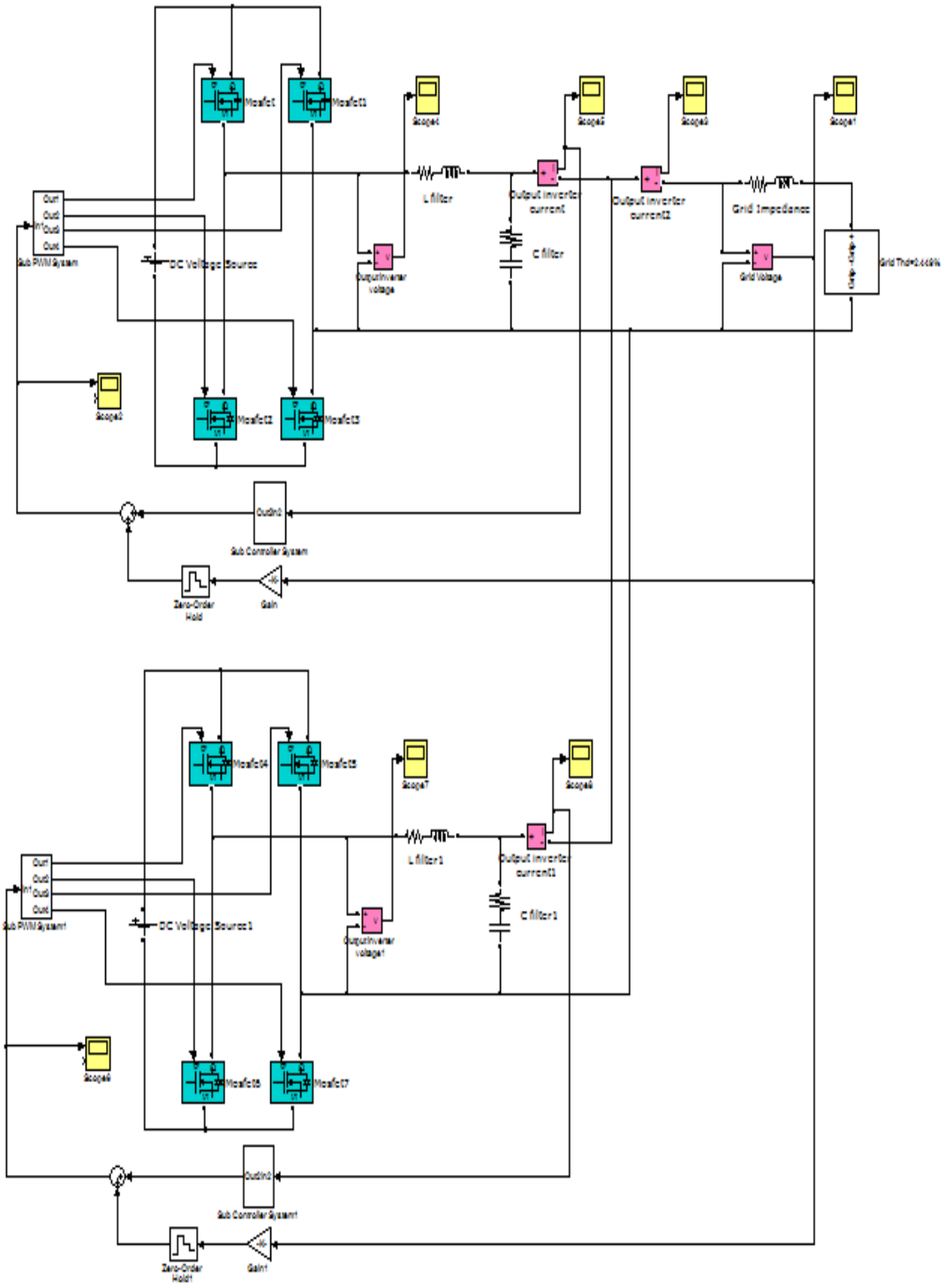

Figure 5-13: Parallel inverter system model.

5.3.1 *Conventional PI Current Controller*

In the simulation, all parameters for the electronic components in both inverter systems remain the same as single inverter system simulation. However, the current controller gains are adjusted by a small amount to optimise the output inverter current. Based on *Kirchoff`s Current Law*, the current injected into the grid is the summation of inverter 1 output current and inverter 2 output current. Therefore, the the grid current is 40 A peak. With greater grid current and fixed grid voltage, the total output power to the supply grid is increased.

In the following results, the simulation model is run for 1.0 s. The time domain waveforms of the signals are captured and downloaded to a personal computer. From this, waveforms and low order harmonic spectra of each individual inverter, and the grid, are post processed using excel. Figure 5-14 shows the error signal between the reference and the actual inverter current for both inverter systems. The output signals for the inverters and the grid together with the low order harmonic profiles are illustrated in Figure 5-15 and Figure 5-16.

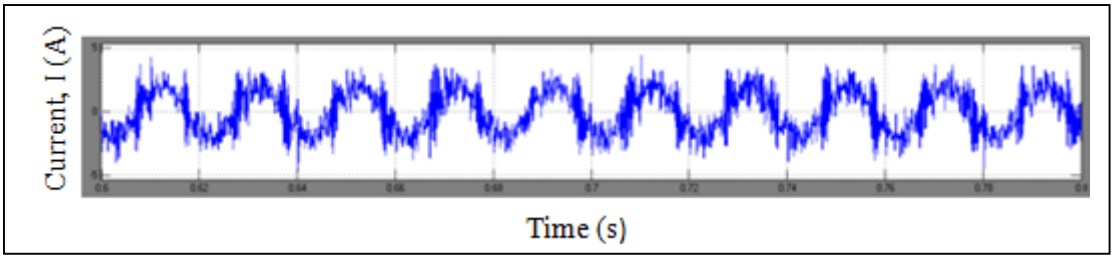

(a)

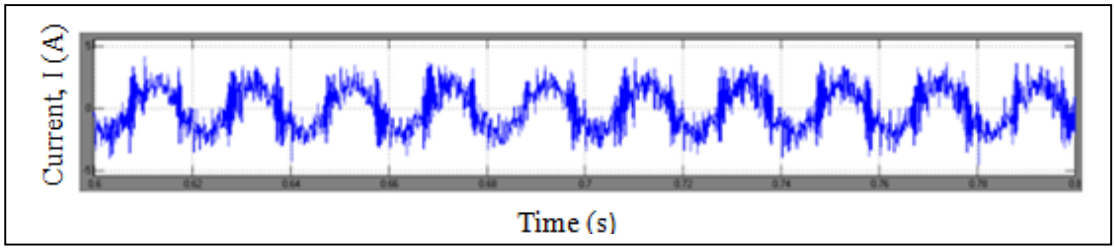

(b)

Figure 5-14: Current error signal of (a) Inverter 1, and (b) Inverter 2, with PI current controller which shows big magnitude errors.

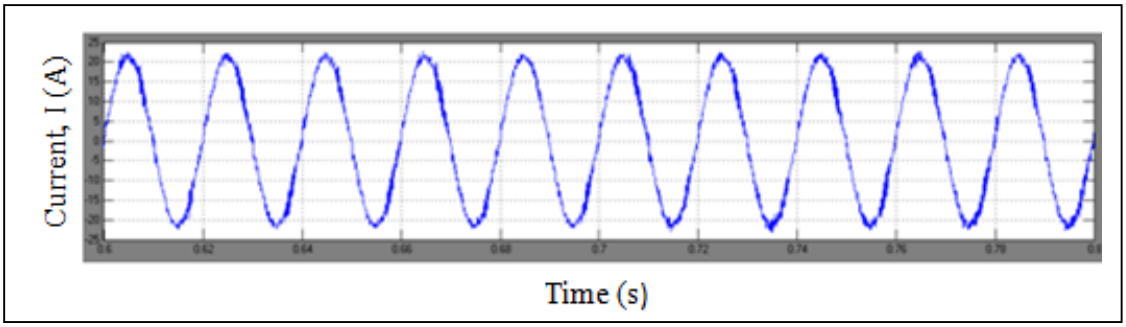

(a)

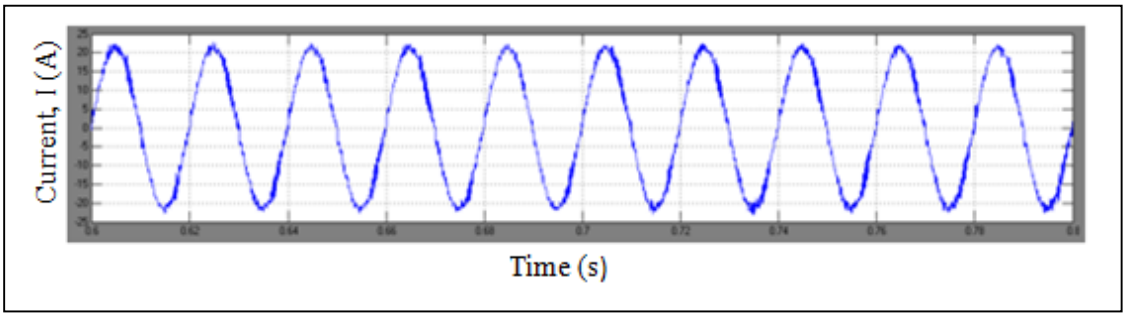

(b)

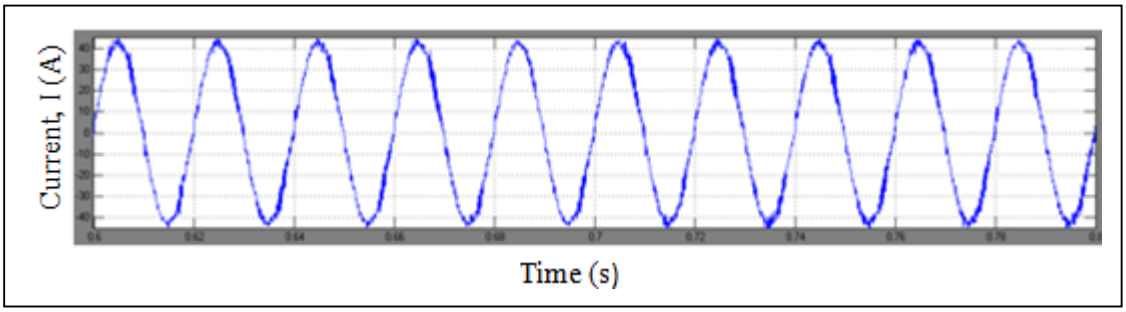

(c)

Figure 5-15: Waveforms of (a) Inverter 1 output current, (b) Inverter 2 output current, and (c) Grid current with PI controller.

From figure 5-15, it can be seen that:

$$I_{grid} = I_{inv1} + I_{inv2}$$

$$= 20 \text{ A peak} + 20 \text{ A peak}$$

$$= 40 \text{ A peak}$$

The low order harmonic magnitude for each inverter current, and overall grid current, is measured using FFT analysis. 10 cycles are taken as a sample for the analysis, between 0.6 s to 0.8 s. Results are shown in figure 5-16 where the harmonic profiles show significant harmonic emissions between the 3rd and 19th order. It is also apparent that a very similar harmonic spectrum exists in each profile.

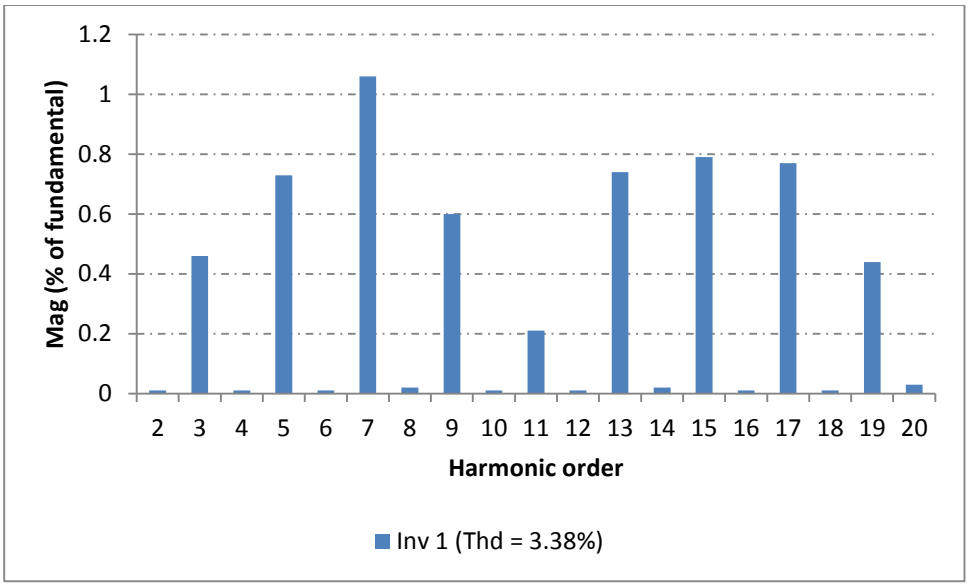
1.2
1
0.8
0.6
0.4
0.2
0
Mag (% of fundamental)
2 3 4 5 6 7 8 9 10 11 12 13 14 15 16 17 18 19 20
Harmonic order
Inv 1 (Thd = 3.38%)

(a)

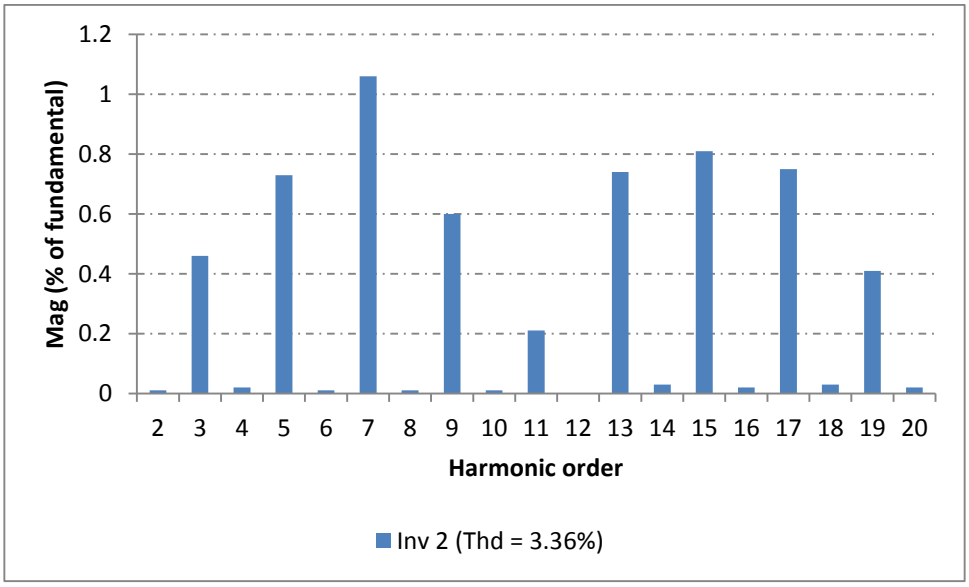
1.2
1
0.8
0.6
0.4
0.2
0
Mag (% of fundamental)
2 3 4 5 6 7 8 9 10 11 12 13 14 15 16 17 18 19 20
Harmonic order
Inv 2 (Thd = 3.36%)

(b)

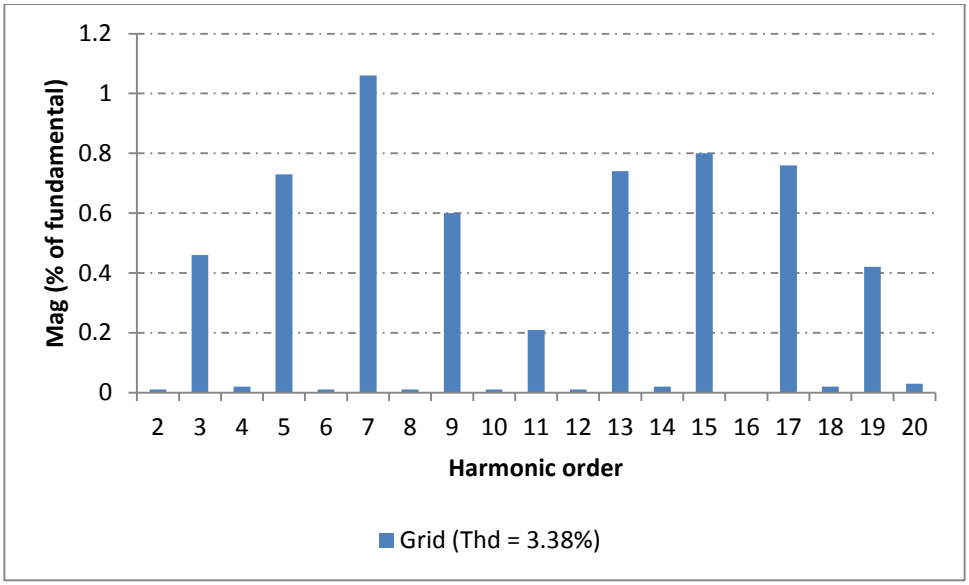

(c)

Figure 5-16: Harmonic profiles of (a) Inverter 1 output current, (b) Inverter 2 output current, and (c) Grid current. All shows significant harmonic emissions between the 3rd and 19th harmonic orders.

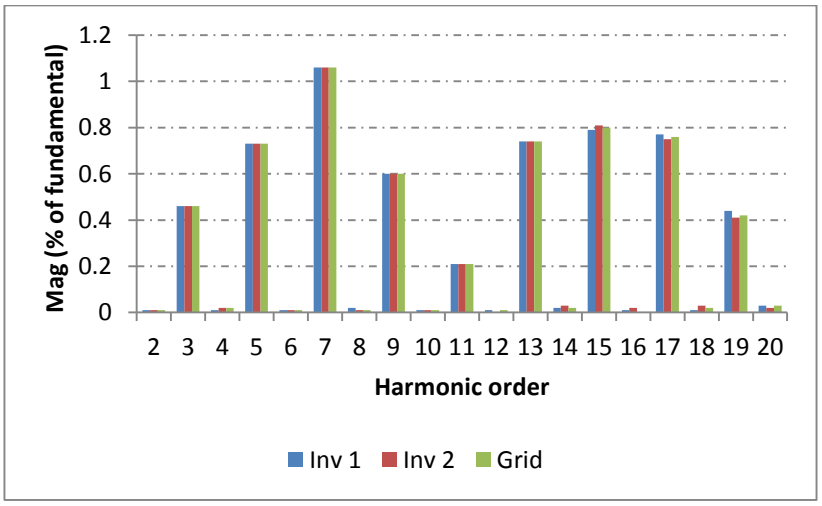

Figure 5-17: Harmonic profiles of inverter 1, inverter 2, and grid current with PI current controller which shows similar harmonic spectrum exists except for the 15th, 17th and 19th order.

5.3.2 *Proportional resonance (PR) control technique*

The next simulation is to run the parallel inverter system using the proportional resonance (PR) control technique. In the simulation model, the parameters for the proportional gain, K_P and the resonant gain, K_R of the controller system are again slightly re-tuned from the single inverter settings to ensure optimum performance is achieved. All waveforms and results are recorded and post processed in Excel. Figure 5-18 shows the error signal between the reference and the actual inverter current for both systems.

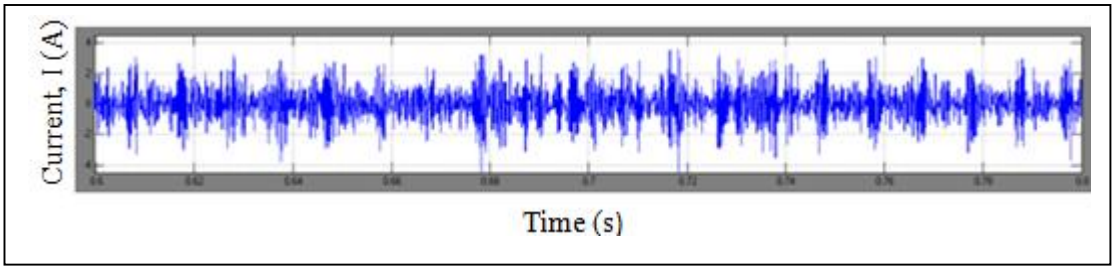

(a)

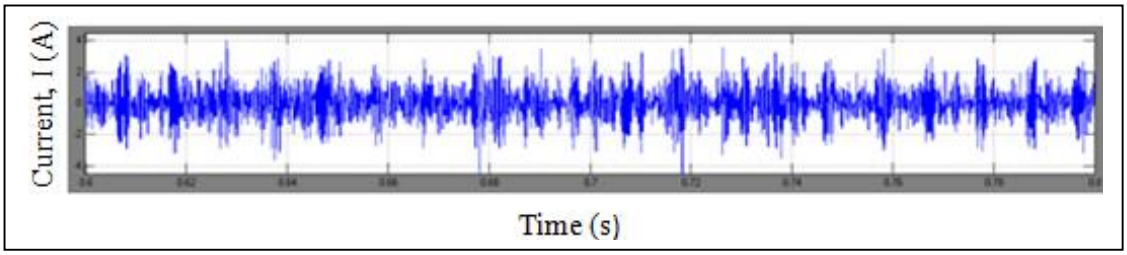

(b)

Figure 5-18: The error signal between reference and the actual current of (a) Inverter 1, and (b) Inverter 2 with PR current controller.

The output current waveforms for each inverter and overall grid current, together with the low order harmonic profiles, can be seen in Figure 5-19.

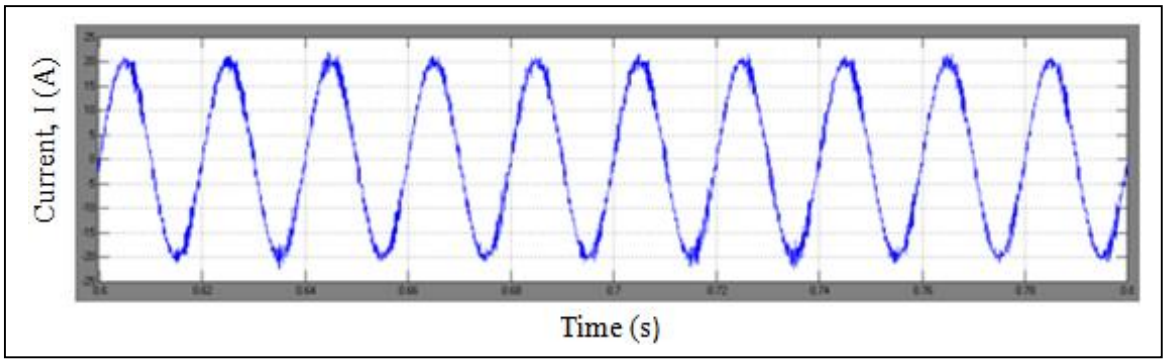

(a)

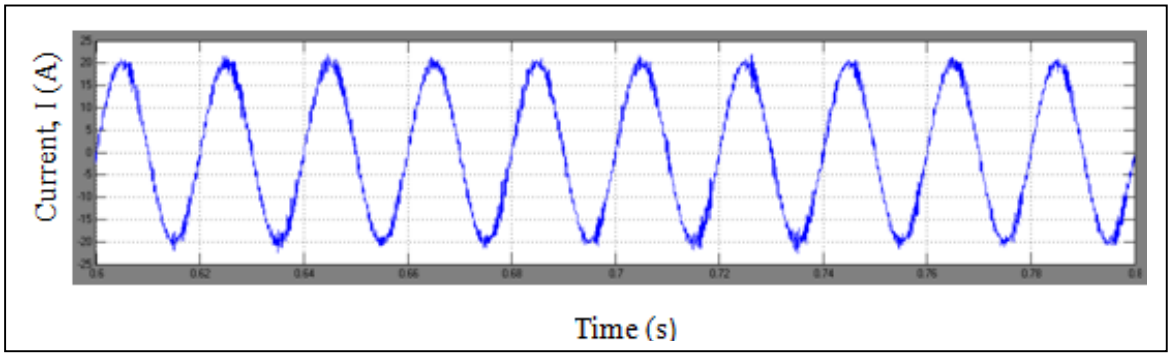

(b)

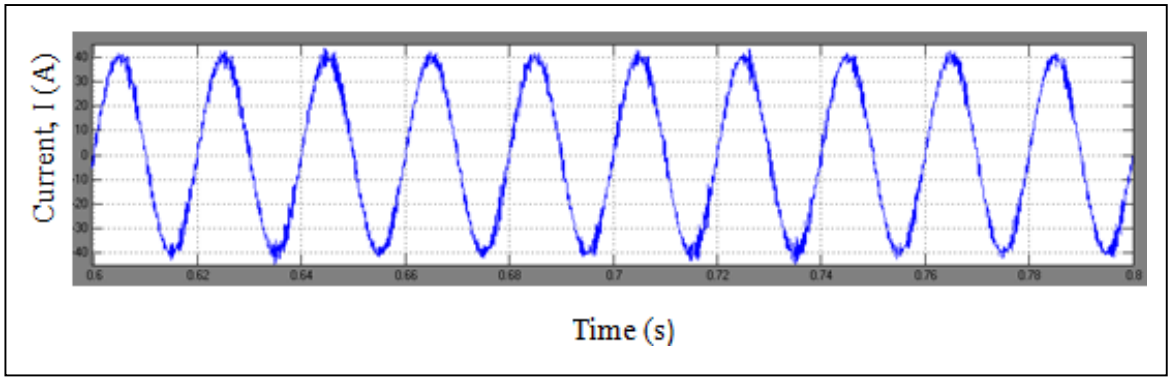

(c)

Figure 5-19: Waveforms of (a) Inverter 1 output current, (b) Inverter 2 output current, and (c) Grid current with PR current controller.

The low harmonic orders for each inverter current and grid current is again measured using FFT analysis and 10 cycles are taken as a sample for the analysis, starting from 0.6 s to 0.8 s. The graphs are then transferred to Excel as shown in Figure 5-20.

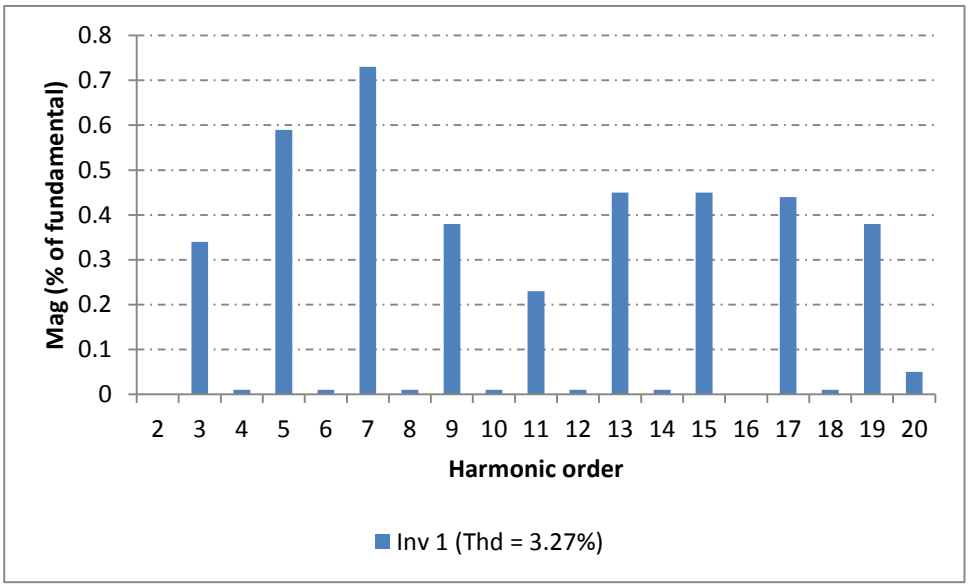
0.8
0.7
0.6
0.5
0.4
0.3
0.2
0.1
0
Mag (% of fundamental)
2 3 4 5 6 7 8 9 10 11 12 13 14 15 16 17 18 19 20
Harmonic order
Inv 1 (Thd = 3.27%)

(a)

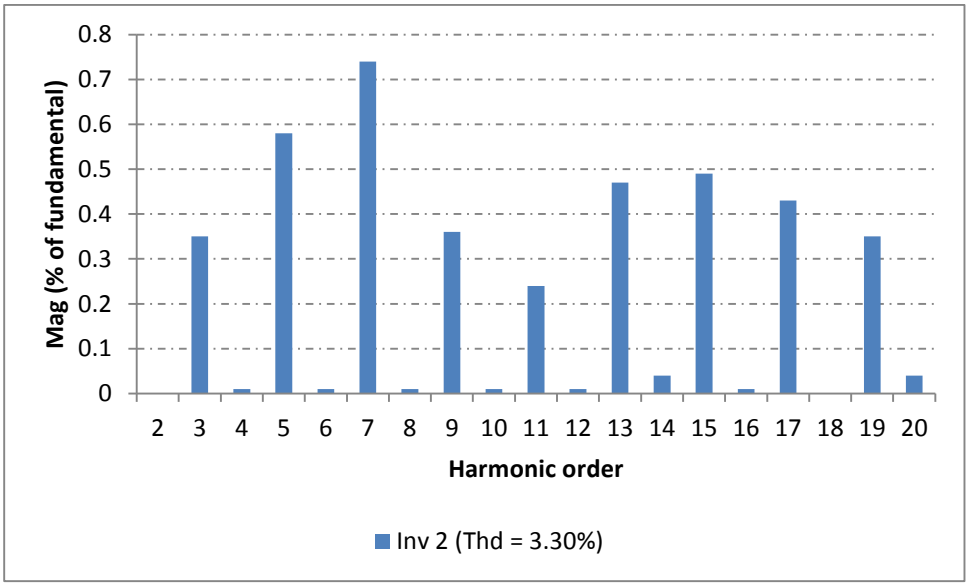
0.8
0.7
0.6
0.5
0.4
0.3
0.2
0.1
0
Mag (% of fundamental)
2 3 4 5 6 7 8 9 10 11 12 13 14 15 16 17 18 19 20
Harmonic order
Inv 2 (Thd = 3.30%)

(b)

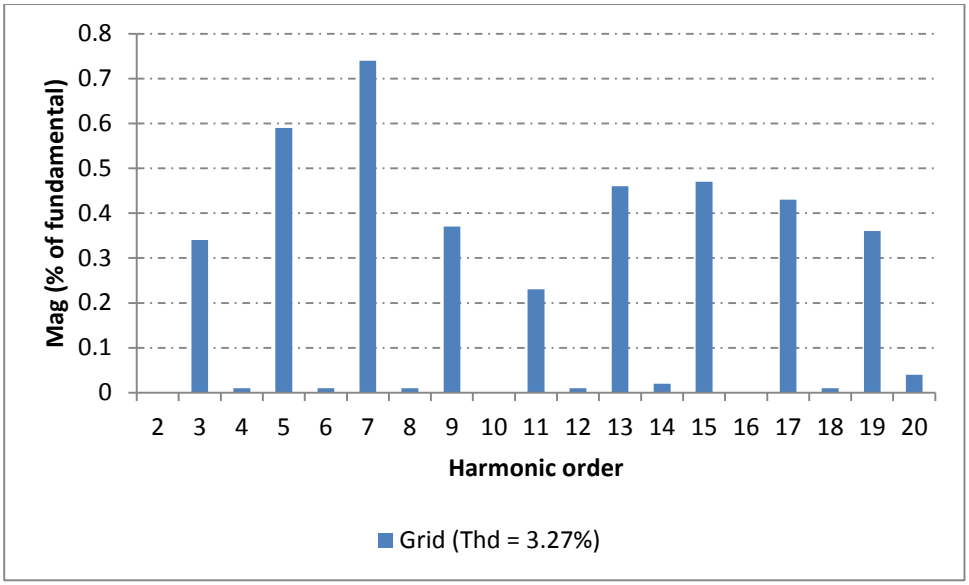

(c)

Figure 5-20: Harmonic profiles with the respective per unit magnitude of (a) Inverter 1 output current, (b) Inverter 2 output current, and (c) Grid current.

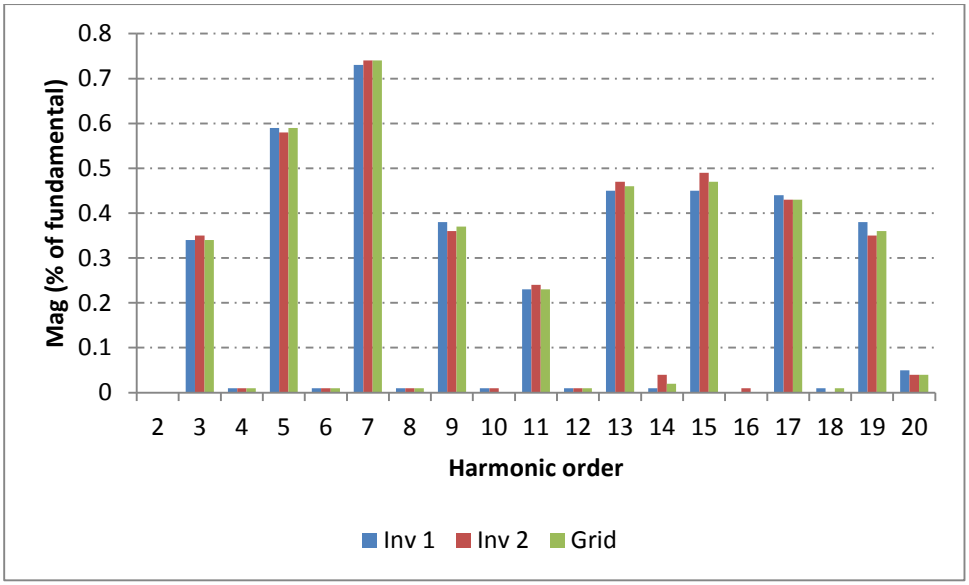

Figure 5-21: Harmonic profiles of Inverter 1, Inverter 2, and Grid current with PR controller in one graph shows harmonics addition and cancellation occurred.

From Figure 5-21, it can be clearly seen that there is some addition as well as cancellation of the harmonic magnitude. For instance, the 3rd and 5th harmonic order magnitudes of inverter 1 output current are 0.34 and 0.59 respectively but the same harmonic order magnitudes of inverter 2 output current are 0.35 and 0.58 respectively. The effect of this controller technique can also be observed on all the low harmonic orders. For that reason, the harmonic profile of the grid current is also affected resulting in an improvement to the grid current THD that is 3.27%; a reduction of approximately 3.25% from the previous parallel inverters simulation when using the conventional PI current controller.

5.3.3 *Modified PR Control Technique*

For this simulation, the modified proportional resonance control technique is applied. In the simulation model, the parameters for the proportional gain, K_P and the resonant gain, K_R of the controller system remain the same as the value used in the second technique. However, the proportional gain is randomly adjusted within a set limit, as explained in section 5.2.3. The model is again run for 1.0 s and all waveforms and results are recorded once again. Figure 5-22 shows the error signal between the reference and the actual inverter current for both inverter systems.

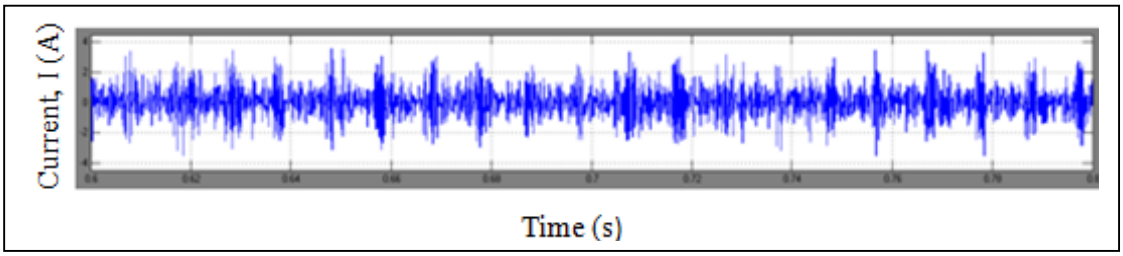

(a)

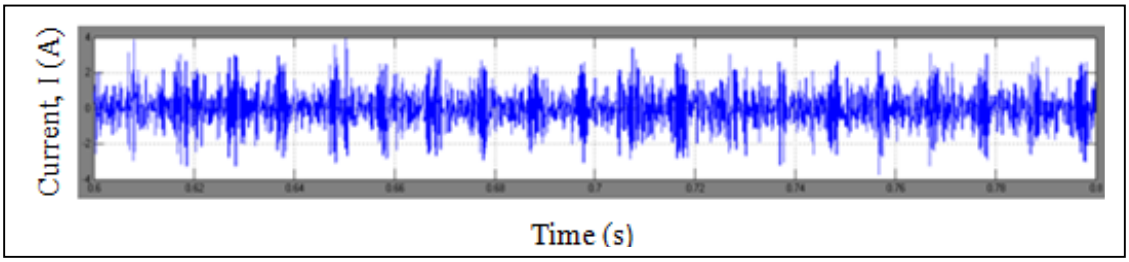

(b)

Figure 5-22: The error signal between reference and the actual current of (a) Inverter 1, and (b) Inverter 2 with modified PR current controller.

The output current waveforms for each inverter, and the grid current, are shown in Figure 5-23.

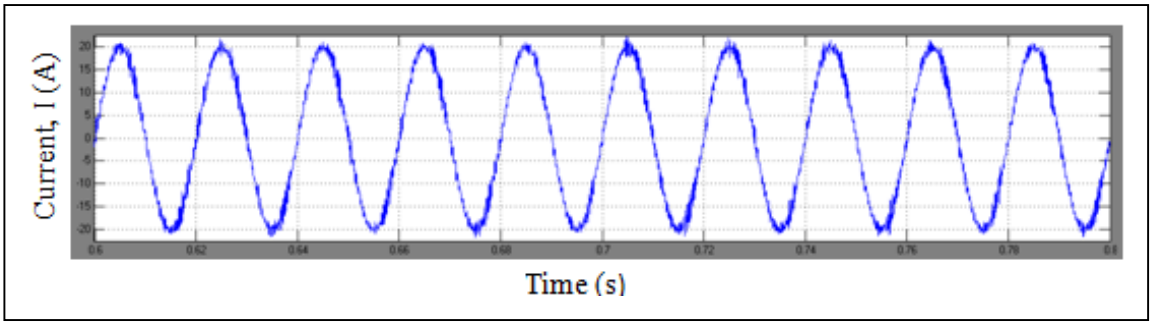

(a)

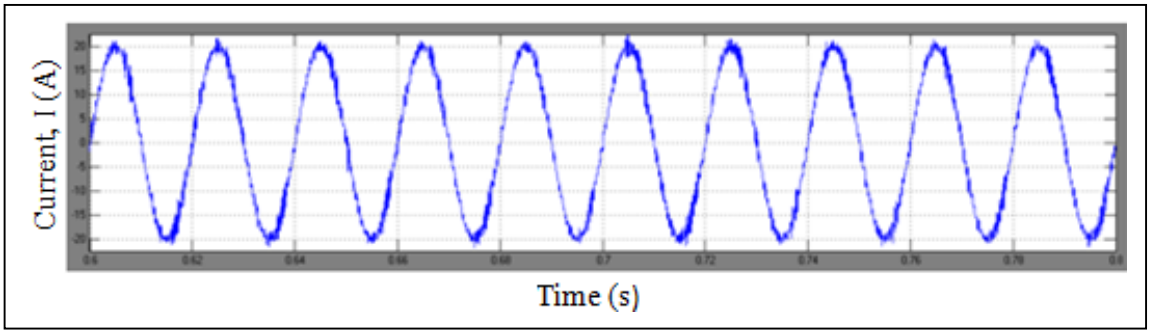

(b)

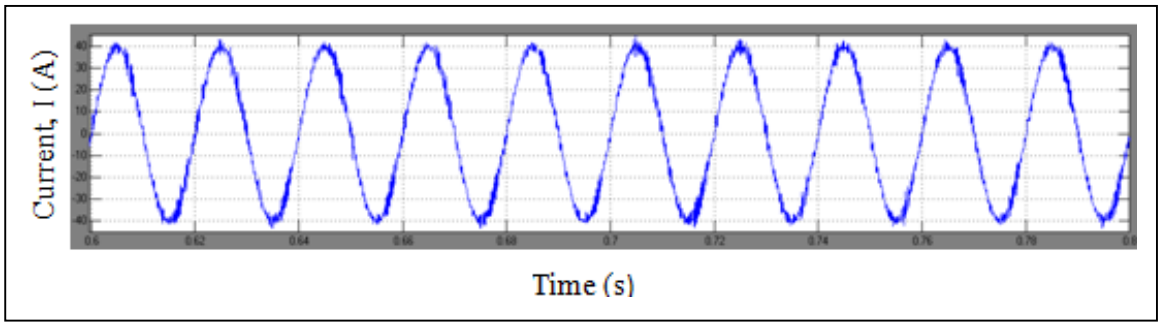

(c)

Figure 5-23: Waveforms of (a) Inverter 1 output current, (b) Inverter 2 output current, and (c) Grid current with modified PR current controller.

The low harmonic orders for each inverter current and grid current is again measured using FFT Analysis. 10 cycles are taken as a window for the analysis, between 0.6 s to 0.8 s. The data is then transferred to Excel, as shown in Figure 5-24.

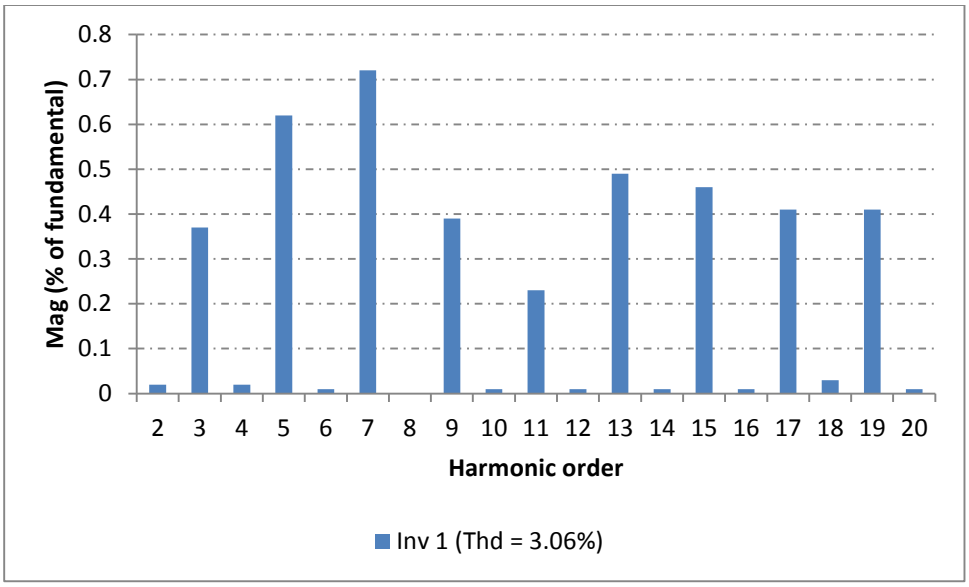
Mag (% of fundamental)
0.8
0.7
0.6
0.5
0.4
0.3
0.2
0.1
0
2 3 4 5 6 7 8 9 10 11 12 13 14 15 16 17 18 19 20
Harmonic order
Inv 1 (Thd = 3.06%)

(a)

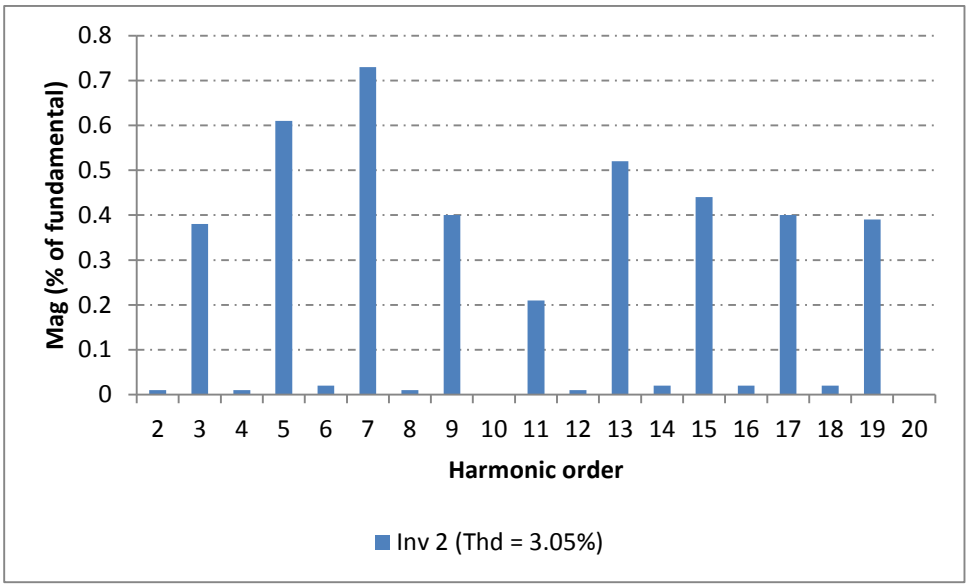
Mag (% of fundamental)
0.8
0.7
0.6
0.5
0.4
0.3
0.2
0.1
0
2 3 4 5 6 7 8 9 10 11 12 13 14 15 16 17 18 19 20
Harmonic order
Inv 2 (Thd = 3.05%)

(b)

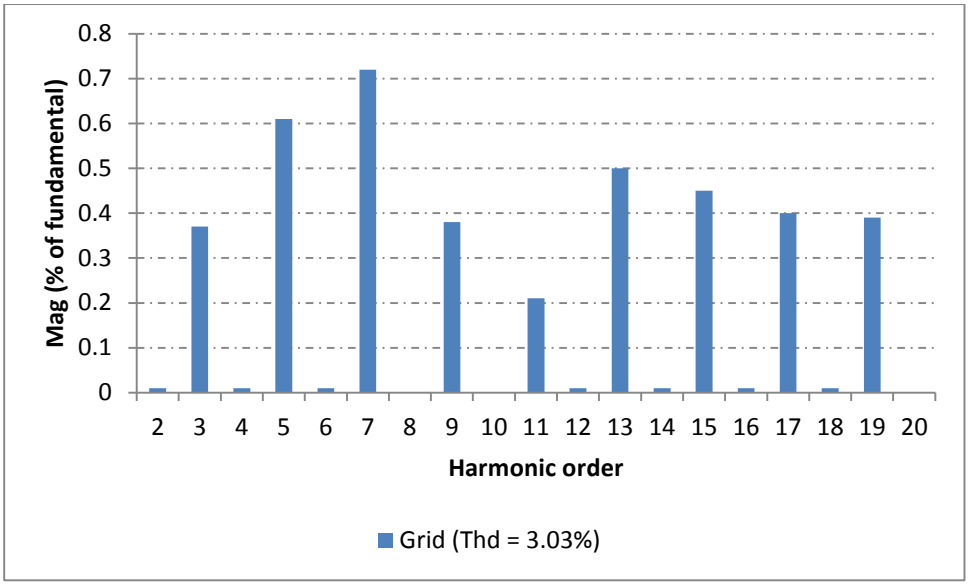

(c)

Figure 5-24: Harmonic profiles with the respective per unit magnitude of (a) Inverter 1 output current, (b) Inverter 2 output current, and (c) Grid current.

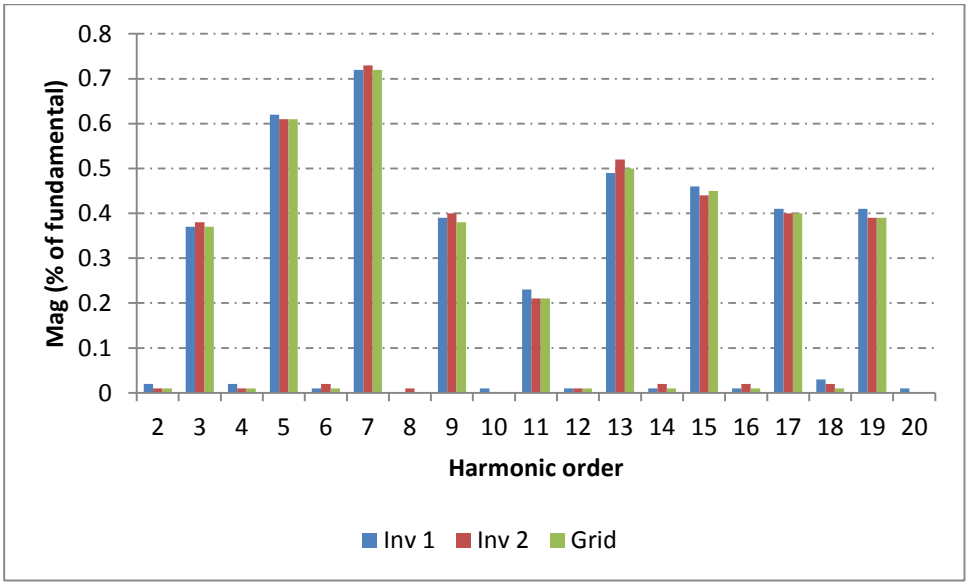

Figure 5-25: Harmonic profiles of inverter 1, inverter 2, and grid current with modified PR controller shows harmonic cancellation and addition leading to a further THD reduction compared to the PR current controller technique.

The grid current THD observed is 3.03% which shows a further improvement compared to the previous simulation when using the proportional resonance controller

technique alone. This also proves that the latter technique works even better when two inverters are connected in parallel to the grid. This is because when a single inverter system is run using the PR and the modified PR control technique which involves the randomized gain in the controller system, the THD improvement observed is approximately 1.1%. However, when two inverter systems are run in parallel using the same techniques, the THD improvement observed is approximately 7.3%. The next following figure compares the harmonic spectrum of the grid current when each controller technique is applied to the parallel inverter system.

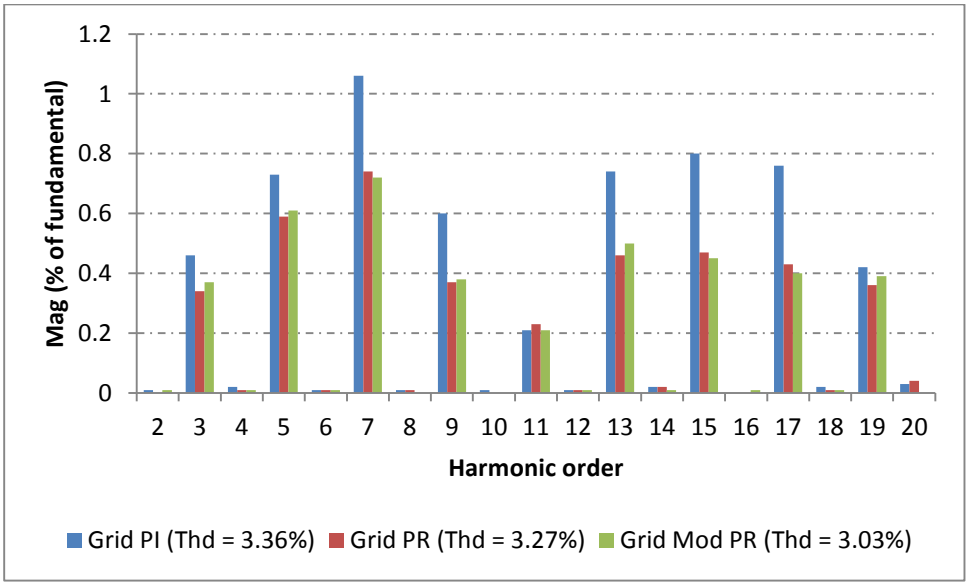

Figure 5-26: Current harmonic profile using PI, PR and modified PR controllers. THD of grid current with modified PR controller shows the lowest value.

From Figure 5-26, it is noticed that a reduction in the overall harmonic content occurs when using the proportional resonance and modified proportional resonance technique, compared to using the conventional PI control technique. When a random signal is added to the proportional gain of the PR controller, a random interaction occurs between the inverters, resulted in a time-varying harmonic spectrum. The simulation results provide a basis for verifying the control technique experimentally.

5.4 Chapter Summary

This chapter compares simulation results for a single, and parallel, operated grid connected inverter system. The impact of three different control schemes have been compared; conventional PI, conventional PR and random parameter variation PR. Results show that in a single inverter system, a THD reduction by 1.1% in the grid current can be achieved with the random parameter PR scheme. Further improvement is observed in the parallel connected inverter system, where a significant 7.3% THD reduction is observed. The research in this chapter has shown for the first time that, in simulation, it is possible to reduce the low order harmonic content of a parallel connected inverter system by utilising a random parameter PR control scheme.

Chapter 6: Experimental Results of Stand Alone Inverter

6.1 Chapter Introduction

This chapter starts by describing the software and hardware used in this research project. Following this, experimental results from applying the three different control methods described in Chapter 4 to a stand-alone inverter system is shown. Finally, a comparison of the results is presented, and conclusions are drawn.

6.2 General Hardware Description

Different tools i.e. the software and hardware are used for the purpose of this research project. The software includes the Multisim and Ultiboard for designing the circuits and the layout boards as well as the Code Composer Studio (CCS) for programming. In total, five PCB boards need to be designed and made. They are the inverter board, the current measurement board, the voltage measurement board, the gate driver board and the DSP interface board. The screen shot of the boards can be seen in Appendixes. To cut a bit of time for this research project, only the inverter board need to be designed in the Multisim and Ultiboard. All the other four boards were designed by a previous student who had the same area of research and they are allowed to be used in this project.

6.2.1 *Inverter Board*

The power inverter board uses four 100 V TO-220 case style Mosfets. The inverter board is then connected to a low pass output filter. The schematic diagram of the power inverter board and filter is shown in Figure 6-1.

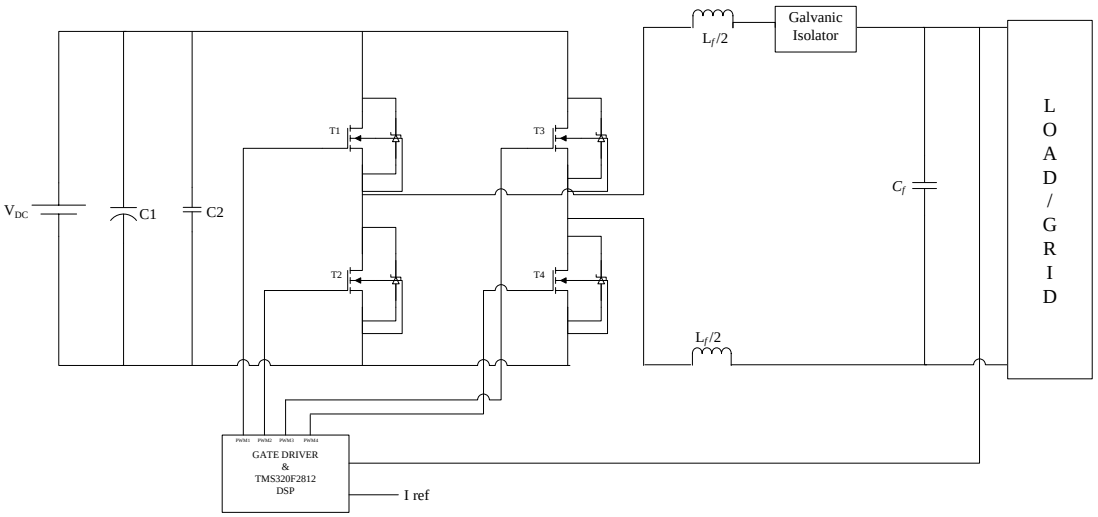

Figure 6-1: Schematic diagram of power inverter board.

6.2.2 *TMS320F2812 Digital Signal Processor*

A Texas Instruments ezDSP, TMS320F2812, processor board is used for this work. This system has four major interface blocks; the parallel port controller interface, the external JTAG interface, the analogue expansion interface and the I/O expansion interface. The block diagram of the eZdsp^{TM} F2812 chip can be seen in Figure 6-2 [81]. The description of all the blocks functions are as follows:

a) Parallel port controller interface – connects to the communication environment such as Code Composer Studio (CCS).

b) External JTAG interface – the emulators interface to the DSPs.

c) Analogue expansion interface – connects to the analogue input for digital conversion purposes.

d) I/O expansion interface – used to get the input and output signals from the DSP.

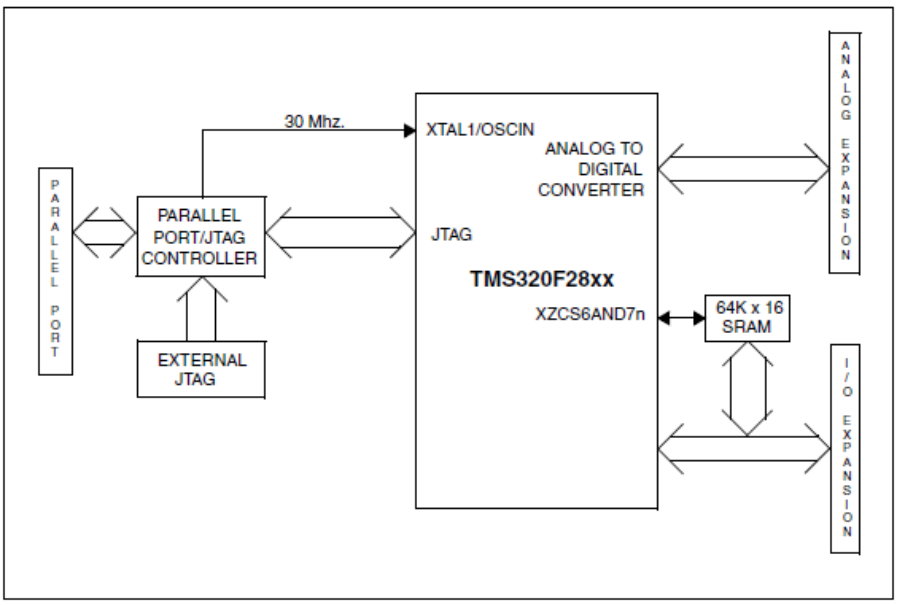

Figure 6-2: Block diagram of the eZdsp^{TM} F2812 [81].

6.3 PI Experiments and Results

As stated in the earlier chapter, this research is concerned with two inverter systems operating in parallel. However, before any further experiments are done, each inverter system need to be tested with a resistive load at the output. This is also known as a stand-alone inverter where no connection with the grid is made. Initially, one of the inverters (Inverter 1) is tested with a conventional PI current control loop. Output waveforms are taken from a normal oscilloscope and the FFT of the harmonic current is taken from a power analyzer which is then transferred to Excel to get the graph. All tests in this stand-alone mode used a 25 V DC supply with a 3 A peak current demand and 5 Ohms resistive load at the end. In order to get the best proportional and integral gains for the system, the software is run with different gain values each time. The purpose is to observe which gain values can get the best output waveform with the best total harmonic distortion (THD) value. Using trial and error method, the optimum value for the proportional gain K_P is 1.6 and the optimum value for the integral gain K_I is 0.275. Figure 6-3 and Figure 6-4 are the screen shots of the current output waveform and the respective FFT for the gains stated with the scope set to 1 A per division.

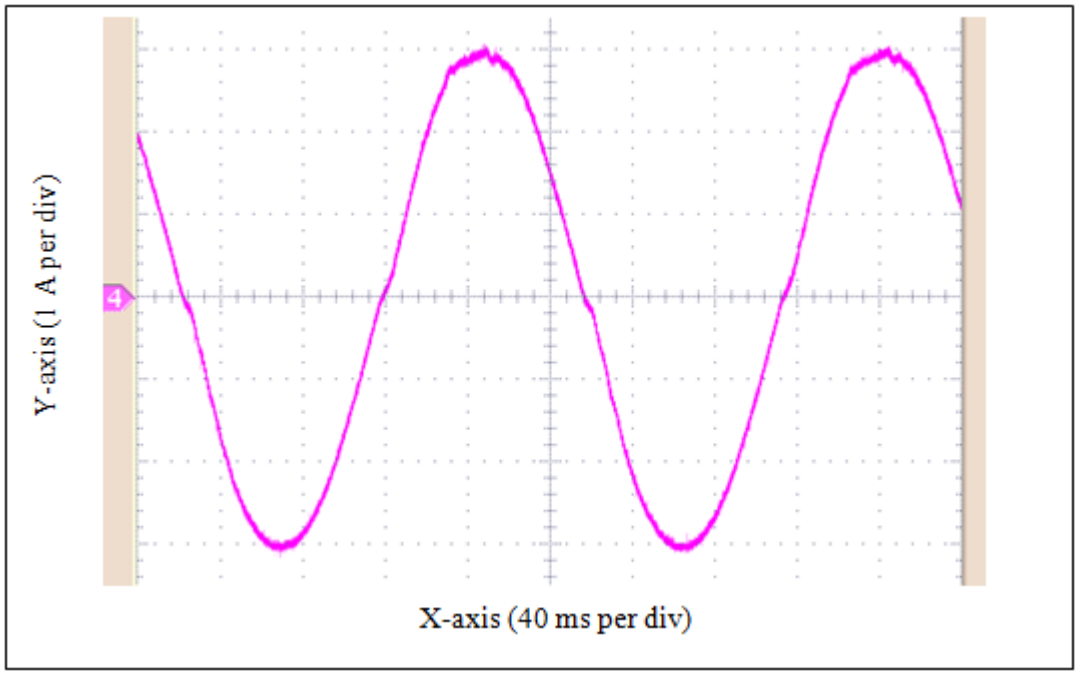

Figure 6-3: Screen shot of current output waveform.

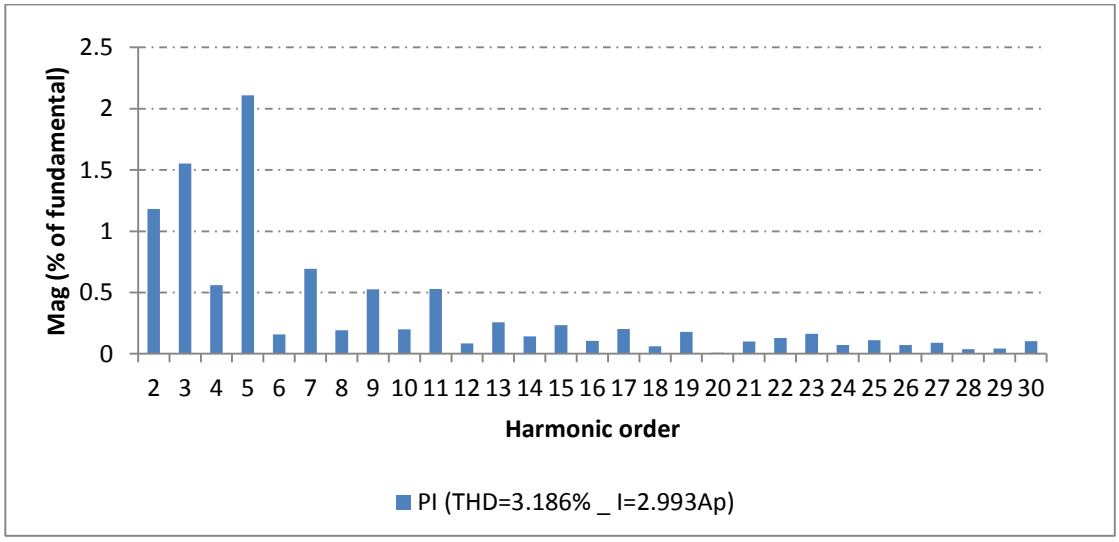

Figure 6-4: FFT of output current.

6.3.1 *Dead time Effect and Its Compensation*

From Figure 6-3, it can be seen that whenever the current crosses the zero line, a small distortion occurred which is known as the PWM dead time effect. Dead time is a short time delay that is applied in the PWM switching to avoid the switches from turning on or off at the same time. It is discussed briefly in Appendix. The effect of dead time is

normally seen at the output waveform as can be seen above. To compensate the effect of dead time to the output results, an adjustment in the software is made. This is done by adding a particular value based on the dead time value used in the PWM switching. In this project a dead time used in the PWM switching is 1.7 µs which is around 3% of the switching time. For the purpose of the compensation, this time delay in per unit need to be multiplied by the maximum magnitude of the modulating signal and then be added to the current controller output. To observe the effect of the dead time compensation to the output waveforms, a test is done with a variable dead time compensation unit of 0.00, 0.01, 0.02, and 0.03 using the same K_P and K_I gain for all tests. Below are the screen shot of the current output waveforms when each of the dead time compensation unit is used in the test.

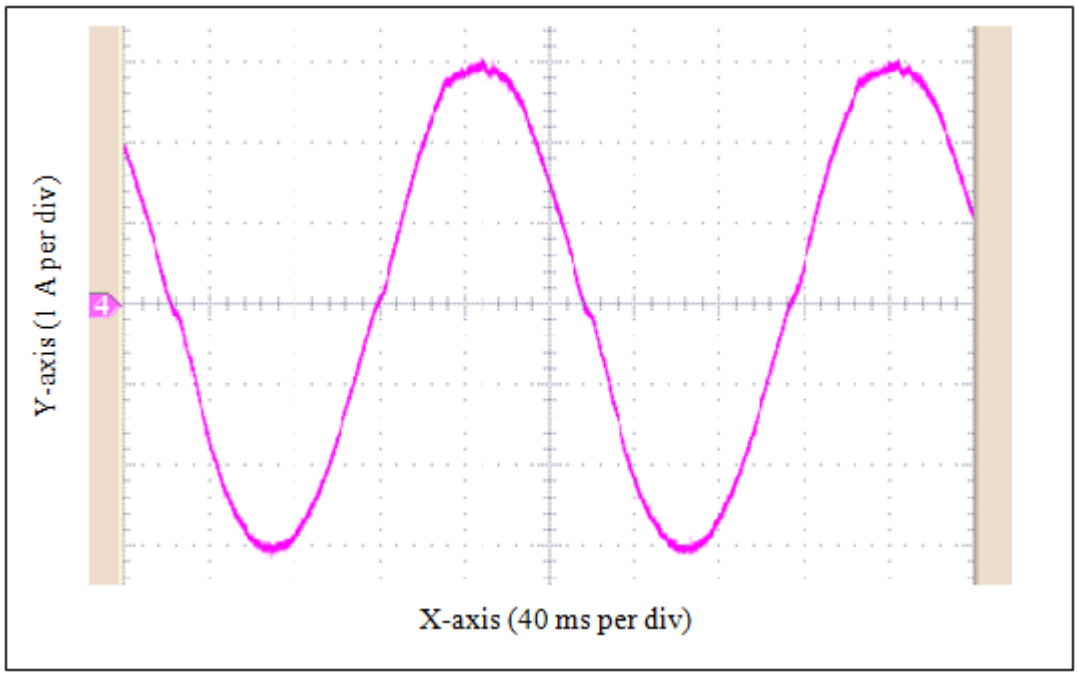

(a) dead time compensation unit of 0.00.

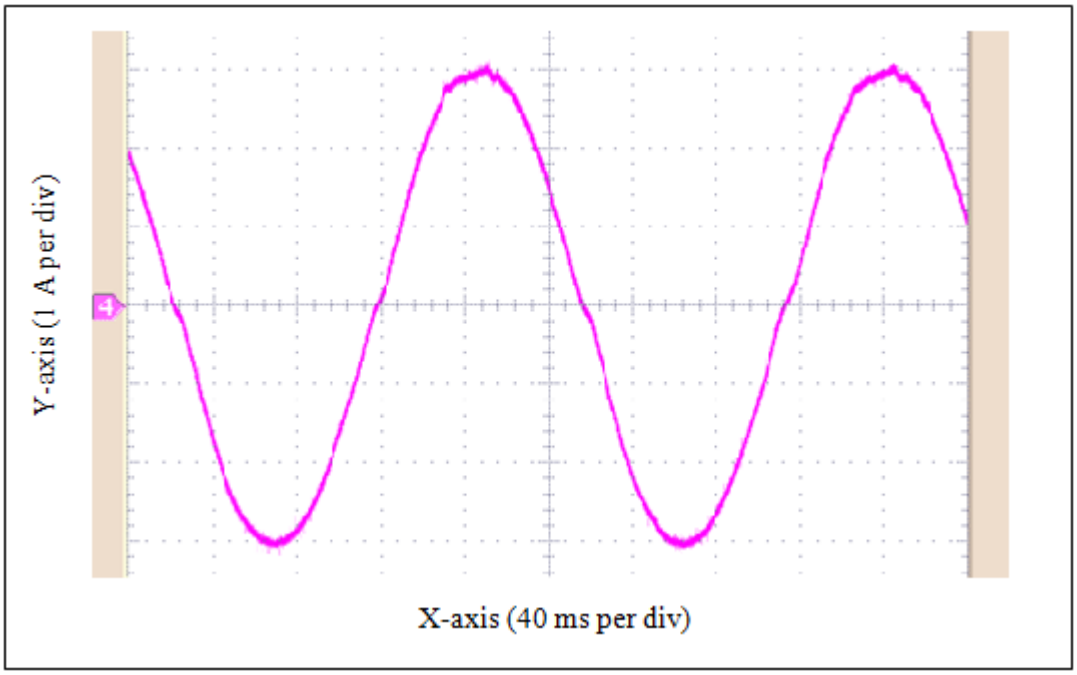

(b) dead time compensation unit of 0.01.

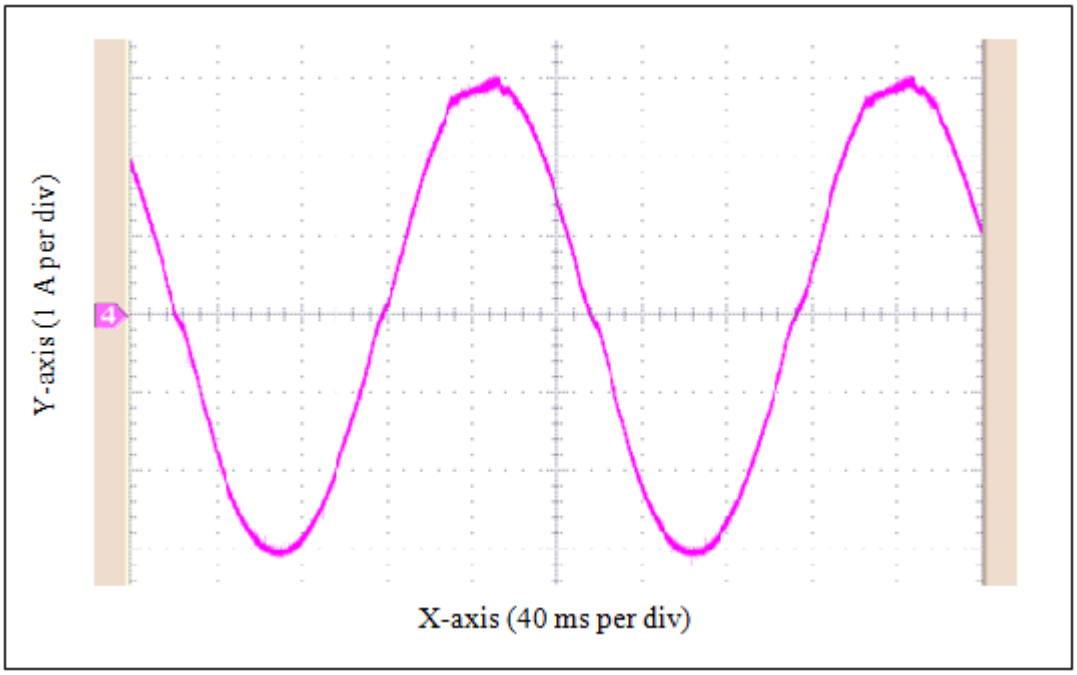

(c) dead time compensation unit of 0.02.

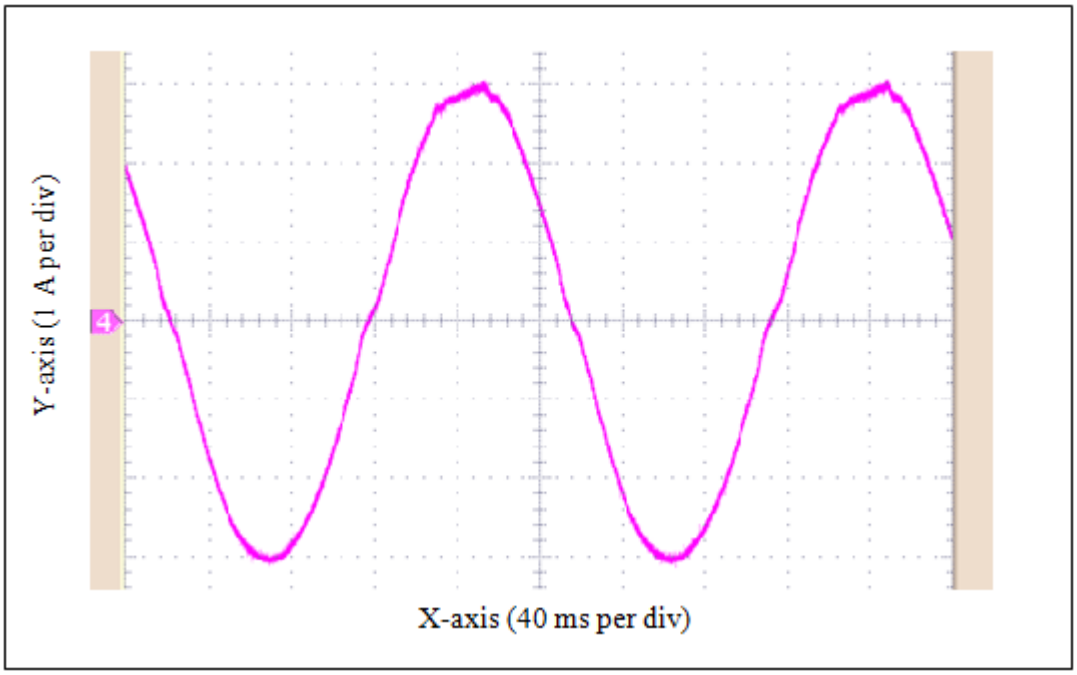

(d) dead time compensation unit of 0.03.

Figure 6-5: Screen shot of the output current waveform with (a) dead time 0.00, (b) dead time 0.01, (c) dead time 0.02, and (d) dead time 0.03.

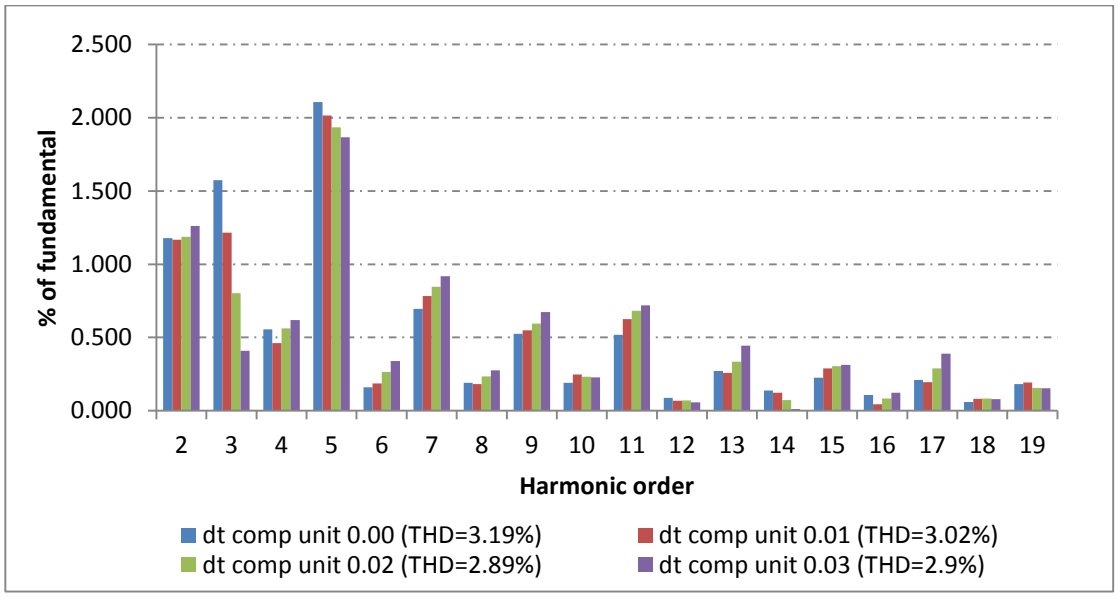

Figure 6-6: Output current FFT for different dead time compensation unit.

Comparing the output waveforms shown in Figure 6-5 above, it is apparent that the output waveform with a dead time compensation unit of 0.03 gives the best waveform of the four. It is clearly seen when the output current reaches zero value where the

distortion is much reduced. Following the figures is the FFT of all four states in one graph for easy comparison. The observed reduction of the distorted waveforms in Figure 6-5 is agreed by the finding results from the FFT analysis shown. As the dead time compensation unit is increased by 0.01, the THD of the output current can be decreased. In addition, the 3rd and the 5th harmonic orders which is known as the hardest order harmonics magnitude to be reduced is reduced in this case. Although the output current THD when using the dead time compensation unit of 0.03 is slightly bigger by 0.01% than output current THD when using the dead time compensation unit of 0.02, the 3rd as well as the 5th harmonic orders of the former are well reduced. These findings conclude that the dead time compensation unit of 0.03 will be used in other test of PI current controller later on.

6.3.2 *Zero Crossing Detection (ZCD)*

In real life, the inverter system is connected to the supply grid to support users demand. For that reason, the current injected from the inverter system must be in phase and synchronised with the current in the supply grid. Moreover, in order to connect several inverter systems in parallel to the same point in the supply grid, the same condition must be met. This is achieved by applying a zero crossing detection (ZCD) in the overall system. For the purpose of completing this research project, a readily available ZCD circuit is used. This circuit consists of step down transformer (240V: 9V); to reduce the grid voltage to a significantly lower voltage to interface with digital interface electronics. This interface comprises of a low pass filter; to filter out noise that can cause false reading of the ZCD, a transceiver; to create rectangular pulse, and a comparator; to compare the filtered voltage with the DC offset. Using an oscilloscope, the output waveform from the ZCD circuit together with the inverter output current is observed and can be seen in Figure 6-7. This output is then interfaced to the DSP. In this research work, each power electronic inverter under investigation is synchronised using its own Zero Crossing Detector Unit and DSP. In this way, each inverter unit operates fully independently as would be the case in a commercial system. For this reason, there are no abnormal synchronisation issues created due to the experimental setup.

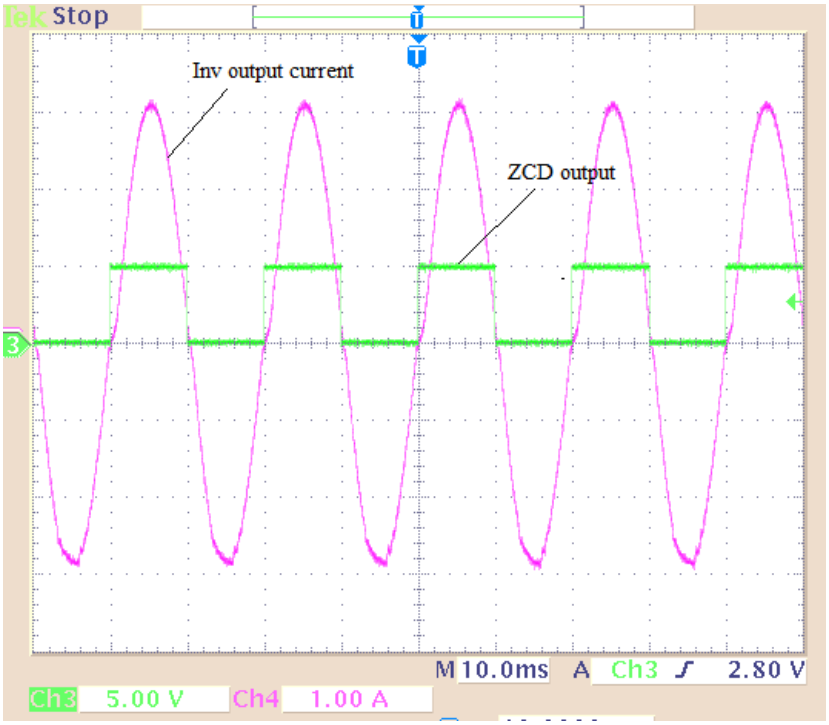

Figure 6-7: Output waveforms of ZCD and inverter system in phase.

6.3.3 *Results on Inverter 1 system*

Before a parallel inverter system is tested, experiments are done for each separate inverter. In this research, Inverter system 1 is tested first and results are recorded.

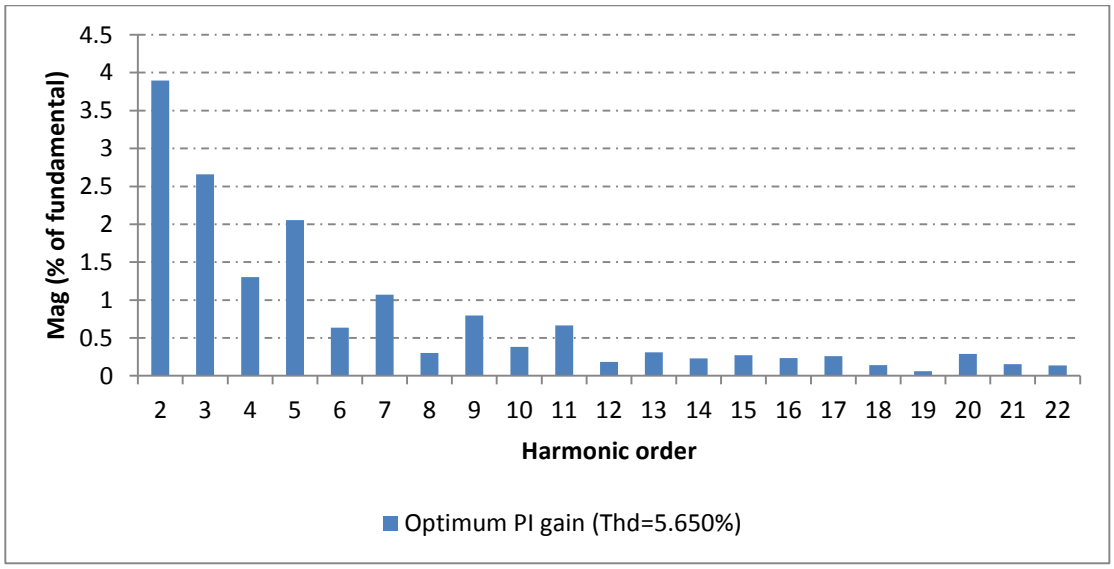

Figure 6-8: Harmonic data of inverter 1 output current.

Figure 6-9 shows the screen shot of the output current and the error between the current demand and the actual current.

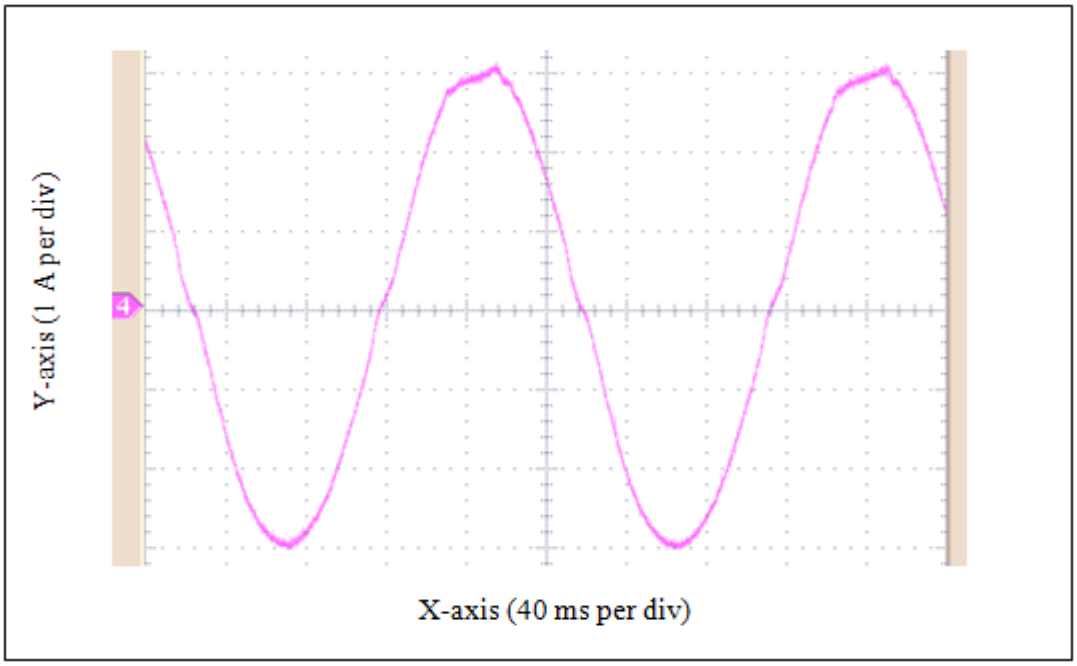

(a)

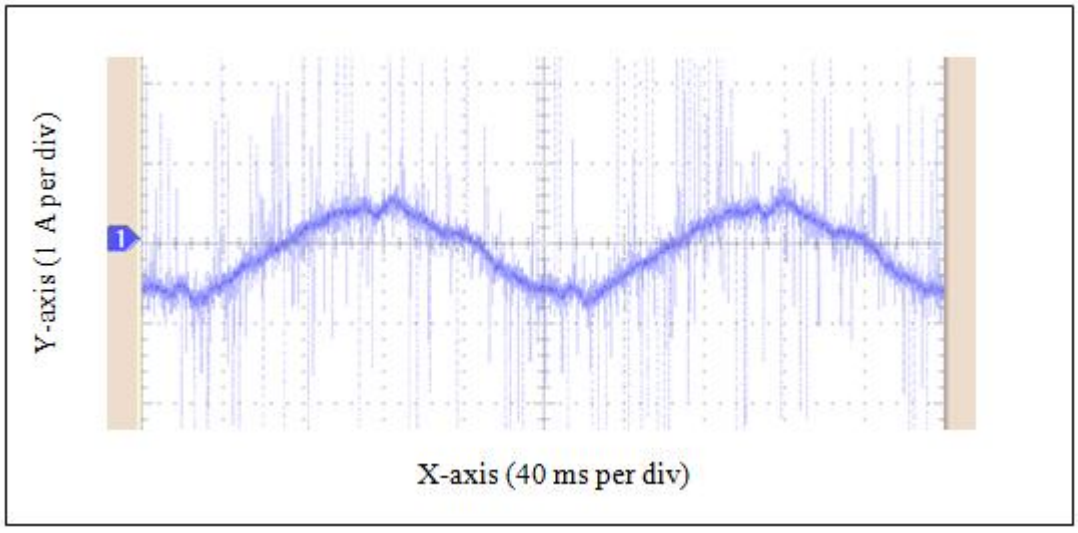

(b)

Figure 6-9: Screen shot of (a) Inverter 1 output current, and (b) Inverter 1 current error.

The software is set to have a dead time compensation unit of 0.03 and a ZCD is connected into the system. The DC input voltage is fixed to 30 V and the resistive load value used is approximately 5 Ohm. The power analyzer is set so that the output current FFT analysis is done by taking an average of 16 fundamental current cycles. The proportional gain, K_P and the integral gain, K_I are tuned once again to acquire the best possible output current with the best THD. For that reason, the chosen K_P and K_I value is 2 and 0.35 respectively. During the tuning process, from the observation of the waveforms and the FFTs, a further increment as well as decrement in the proportional gain, K_P will push the waveform to instability. For the tuning of the integral part, a further increment of the gain, K_I will also push the waveform to instability whilst a further decrement of the gain, K_I will reduced the output current magnitude. Four readings are taken and the average data is calculated and shown in Figure 6-8.

With the chosen proportional and integral gains, the THD achieved is 5.65%. Furthermore, it can be observed from Figure 6-8 that the most dominant low order harmonic are of the 3rd and 5th orders which are approximately 2.5% and 2% of the fundamental value. Other than that, a problem spotted in the 2nd harmonic order. Despite that it should be in a low magnitude value, it shows a definite high value which in fact higher than the other harmonic orders. The reason for this is believed to be because of the resistive load used which has some inductive value in it. At the time of the experiments are done, this is the only type of resistor (linear resistor) that is available in the lab. Next, the results from Inverter 2 are demonstrated, all with the same DC input voltage and resistive load value.

6.3.4 *Results on Inverter 2 system*

With the same DC input voltage of 30V and resistive load value of 5 Ohm, a second inverter system, Inverter 2 is tested, all using the same type and value of electronic components. The proportional and integral gains chosen are 2 and 0.11 respectively. Four readings are taken in the experiment of Inverter 2 stand alone system. The average data of the harmonic spectrum is then calculated and shown in Figure 6-10.

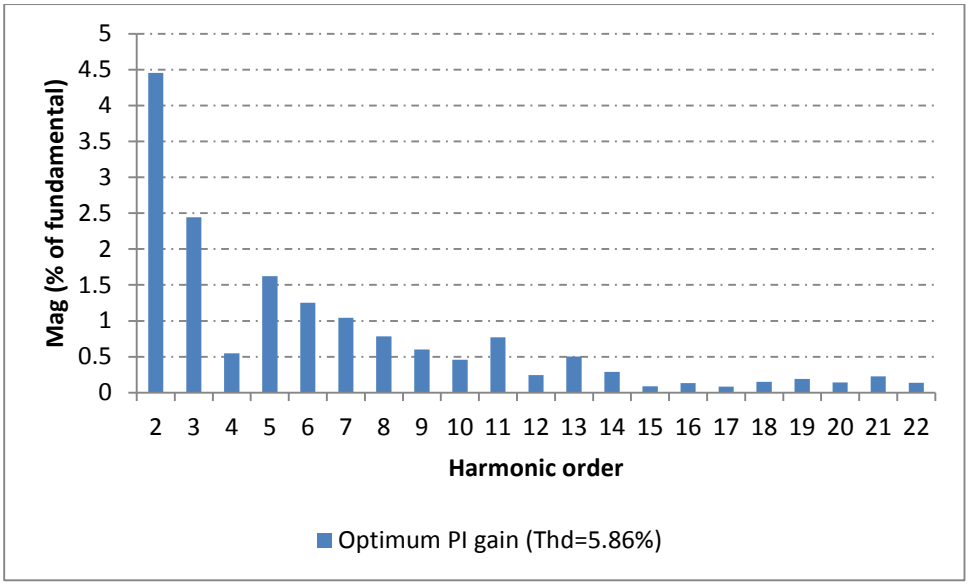

Figure 6-10: Harmonic data of inverter 2 output current using PI control.

As can be seen in Figure 6-10, the output current THD observed is 5.86% with high harmonics magnitude in the lower order. Figure 6-11 below combines the harmonic spectrums in Figure 6-8 and Figure 6-10 in the same graph.

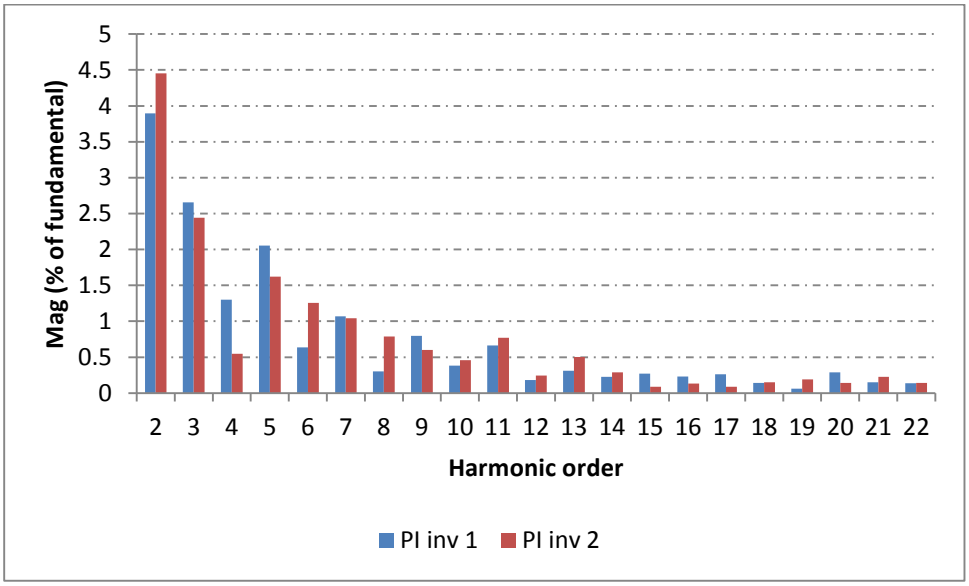

Figure 6-11: Harmonic spectrums of Inv 1 and Inv 2 with PI current control.

Although theoretically the spectrum as in Figure 6-11 should resemble each other because of the same values used for the components in both inverters, this is not the case in the research. After much effort has been done to the experimental area; such as

shorten the wire connector, reduce noise by wrapping wires with a tape and placing the DSP further with the inverter output point, the inequality to the output current harmonic spectrum could not be resolved. Therefore, the only reason for that to happen is because of the components used are physically different even though the same value of components are used for both inverters.

6.4 PR Experiments and Results

The next step in this research is implementing the Proportional Resonant (PR) controller in the inverter system. Once again, before the experiment is done with a grid connected system, a stand-alone system with the same value of resistive load as in PI experiments is used. It has to be noted here that the DC input voltage used and the current demand are also the same as when experimenting with the conventional PI current controller. For the purpose of this test, a new programming code based on the digitized PR transfer function is added to the software. After the code is loaded and run, two gains; the proportional gain, K_P and the resonant gain, K_R need to be tuned to get the best output current waveform with the best THD possible.

There are a number of papers [80, 82, 83] mentioning that using a PR controller without adding a cut off frequency in the system will make the system unstable. Based on a paper by [84], after a cut-off frequency is added to the system, the analogue transfer function becomes as follows.

$$H_{PR}(s) = K_P + \frac{2K_R\omega_c s}{s^2 + 2\omega_c s + \omega_o^2}$$

$$= \frac{K_P(s^2 + 2\omega_c s + \omega_o^2) + 2K_R\omega_c s}{s^2 + 2\omega_c s + \omega_o^2}$$

(Eq. 6-1)

By means of Tustin transformation, (Eq. 6-1) can be described as:

$$H_{PR}(z) = \frac{K_P\left[\left(\frac{2}{T}\frac{1-z^{-1}}{1+z^{-1}}\right)^2 + 2\omega_c\left(\frac{2}{T}\frac{1-z^{-1}}{1+z^{-1}}\right) + \omega_o^2\right] + 2K_R\omega_c\left(\frac{2}{T}\frac{1-z^{-1}}{1+z^{-1}}\right)}{\left(\frac{2}{T}\frac{1-z^{-1}}{1+z^{-1}}\right)^2 + 2\omega_c\left(\frac{2}{T}\frac{1-z^{-1}}{1+z^{-1}}\right) + \omega_o^2}$$

$$= \frac{K_P\left[\left(\frac{4}{T^2}\right)\left(\frac{1-2z^{-1}+z^{-2}}{1+2z^{-1}+z^{-2}}\right)+\frac{4\omega_c}{T}\left(\frac{1-z^{-1}}{1+z^{-1}}\right)+\omega_0^2\right]+\frac{4K_R\omega_c}{T}\left(\frac{1-z^{-1}}{1+z^{-1}}\right)}{\left(\frac{4}{T^2}\right)\left(\frac{1-2z^{-1}+z^{-2}}{1+2z^{-1}+z^{-2}}\right)+\frac{4\omega_c}{T}\left(\frac{1-z^{-1}}{1+z^{-1}}\right)+\omega_0^2}$$

$$= \frac{K_P\left[\frac{4(1-2z^{-1}+z^{-2})}{T^2(1+2z^{-1}+z^{-2})}+\frac{4T\omega_c(1-z^{-2})}{T^2(1+2z^{-1}+z^{-2})}+\frac{\omega_o^2T^2(1+2z^{-1}+z^{-2})}{T^2(1+2z^{-1}+z^{-2})}\right]+\frac{4TK_R\omega_c(1-z^{-2})}{T^2(1+2z^{-1}+z^{-2})}}{\frac{4(1-2z^{-1}+z^{-2})}{T^2(1+2z^{-1}+z^{-2})}+\frac{4T\omega_c(1-z^{-2})}{T^2(1+2z^{-1}+z^{-2})}+\frac{\omega_o^2T^2(1+2z^{-1}+z^{-2})}{T^2(1+2z^{-1}+z^{-2})}}$$

(Eq. 6-2)

To simplify (Eq. 6-2) above, the transfer function becomes:

$$H_{PR}(z) = \frac{4K_P(1-2z^{-1}+z^{-2})+4TK_P\omega_c(1-z^{-2})+K_P\omega_o^2T^2(1+2z^{-1}+z^{-2})+4TK_R\omega_c(1-z^{-2})}{4-8z^{-1}+4z^{-2}+4T\omega_c-4T\omega_cz^{-2}+\omega_o^2T^2+2\omega_o^2T^2z^{-1}+\omega_o^2T^2z^{-2}}$$

(Eq. 6-3)

Re-arranging (Eq. 6-3), the transfer function becomes:

$$H_{PR}(z) = \frac{(4K_P+4K_PT\omega_c+K_P\omega_o^2T^2+4TK_R\omega_c)+(2K_P\omega_o^2T^2-8K_P)z^{-1}+(4K_P-4K_PT\omega_c+K_P\omega_o^2T^2-4TK_R\omega_c)z^{-2}}{(4+4T\omega_c+\omega_o^2T^2)+(2\omega_o^2T^2-8)z^{-1}+(4-4T\omega_c+\omega_o^2T^2)z^{-2}}$$

(Eq. 6-4)

Based on (Eq. 6-4), the transfer function can be re-written as:

$$H_{PR}(z) = \frac{b_o+b_1z^{-1}+b_2z^{-2}}{1+a_1z^{-1}+a_2z^{-2}}$$

(Eq. 6-5)

Where;

$$b_o = \frac{\left(4K_P+4K_PT\omega_c+K_P\omega_0^2T^2+4K_R\omega_cT\right)}{(4+4T\omega_c+T^2\omega_0^2)}$$

$$b_1 = \frac{\left(2K_P\omega_0^2T^2-8K_P\right)}{(4+4T\omega_c+T^2\omega_0^2)}$$

$$b_2 = \frac{\left(4K_P-4K_PT\omega_c+K_P\omega_0^2T^2-4K_R\omega_cT\right)}{(4+4T\omega_c+T^2\omega_0^2)}$$

$$a_1 = \frac{\left(2T^2\omega_0^2 - 8\right)}{(4 + 4T\omega_c + T^2\omega_0^2)}$$

$$a_2 = \frac{(4 + 4T\omega_c + T^2\omega_0^2)}{(4 + 4T\omega_c + T^2\omega_0^2)}$$

T is 50 µs, ω_o is 100 π, and ω_c is the controller cut off frequency. In a study by A. Hasanzadeh et al [80], they identify a range of practical cut off frequency value that can be used in the PR controller system. It is between 10 to 100 rad/s. Based on that range, several different values of cut off frequency between 10 to 100 rad/s are applied and tested in the experiment. Following that, it is noticed that the harmonic data of the inverter output current waveform is much improved following the increased value of cut off frequency. Besides, the output current waveform as well as the corresponding THD is also improved. For the purpose of the research, a cut off frequency of 30 rad/s is chosen as the output current harmonic spectrum shows an optimum performance of all.

6.4.1 *Results on Inverter 1 System*

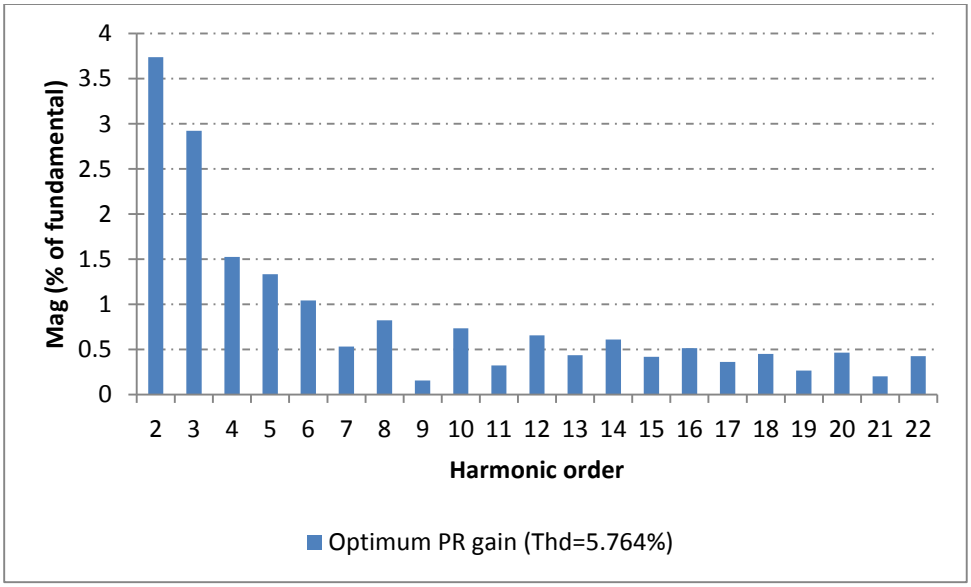

Figure 6-12: Harmonic data of inverter 1 output current using PR control.

Similar to previous experiment with PI controller, the software is set to have a dead time compensation unit of 0.03 and a ZCD is connected into the system. The power

analyzer is set so that the output current FFT analysis is done by taking an average of 16 fundamental current cycles.

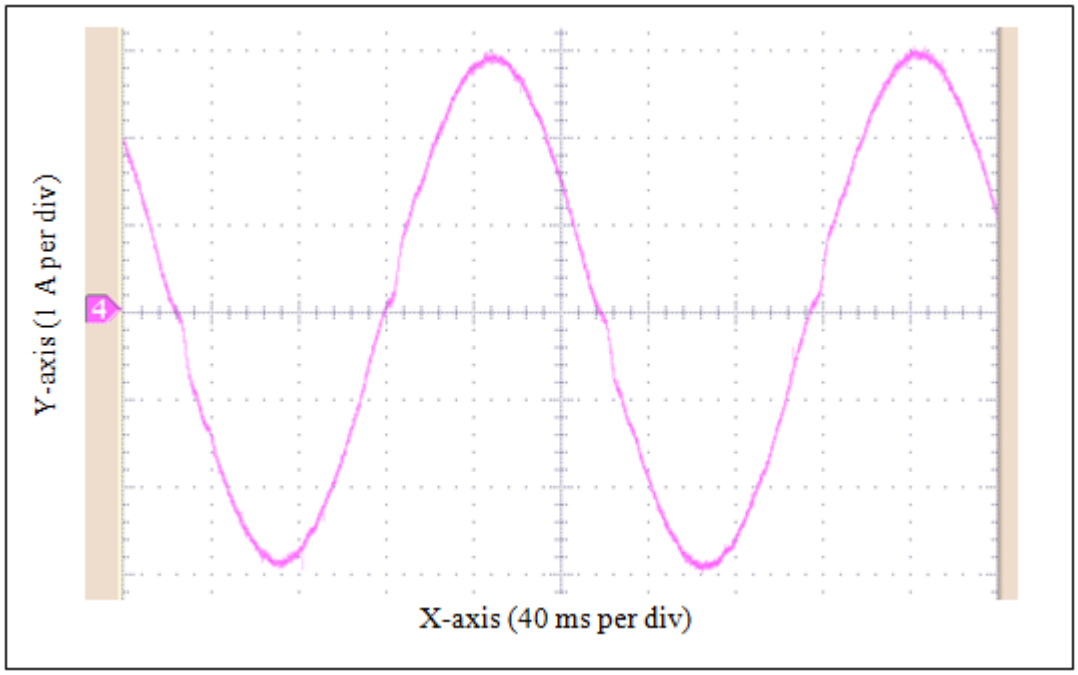

(a)

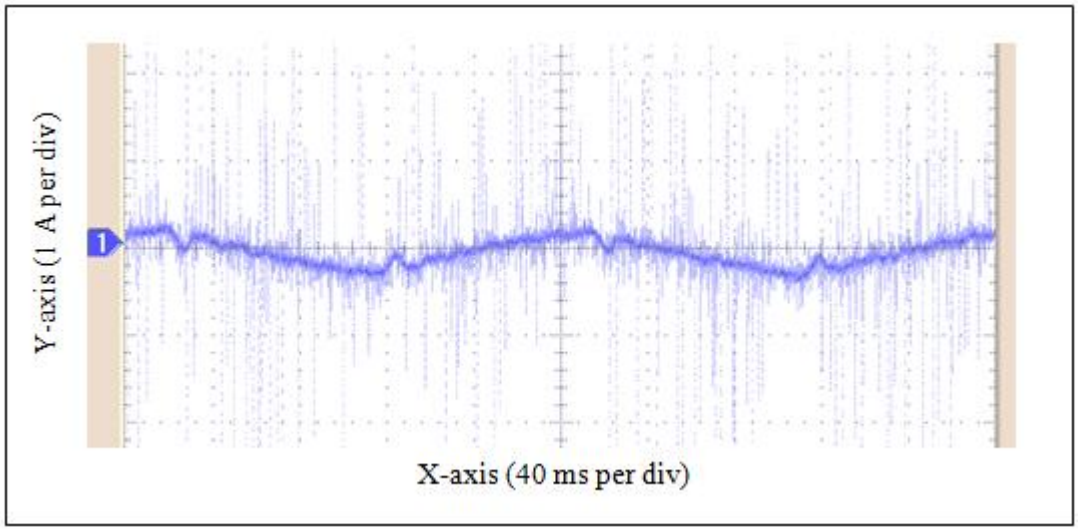

(b)

Figure 6-13: Screen shot of (a) output current waveform with reference 3 A peak ; and (b) current error waveform which shows approximately 0.2 A peak.

The proportional gain, K_P and the integral gain, K_R are tuned to acquire the best possible output current with the best THD. For that reason, the chosen K_P and K_R value is 2 and 410 respectively. During the tuning process, from the observation of the waveforms and the harmonic data, a further increment as well as decrement in the proportional gain, K_P and the resonance gain, K_R will push the waveform to instability. Using the chosen gains, four readings are taken and the average data is calculated and shown in Figure 6-12. It can be noticed that high harmonics appear between the 2nd to 6th orders. The reason for the high magnitude of the even harmonic numbers is similar to the experiment when the inverter system is tested with PI control. Figure 6-13 shows the screen shot of the output current waveform and the current error when the reference current of 3 A peak is compared with the measured output current.

6.4.2 *Results on Inverter 2 system*

Following the testing of inverter 1 system using PR control, inverter 2 system with the same type and parameter values is tested. The gains are tuned so that the lowest THD is obtained. Again, it has to be noted that although inverter 2 system is of the same type and use the same parameter values, the physical of components are different which leads to different gains value. As a result, the proportional gain, K_P and the resonant gain, K_R is 1.8 and 100 respectively.

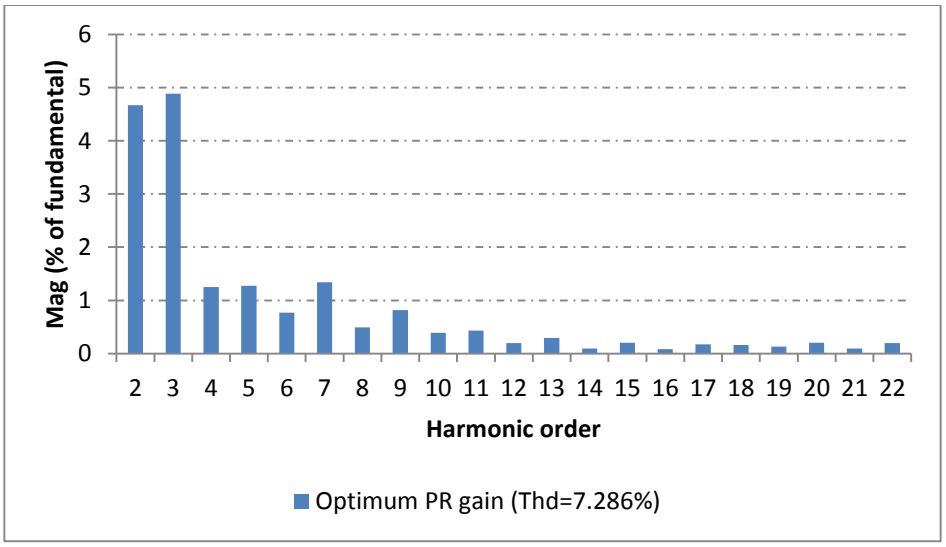

Figure 6-14: Harmonic data of inverter 2 output current using PR control

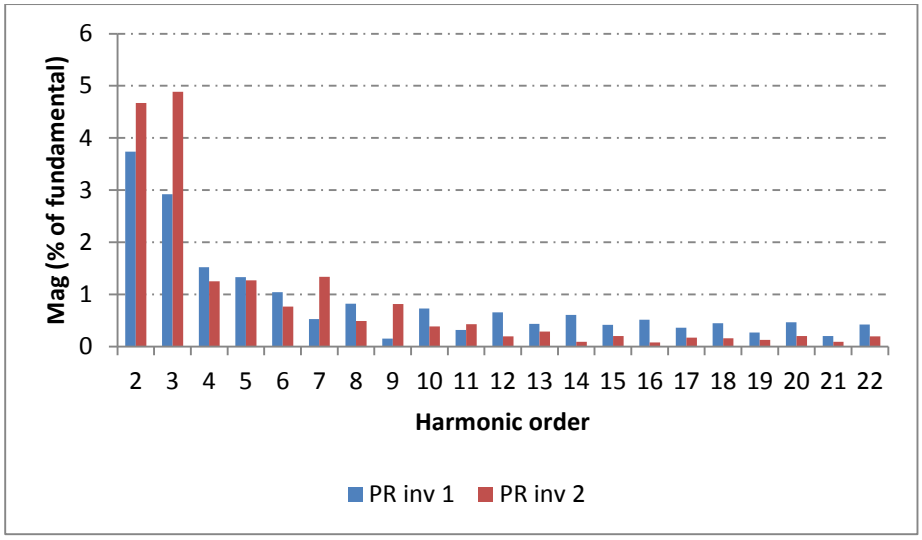

Figure 6-15: Harmonic spectrums of Inv 1 and Inv 2 with PR current control.

Figure 6-14 illustrates the averaged harmonic data of the inverter output current after four readings are taken from the power analyzer. As can be seen, the output current THD obtained is 7.286%. The highest harmonics magnitude are of the 2nd and 3rd order. Figure 6-15 combines the harmonic spectrums in Figure 6-12 and Figure 6-14 in the same graph. Once again, the dissimilarity of the harmonic spectrum between both inverters are due to the components that are physically different even though the same value of components are used for both inverters.

6.5 Comparison between the PI and PR Controller System

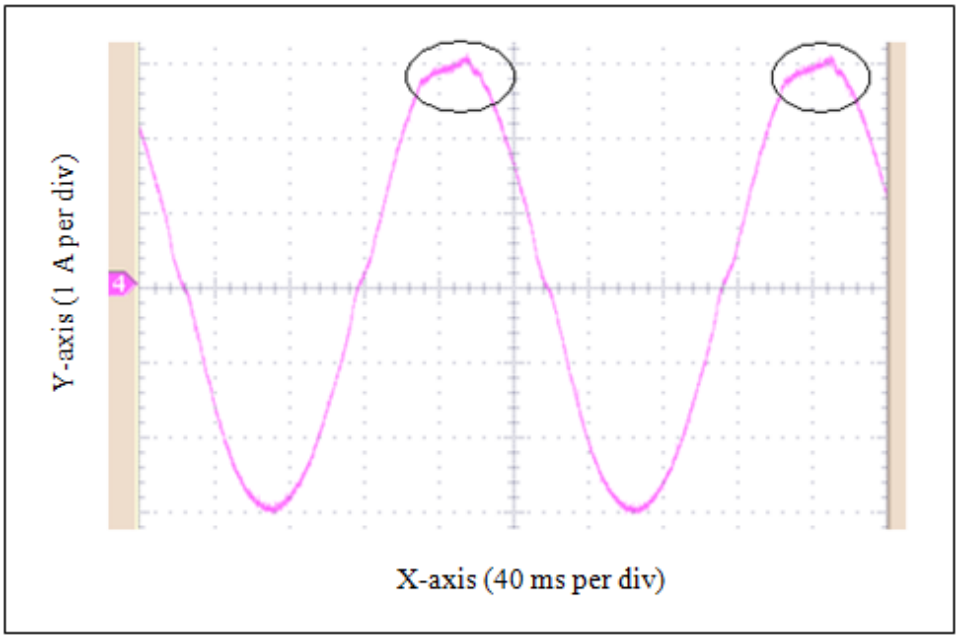

(a)

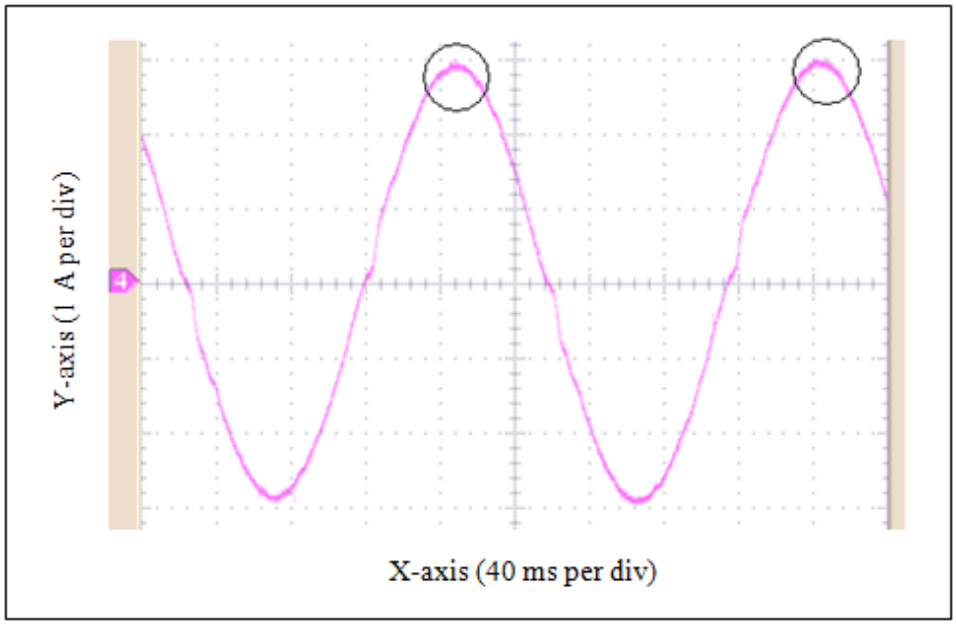

(b)

Figure 6-16: Compare output current waveform of two controller systems (a) Output current from PI controller shows distortion at the top, and (b) output current from PR controller shows smooth curve at the top.

Figure 6-16 compares the output current waveform of two controller systems. Each current errors are illustrated in Figure 6-17. From observation, the reason for that is because the PR controller system can reduce the steady state error between the demand and the actual current.

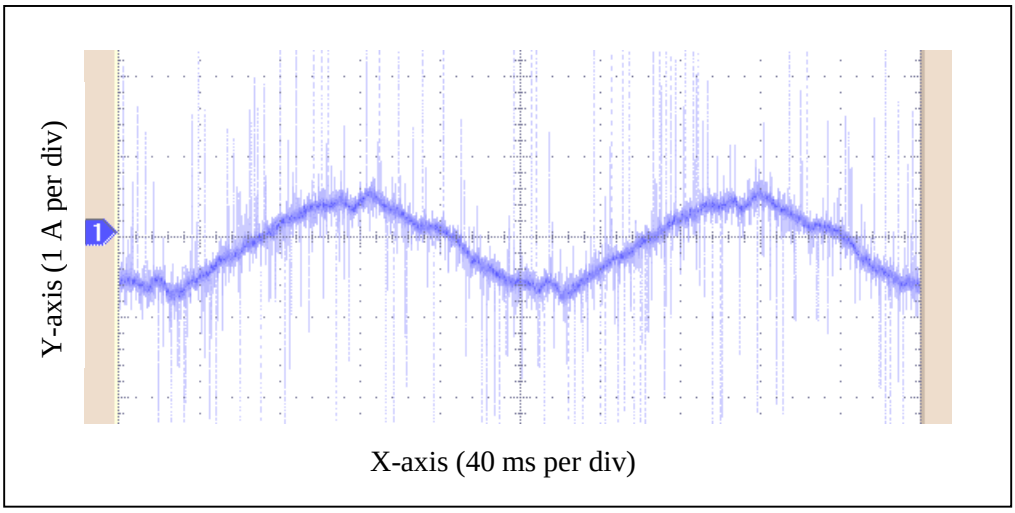

(a)

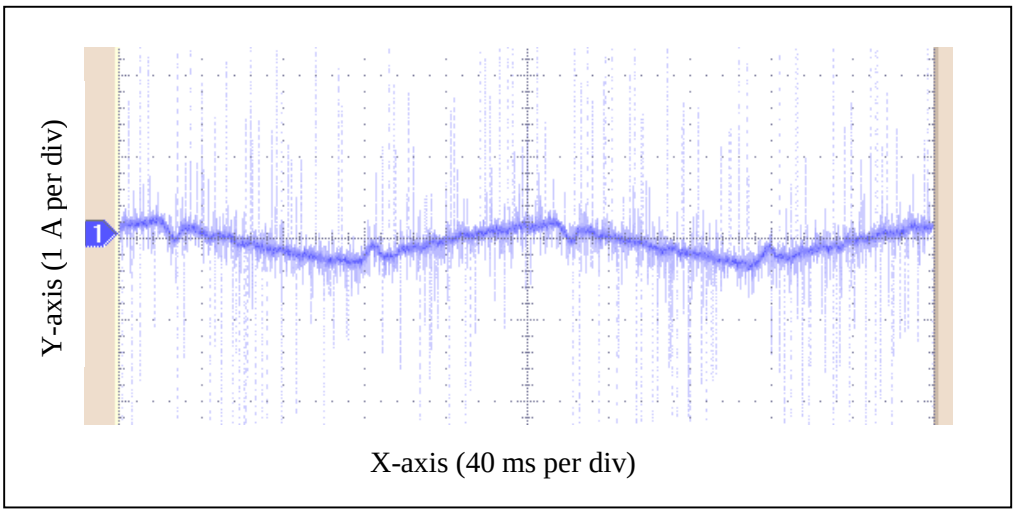

(b)

Figure 6-17: Compare error of two controller systems (a) current error with PI controller system is approximately 0.5 A peak; and (b) current error with PR controller system is reduced to approximately 0.2 A peak.

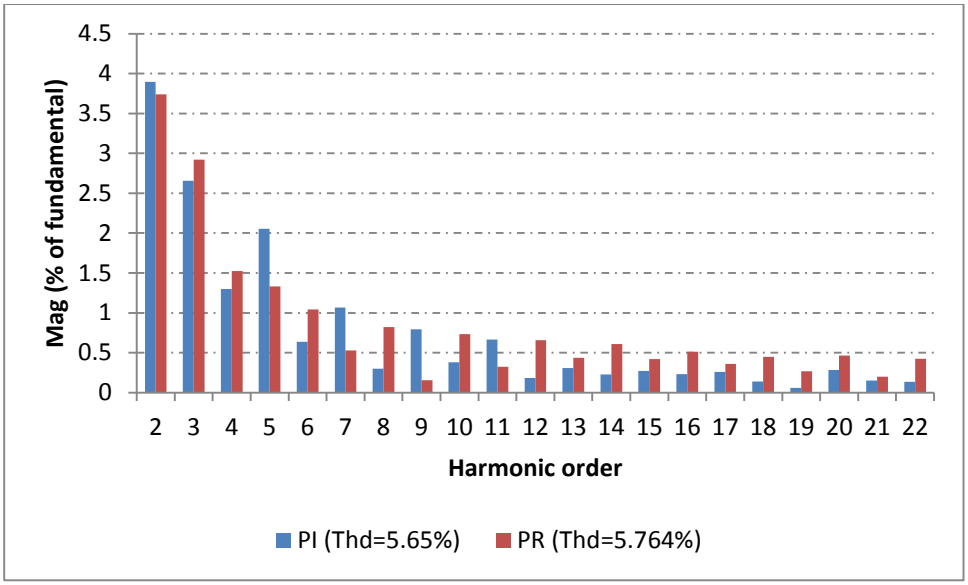

Figure 6-18: Compare FFT of two controller systems.

Yet, when comparing the harmonic profile of inverter 1 system with the PI and PR controller system, the harmonics of the 5^{th}, 7^{th}, 9^{th} and 11^{th} of the PR controller system are reduced significantly, that is between 25% to 75%, lower than the harmonics of the PI controller system. The results thus demonstrate that the same output in the R.Teodorescu et al [59] study as explained in Chapter 2 is achieved. This can be seen in Figure 6-18. The same figure also shows the output current Total Harmonic Distortion (THD) of the two controller systems. It shows an output current THD of 5.65% when using PI control and 5.764% PR control system.

The THD results show that both current control methods yield similar THD performance. However, with respect to the lowest harmonic orders (3^{rd} 5^{th} 7^{th}), the PR controller achieves lower individual harmonic components. This is an important result. In previous works, the lowest order harmonics are often cited as being problematic in grid connected inverter systems. Therefore, in terms of meeting the imposed recommendations for individual harmonics (<2% for a commercial system), the PR controller offers some performance advantages.

Based on the objective of this research project, a random gain is used in the controller system instead of a fixed gain value. The modified controllers are then tested and results are described in the following section.

6.6 Parameter Randomization Controller Technique

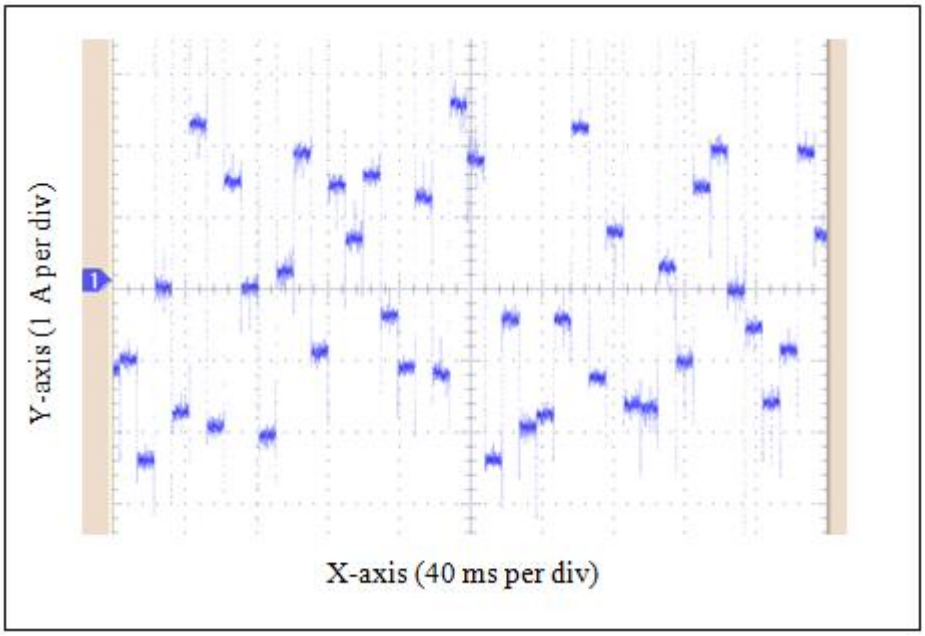

(a)

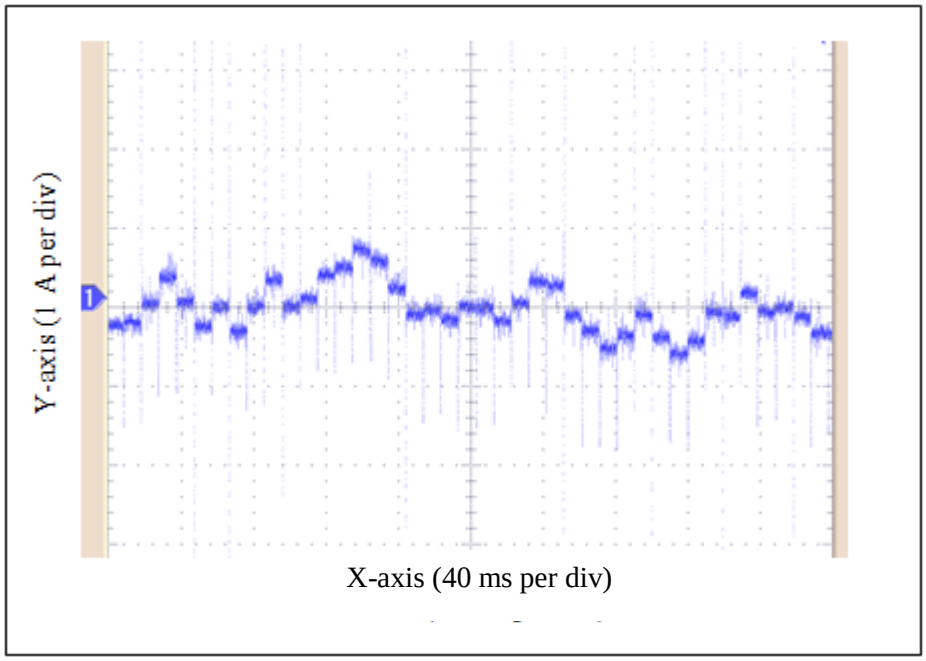

(b)

Figure 6-19: Random signal generation (a) generation of random signal more scattered around before filtering process ; and (b) random signal becomes smoother like a waveform after filtering process.

In order to improve the harmonic spectrum thus reduces the overall output current THD, a random signal is added to the proportional and integral gain of the conventional PI current controller. This random signal is generated using the software and is limited to a certain range so that the output current instability is prevented by the adjusted gain, R_{PI} and R_{KI} tuning. The range of the signal is determined by testing the inverter system with different values of gains. The maximum and minimum gain value before the output current becomes unstable is then chosen as the random signal limit. Following this, when the limit is added to the gains, the new randomized gains, R_{PI} and R_{KI} are adjusted automatically while the inverter system is on test. A simple digital low pass filter is also added after the random number generation for smooth variation signal. This filter has a cut off frequency of approximately 560 Hz. It is observed that higher cut off frequency will not make the random signal any smoother and lower cut off frequency will limit the range of the random signal. The filtered random signal is then added to the gains to form the newly randomized gains which in turn used in the current control of the inverter system. Figure 6-19 shows the waveforms of the random signal before and after filtering.

6.6.1 *Results on Randomized PI on Inverter 1 System*

Two tests were carried out in order to gain the best implementation of the randomized signal. Firstly, the test of randomized signal being added to the proportional gain to become the randomized proportional gain, R_{KP} whilst the integral gain, K_I remain fixed and secondly, the test of randomized signal being added to the integral gain to become the randomized integral gain, R_{KI} whilst the proportional gain, K_P remain fixed. In the first test, the randomized proportional gain, R_{KP} is set to be in a range from 1.3 to 2.7 while the integral gain is set to be fixed at 0.35. After four readings are taken from the power analyzer which has been set to calculate the output waveform of up to 16 fundamental cycles, an average in then calculated in Excel. The harmonic spectrum is illustrates in Figure 6-20.

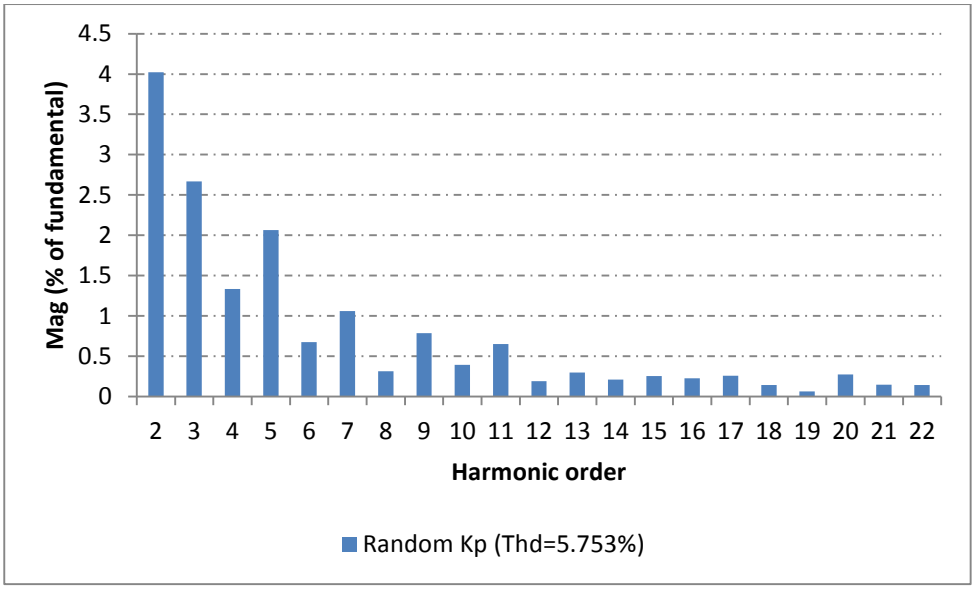

Figure 6-20: Output current harmonic spectrum of inverter 1 system using a randomized proportional gain of PI control technique.

In the second test, the randomized integral gain, R_{KI} is set to be in a range from 0.2 to 0.5 while the integral gain is set to be fixed at 2. Again, four readings of harmonic data are taken from the power analyzer and an average data value is then calculated in Excel. The output current harmonic spectrum is illustrates in Figure 6-21.

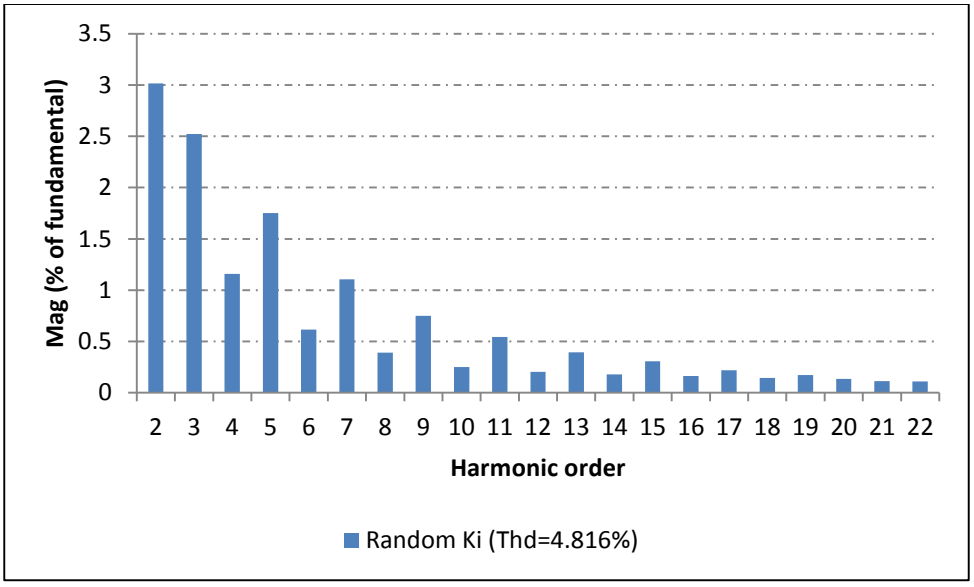

Figure 6-21: Output current harmonic spectrum of inverter 1 system using a randomized integral gain of PI control technique.

Figure 6-22 shows the comparison between the three graphs; Figure 6-8, Figure 6-20 and Figure 6-21, when inverter 1 system is tested using the conventional PI and the randomized PI control technique.

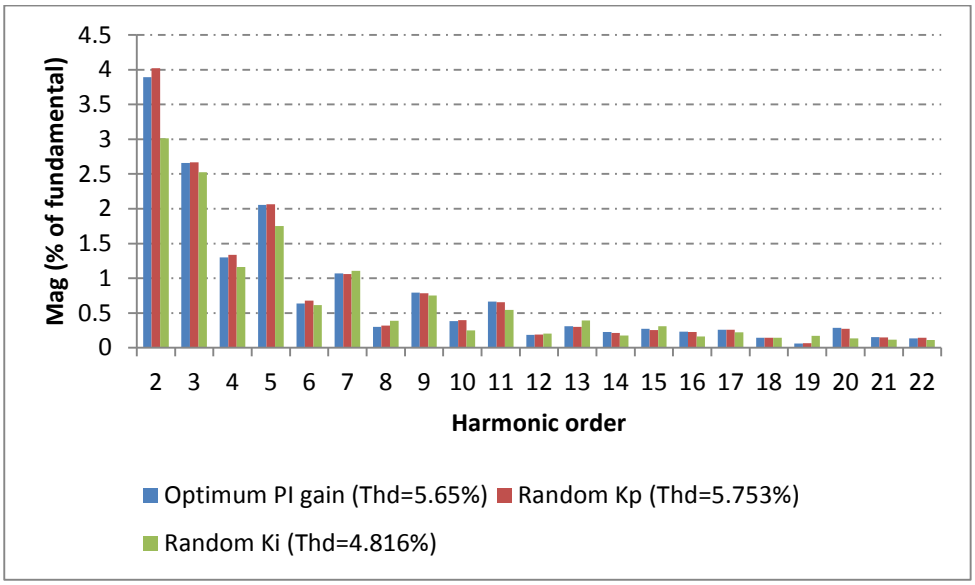

Figure 6-22: Harmonic spectrum of inverter 1 system using a conventional, randomized proportional, and randomized integral gain of PI control technique.

From the graph, it can be easily compared that when random gains are applied to the inverter 1 system, the output current harmonic spectrum is slightly changed which in turns affected the trend of the spectrum. As a result, the THD of the output current is also affected. As seen in Figure 6-22, implementing the randomized integral gain to the conventional PI current technique can improve the THD of inverter 1 system. The THD reduced from 5.65% to 4.816% which is a reduction by approximately 15%. Most importantly, the magnitude of the lower order harmonics that is from the 2^{nd} to the 11^{th} harmonic orders are mostly decreased except for the 7^{th} and 8^{th} orders which have a small increment. Harmonic orders beyond the 11^{th} show a fair reduction as well as increment. This behaviour of having a reduction and increment in harmonic orders magnitude is the reason of the reduced Total Harmonic Distortion (THD) of inverter 1 system when using the randomized integral gain, R_{KI}.

Next, randomized proportional and integral gain of the conventional PI control technique are applied and tested in inverter 2 system.

6.6.2 *Results on Randomized PI on Inverter 2 System*

The same test is then performed with the second inverter, inverter 2 system. As the value of the gains when an optimum output current of inverter 2 result is achieved are 2 and 0.11 for K_P and K_I respectively, the limitation for the random signal need to be set differently. Again, this is done by setting the gains slightly higher and slightly lower to the point before the system goes unstable. After several gain changes, it is agreed that when K_I is fixed to 0.11, the lower limit for K_P is 1.6 and the upper limit is 2.4. Whereas when K_P is fixed to 2, the lower limit for K_I is 0.095 and the upper limit is 0.13. Figure 6-23 and Figure 6-24 shows the averaged data values of the output current harmonic spectrum when the randomized proportional gain, R_{KP} and the randomized integral gain, R_{KI} is applied to the conventional PI system in the inverter 2 system.

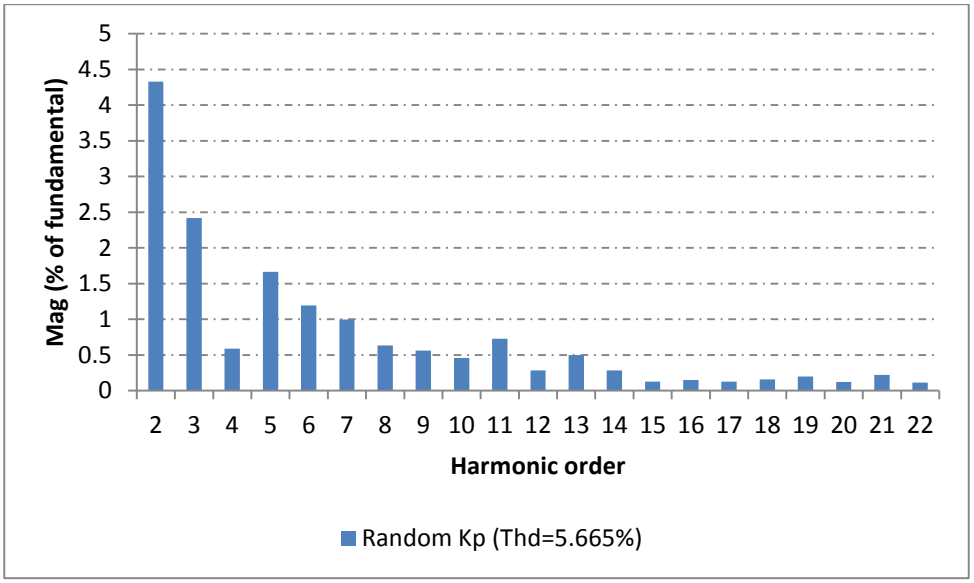

Figure 6-23: Output current harmonic spectrum of inverter 2 system using a randomized proportional gain of PI control technique.

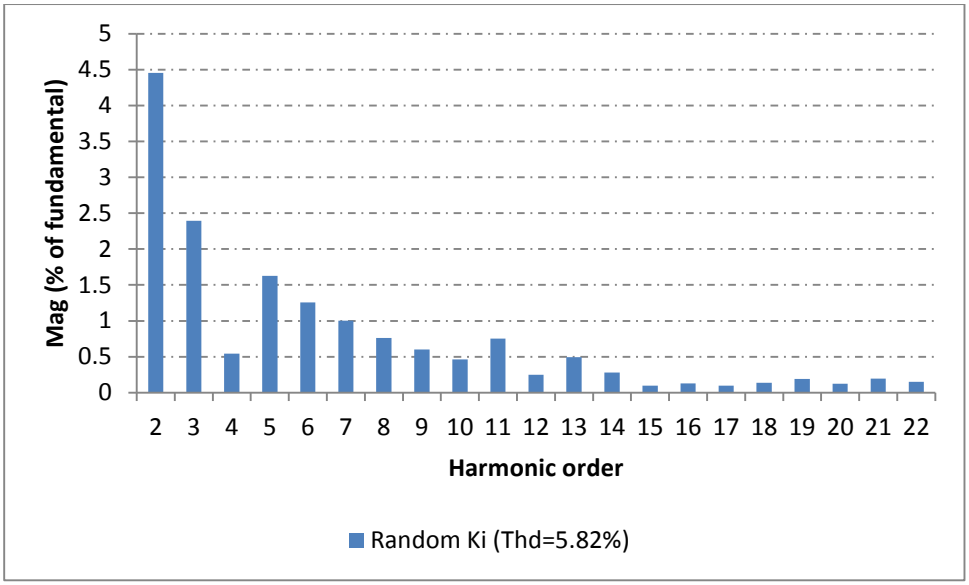

Figure 6-24: Output current harmonic spectrum of inverter 2 system using a randomized proportional gain of PI control technique.

Figure 6-25 shows the comparison between the three graphs; Figure 6-10, Figure 6-23 and Figure 6-24.

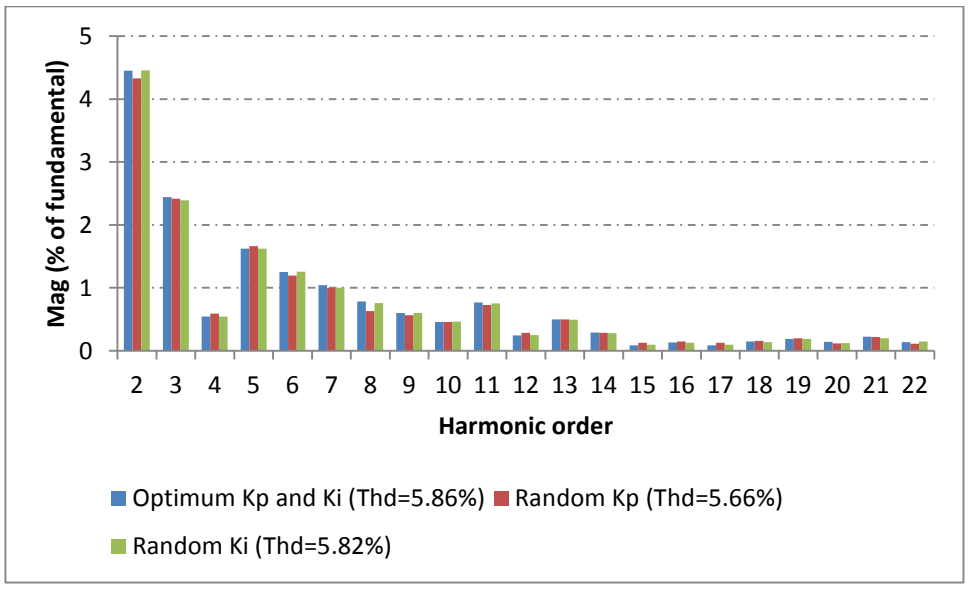

Figure 6-25: Harmonic spectrum of inverter 2 system using a conventional, randomized proportional, and randomized integral gain of PI control technique.

While different trends are achieved when random gains of PI control are applied to the inverter 1 system, this is not the case when the same techniques are tested on inverter 2. It can be seen in Figure 6-25 that only a small changes; increment and decrement are observed to the output current harmonic spectrum which yields to almost no changes to the THD. There is no exact explanation to the result as above. The only reason at the time when the test is done is because of the difference in the physical of the components used. Because of that, further experiment to answer about the question of why results of inverter 2 system is not similar to the results of inverter 1 system is suggested in future.

6.6.3 *Results on Randomized PR in Inverter 1 System*

Following the tests of randomized PI in both inverter systems, tests of randomized PR are performed next. Again, randomized proportional gain of PR control is tested first before the randomized integral gain is applied to the PR control. Results of the tests are illustrated in Figure 6-26, Figure 6-27 and Figure 6-28.

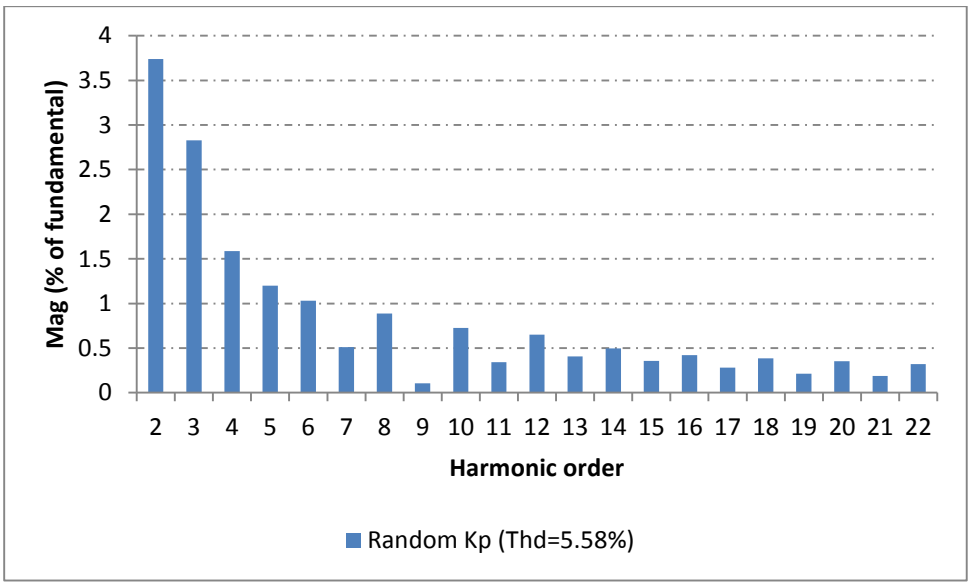

Figure 6-26: Output current harmonic spectrum of inverter 1 system using a randomized proportional gain of PR control technique.

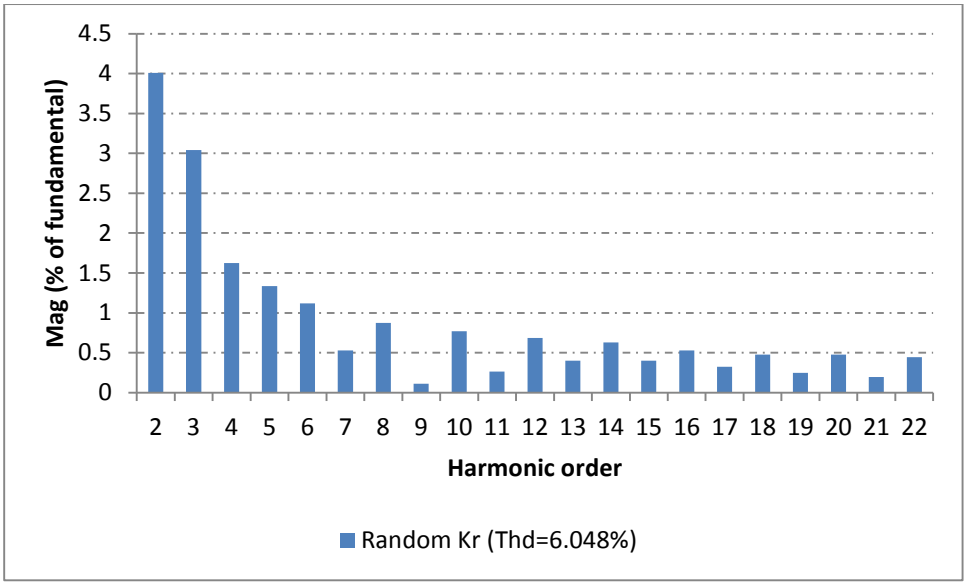

Figure 6-27: Output current harmonic spectrum of inverter 1 system using a randomized resonant gain of PR control technique.

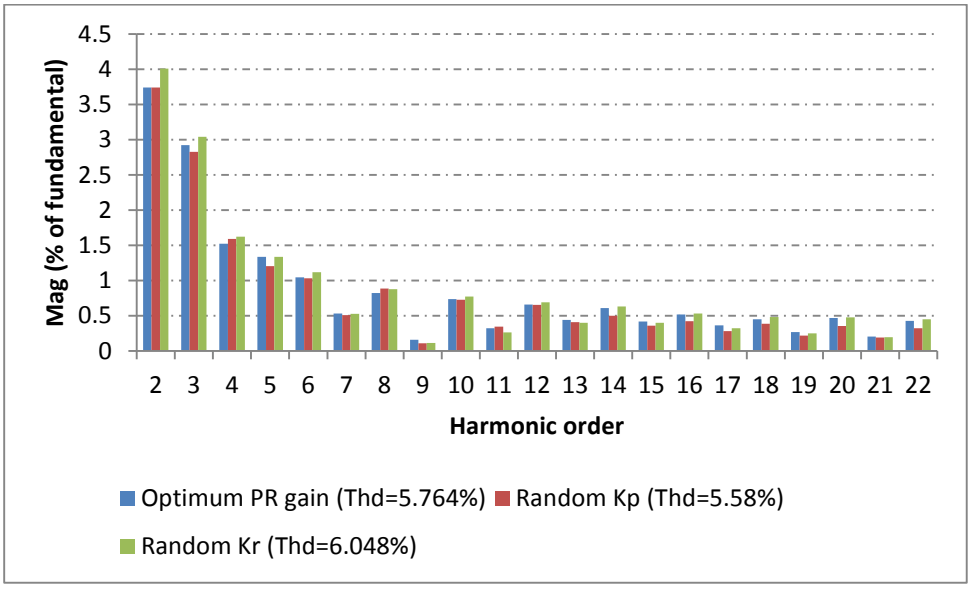

Figure 6-28: Harmonic spectrum of inverter 1 system using a conventional, randomized proportional and randomized resonant gain of PR control technique.

The first test is done when the resonant gain is fixed to 410 while the randomized proportional gain limit is set to be in the range between 1.4 to 2.6. The second test is done when the proportional gain is fixed to 2 while the randomized resonant gain limit is set to be in the range between 370 to 450. From Figure 6-28, different trends are observed in the harmonic spectrum of the inverter output current. The critical part to

notice is the improvement to the THD when randomized proportional gain, R_{KP} is applied to the PR control. Although it shows a small THD reduction, it is believed that the outcome can be improved when a higher DC voltage is used.

6.6.4 *Results on Randomized PR in Inverter 2 System*

For the tests of inverter 2 system, the randomized proportional gain is limited between 1.4 to 2.2 whilst the randomized resonant gain is limited between 85 to 115. Again, it has to be noted that the limitation given is based in the test when different gain values are in the beginning to observe the stability. Figure 6-29 and Figure 6-30 shows the individual harmonic spectrum when the randomized proportional gain, R_{KP} and the randomized resonant gain, R_{KR} are applied to the conventional PR control technique.

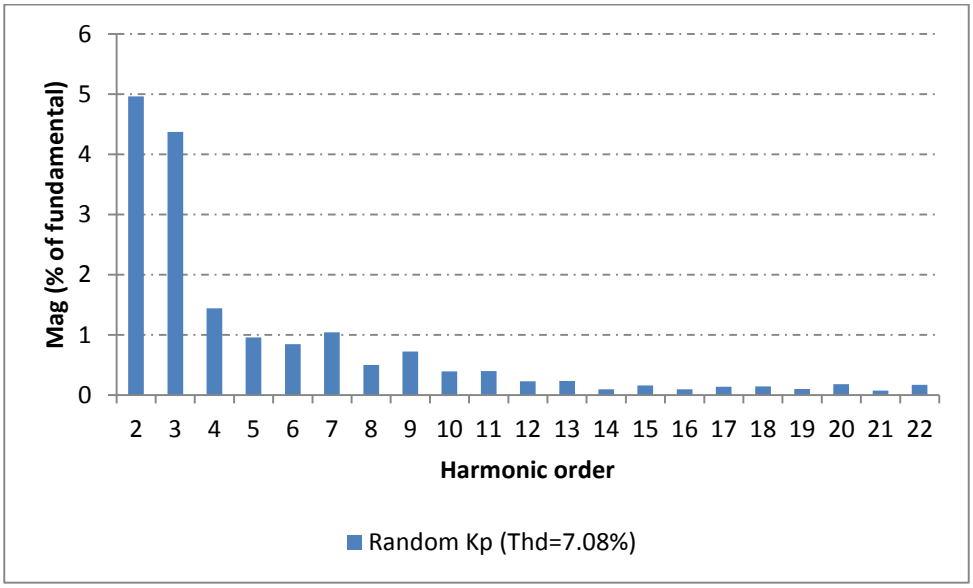

Figure 6-29: Output current harmonic spectrum of inverter 2 system using a randomized proportional gain of PR control technique.

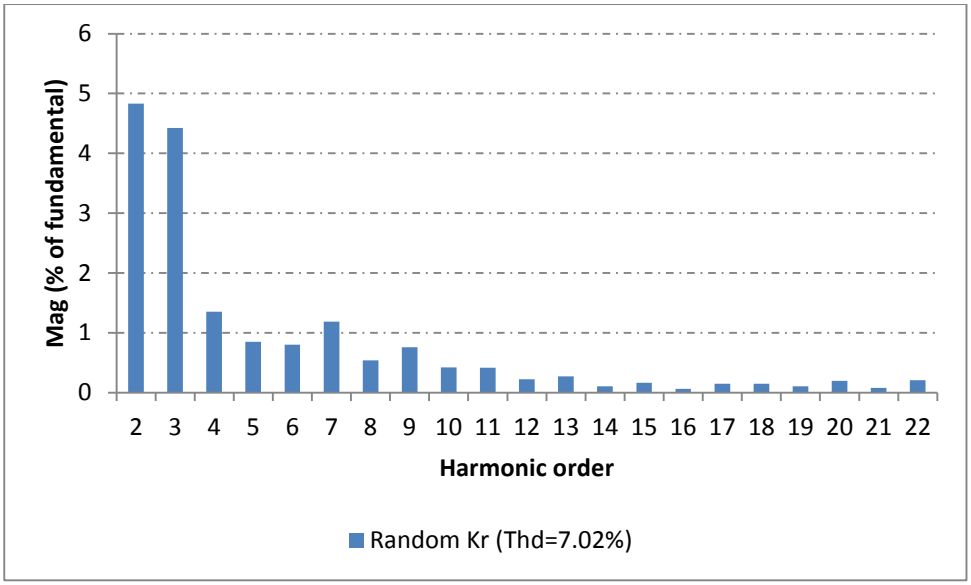

Figure 6-30: Output current harmonic spectrum of inverter 2 system using a randomized resonant gain of PR control technique.

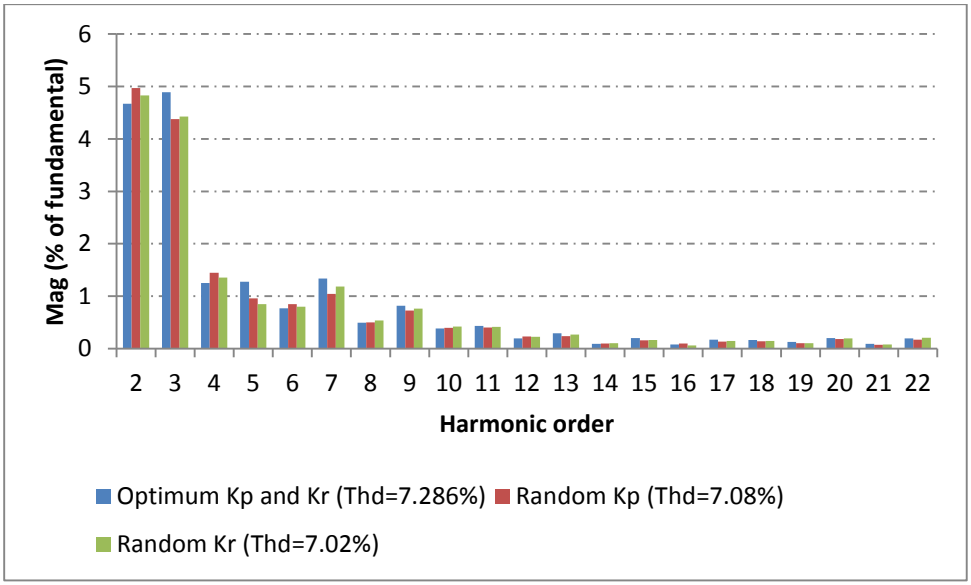

Figure 6-31: spectrum of inverter 2 system using a conventional, randomized proportional, and randomized resonant gain of PR control technique.

From Figure 6-31, it can be seen that increment as well as decrement of harmonics magnitude are achieved especially to the harmonic orders between the 2nd to the 7th. These in turn yield to the improvement in the total harmonic distortion, THD of the inverter 2 system.

6.7 Chapter Summary

The overall of this chapter showed significant results using three different control methods in a stand-alone system. It can be concluded here that by using a random signal gain to the conventional controller, PI and PR, improvement in the output current THD is achieved. From the results, it shows that using the randomized integral gain, R_{KI} in the conventional PI controller is better than using a fix integral gain, K_I alone. It also shows that using the randomized proportional gain, R_{KP} in the conventional PR controller is better than using a fix proportional gain, K_P alone.

Chapter 7: Experimental Results of Grid Connected Inverters

7.1 Introduction

This chapter presents results for the parallel inverter system described in Chapter 6. The chapter is split into three sections. The first section concentrates on the performance of the parallel inverter system when operated with a conventional PI current controller scheme. The second section considers the performance of the parallel inverter system when run with the random parameter controller scheme. In both sections, the performance of each inverter unit operating as an independent grid connected unit is initially assessed. Specifically, the harmonic profile of each inverter is shown, and performance comparisons are made between individual inverter units. Attention is then given to assessing the performance of each inverter when operated in parallel. The effect of each inverters harmonic profile on the overall harmonic performance of the parallel inverter system is then considered. Finally, the performance of the random parameter control technique is assessed via direct comparison of results with the conventional PI control scheme.

7.2 Experimental results with conventional PI current control techniques

This sub-section concentrates on the performance of the parallel inverter system when operated with a conventional PI current controller scheme first and followed by the parallel system operated with a parameter randomisation of PI current controller scheme. For each technique, a single inverter system is tested first followed by two inverters working in parallel.

7.2.1 *Conventional PI Current Control of Individual Inverter Units*

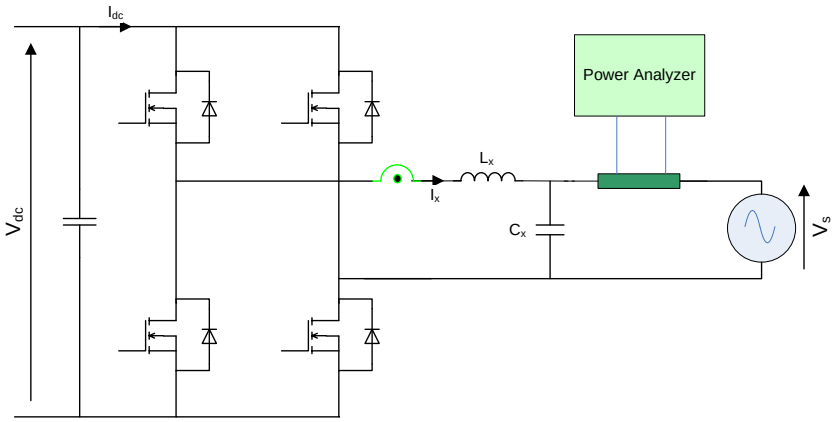

Figure 7-1: Experimental H-Bridge inverter. Single inverter grid connected system

Initially, each inverter is operated independently as a single grid connected unit with a conventional current control loop (Figure 7-1). Each inverter operates from an independent 50 V DC bus, and is connected to a 20 V AC grid voltage. Importantly, each inverter is synchronised to the network via its own Zero Crossing Detector Unit and Digital Control System. In this way, each inverter unit operates fully independently as would be the case in a commercial system and there are no abnormal synchronisation issues created due to the experimental setup. Harmonic data is acquired through the use of a Yokogawa power analyser. The power analyser is set up to acquire the harmonic data over 16 fundamental current cycles, utilising a Hanning sampling window. All harmonic and THD results presented are acquired under these conditions. Each inverter is tuned independently via the software parameters: proportional gain, K_P and integral gain, K_I, to achieve the best output current fidelity possible. Each inverter is controlled to operate at unity power factor with respect to the grid voltage. Via the power analyser, the harmonic spectrum of the output current is recorded for each inverter. The results obtained represent a snap shot in time of the performance of each inverter. To evaluate the average performance of each inverter over time, the harmonic spectrum of each inverter is recorded at three separate intervals. From this, an averaged harmonic spectrum may be calculated and considered to be a typical measure of inverter performance. The averaged harmonic data is imported into Microsoft® Excel® for

presentation in graphical format. Conclusions are drawn from the averaged harmonic performance of each inverter.

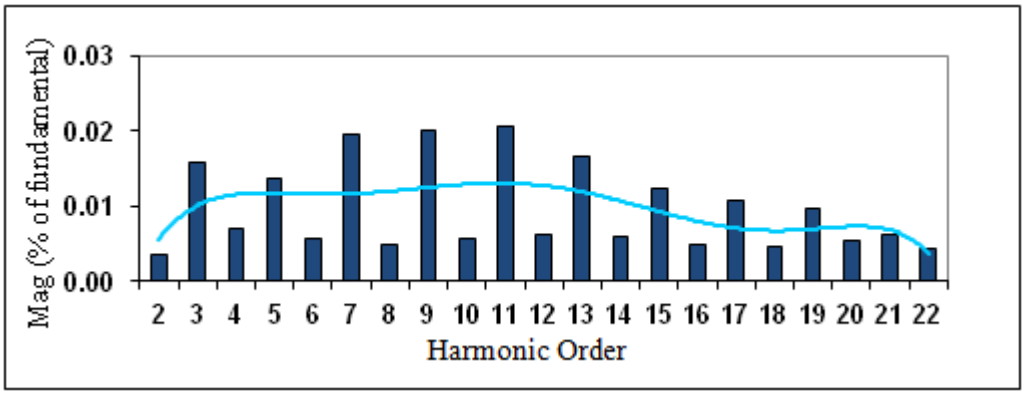

(a)

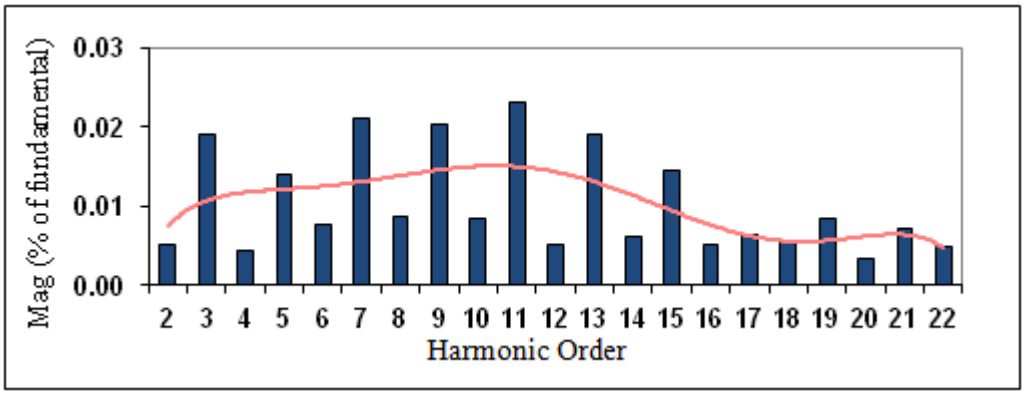

(b)

Figure 7-2: Low order harmonic spectra of (a) Inverter 1 output current with conventional PI control: predominant harmonics appear between the 3rd and 15th harmonic and (b) Inverter 2 output current with conventional PI control: predominant harmonics appear between the 3rd and 15th harmonic.

The averaged harmonic performance of each individual inverter operating independently is shown in Figure 7-2. This shows the per unit magnitude of all harmonics between the 2nd and 22nd harmonic. For both inverters, the predominant harmonics appear between the 3rd and the 15th harmonic. The harmonics become less problematic beyond the 19th harmonic. This is to be expected, since the output inductor and capacitor components yield a low pass filter with an approximate 800 Hz cut-off frequency. Using the Microsoft® Excel® trend line function, a 6th order polynomial trend line is imposed on each graph. This produces a harmonic profile for each inverter

over the averaged set of harmonic data. This approach is consistent with the work by Armstrong [33], and allows for easy comparison between results. As reported by Armstrong, the 6th order polynomial fit provides a good smooth average trend line across the harmonic range. Lower order fits are more sensitive to individual harmonic components [33]. The results show a strong correlation in harmonic profile for each of the two inverters under test. The THD performance of the inverters is summarised in Table 7-1 and indicates the average harmonic performance of each inverter when operating independently is 5.74%.

Table 7-1: THD figures for independently operated, grid connected, inverters using conventional PI current control

Operating Inverter	THD SYSTEM OUTPUT
Inverter 1	5.82%
Inverter 2	5.65%
Single inverter average	**5.74%.**

7.2.2 *Conventional PI Current Control of Two Inverters in Parallel*

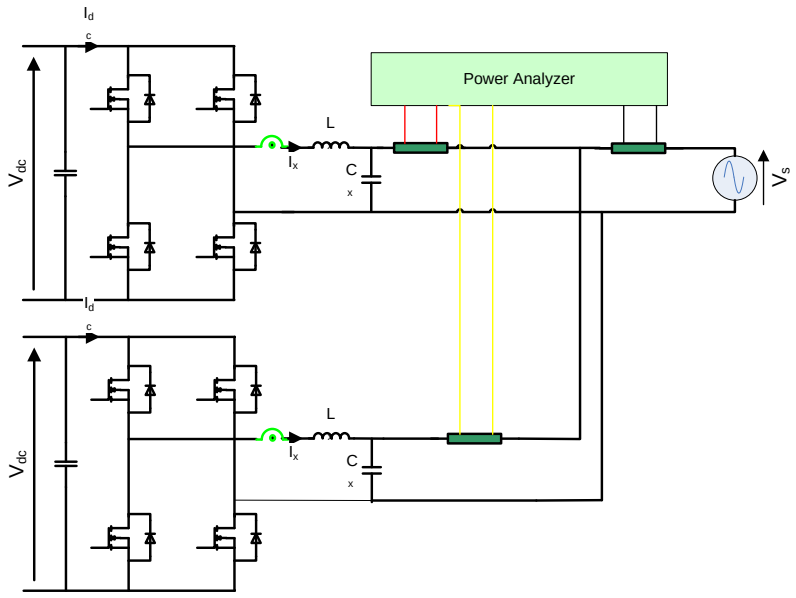

Figure 7-3: Experimental, parallel connected inverter system comprising of two inverter units.

Having tuned and assessed the performance of the inverters operating independently, the inverters are then configured to form a parallel, two inverter, grid connected system.

The circuit topology is shown in Figure 7-3. Current measurements are made by the power analyser at the output of each individual inverter.

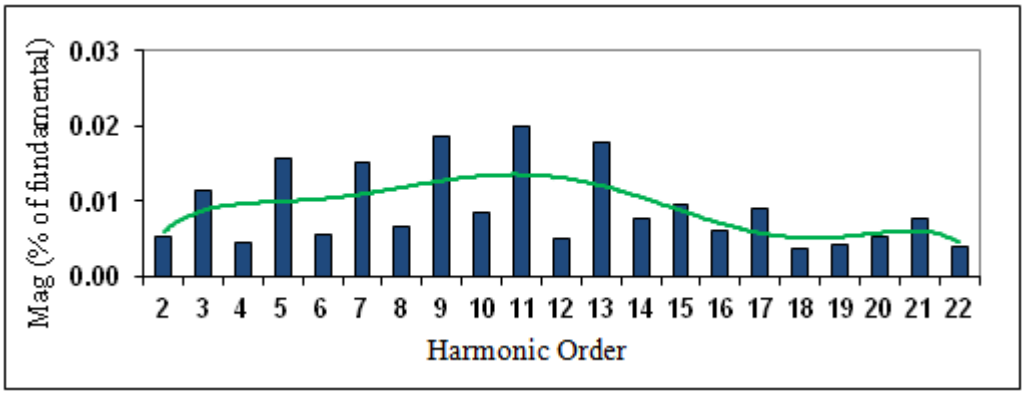

(a)

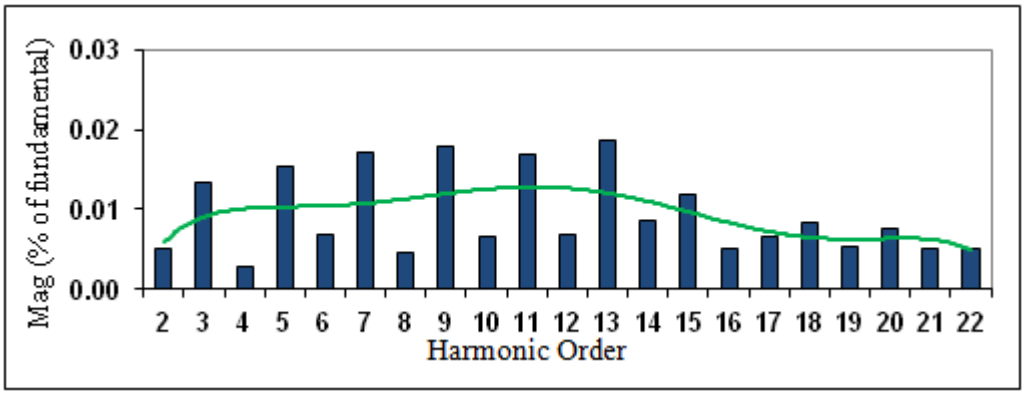

(b)

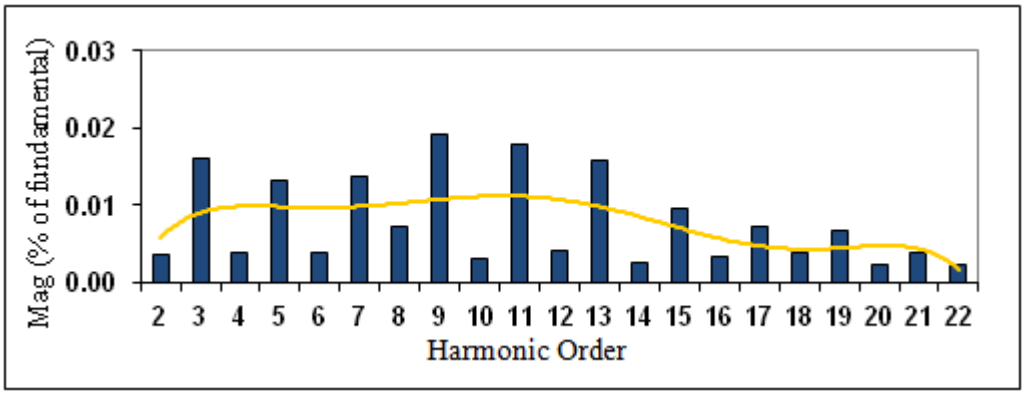

(c)

Figure 7-4: Low order harmonic spectra of parallel inverters with PI current control. (a) Results of inverter 1 output current; (b) Results of Inverter 2 output current; and (c) Results of the parallel system output current. All shows strong correlation between them with predominant harmonics appear between the 3rd and 15th harmonic.

To record the overall parallel system performance, an additional current measurement is made at the point of common coupling. Each inverter is current controlled with the same controller tuning as determined previously during independent operation. In each case, the two applicable inverters are set to operate at unity power factor with respect to the grid voltage. As before, three sets of harmonic data are collected and an averaged harmonic spectrum is determined for each inverter (Figure 7-4). The recorded THD of each individual inverter, along with the parallel inverter system output THD, is summarised in Table 7-2. The results show that the average THD of the parallel system output is 5.36%.

Table 7-2: THD Performance of Two Inverter Parallel System with conventional PI control

PARALLEL COMBINATION	THD INV 1	THD INV 2	THD SYSTEM OUTPUT
Inverter 1 & Inverter 2	5.64%	5.42%	5.36%

7.2.3 *Summary: Conventional PI Current Control*

For all the results presented with conventional PI current control, the same general trend line is seen in the harmonic profile of the output current of each individual inverter unit. In particular, the results show that the largest distortion components are at the 3rd, 7th, 9th and 11th harmonic. When operated as a parallel inverter system, this same harmonic trend is observed in the parallel system output current, and similar individual harmonics dominate. With respect to THD, each inverter typically operates with a THD around 5.5%. When operated as a parallel inverter system, a comparable THD level is observed at the point of common coupling. This behaviour clearly demonstrates the additive nature of the harmonics at the output from individual inverters. It is this harmonic addition at the multiple inverter output which is undesirable, as originally reported by Armstrong et al.

7.2.4 *Experimental Results with Randomised PI Current Control Techniques*

The second section of this chapter presents results for the parallel inverter system when controlled via the randomised parameter PI control method. In order to assess the

performance of this proposed methodology, the same sequence of tests is carried out as presented for the conventional PI current control method. Once again, the harmonic performance of each inverter operating as an independent grid connected unit is considered. This is followed by the harmonic assessment of each grid connected inverter when operating in a parallel connected system. From this, the impact of the randomised control scheme on the parallel inverter system output current is determined. Once again, due to the inclusion of the controller randomisation, the harmonic performance of each inverter varies with time. Therefore, a definitive assessment of the randomised control strategy cannot be determined from one set of results taken at a single instance in time. For this reason, the performance of each inverter is again determined through averaging three sets of harmonic data. In this way, a statistical conclusion is made possible, based on a number of experimental results taken over time.

7.2.5 *Parameter Randomisation PI Current Control of Individual Inverter Units*

Figure 7-5 shows the averaged harmonic spectrum of each inverter when operated as a single inverter system. Importantly, the harmonic profile of each inverter is now different. This is shown through the differing trend line patterns and is in contrast to the almost identical set of harmonic profiles observed with conventional current control (Figure 7-2). This indicates that the random component in the current controller has reduced the degree of correlation in the harmonic profile of each inverter. When the inverter system is connected to the grid, the impact of the randomisation is much more noticeable, due to the low order disturbance effect of the grid on the current control loop. This effect was also observed by Armstrong et al [34]. It is this uncorrelated performance which may be utilised to advantage in a parallel inverter system, since it yields improved opportunities for harmonic cancellation at the system output. The recorded THD at the parallel inverter system output, as measured by the power analyser, is 5.15% (Table 7-3).

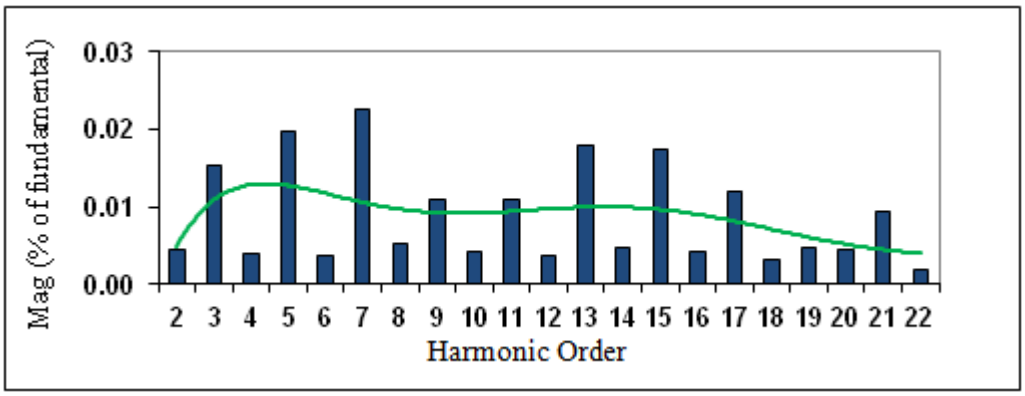

(a)

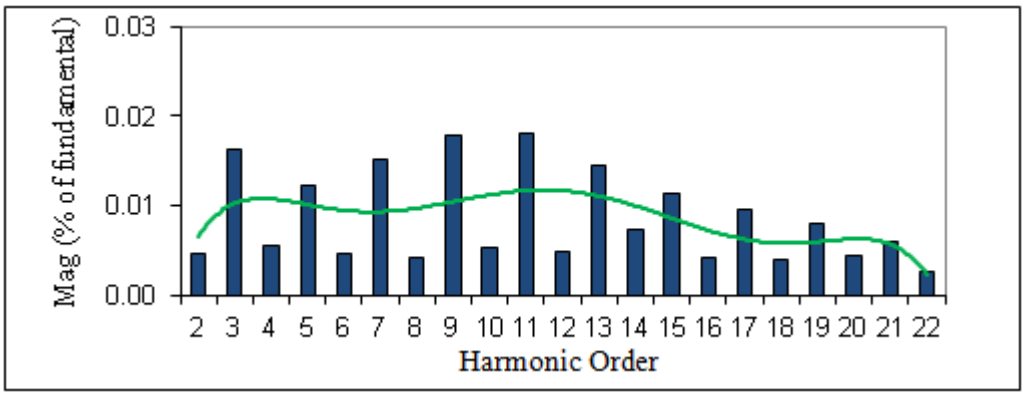

(b)

Figure 7-5: Low order harmonic spectra of (a) Inverter 1 output current with randomised PI control; and (b) Inverter 2 output current with randomised PI control; where difference trend lines are observed between the two inverters.

Table 7-3: THD Performance of Two Inverter Parallel System with conventional control

PARALLEL COMBINATION	THD SYSTEM OUTPUT
Inverter 1	5.07%
Inverter 2	5.22%
Single Inverter Average	**5.15%**

7.2.6 *Parameter Randomisation PI Current Control of Two Inverters in Parallel*

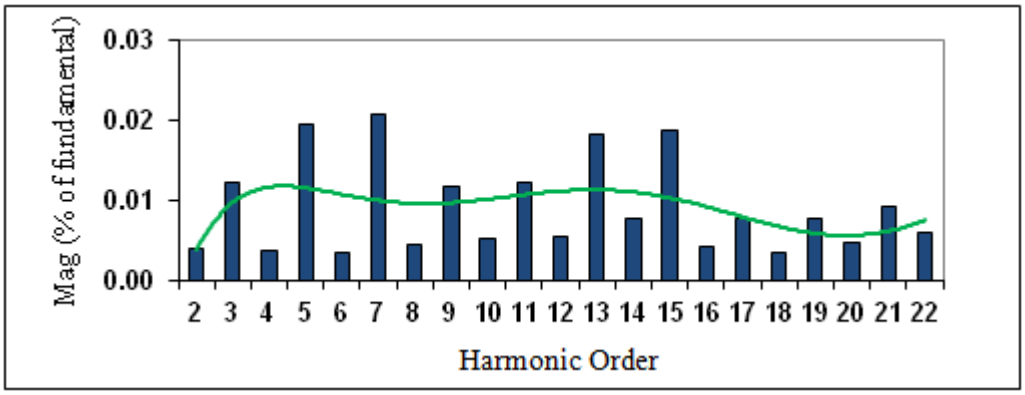

(a)

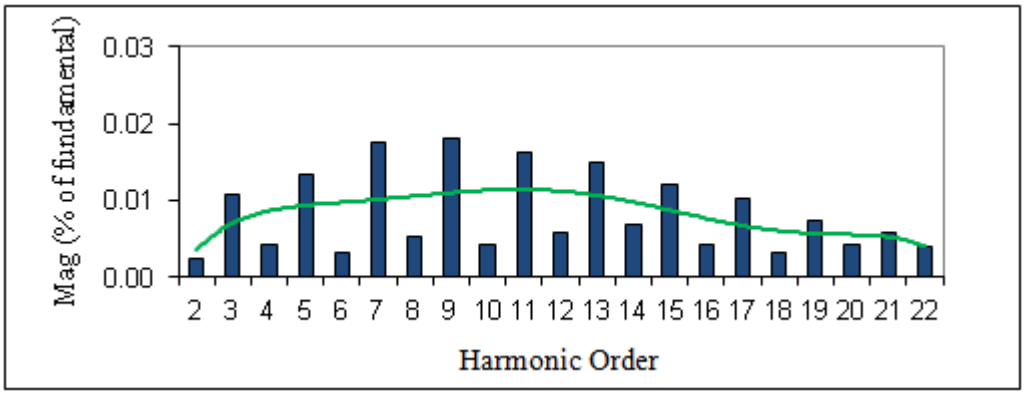

(b)

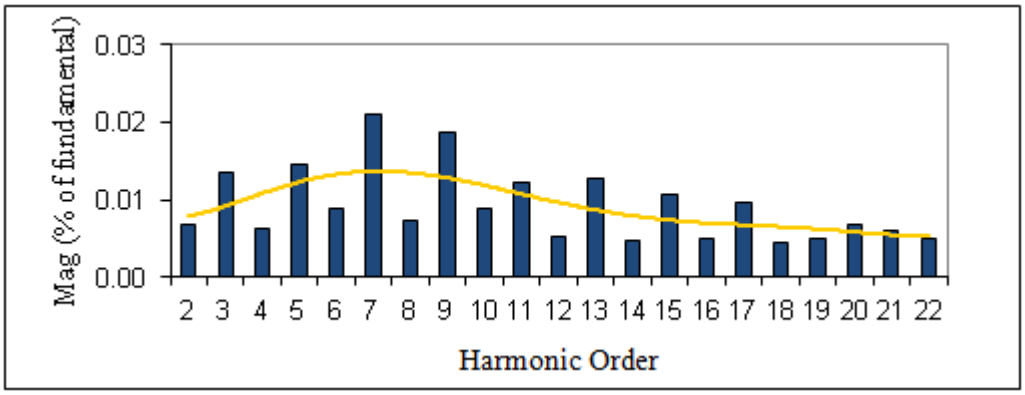

(c)

Figure 7-6: Harmonic spectra of parallel inverters with randomised PI current control. (a) Results of inverter 1 output current; (b) Results of Inverter 2 output current; and (c) Results of the parallel system output current. Different trend lines are observed.

Having assessed the performance of the inverters operating independently, the inverters are then configured to form a parallel, two inverter, grid connected system. The circuit topology remains the same as described for the conventional PI current control scheme; whereby current measurements are made by the power analyser at the output of each individual inverter, and the point of common coupling. Three sets of harmonic data are collected, and an averaged harmonic spectrum is determined for each inverter Figure 7-6. The recorded THD of each individual inverter, along with the parallel inverter system output THD, is summarised in Table 7-4. The results show that the average THD of the parallel system output is 4.62%.

The risk of circulating current is always a potential problem in parallel connected inverter systems. In this work, although possible circulating current was not directly measured, there did not appear to be any practical evidence of it causing any problems with the operation of the inverter units, or the control system. This is concluded from knowledge that the characteristics of each inverter are similar regardless or individual or parallel operation.

Table 7-4: THD Performance of Two Inverter Parallel System with random parameter control

PARALLEL COMBINATION	THD INV 1	THD INV 2	THD SYSTEM OUTPUT
Inverter 1 & Inverter 2	5.34%	5.42%	4.62%

7.2.7 *Summary, Parameter Randomisation PI Current Controller*

The results presented for the random parameter PI current controller confirm that it is possible to adjust the harmonic performance of each inverter unit. By using the random parameter controller, the harmonic profile of each inverter unit now dynamically varies with time. The fixed harmonic trend line observed with the conventional PI control scheme is no longer typical of the behaviour of the system. Whilst the THD of each inverter individual unit is still typically just over 5.3%, when operated as a parallel inverter system a lower average THD is observed at the point of common coupling. For a two inverter parallel system, the average THD is measured as 4.62%. This marks a significant improvement in the net harmonic performance of the parallel inverter system compared to the conventional PI current controller. However, as discussed by

Armstrong et al, there is still a significant contribution from the very low order harmonics; 3rd to 9th, despite the introduction of the controller randomisation.

7.3 Experimental Results with Randomised PR Current Control Techniques

The experimental conditions in this section are identical to those presented for the PI current controller. The only difference is the control algorithm where PR current control is used instead of the PI current control.

7.3.1 *Fixed PR Current Control of Individual Inverter Units*

Again, initially, each inverter is operated independently as a single grid connected unit with a conventional PR current control loop (Figure 7-1). Each inverter is tuned independently via the software parameters: proportional gain, K_P and resonant gain, K_R, to achieve the best output current fidelity possible. Each inverter is controlled to operate at unity power factor with respect to the grid voltage. Via the power analyser, the harmonic spectrum of the output current is recorded for each inverter. To evaluate the average performance of each inverter over time, the harmonic spectrum of each inverter is recorded at three separate intervals. Conclusions are drawn from the averaged harmonic performance of each inverter.

The averaged harmonic performance of each individual inverter operating independently is shown in Figure 7-7. As anticipated, the results show some degree of correlation in harmonic profile for each of the two inverters under test.

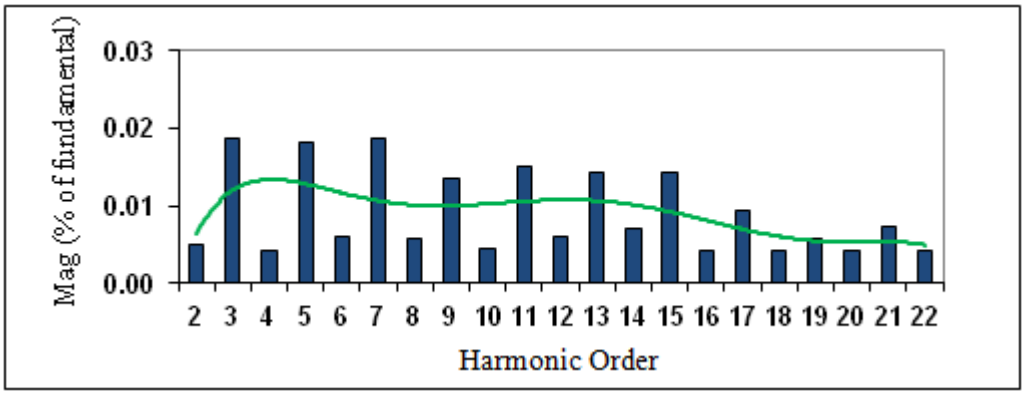

(a)

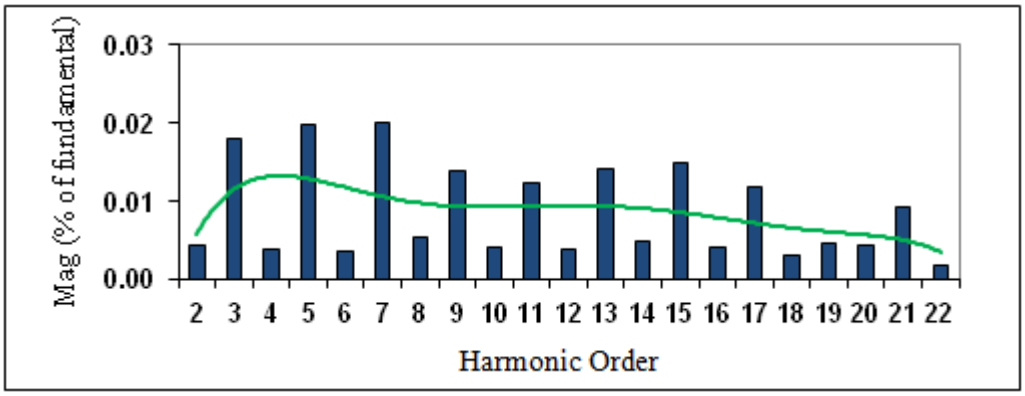

(b)

Figure 7-7: Low order harmonic spectra of (a) Inverter 1 output current with conventional PR control; and (b) Inverter 2 output current with conventional PI control. Results show some degree of correlation in harmonic profile for each of the two inverters.

Table 7-5: THD figures for independently operated, grid connected, inverters using conventional PR current control

Operating Inverter	THD SYSTEM OUTPUT
Inverter 1	4.98%
Inverter 2	4.92%
Single inverter average	**4.95%.**

7.3.2 *Fixed PR Current Control of Two Inverters in Parallel*

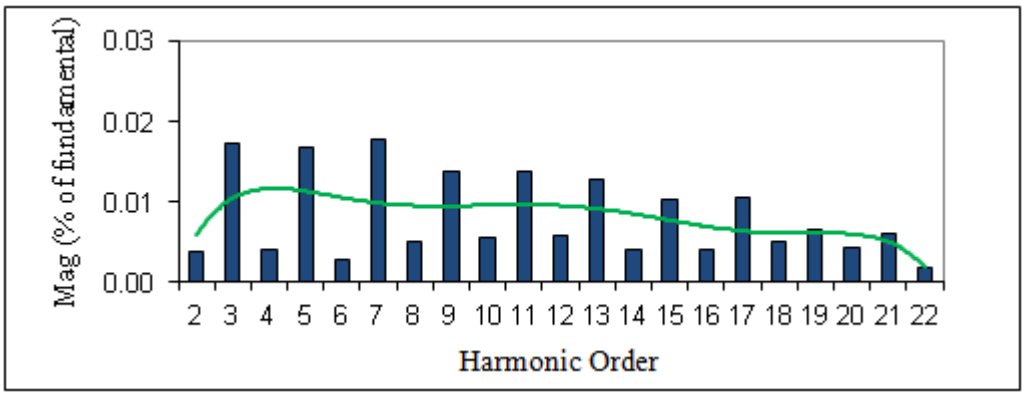

(a)

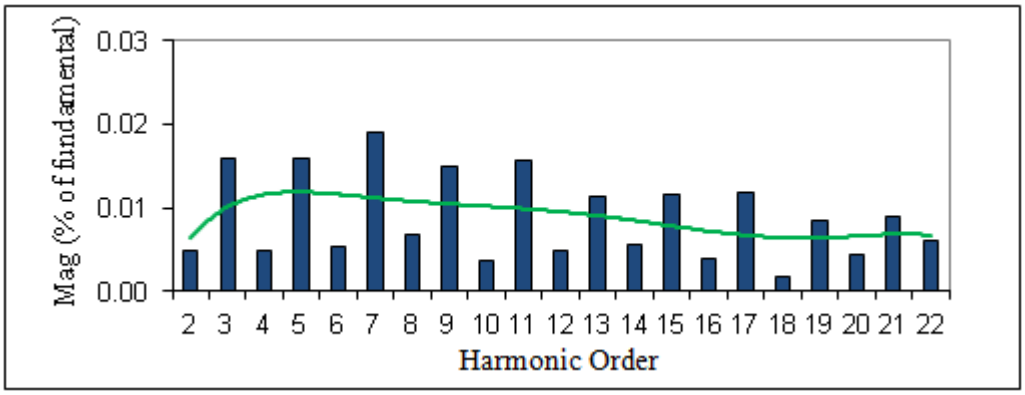

(b)

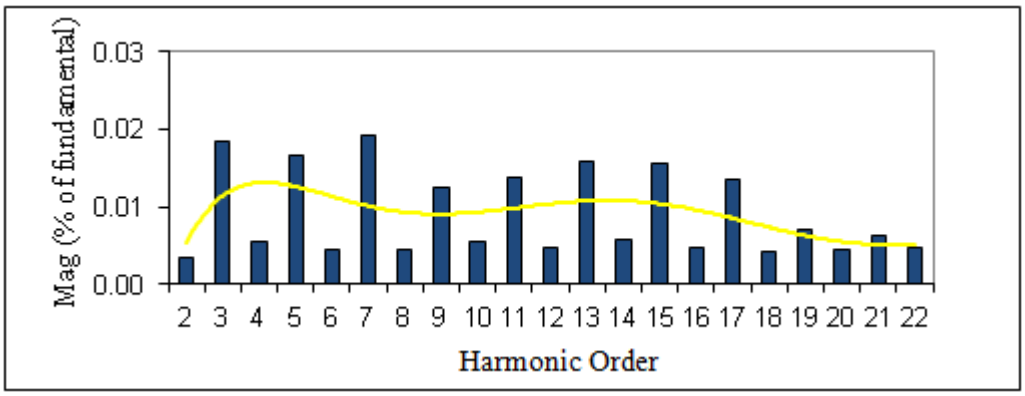

(c)

Figure 7-8: Low order harmonic spectra of parallel inverters with PR current control. (a) Results of inverter 1 output current; (b) Results of Inverter 2 output current; and (c) Results of the parallel system output current. Small cancellation and addition of harmonics are observed at the system output current.

Table 7-6: THD Performance of Two Inverter Parallel System with conventional PR control.

PARALLEL COMBINATION	THD INV 1	THD INV 2	THD SYSTEM OUTPUT
Inverter 1 & Inverter 2	4.98%	5.14%	5.06%

Each inverter is current controlled with the same controller tuning as determined previously during independent operation. In each case, the two applicable inverters are set to operate at unity power factor with respect to the grid voltage. As before, three sets of harmonic data are collected and an averaged harmonic spectrum is determined for each inverter (Figure 7-8). The recorded THD of each individual inverter, along with the parallel inverter system output THD is summarised in Table 7-6. The results show that the average THD of the parallel system output is 5.06% which is better than the average THD of the parallel system when using the conventional PI control.

7.3.3 *Summary: Fixed PR Current Controller*

For the results presented with conventional PR current control, a typical harmonic profile exists, although it differs that observed with the conventional PI controller. Results show that the largest distortion components are at the 3rd, 7th, 9th and 11th harmonic, although importantly these are less of a problem. Similar characteristics are observed when the two converters are operated in parallel, and at the point of common coupling there are still signs of harmonic addition.

7.3.4 *Experimental Results with Randomised PR Current Control Techniques*

This sub-section presents results for the parallel inverter system when controlled via the randomised parameter of the PR control method. Each inverter is tuned independently via the software parameters.

7.3.5 *Parameter Randomisation PR Current Control of Individual Inverter Units*

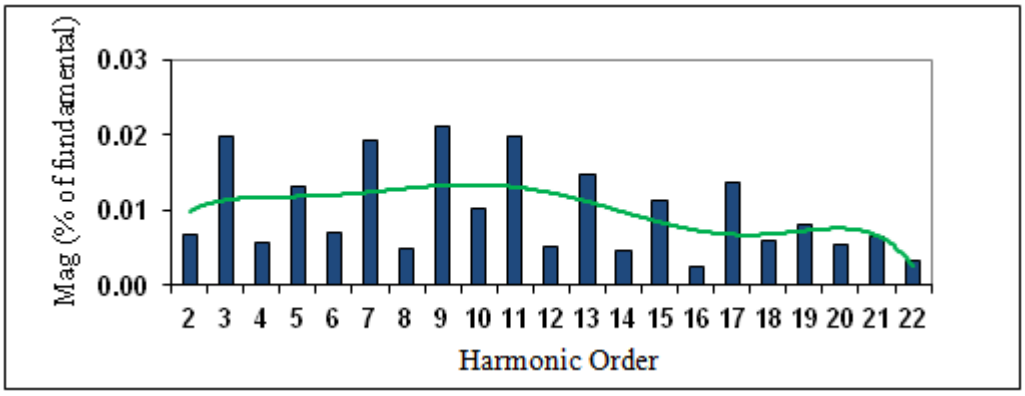

(a)

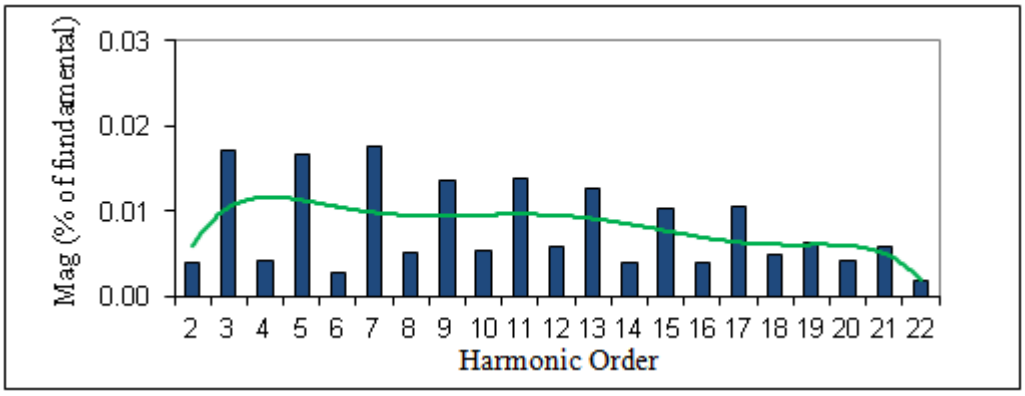

(b)

Figure 7-9: Low order harmonic spectra of (a) Inverter 1 output current with randomised PR control; and (b) Inverter 2 output current with randomised PR control. Different trend line patterns indicate the reduction in the degree of correlation in the harmonic profile.

Figure 7-9 shows the averaged harmonic spectrum of each inverter when operated as a single inverter system. The results demonstrate the success of the controller randomisation in generating differing trend line patterns, thus indicating a reduction in the degree of correlation in the harmonic profile of each inverter. This result suggests

that the controller randomisation technique is well suited to a grid connected inverter system employing a PR controller. In terms of the aims and objectives of this work, this is a successful outcome and one of the main contributions to knowledge.

Table 7-7: THD figures for independently operated, grid connected, inverters using randomised PR current control.

Operating Inverter	THD SYSTEM OUTPUT
Inverter 1	4.98%
Inverter 2	5.12%
Single inverter average	**5.05%.**

7.3.6 *Parameter Randomisation PR Current Control of Two Inverters in Parallel*

Having assessed the performance of the inverters operating independently, the inverters are again configured to form a parallel, two inverter, grid connected system. The circuit topology remains the same as described for the conventional PI current control scheme; whereby current measurements are made by the power analyser at the output of each individual inverter, and the point of common coupling. Three sets of harmonic data are collected, and an averaged harmonic spectrum is determined for each inverter Figure 7-10. The recorded THD of each individual inverter, along with the parallel inverter system output THD, is summarised in Table 7-8. The results show that the average THD of the parallel system output is 4.36%.

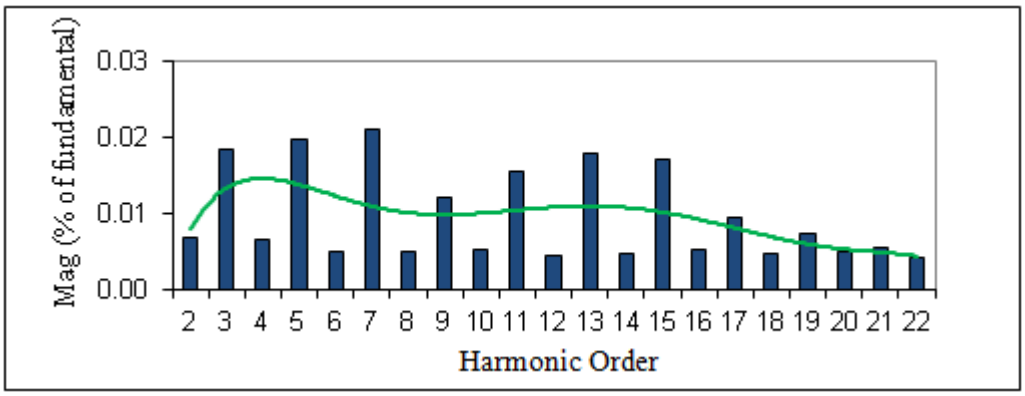

(a)

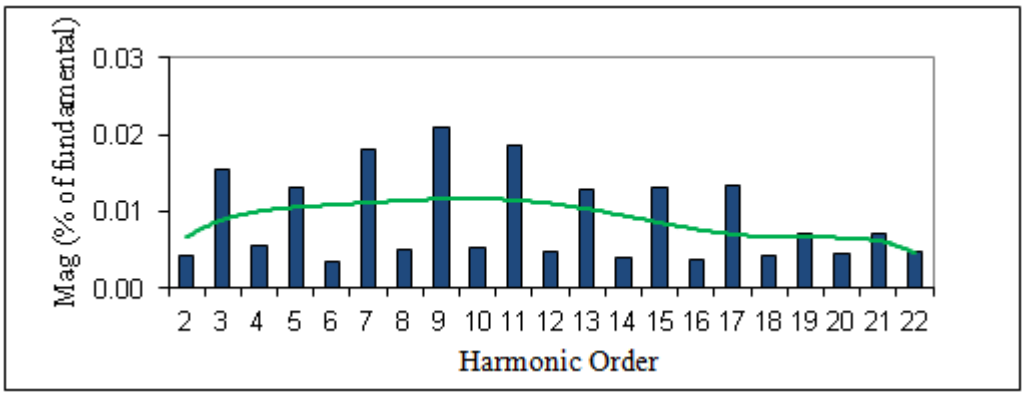

(b)

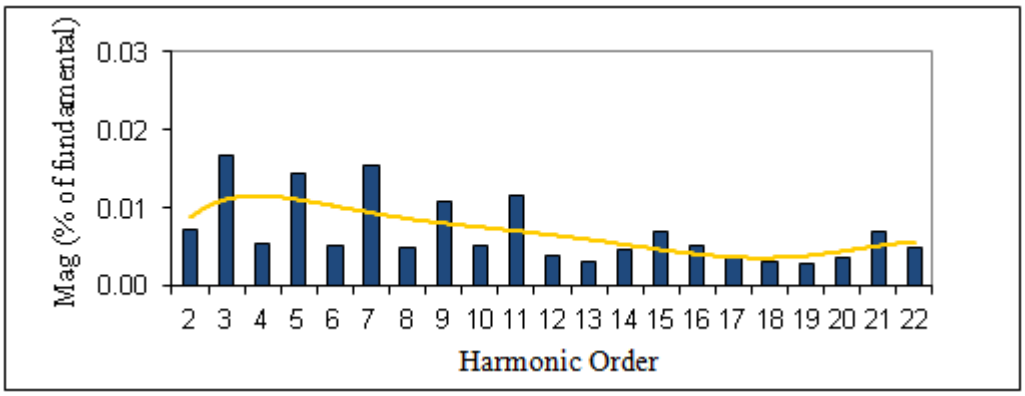

(c)

Figure 7-10: Low order harmonic spectra of parallel inverters with randomised PR current control. (a) Results of inverter 1 output current; (b) Results of Inverter 2 output current; and (c) Results of the parallel system output current. Harmonics magnitude reduction are observed at the parallel system output current between the 7^{th} and 19^{th} order.

Table 7-8: THD Performance of Two Inverter Parallel System with randomised PR control.

PARALLEL COMBINATION	THD INV 1	THD INV 2	THD SYSTEM OUTPUT
Inverter 1 & Inverter 2	4.88%	5.02%	4.34%

7.3.7 *Summary: Parameter Randomisation PR Current Controller*

The results presented for the random parameter PR current controller confirm that it is possible to adjust the harmonic performance of each inverter unit. By using the random parameter PR controller, the harmonic profile of each inverter unit now dynamically varies with time in a similar way to that observed in the PI controller case. It is believed that this is the first time that this approach has been applied to the PR controller in a grid connected power converter system.

The THD of each inverter individual unit is still typically just under 5%, when operated as a parallel inverter system a lower average THD is observed at the point of common coupling. For a two inverter parallel system, the average THD is measured as 4.34%.

This marks a significant improvement over the individual inverter case. Furthermore, it also represents a further reduction in harmonic content compared to the conventional PI current controller approach. Whilst some caution has to be paid to the deliberately induced random nature of the results, it is apparent that there is an improvement in the low order harmonics around the 7^{th} and 9^{th} harmonic. This is an area which is difficult to address with the PI controller approach.

Due to the randomised nature of the proposed controller, the harmonic profile tends to become flatter once inverters are operating in parallel. This is to be expected, since harmonic cancellation starts to take place once the randomised controller is applied. This is in contrast to the fixed parameter controller, where the harmonics typically reinforce due to the similar harmonic profiles.

As the number of parallel inverters increases, the opportunities for harmonic cancellation will increase, hence the harmonic profile should tend to flatten out further. However, as noted by Armstrong and in this work, the lowest order harmonics tend to

be dominant, hence these are the most difficult to eradicate. Therefore, a point is likely to be reached where increasing the number of inverters in parallel brings a diminishing return in terms of overall harmonic performance. The point of which this happens is presently unknown. It would require complex statistical mathematics to be applied, which is presently beyond the scope of this work. However, it does provide scope for potential future research work for optimising the scale of the system.

7.4 Chapter Summary

This chapter has presented experimental results for a grid connected parallel inverter system, implementing both conventional PI, and randomised parameter control techniques. The results show that, on average, the current THD at the parallel inverter system output is lower when using the randomised current control method. With conventional current control, the harmonic spectrum of each inverter demonstrates a high degree of correlation with the harmonic spectra of all other inverters in the parallel system. This results in reinforcement of current harmonics at the parallel inverter system output. By introducing randomised parameter current control, the harmonic spectrum of each inverter is likely to differ from that of all other inverters. Therefore, there is less chance of harmonic reinforcement at the parallel inverter system output. The differing harmonic profiles enhance the opportunities for harmonic cancellation in the system output current. This is reflected in the reduced current total harmonic distortion of the parallel inverter system output.

Chapter 8: Conclusions

8.1 Conclusions

This thesis has presented research into power quality improvement of grid connected inverter systems. In grid connected system, it is vital to inject a unity power factor current into the grid with low levels of harmonic distortion. This can be achieved with an appropriate choice of inverter topology, PWM switching scheme, passive filter components, and current control scheme.

This work has specifically focused on improving the low order harmonic performance of grid connected inverters by investigating the impact of different current control methods. In this work, three techniques have been analysed, simulated, and experimentally validated. They are the conventional PI control technique, the proportional resonant (PR) control technique, and a novel modified proportional resonant control technique.

The classic PI controller is very well understood and often applied by engineers in industry. It has been successfully applied in grid connected inverter applications, and shown it provide good overall performance. Literature shows that many different tuning algorithms have been applied to the PI controller. Furthermore, novel approaches such as gain randomisation have successfully been applied to achieve better low order harmonic performance.

Despite the general merits of the PI controller, literature also shows a move away from this control technique in grid connected applications. It is reported that the PI controller suffers from steady state error when tracking AC signals. Such characteristics have been confirmed in this research by considering the PI controller error signal.

For this reason, investigators are now leaning to alternative control methods such as the Proportional Resonant (PR) controller. It is stated that this controller does not exhibit the same steady state error when tracking AC signals. The work carried out in this thesis appears to agree with conclusion, since the controller error signal is improved compared to the PI controller. From this, it appears that there are distinct advantages to applying the PR controller.

For this reason, following the same methodology as first applied to the PI controller by Armstrong [33], this thesis set out to test the hypothesis that the gains for the PR controller can also be randomised with a view to improving harmonic performance of parallel connected inverters. Whilst the performance of each individual inverter may not necessarily be improved directly, the overall harmonic injection into the grid may be reduced if the controllers exhibit some degree of randomisation. The author believes that this is the first time that such a technique has been applied to the PR controller in a grid connected inverter system.

In this work it is shown, via simulation and experimental validation that using a modified Proportional Resonant with random proportional gain can modestly improve the THD of the injected grid current in a parallel connected inverters system. The degree of improvement is admittedly only small, but it is believed that better results may have been observed with a larger number of inverters operating in parallel. However, due to limitation of resources for the project, this work was restricted to two inverters only. In principle more inverters operating together should present greater opportunities for harmonic cancellation. Verification of the scheme on a larger scale system is one of the first suggested areas for future work and investigation.

However, the important outcome from this work is knowledge that gain randomisation will work with the PR controller in grid connected inverters has been achieved by this work. This is important given the shift towards this type of controller in grid connected applications.

In Chapter 6, it is identified that the harmonic performance of the conventional PI controller can also be improved by using a random integral gain, R_{KI} instead of a fixed integral gain, K_I . Such Integral gain randomisation was avoided by Armstrong due to concerns over maintaining unity power factor. However, it has been shown in this work, believed to be for the first time, that the integral gain can be modified to improve harmonic performance. Provided the limits of variation are kept very small, the impact on power factor seems minimal. For this reason, the author believes that further studies into variation of all controller parameters may yield further improvement in harmonic performance. At present, the level of randomisation applied is very much determined by a trial and error approach. By observing the performance of the system, and applying cautious limits, the integrity of the system is preserved and performance improvement

is simply recorded. It is therefore suggested that a more comprehensive analytical approach to the problem may reveal more about methods of system optimisation. Furthermore, it could be used to better quantify the robustness of the controller and its system sensitivity to parameter changes. This would

Finally, it is worth noting that this work concentrates solely on small scale single phase inverter systems– typically inverters designed for domestic installation (<3kW). In theory, the controller principles investigated should be applicable to three phase systems. However, this would require a significant amount of additional research work to verify. A number of key points would need to be considered; the recommendations on harmonic limits are different for larger scale inverter systems, the inverter topologies are different, and the control algorithms are fundamentally different – for example Space Vector Modulation techniques. Therefore, in the future, there is potential for investigation into three phase applications.

Appendix A Multisim and Ultiboard Designing Tool

Before a PCB is made, the schematic diagrams of the circuit are designed in the circuit design suite called Multisim.

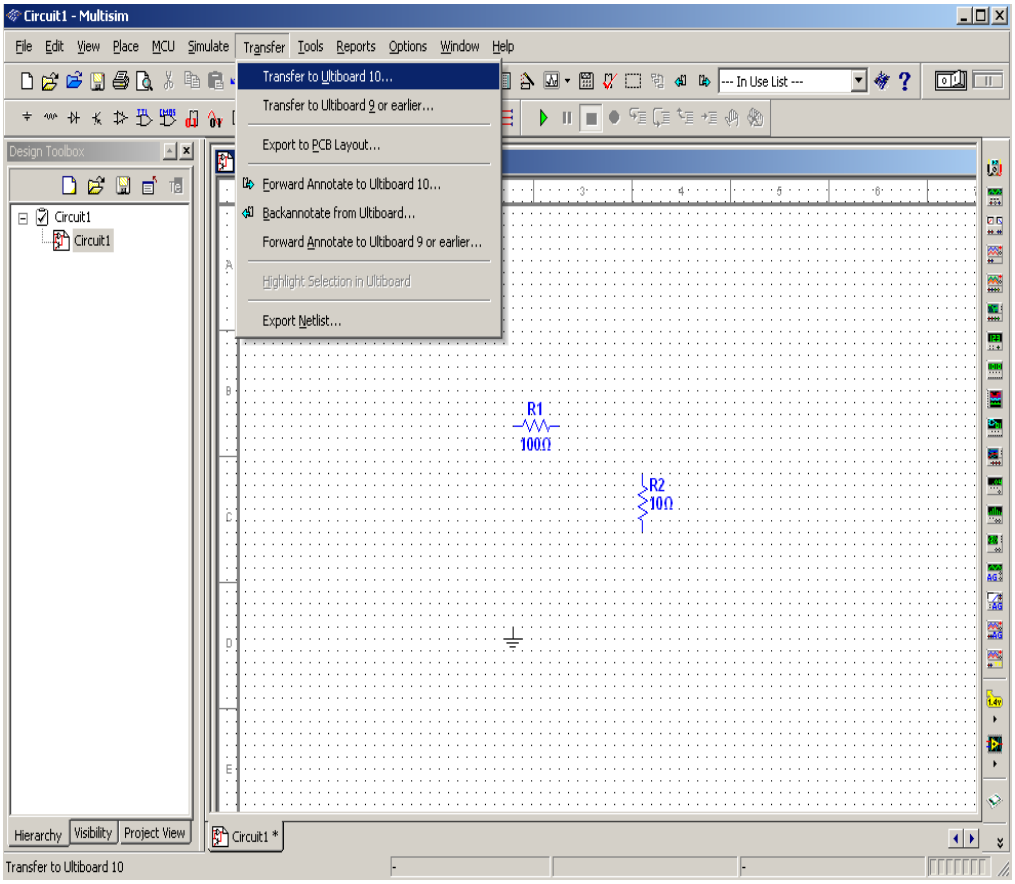

Figure A-1: Screen shot of Multisim designing tool

After all the required components have been placed on the schematic capture space, with point and click, the designs are then transferred to another tool in the circuit design suite called Ultiboard 10.1 as shown in the Figure A-2. This tool will allow the user to create and design the intended PCB.

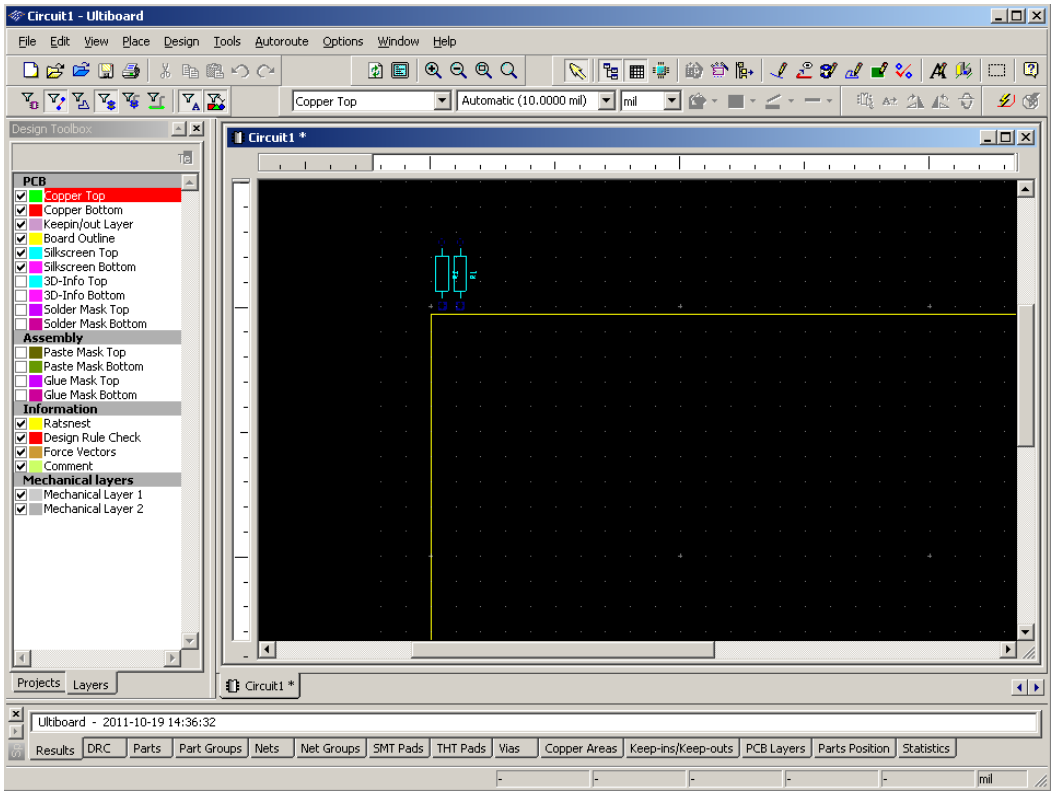

Figure A-2: Screen shot of Ultiboard designing tool

There are five PCBs that were needed to be made in this project. They are the power inverter board, the voltage measurement board, the current measurement board, the gate driver board, and the extension board for the processor. As mentioned in earlier chapter, a TMS320F2812 Digital Signal Processor (DSP) is used as the processor for this project and has been briefly discussed in Chapter 6 . The next following figures are the pictures of the PCBs. The gate driver layout, voltage measurement layout, current measurement layout, and interface layout for the DSP are designed by the previous lab members. However, they are permitted to be used in this research project.

Appendix B Screen Shot of the PCBs

The following pictures are the experimental boards that were used in this research project.

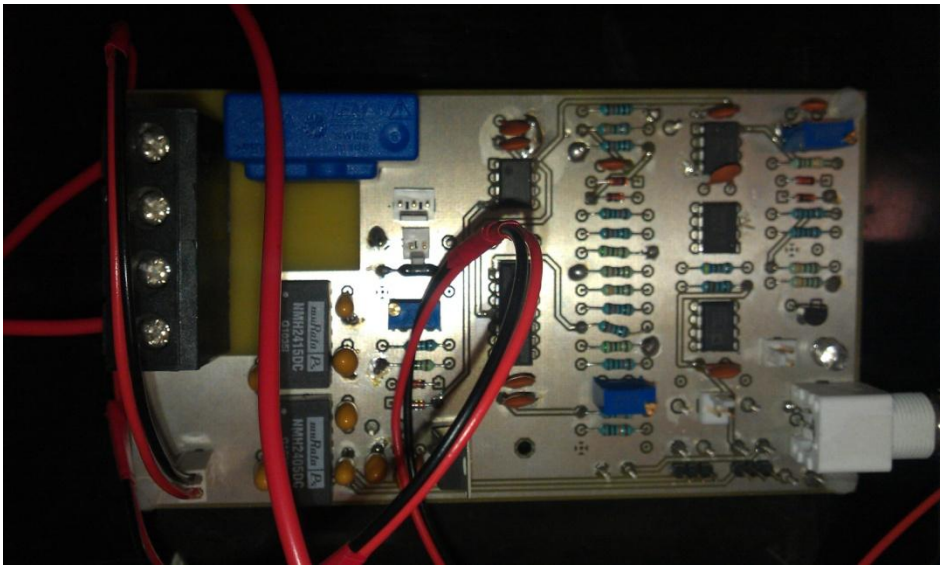

(a) Current measurement board.

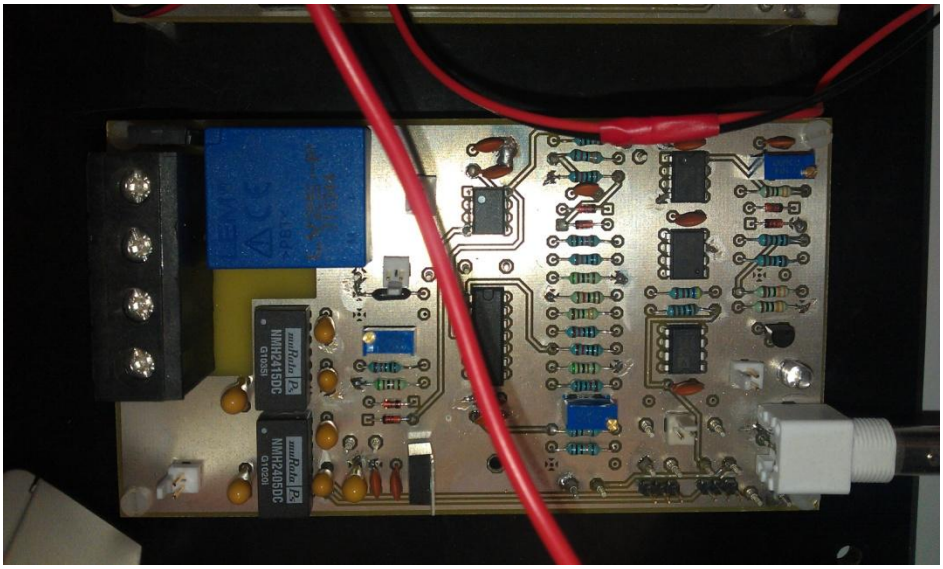

(b) Voltage measurement board.

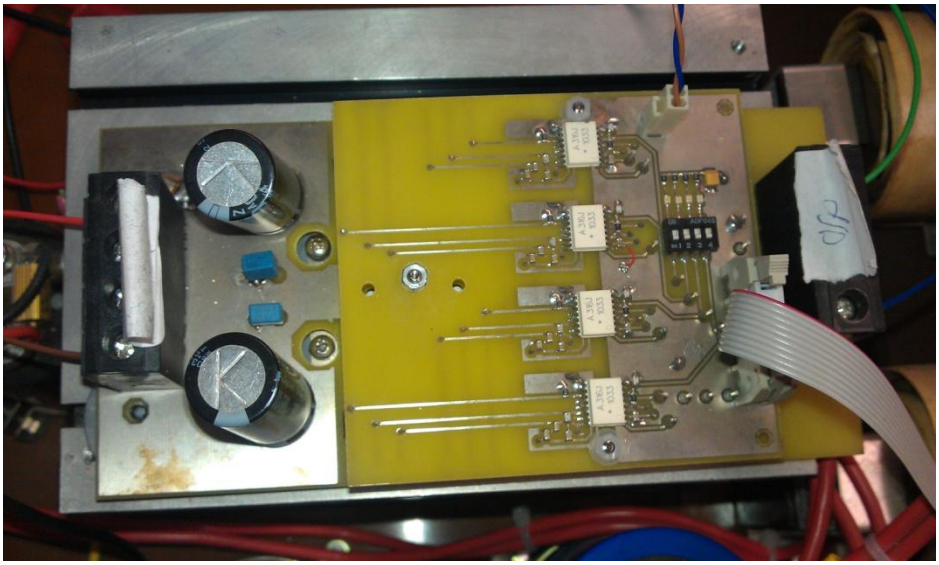

(c) Gate driver and inverter board.

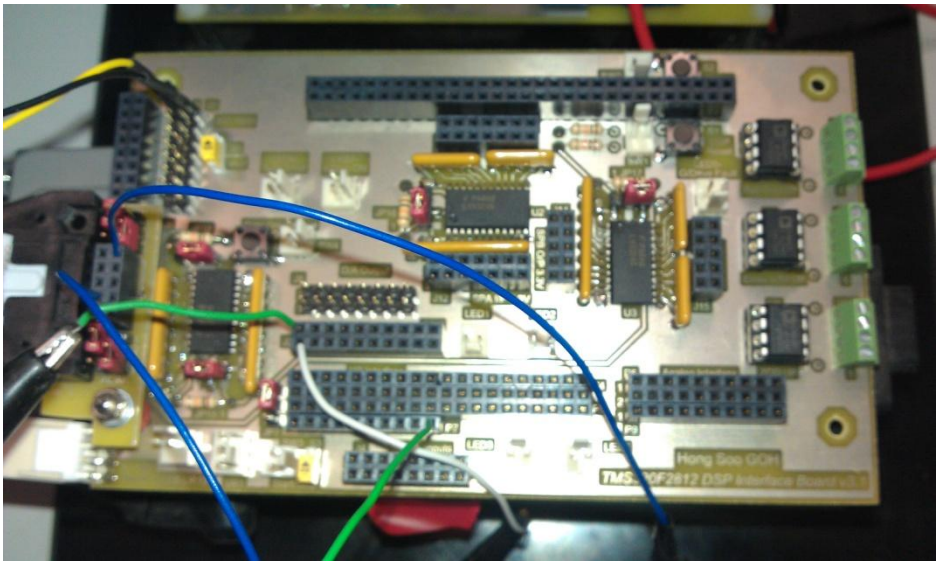

(d) Extension DSP board.

Figure B-1: Screen shot of the PCBs. (a) Current measurement board, (b) Voltage measurement board, (c) Gate driver and inverter board, and (d) Extension DSP board.

Appendix C Schematic Diagram of Single Inverter System

Figure C-1 shows the full circuit diagram of the power inverter board that includes the DC blocking circuit.

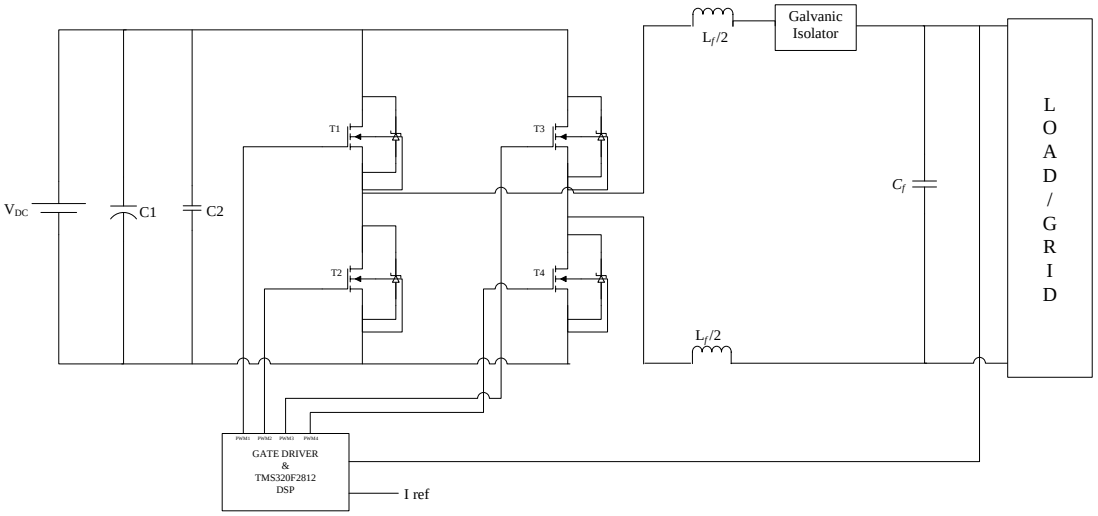

(a) power inverter with filter.

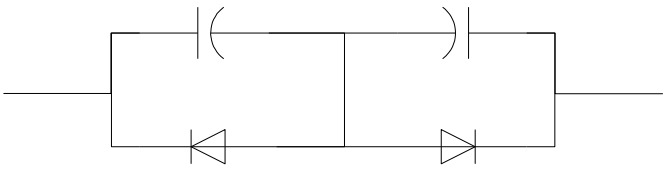

(b) DC blocking circuit.

Figure C-1: Circuit diagram of (a) power inverter board and (b) DC blocking circuit.

The low pass filter consists of two inductors, L_f, of 160 µH each and one 20 µF capacitor, C_f. Besides the filter circuit, another small circuit that consists of capacitors and diodes is connected in series with the output filter. This acts as an isolator to prevent the flowing of DC current to the AC side of the inverter.

Appendix D PWM Generation

The generation of PWM signals can be done using the I/O interface of the DSP. There are two event manager modules; the Event Manager A (EVA) and Event Manager B (EVB). Only the EVA is used in this project where it contains pins of PWM1, PWM2, PWM3, and PWM4 and are used to drive the inverter system. The General Purpose Timer 1 in this module has a compare register T1CMPR and is used to compare the PWM signals with the carrier signal. The following statements explain the step by step way of generating a PWM signal. First, the carrier signal needs to be generated. In order to do this, the period and frequency have to be set as in equation below

$$T1PR = \frac{GPTIMER\_Freq}{2\ x\ PWM\_Freq}$$

(Eq. D.1)

$T1PR$ is the amplitude of the carrier signal, PWM_Freq used in this project was 20 kHz and the $GPTIMER\_Freq$ depends on the determination of a few other registers such as the HISPCP bit 2-0 and T1CON bit 10-8. Below is the adapted diagram to help with the calculation of $GPTIMER\_Freq$ [85].

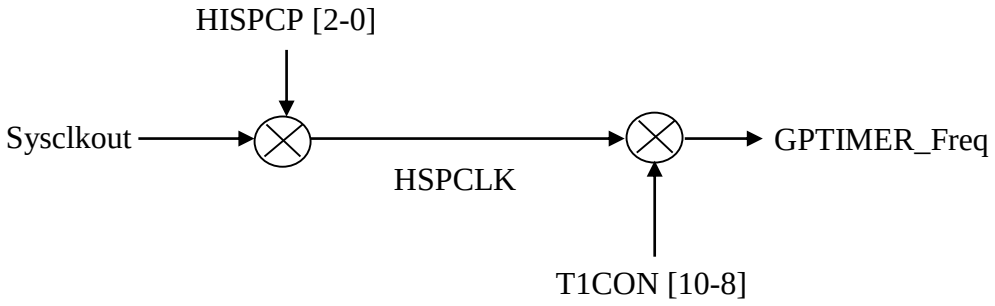

Figure D-1: Diagram to determine the $\boldsymbol{GPTIMER\_Freq}$

From the figure, it can be seen that the system clock out, Sysclkout is scaled for two times in order to get the $GPTIMER\_Freq$. The first scaling depends on bit 2 to bit 0 in

High-Speed Peripheral Clock Prescaler (HISPCP). In this project, the corresponding bits are 000 which is equal to the Sysclkout divided by 1. Sysclkout is equal to the clock into the CPU that is 150 MHz. So, HSPCLK will be 150 MHz as well. The second scaling depends on bit 10 to bit 8 in Timer 1 Control Register (T1CON) which in this project was chosen as 000. This means that HSPCLK must be again divided by 1 and will then give the value of 150 MHz for the $GPTIMER\_Freq$. According to equation 1, the amplitude of the carrier signal, $T1PR$ is 3750.

To get signals from the PWM pins, the compare register T1CMPR need to be loaded to a value in the range of 0 to T1PR. This will give the duty cycles of the PWM pulses. For instance, a pulse of 90% duty cycle can be obtained when the value of T1CMPR is 3750 times 0.9. A pulse of 70% duty cycle can be obtained when the value of T1CMPR is 3750 times 0.7. A pulse of 50% duty cycle can be obtained when the value of T1CMPR is T1PR times 0.5 which is half of T1PR and so on. The following figure is the output signal from pin PWM1 which is copied from the oscilloscope images.

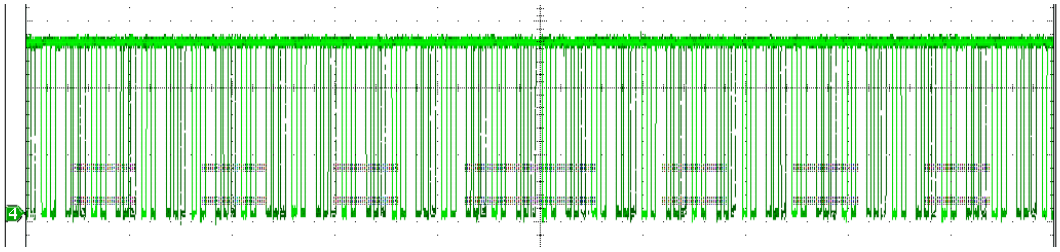

(a) 90% duty cycle.

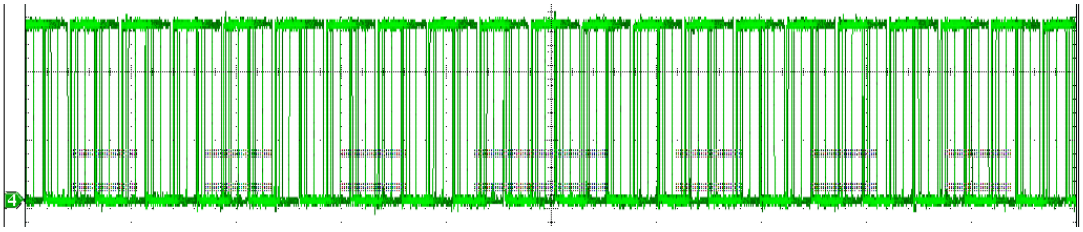

(b) 50% duty cycle.

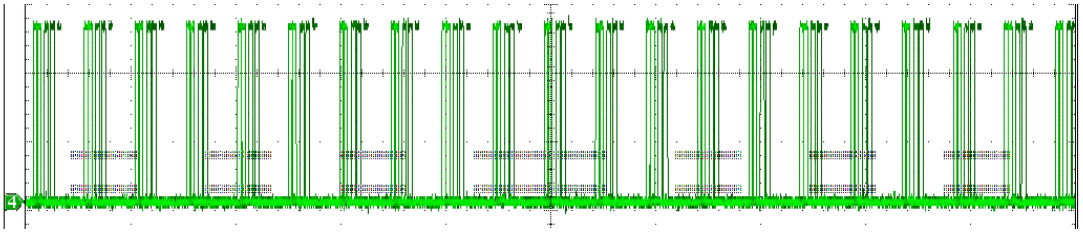

(c) 10% duty cycle.

Figure D-2: Output pin PWM1 with (a) 90% duty cycle, (b) 50% duty cycle, and (c) 10% duty cycle.

Appendix E Dead-time

Often, a short time delay must be applied between the turn on of one Mosfet and the other in the same leg of the inverter. This is to ensure a complete turn off of the upper Mosfet before the turning on the lower Mosfet. It prevents overlap current from each other thus avoiding a shoot-through fault. Shoot-through occurs when both Mosfets are in the on position at one same particular time. Therefore, a dead-time is introduced. In order to set the time, the DBTCONA registers have to be properly setup. For simplicity, below shows the calculation of the dead-time.

$$\text{Dead-time} = p \times m \times \text{HSPCLK} \qquad \text{(Eq. E.1)}$$

where *p* will depend on bit 4 to bit 2 of DBTCONA registers and *m* will depend on bit 11 to bit 8 of DBTCONA registers. Previously, it is known that HSPCLK is equal to 150 MHz which will be 6 ns when it is converted to time. Based on the dead-time formula stated above, a dead-time of approximately 1.7 µs can be set if bit 11 to bit 8 of DBTCONA registers is set to 1000, which is 8 in decimal value, and bit 4 to bit 2 of DBTCONA registers is set to 110, which gives p of 32. Output of the PWM pins are shown in Figure E-1.

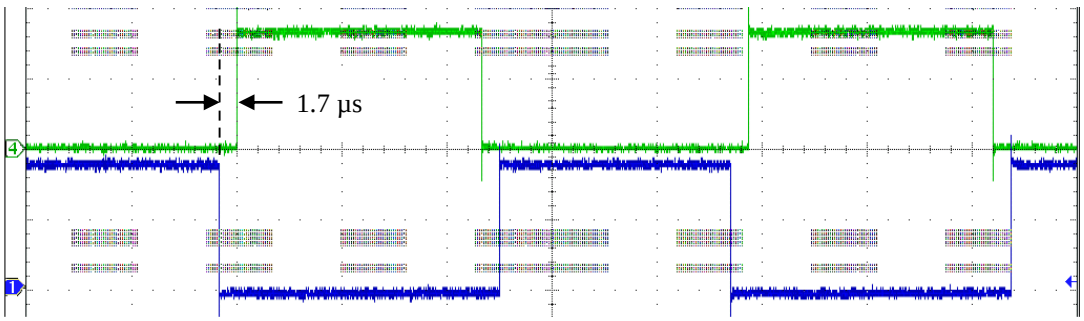

Figure E-1: Signals of PWM1 and PWM2 with approximately 1.7 µs dead-time.

Appendix F Code Composer Studio (CCS)

This software is the development software tool for this project. Here, the user can write codes, edit, and debug. Figure below shows the screen shot of the software.

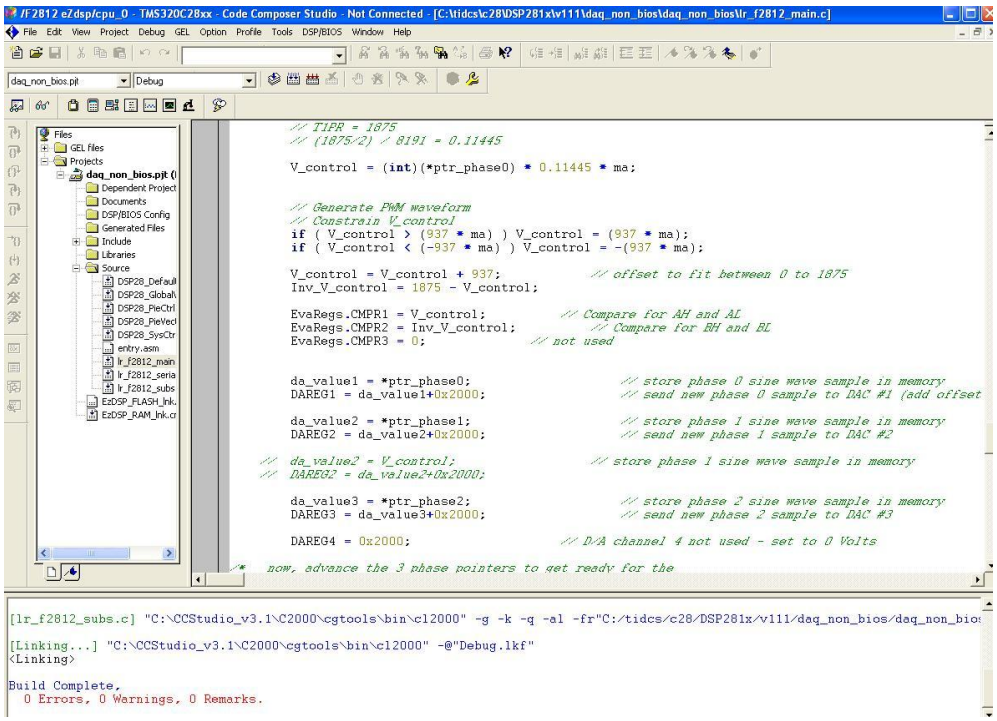

Figure F-1: CCS Software.

After a project has been created and source files have been added, they need to be linked together before the program can be loaded to the DSP. The DSP must be connected as a ‘target’ in order to run the program. This software has a window called the ‘Watch Window’ to watch the program’s variables. There is a tutorial supplied with the software to get a better understanding from creating to compiling a project. Figure F-1 is the C programming code that is written in this software and used to generate the PWM signals. In order to generate PWM signals, a modulating signal has to be created. This modulating signal is a sine waveform and it has already been written into the DSP`s memory originally. For the purpose of this research project, the tasks are; to get a 50 Hz signal with a sampling rate of 20 kHz and to ensure that the peak to peak of the sine waveform will not equal to or more than 3750, which is the peak value of the triangular signal. Therefore, in order to change the sampling rate to 20 kHz or 50 µs,

and to create a 50 Hz sine wave, the table step size need to be increased to 150. This works as follows;

i- the original table size is 60000

ii- 0.02 s ÷ 0.00005 s = 400 steps

iii- equation above means that it must have 400 steps from table size 0 to table size 60000.

iv- that works out to 150 table size increment for each step.

It is known that the amplitude of the original sine wave is 1875. It oscillates between +1875 to -1875. However the triangular waveform is between the values of 0 to 3750. In order to get the PWM signals with modulating amplitude, ma not equal to or more than 1, the modulating signal or the sine wave need to be in the same range as the triangular waveform. To achieve that, a modulating amplitude, ma of 0.95 is set. An offset of 1875 must then be added to the amplitude of the original sine wave and it is then multiplied by the ma. A limit is set to ensure that the sine wave will not go beyond that value. This makes the sine wave oscillates between values of 188 to 3562.

For a unipolar PWM to be generated, two modulating signals of 180° phase difference from one to another have to be compared with the triangular signal. This is done by setting the CMPR1 register to the first modulating signal and setting the CMPR2 register to the inversion of the first modulating signal. Figure F-2 shows an example of the output of PWM1 pin.

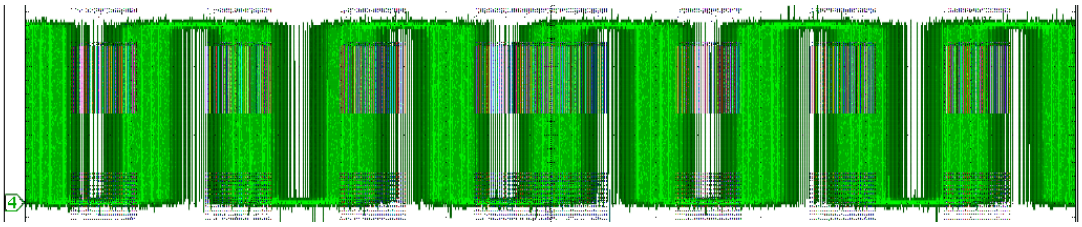

Figure F-2: Output of PWM1 pin after the triangular waveform is compared to the modulating signal ($\boldsymbol{ma}$ = 0.95).

Appendix G Testing an Open Loop System

Before a close loop with any controller system is applied, the power inverter board is tested. A small DC power supply of 10 V is fed to the inverter system and the signals from the PWM pins are connected to the gate driver board to switch the Mosfets. Without connecting a load at the output, the voltage of the output filter is observed on the oscilloscope. It can be seen in Figure G-1 that the amplitude of the waveform is approximately 10 V, which is to be expected. This confirms that the power inverter board connections are correct and can be used for further tests.

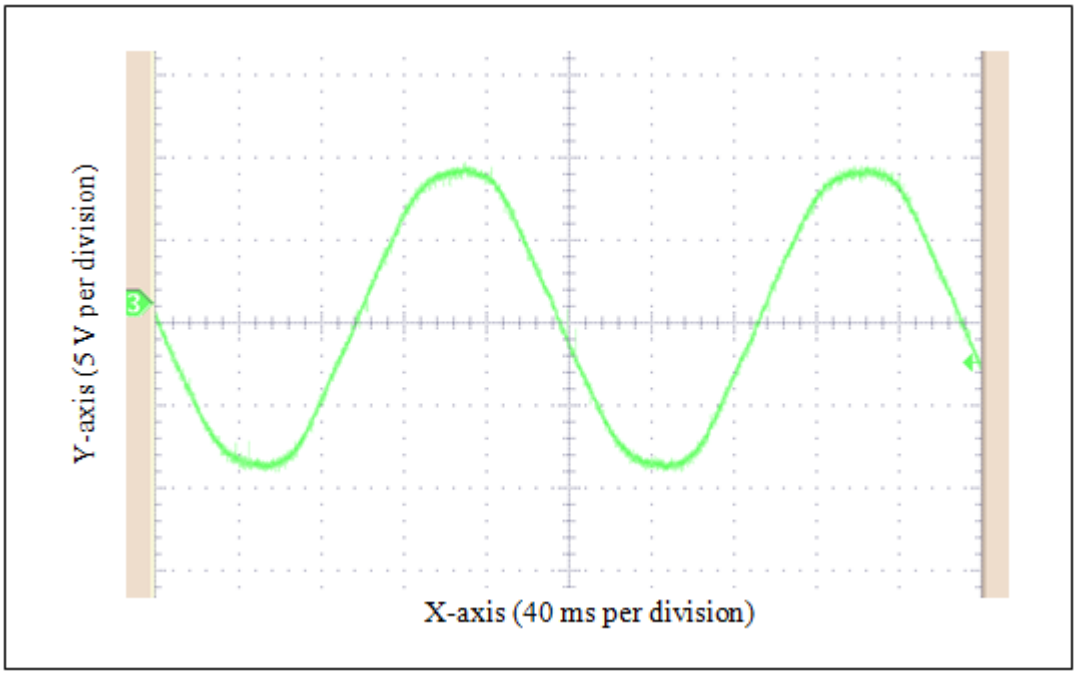

Figure G-1: Waveform of output filter without load

Following that, a resistive load of approximately 5 Ohms is connected at the output of the inverter system. A current probe as in the Figure G-2 is used to measure the current through the load and it is set to 100 mV/A. This setting is then need to be adjusted on the oscilloscope setting so that the reading is in Ampere. This makes one easily read the output current reading on the scope without the need to do any calculation later on.

Figure G-2: Current probe.

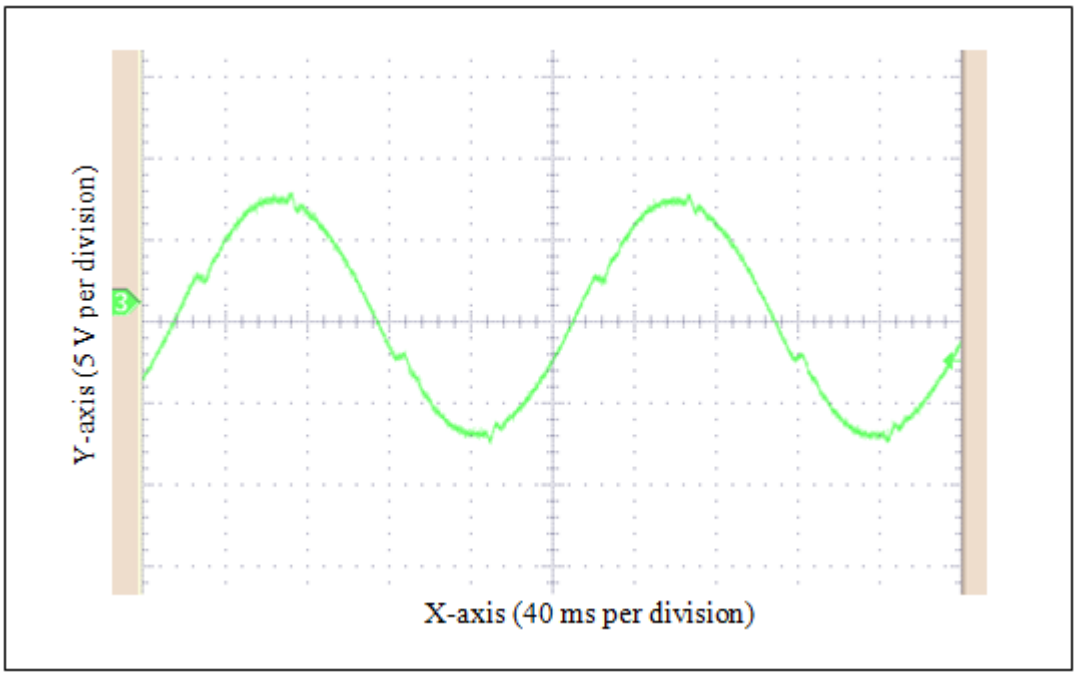

Figure G-3: Waveform of output filter after a resistive load is connected.

From Figure G-1 and Figure G-3, it is clearly seen that the latter has some distortion on the line and magnitude is reduced. This distortion occurred as a result from using dead time in the PWM switching. As for the magnitude reduction, it is expected from the beginning because of the voltage drop.

Appendix H Current Sensor

Gain Adjustment

Aiming that this research project will not give an output current of more than 15 A peak, the gain at the current sensor measurement board has to be adjusted corresponds with the Analogue to Digital (ADC) channel of the DSP board. This is done by connecting the current sensor board with a DC supply voltage and a fixed resistive load at the end where in this case, a load of 2 Ohms is used. Several tests are done with different DC voltages. For example, a DC voltage of 3 V will give a current of 1.5 A and should therefore give a 1 V output at the end of the sensor board. In order to get the 1 V output, the gain in the sensor board need to be adjusted. Following that, with the adjusted gain, the DC supply voltage is increased to 6 V in order to give the output current of 3 A. The voltage at the output of the sensor board is then measured and it must be confirmed to give the value of 2 V. Same step is repeated with this time a DC supply voltage of 9 V. When the measured output voltage of the sensor board is 3 V, the current sensor board is ready to be used for this project.

Accuracy

Accuracy of any analogue to digital (ADC) channel measurement is a very important aspect to look at. It is called the resolution. Using a low resolution of ADC basically means that the measurement is not accurate and a high resolution ADC will give a very high accuracy measurement. As the ADC used in this research project is of 14 bits and in the range of ±10V, the resolution is then can be calculated using the formula as in Eq. H.1.

$$Q_v = \frac{V_{FSR}}{2^N - 1}$$

(Eq. H.1)

$$= \frac{20}{2^{14} - 1}$$

$= 1.2\ mV$

Earlier, it is known that 1 V output measured from the current sensor is equal to 1.5 A current from the input. Equation above means that there need to be a change of at least 1.2 mV or 0.012 mA in the input for the output to change. This shows that the resolution of the ADC is very high, accurate, and very acceptable to be used for this research project.

References:

[1] R. DeGunther (2009). "*Alternative Energy For Dummies*." Wiley Publishing. ISBN 9780470430620.

[2] P. Chiradeja, "Benefit of Distributed Generation: A Line Loss Reduction Analysis," in *Transmission and Distribution Conference and Exhibition: Asia and Pacific, 2005 IEEE/PES*, 2005, pp. 1-5.

[3] Y. Ma *et al*, "Distributed generation system development based on various renewable energy resources," in *Control Conference (CCC), 2011 30th Chinese*, 2011, pp. 6203-6207.

[4] D. Chen and L. Xu, "DC microgrid with variable generations and energy storage," in *Renewable Power Generation (RPG 2011), IET Conference on*, 2011, pp. 1-6.

[5] B. Williams *et al*, "Using microgrids to integrate distributed renewables into the grid," in *Innovative Smart Grid Technologies Conference Europe (ISGT Europe), 2010 IEEE PES*, 2010, pp. 1-5.

[6] S. Jahdi *et al*, "Grid integration of wind-solar hybrid renewables using AC/DC converters as DG power sources," in *Sustainable Technologies (WCST), 2011 World Congress on*, 2011, pp. 171-177.

[7] L. O. Williams (2002). "*An end to global warming"*. Pergamon, ISBN 9780080440453.

[8] K. F. Katiraei *et al*, "Solar PV Integration Challenges," *Power and Energy Magazine, IEEE*, vol. 9, pp. 62-71, 2011.

[9] REN21, "Renewables 2010 Global Status Report," ed, 2010.

[10] R. Foster *et al (2009).* "*Solar Energy: Renewable Energy and the Environment"*. CRC Press. ISBN 978-1420075663.

[11] R. A. Ewing and D. Pratt (2005), "*Got sun? go solar: get free renewable energy to power your grid-tied home*". PixyJack Press. ISBN 9780977372461.

[12] F. C. Treble (1991). "*Generating electricity from the sun*". Pergamon Press. ISBN 9780080409368.

[13] B. K. Hodge (2010). "*Alternative energy systems and applications*". Wiley. ISBN 9780470142509.

[14] B. M. Hasaneen and A. A. Elbaset Mohammed, "Design and simulation of DC/DC boost converter," in *Power System Conference, 2008. MEPCON 2008. 12th International Middle-East*, 2008, pp. 335-340.

[15] C.-T. Tsai and S.-H. Chen, "PV Power-Generation System with a Phase-Shift PWM Technique for High Step-Up Voltage Applications," *International Jurnal of Photoenergy*, vol. Volume 2012, Article ID 838231, 2012.

[16] T.Chaitanya *et al*, "Modelling and Simulation of PV Array and its Performance Enhancement Using MPPT (P&O) Technique," *International Journal of Computer Science & Communication Networks*, vol. Vol 1, September-October 2011.

[17] C. Hanju and T. K. Vu, "Comparative analysis of low-pass output filter for single-phase grid-connected Photovoltaic inverter," in *Applied Power Electronics Conference and Exposition (APEC), 2010 Twenty-Fifth Annual IEEE*, 2010, pp. 1659-1665.

[18] J. Selvaraj and N. A. Rahim, "Multilevel Inverter For Grid-Connected PV System Employing Digital PI Controller," *Industrial Electronics, IEEE Transactions on*, vol. 56, pp. 149-158, 2009.

[19] K. Kang-Hoon *et al*, "The power factor control system of photovoltaic power generation system," in *Power Conversion Conference, 2002. PCC Osaka 2002. Proceedings of the*, 2002, pp. 643-646 vol.2.

[20] J. Selvaraj *et al*, "Digital PI current control for grid connected PV inverter," in *Industrial Electronics and Applications, 2008. ICIEA 2008. 3rd IEEE Conference on*, 2008, pp. 742-746.

[21] M. Katiamoorthy *et al*, "A new single-phase PV fed five-level inverter topology connected to the grid," in *Communication Control and Computing Technologies (ICCCCT), 2010 IEEE International Conference on*, 2010, pp. 196-203.

[22] W. Xiaojin *et al*, "Optimal Design of Structures of PV Array in Photovoltaic Systems," in *Intelligent System Design and Engineering Application (ISDEA), 2010 International Conference on*, 2010, pp. 9-12.

[23] M. Ciobotaru *et al*, "Control of single-stage single-phase PV inverter," in *Power Electronics and Applications, 2005 European Conference on*, 2005, pp. 10 pp.-P.10.

[24] Z. Zhe *et al*, "An optimal control method for grid-connected photovoltaic micro-inverter to improve the efficiency at light-load condition," in *Energy Conversion Congress and Exposition (ECCE), 2011 IEEE*, 2011, pp. 219-224.

[25] M. Johns, *et al.* Grid-Connected Solar Electronics. [Contemporary Energy Issues].

[26] K. Jung-Min *et al*, "Grid-Connected Photovoltaic Multistring PCS With PV Current Variation Reduction Control," *Industrial Electronics, IEEE Transactions on*, vol. 56, pp. 4381-4388, 2009.

[27] R. H. Wills *et al*, "The AC photovoltaic module," in *Photovoltaic Specialists Conference, 1996., Conference Record of the Twenty Fifth IEEE*, 1996, pp. 1231-1234.

[28] K. S.K. *et al*, "Power Quality in Grid connected Renewable Energy Systems: Role of Custom Power Devices," *International Conference on Renewable Energies and Power Quality (ICREPQ'10)*, 2010.

[29] M. Calais *et al*, "Inverters for single-phase grid connected photovoltaic systems-an overview," in *Power Electronics Specialists Conference, 2002. pesc 02. 2002 IEEE 33rd Annual*, 2002, pp. 1995-2000.

[30] G. T. Heydt, "Electric power quality: a tutorial introduction," *Computer Applications in Power, IEEE*, vol. 11, pp. 15-19, 1998.

[31] "IEEE Recommended Practice for Utility Interface of Photovoltaic (PV) Systems," *IEEE Std 929-2000*, 2000.

[32] E. Caamano *et al*, "State-of -the-art on dispersed PV power generation: Publications review on the impacts of PV distributed generation and electricity networks," Intelligent Energy Europe 2007-07-23 2007.

[33] M. Armstrong *et al*, "Low order harmonic cancellation in a grid connected multiple inverter system via current control parameter randomization," *IEEE Transactions on Power Electronics*, vol. 20, pp. 885-892, 2005.

[34] M. Cespedes and J. Sun, "Renewable Energy Systems Instability Involving Grid-Parallel Inverters," in *Applied Power Electronics Conference and Exposition, 2009. APEC 2009. Twenty-Fourth Annual IEEE*, 2009, pp. 1971-1977.

[35] George J. Wakileh (2010). "Power Systems Harmonics: Fundamentals, Analysis and Filter Design". Springer. ISBN 9783642075933.

[36] J. Schlabbach *et al*, "Influence of Harmonic System Voltages on the Harmonic Current Emission of Photovoltaic Inverters," in *Power Engineering, Energy and Electrical Drives, 2007. POWERENG 2007. International Conference on*, 2007, pp. 545-550.

[37] G. Chicco *et al*, "Characterisation and assessment of the harmonic emission of grid-connected photovoltaic systems," in *Power Tech, 2005 IEEE Russia*, 2005, pp. 1-7.

[38] A. Celebi and M. Colak, "The effects of harmonics produced by grid connected photovoltaic systems on electrical networks."

[39] J. S. Subjak, Jr. and J. S. McQuilkin, "Harmonics-causes, effects, measurements, and analysis: an update," *Industry Applications, IEEE Transactions on,* vol. 26, pp. 1034-1042, 1990.

[40] V. E. Wagner *et al*, "Effects of harmonics on equipment," *Power Delivery, IEEE Transactions on,* vol. 8, pp. 672-680, 1993.

[41] D. G. Infield *et al*, "Power quality from multiple grid-connected single-phase inverters," *Power Delivery, IEEE Transactions on,* vol. 19, pp. 1983-1989, 2004.

[42] I. T. Papaioannou *et al*, "Harmonic impact of small photovoltaic systems connected to the LV distribution network," in *Electricity Market, 2008. EEM 2008. 5th International Conference on European*, 2008, pp. 1-6.

[43] A. Kotsopoulos *et al*, "Zero-crossing distortion in grid-connected PV inverters," *Industrial Electronics, IEEE Transactions on*, vol. 52, pp. 558-565, 2005.

[44] G. Hong Soo *et al*, "The effect of grid operating conditions on the current controller performance of grid connected photovoltaic inverters," in *Power Electronics and Applications, 2009. EPE '09. 13th European Conference on*, 2009, pp. 1-8.

[45] "IEEE Recommended Practices and Requirements for Harmonic Control in Electrical Power Systems," *IEEE Std 519-1992*, 1993.

[46] M. Armstrong *et al*, "Auto-calibrating dc link current sensing technique for transformerless, grid connected, H-bridge inverter systems," *IEEE Transactions on Power Electronics*, vol. 21, pp. 1385-1393, 2006.

[47] A. Testa *et al*, "Interharmonics: Theory and Modeling," *Power Delivery, IEEE Transactions on,* vol. 22, pp. 2335-2348, 2007.

[48] T. Abeyasekera *et al*, "Suppression of line voltage related distortion in current controlled grid connected inverters," *Power Electronics, IEEE Transactions on*, vol. 20, pp. 1393-1401, 2005.

[49] H. Zhang *et al*, "Switching harmonics in the DC link current in a PWM AC-DC-AC converter," in *Industry Applications Conference, 1995. Thirtieth IAS Annual Meeting, IAS '95., Conference Record of the 1995 IEEE*, 1995, pp. 2649-2655 vol.3.

[50] S. Ma *et al*, "On suppression technologies of switching harmonics based on VVVF," in *Control Conference (CCC), 2011 30th Chinese*, 2011, pp. 5137-5141.

[51] I. E. P. Copper Development Association. *Power Quality Application Guide: Harmonics-Interharmonics*.

[52] C. Li *et al*, "Interharmonics: Basic concepts and techniques for their detection and measurement," *Electric Power Systems Research*, vol. 66, pp. 39-48, 2003.

[53] Z. Leonowicz, "Analysis of sub-harmonics in power systems," in *Environment and Electrical Engineering (EEEIC), 2010 9th International Conference on*, 2010, pp. 125-127.

[54] V. Salas *et al*, "DC Current Injection Into the Network from PV Grid Inverters," in *Photovoltaic Energy Conversion, Conference Record of the 2006 IEEE 4th World Conference on*, 2006, pp. 2371-2374.

[55] L. Gertmar *et al*, "On DC injection to AC grids from distributed generation," in *Power Electronics and Applications, 2005 European Conference on*, 2005, pp. 10 pp.-P.10.

[56] R. Gonzalez *et al*, "High-Efficiency Transformerless Single-phase Photovoltaic Inverter," in *Power Electronics and Motion Control Conference, 2006. EPE-PEMC 2006. 12th International*, 2006, pp. 1895-1900.

[57] H. S. Patel and R. G. Hoft, "Generalized Techniques of Harmonic Elimination and Voltage Control in Thyristor Inverters: Part I--Harmonic Elimination," *Industry Applications, IEEE Transactions on*, vol. IA-9, pp. 310-317, 1973.

[58] R. Teodorescu *et al*, "A new control structure for grid-connected LCL PV inverters with zero steady-state error and selective harmonic compensation," in *Applied Power Electronics Conference and Exposition, 2004. APEC '04. Nineteenth Annual IEEE*, 2004, pp. 580-586 Vol.1.

[59] S. Xiu'e *et al*, "Proportional-resonant current control of single-phase grid-tied PV inverter system," in *Electricity Distribution (CICED), 2010 China International Conference on*, 2010, pp. 1-4.

[60] S. Guoqiao *et al*, "A New Current Feedback PR Control Strategy for Grid-Connected VSI with an LCL Filter," in *Applied Power Electronics Conference and Exposition, 2009. APEC 2009. Twenty-Fourth Annual IEEE*, 2009, pp. 1564-1569.

[61] S. Guoqiao *et al*, "An Improved Control Strategy for Grid-Connected Voltage Source Inverters With an LCL Filter," *Power Electronics, IEEE Transactions on*, vol. 23, pp. 1899-1906, 2008.

[62] M. Castilla *et al*, "Linear Current Control Scheme With Series Resonant Harmonic Compensator for Single-Phase Grid-Connected Photovoltaic Inverters," *Industrial Electronics, IEEE Transactions on*, vol. 55, pp. 2724-2733, 2008.

[63] R. A. Villarreal-Ortiz *et al*, "Centroid PWM technique for inverter harmonics elimination," *Power Delivery, IEEE Transactions on*, vol. 20, pp. 1209-1210, 2005.

[64] L. G. Franquelo *et al*, "A Flexible Selective Harmonic Mitigation Technique to Meet Grid Codes in Three-Level PWM Converters," *Industrial Electronics, IEEE Transactions on*, vol. 54, pp. 3022-3029, 2007.

[65] H. Qunhai *et al*, "A new method for the photovoltaic grid-connected inverter control," in *Electric Utility Deregulation and Restructuring and Power Technologies, 2008. DRPT 2008. Third International Conference on*, 2008, pp. 2626-2629.

[66] M. A. A. Younis *et al*, "Distributed generation with parallel connected inverter," in *Industrial Electronics and Applications, 2009. ICIEA 2009. 4th IEEE Conference on*, 2009, pp. 2935-2940.

[67] M. A. A. Younis *et al*, "High efficiency THIPWM three-phase inverter for grid connected system," in *Industrial Electronics & Applications (ISIEA), 2010 IEEE Symposium on*, 2010, pp. 88-93.

[68] A. M. Roslan *et al*, "Improved Instantaneous Average Current-Sharing Control Scheme for Parallel-Connected Inverter Considering Line Impedance Impact in Microgrid Networks," *Power Electronics, IEEE Transactions on*, vol. 26, pp. 702-716, 2011.

[69] M. Jafari *et al*, "Robust controller design for parallel multi-inverter systems-synthesis," in *Power and Energy Conference, 2008. PECon 2008. IEEE 2nd International*, 2008, pp. 619-624.

[70] M. Khodsuz and A. Sheikholeslami, "Voltage regulation and harmonic compensation in stand-alone inverter-based distributed generation using non-sinusoidal hysteresis voltage control," in *Power Electronics and Intelligent Transportation System (PEITS), 2009 2nd International Conference on*, 2009, pp. 44-49.

[71] B. Geethalakshmi *et al*, "Harmonic compensation using multilevel inverter based shunt active power filter," in *Power Electronics, Drives and Energy Systems (PEDES) & 2010 Power India, 2010 Joint International Conference on*, 2010, pp. 1-6.

[72] N. Mahamad *et al*, "Application of LC filter in harmonics reduction," in *Power and Energy Conference, 2004. PECon 2004. Proceedings. National*, 2004, pp. 268-271.

[73] A. Zabihinejad and J. S. Moghani, "Implementation of a novel vector-controlled drive by Direct Injection of Random Signal," in *Vehicle Power and Propulsion Conference, 2008. VPPC '08. IEEE*, 2008, pp. 1-5.

[74] L. Bowtell and A. Ahfock, "Comparison between unipolar and bipolar single phase gridconnected inverters for PV applications," in *Power Engineering Conference, 2007. AUPEC 2007. Australasian Universities*, 2007, pp. 1-5.

[75] R. Sharma and J. A. R. Ball, "Unipolar switched inverter low-frequency harmonics caused by switching delay," *Power Electronics, IET*, vol. 2, pp. 508-516, 2009.

[76] T. Abeyasekera, "Improvements to grid connected photovoltaic inverters," Newcastle University, Newcastle upon Tyne, 2005.

[77] J. D. P. Gene F. Franklin, Michael L. Workman (1997). "*Digital Control of Dynamic Systems"*. ISBN 9780201820546.

[78] R. Teodorescu *et al*, "Proportional-resonant controllers and filters for grid-connected voltage-source converters," *Electric Power Applications, IEE Proceedings* vol. 153, pp. 750-762, 2006.

[79] S. Buso and P. Mattavelli (2006). "*Digital Control in Power Electronics"*. Morgan & Claypool Publishers. ISBN 9781598291124.

[80] A. Hasanzadeh *et al*, "A Proportional-Resonant Controller-Based Wireless Control Strategy With a Reduced Number of Sensors for Parallel-Operated UPSs," *Power Delivery, IEEE Transactions on*, vol. 25, pp. 468-478, 2010.

[81] S. D. Inc., "eZdsp F2812 Technical Reference," 2003.

[82] Z. Ye *et al*, "PR and harmonic compensation control scheme with current state feedback for an single-phase Active Voltage Quality Regulator," in *Power Electronics and ECCE Asia (ICPE & ECCE), 2011 IEEE 8th International Conference on*, 2011, pp. 2749-2756.

[83] D. Sera *et al*, "Low-cost digital implementation of proportional-resonant current controllers for PV inverter applications using delta operator," in *Industrial Electronics Society, 2005. IECON 2005. 31st Annual Conference of IEEE*, 2005, p. 6 pp.

[84] X. Guo *et al*, "A Single-Phase Grid-Connected Inverter System With Zero Steady-State Error," in *Power Electronics and Motion Control Conference, 2006. IPEMC 2006. CES/IEEE 5th International*, 2006, pp. 1-5.

[85] K. C. B. Mehmet Tumay, Mehmet Ugras CUMA, Ahmet TEKE, "Experimental Setup For a DSP Based Single-Phase PWM Inverter," 2005.